Faculty of Aerospace Engineering, Delft University of Technology
Energieonderzoek Centrum Nederland

Technical Report

Comparison and Application of Unsteady Integral Boundary Layer Methods
using various numerical schemes

by

Bram van Es
November 16, 2009

Supervisors: Hüseyin Özdemir (ECN) & Bas van Oudheusden (TUDelft)

To well predicted boundary layers

Preface

With great relieve I write the final words of my thesis and yet with great sadness I close off one of the richest periods in my life.

More than a year ago I moved to Heiloo to do my thesis work at ECN. I was somewhat shivery about living with a stranger, since you never know who you might end up with. It turned out to be one of the most polite and kind people I ever met, a South-African master student from my own faculty with whom I would be spending most of my time since he was also my office mate.

Together with my newly found friend I moved to Alkmaar, the Jan van Goyenstraat to be exact. Here a rich social life developed with a large group of friends representing a wide variety of nationalities. In fact most of the time I was the only Dutch person in the group which made me appreciate my own country in a different way. Many activities, dinners, get-togethers were organised, if not through talking in the ECN-bus about the stuff we could do after work then by participating in the ECN/JRC/NRG mailing list (dubbed the "spamlist") which always contained some excuse to go to the beach or to grab a beer.

All and all I met an interesting bunch of international(ly minded) people (and trying to list them here would add another page to an already lengthy report) and did many interesting things (listing them would do the same..). Those who are closest to my heart I will meet again, sooner rather than later.

I had a taste of being a stranger in my own country, in the near future I will be a stranger in a different country since by the suggestion of one of my new French friends I will pursue a PhD in Paris.

I wish my supervisor Hüseyin Özdemir all the luck in the world, with the implementation of the schemes which will be a daunting task for implicit time stepping (especially for DG) but especially with Belgin (who cares about schemes anyway). I have come to know you as a kind and warm person and I doubt I will ever again have such a friendly and informal relation with a supervisor. Out of interest I will continue the work on the schemes myself and I hope this will end up in a collaboration of some sort.

Based on the studied literature it is my conviction that this Msc thesis is probably the most complete treatise on unsteady IBL methods that is currently available. I hope it is considered useful beyond the walls of ECN and the TUDelft.

Velserbroek, 15 November 2009

Bram van Es

Contents

Abstract

ECN's project Rotorflow is focused on the development of an aerodynamic module which is able to model the unsteady flow over wind turbine blades. This module is to be coupled to structural dynamics modules for the analysis of wind turbine aeroelasticity . For this aerodynamic module a zonal approach will be used which incorporates an external unsteady potential flow solver and an unsteady integral boundary layer method(IBLM). It was my task to develop an unsteady two-dimensional IBLM from existing methods and then to apply the method using several Finite Differencing Methods (FDM), Finite Volume Methods (FVM) and a particular Finite Element Method(FEM) namely Discontinuous Galerkin (DG). Several systems of IBL equations as well as closure relations have been considered in some detail. All of the considered systems for the IBLM turn out to be hyperbolic and thus warrant the implementation of a Riemann solver. Various test cases were performed and compared with literature, most notably, the impulsively moved and oscillating flat plate and the impulsively moved cylinder. Results show that the unsteady IBLM is able to model the transient behavior correctly, even close to separation, for very high Reynolds number numerical smoothing is required. All finite difference schemes performed well, the same is expected for the finite volume methods. It is advised to apply the closure relations by Matsushita et al for laminar boundary layer flow. Further development is necessary for the DG method as the closure relations may give problems in combination with an expansion in basis functions for the flux vector and the source vector.

Part I

General Introduction and Literature Review

Chapter 1

Introduction

1.1 Wind energy and ECN

The Energy research Center of the Netherlands is active in a multitude of areas which can roughly be divided into technical research and policy studies. The technical research is divided over several units with their own specialisation, ranging from biomass to wind energy.

The wind energy unit has three research groups which focus on aerodynamics, integrated wind turbine design, and operation and maintenance. The current thesis falls within the framework of the aerodynamics research group and the integrated wind turbine design research group.

To design windturbines the aerodynamic loading and the coupling of this loading with the structural dynamics is crucial. To model the aeroelastic behavior time dependency can not be neglected and the loading should be physically correct, to that end separation and wake effects should also be resolved to some extent.

Current structural design tools that allow coupling are PHATAS (Program for Horizontal Axis wind Turbine Analysis and Simulation), TURBU and SIMPACK, which examine the mechanical loading of the wind turbines or wind turbine blades, a multibody-FEM is currently under development. The input of these structural design tools can be provided by different aerodynamic programs/models. Currently the input methods are, in increasing order of complexity, the BEM(Blade Element Momentum) theory, AWSM (Aerodynamic Windturbine Simulation Module,which is based on a vortex line model) and the Reynolds Averaged Navier-Stokes equations.

Both BEM and AWSM assume steady flow. Although BEM allows dynamic inflow conditions BEM is very limited in the amount of physics that is resolved, using modified actuator disc theory (including radial difference of inflow velocity due to a rotating wake) to approximate the forces per chord section. AWSM is more advanced, using lifting line theory, however it still requires user defined relations for the effect of viscosity, it lacks time-dependency and turbulence modelling. RANS contains much of the fluid physics, however like most turbulence models the practical application is limited due to computational cost in case of very high Reynolds numbers which is typical for wind turbines.

1.2 Problem Description

The need for an efficient but physically accurate time-dependent solver for aeroelastic simulations of wind turbines and accurate flow modelling around wind turbines defines the framework of the current thesis, which is captured in project Rotorflow. Rotorflow

is meant to produce an aerodynamic model (or set of models) which can simulate the unsteadiness of the flow field over wind turbine rotors with incorporation of viscosity and possibly also compressibility and which can serve as the input for the structural design tools. The aim is that Rotorflow is physically more correct than AWSM in that the most important features are present but can still be run on a normal desktop computer, thus filling the gap between AWSM and RANS. Rotorflow is particularly relevant for the analysis of fatigue loading which is primarily dependent on the time varying solution and thus the quality of the unsteady flow determination becomes important.

To fulfill the requirements set out for Rotorflow a zonal approach is taken, the solution domain is divided in an outer flow and a boundary layer flow, for both domains a different approximation is used. The coupling of the two domains is handled through an interaction law. Each aspect, the outer flow, the boundary layer flow and the coupling method are separate topics which cannot all be addressed in this thesis.

The outer flow is considered to be incompressible and non-viscous which allows for a potential flow solver, where the boundary layer flow is considered to be viscous which can be solved by the boundary layer equations. The unsteady incompressible potential flow solver to be used is a multilevel unsteady panel method, which should show a considerable speed-up compared to conventional panel methods. The boundary layer equations are solved in the integral form which reduces the problem dimension by one and which should decrease the computation time for the boundary layer by an order of magnitude compared to the non-integral formulation (to be called the field form). An unsteady Integer Boundary Layer Method (IBLM from now on) coupled to an unsteady panel code should be able to capture the main viscous effects and the unsteady behavior while maintaining a low computational footprint.

The existing code XFOIL and the more wind dedicated RFOIL use an integral boundary layer method and are based on a coupled viscid-inviscid solver. They are however based on steady formulations. The focus of this thesis will be the development of a two-dimensional *unsteady* IBLM, which is implemented with several numerical methods.

1.2.1 Goal of this Thesis

From a range of existing closure relations and solution methods this thesis will present a system of equations to solve the unsteady two-dimensional IBL equations, subsequently this system will be solved using a Finite Difference Method(FDM), a Finite Volume Method(FVM) and a Finite Element Method(FEM). The overlying objective is to provide some experience for the final unsteady three-dimensional compressible integral boundary layer equations which are to be coupled to an unsteady panel method.

1.3 Report outline

The report consists of three parts, the first part will describe the existing literature and will give an overview of the closure models that can be used, the second part describes the selection of the closure models and solution methods based on the literature research, some preliminary tests with steady models and a description of the numerical methods, the third part describes the test cases and the results.

Part i In chapter two the integral boundary layer equations are derived starting from the full Navier-Stokes equations. Chapter three gives a description of the basic problems in boundary layer and so-called closure models used in literature.

Part ii Chapter four describes some of the solution methods found in literature, solution methods being the combination of the closure models, a certain set of integral boundary layer equations and some numerical method to solve the system. Starting from the

knowledge of part i several combinations of closure models and integral boundary layer equations are discussed at the end of chapter four from which a selection is made which will be used for the final implementation. Chapter five discusses in general implementation issues such as stability, hyperbolicity, etc. Chapter six will deal with the numerical methods which have been implemented.

Part iii Chapter 7 describes the test cases and results obtained with the current implementation[1], chapter 8 finally contains the conclusion and recommendations.

Administrative notes by the author

- when there is a mentioning of dimensions the reader should assume physical dimensions unless stated otherwise
- when there is a mentioning of inner solution or inner approximation the reader should assume that it refers to the solution at the inner grid points
- when there is a mentioning of travelling information and directionality of information the reader should interpret this as solution information travelling through the solution domain in physical time
- when results are plotted abbreviations will be used for the specifications, e.g. second order Runge-Kutta integration is RK2, a Courant-Friedrich-Lewy condition of 0.5 is $CFL = 0.5$
- edge velocity is synonym to tangential inviscid velocity
- 'scheme' refers to a numerical discretisation scheme
- whenever there is a reference to an 'equation', say 'equation 3.1' equation 3.1 may be a single equation or a system/set of equations
- when there is a mentioning of outer solution the reader should interpret this is as the solution of the inviscid equations 'outside' the boundary layer
- for the description of the DG method cell faces actual refer cell points, however the term 'face' is more intuitive in relation to fluxes
- the kinetic energy integral equation and the moment-of-momentum equation refer to the same equation

[1] It must be noted here that not all the implemented (read 'coded') methods have actually been tested

Chapter 2

Integral Boundary Layer equations

As was said in the problem description the integral boundary layer(or IBL) equations will form the basic equations with which the boundary layer velocity profile will be solved. The IBL equations originate from the boundary layer (or BL) equations which in turn originate from the full equations of motions for a fluid. This chapter will elaborate on the IBL equations, explaining the derivation in some detail, and reviewing the relations used to close the resulting system of equations.

The next section will explain the physical aspect of the boundary layer and the boundary layer equations resulting from the simplifications. First very shortly the general flow equations for a fluid are discussed.

2.1 General Flow Equations

Conventionally the problem of fluid flow is considered as a continuum mechanical problem. This means that the properties of the myriad of colliding atomic particles is described by a continuous model. The continuous model for a Newtonian fluid is based on the idea that (besides a continuum medium) the shear stress on the surface of a fluid control volume can be directly related to the velocity gradient perpendicular to the surface, i.e.

$$\overline{\overline{\tau}}_{surface} = \mu \frac{\partial \overline{u}}{\partial \overline{n}} \tag{2.1}$$

where μ is denoted as the viscosity which is basically an exchange of momentum through molecular diffusion. The continuous model is characterised by several conservation laws. These conservation laws state that each infinitesimal control volume has a balanced gain and loss of mass, momentum and energy. Effectively it means that the transport/creation/destruction of these properties is equal to the time rate of change of these properties in the control volume. Based on the control volume these balances can be cast into differential equations by taking the limit to zero for $\Delta t, \Delta x, \Delta y$ and Δz. For a detailed derivation off the equations of fluid motion, see for instance Warsi[151], Anderson[5]. Commonly used is the Einstein or tensor notation which allows for a more concise formulation, the conservation laws are written in Einstein notation as

$$\begin{aligned} \frac{\partial \rho}{\partial t} + \frac{\partial \rho u_i}{\partial x_i} &= 0, \\ \frac{\partial \rho u_i}{\partial t} + u_j \frac{\partial \rho u_i}{\partial x_j} &= \frac{\partial \sigma_{ij}}{\partial x_j} + \rho f_n, \\ \frac{\partial \rho E}{\partial t} + \frac{\partial \rho E u_i}{\partial x_i} &= \rho u_i \, f_n + \frac{\partial u_i \sigma_{ij}}{x_j} - \frac{\partial q_i}{\partial x_i}, \end{aligned} \tag{2.2}$$

with

$$\begin{aligned}
\text{total stress tensor:} \quad & \sigma_{ij} = -p\delta_{ij} + \tau_{ij}, \\
\text{viscous stress tensor:} \quad & \tau_{ij} = \mu\left(\frac{\partial u_i}{\partial x_j} + \frac{\partial u_j}{\partial x_i}\right) + \lambda\frac{\partial u_m}{\partial x_m}\delta_{ij}, \\
\text{heat flux:} \quad & q_i = -k\frac{\partial T}{\partial x_i}, \\
\text{total energy:} \quad & E = e + \frac{1}{2}u_i\,u_i, \\
\text{bulk viscosity:} \quad & \lambda, \\
\text{body forces:} \quad & f_n.
\end{aligned}$$

Following the Stokes hypothesis it is assumed that $\lambda = -\frac{2}{3}\mu$, see i.e. White[154]. For an ideal gas the following relationships also hold

$$\begin{aligned}
p &= \rho RT, \\
e &= c_v T, \\
R &= c_p - c_v,
\end{aligned}$$

Here c_p and c_v are the specific heats for constant pressure and volume respectively. Although historically incorrect, the above set of equations shall be called the Navier-Stokes(NS) equations. The above formulation of the equations of fluid motion has not been solved analytically and in aerospace practice it is rarely applied numerically without severe simplifications simply due to the computational cost. For the application to boundary layer flows, the simplifications are many fold, on top of these simplifications the resulting boundary layer equations will be integrated to reduce the problem dimension.

2.2 Boundary Layer Equations

For very high Reynolds numbers the incompressible NS equations can be simplified to the boundary layer equations which were first derived by Prandtl in 1904. The boundary layers described by the boundary layer equations emerge in flows over objects and at the interfaces of multiple-fluid flows (shear layers). The flow problem at hand deals with the flow over a flat plate, consider the flow domain in figure (2.1) for the nomenclature of the flow problem. For high Reynolds numbers the boundary layer represents a very

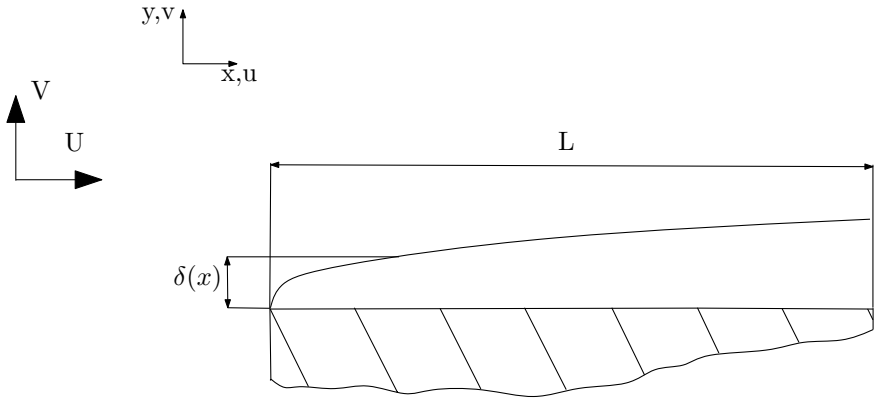

Figure 2.1: Flat plate boundary flow, nomenclature.

thin layer with thickness $\delta \ll L$ in which the flow adapts from the static wall where

the tangential velocity is 0 (to be called the no-slip condition) to the outer flow where viscosity has negligible influence.

Starting with the unsteady NS equations for compressible flow (see equation (2.2)), the boundary layer equations will be derived by adding simplifications.

As stated in the introduction the flow is assumed to be incompressible where all time derivatives of density ρ can be ignored. Applying this assumption the continuity equation reduces to

$$\frac{\partial u_i}{\partial x_i} = 0, \tag{2.3}$$

leading to a simplification in the formulation for τ_{ij}

$$\tau_{ij} = \mu \left(\frac{\partial u_i}{\partial x_j} + \frac{\partial u_j}{\partial x_i} \right). \tag{2.4}$$

Using equation (2.4) and the continuity equation the stress term σ_{ij} can be rewritten

$$\begin{aligned} \frac{\partial \sigma_{ij}}{\partial x_j} &= \frac{\partial p}{\partial x_i} + \frac{\partial \tau_{ij}}{\partial x_j}, \\ &= \frac{\partial p}{\partial x_i} + \mu \left(\frac{\partial}{\partial x_j} \left(\frac{\partial u_i}{\partial x_j} \right) + \frac{\partial}{\partial x_i} \left(\frac{\partial u_j}{\partial x_j} \right) \right), \\ &= \frac{\partial p}{\partial x_i} + \mu \frac{\partial}{\partial x_j} \left(\frac{\partial u_i}{\partial x_j} \right). \end{aligned} \tag{2.5}$$

The momentum equation and the energy equation can now be written as

$$\frac{\partial u_i}{\partial t} + u_j \frac{\partial u_i}{\partial x_j} = \frac{1}{\rho} \left(\frac{\partial p}{\partial x_i} + \mu \frac{\partial}{\partial x_j} \left(\frac{\partial u_i}{\partial x_j} \right) \right) + f_n, \tag{2.6}$$

$$\frac{\partial E}{\partial t} + \frac{\partial E u_i}{\partial x_i} = \frac{1}{\rho} \left(u_i \frac{\partial \sigma_{ij}}{\partial x_j} + \sigma_{ij} \frac{\partial u_i}{\partial x_j} - \frac{\partial q_i}{\partial x_i} \right) + u_i \, f_n. \tag{2.7}$$

For Newtonian gases the viscosity coefficient μ is assumed to be a function of pressure and temperature (see i.e White [154]). Since the gas is assumed to be incompressible the pressure is related directly to the temperature through the equation of state. However the temperature dependence of the viscosity will also be ignored for the very simple reason that the assumption of incompressibility (and thus low subsonic velocities) brings along that the flow induced temperature effects will be of minor importance. When supersonic velocities are considered the incorporation of varying viscosity might be required.
Equations (2.3) and (2.6) describe the two dimensional incompressible flow where viscosity is assumed to be constant.
Using the assumption that $\delta < L$ these equations are non-dimensionalised using the following non-dimensional variables

$$\begin{aligned} u^* &= \frac{u}{U} & v^* &= \frac{v}{V}, \\ x^* &= \frac{x}{L} & y^* &= \frac{y}{\delta}, \\ t^* &= t \, \frac{\sqrt{U^2 + V^2}}{L} & p^* &= \frac{p}{\rho_0 \sqrt{U^2 + V^2}}, \\ \rho^* &= \frac{\rho}{\rho_0} & \mu^* &= \frac{\mu}{\mu_0}, \end{aligned}$$

where ρ_0 and μ_0 are the reference values for the density and the viscosity respectively. Here gravity is ignored but please note that body forces play an important role when

considering the rotation of the blade in three dimensions (see Van Garrel [52]). Applying the non-dimensional variables to the continuity equation results in

$$\frac{U}{L}\frac{\partial u^*}{\partial x^*} + \frac{V}{\delta}\frac{\partial v^*}{\partial y^*} = 0. \tag{2.8}$$

Now $\frac{\partial u^*}{\partial x^*} \sim \frac{\partial v^*}{\partial y^*} = O(1)$ only if $\frac{L}{U}\frac{V}{\delta} = O(1)$ which results in $V \sim U\frac{\delta}{L}$ (see i.e. Veldman [145]). So the velocity tangential to the body surface can be assumed to be much larger than the velocity normal to the surface, i.e. $V \ll U$ and subsequently $U^2 + V^2 \approx U^2$. Writing out σ_{ij} and substituting the non-dimensional variables the non-dimensionalised momentum equation in x-direction is written as

$$L\frac{\partial u^*}{\partial t^*} + \frac{U^2}{L}u^*\frac{\partial u^*}{\partial x^*} + \frac{U^2}{L}v^*\frac{\partial u^*}{\partial y^*} = -\frac{U^2}{L}\frac{\partial p^*}{\partial x^*} + \frac{\mu_0 U}{\rho_0 L^2}\frac{\partial^2 u^*}{\partial x^{*2}} + \frac{\mu_0 U}{\rho_0 \delta^2}\frac{\partial^2 u^*}{\partial y^{*2}}, \tag{2.9}$$

and for the momentum equation in y-direction

$$\delta\frac{\partial v^*}{\partial t^*} + \frac{U^2\delta}{L}v^*\frac{\partial v^*}{\partial y^*} + \frac{U^2\delta}{L}u^*\frac{\partial v^*}{\partial x^*} = -\frac{U^2}{\delta}\frac{\partial p^*}{\partial y^*} + \frac{\mu_0 U}{\rho_0 L\delta}\frac{\partial^2 v^*}{\partial y^{*2}} + \frac{\mu_0 U\delta}{\rho_0 L^3}\frac{\partial^2 v^*}{\partial x^{*2}}. \tag{2.10}$$

Since the future three dimensional formulation will be applied to rotating profiles unsteady behaviour may be prominent due to crossflow, also the inviscid outerflow is unsteady therefore the time derivative will not be neglected. Also, the unsteady formulation is noted to be more robust by Van der Wees en Van der Muijden (referenced by Van Garrel[52]). Continuing with equations (2.8), (2.9) and (2.10) further simplifications are possible.
Since the boundary layer is considered specifically the nomenclature will be changed somewhat, the index 0 is usually the indicator for either free stream or initial conditions, neither is suitable for the boundary layer, instead e will be used to indicate the values at the edge of the boundary layer. The edge of the boundary layer is defined as the value of y for which $u = m\,u_e$, where m is a constant and is usually 0.99 (see i.e. Schlichting[118]), see figure (2.2). Dividing by the factor for the pressure term and using

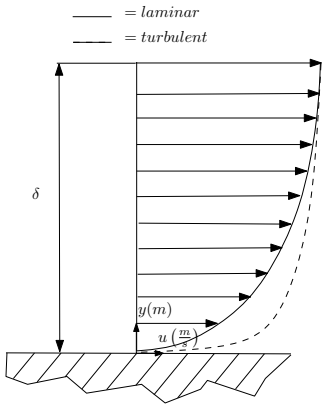

Figure 2.2: Velocity distribution in the boundary layer, δ is the boundary layer thickness.

$$Re = \frac{u_e L}{\nu^*}, \tag{2.11}$$

the conservation of momentum in x-direction is written as

$$\frac{L^2}{u_e^2}\frac{\partial u^*}{\partial t^*} + \left(u^*\frac{\partial u^*}{\partial x^*} + v^*\frac{\partial u^*}{\partial y^*}\right) = -\frac{\partial p^*}{\partial x^*} + \frac{1}{Re}\frac{\partial^2 u^*}{\partial x^{*2}} + \frac{L^2}{\delta^2}\frac{1}{Re}\frac{\partial^2 u^*}{\partial y^{*2}}. \tag{2.12}$$

Likewise for the conservation of momentum in y-direction

$$\frac{\delta^2}{u_e^2}\frac{\partial v^*}{\partial t^*} + \frac{\delta^2}{L^2}\left(v^*\frac{\partial v^*}{\partial y^*} + u^*\frac{\partial v^*}{\partial x^*}\right) = -\frac{\partial p^*}{\partial y^*} + \frac{1}{Re}\frac{\partial^2 v^*}{\partial y^{*2}} + \frac{\delta^2}{L^2}\frac{1}{Re}\frac{\partial^2 v^*}{\partial x^{*2}}. \tag{2.13}$$

If it is required that neither convection nor diffusion dominate in y-direction then $\frac{\delta}{L} \sim \sqrt{\frac{1}{Re}}$, subsequently it follows that

$$\nu\frac{\partial^2 v}{\partial y^2} \sim u\frac{\partial v}{\partial x} + v\frac{\partial v}{\partial y} = \frac{u_e^2\delta}{L^2}.$$

Neglecting all terms where the factor is $\ll 1$ results in the boundary layer equations

$$\frac{\partial u}{\partial x} + \frac{\partial v}{\partial y} = 0, \tag{2.14}$$

$$\frac{\partial u}{\partial t} + u\frac{\partial u}{\partial x} + v\frac{\partial u}{\partial y} = -\frac{1}{\rho}\frac{\partial p}{\partial x} + \nu\frac{\partial^2 u}{\partial y^2}, \tag{2.15}$$

$$0 = -\frac{1}{\rho}\frac{\partial p}{\partial y}. \tag{2.16}$$

Since the pressure gradient is zero in y-direction we can replace the value of pressure p at any location along the cross-section of the boundary layer with the pressure p_e defined at the inviscid outer flow. To obtain the pressure distribution outside the boundary layer the fluid is assumed to be inviscid and parallel to the surface(therefore $v_e = 0$). Using these assumptions the momentum equation outside the boundary layer can be written as

$$\frac{\partial u_e}{\partial t} + u_e\frac{\partial u_e}{\partial x} = -\frac{1}{\rho}\frac{\partial p_e}{\partial x}, \tag{2.17}$$

and inserting into equation (2.15) results in

$$\frac{\partial u}{\partial t} + u\frac{\partial u}{\partial x} + v\frac{\partial u}{\partial y} = \frac{\partial u_e}{\partial t} + u_e\frac{\partial u_e}{\partial x} + \nu\frac{\partial^2 u}{\partial y^2}. \tag{2.18}$$

Equations (2.14) and (2.18) are the field form of the boundary layer equations. Using the continuity equation and the chain rule the momentum equation can be rewritten to conservative form

$$\frac{\partial u}{\partial t} + \frac{\partial u^2}{\partial x} + \frac{\partial v\,u}{\partial y} = \frac{\partial u_e}{\partial t} + u_e\frac{\partial u_e}{\partial x} + \nu\frac{\partial^2 u}{\partial y^2}. \tag{2.19}$$

The boundary layer equations is also commonly derived starting from the RANS equations, the boundary layer equation then contain a Reynolds stress term (see appendix (K)). The field form is already a significant simplification from the form in equation (2.2) but a further reduction is possible through integration, this will lead to the IBL equations. The IBL equations will be derived in section (2.3).

2.3 Integral Boundary Layer Equations

The boundary layer equations (2.14) can be rewritten using the integral formulation for the displacement thickness and the momentum thickness, see appendix (B). Using the fact that the continuity equation is identically zero, families of momentum equations can be derived which in turn can be integrated. One such family is formed by (see i.e. Matsushita[91], Mughal[99])

$$\text{[Continuity equation]} \times \left(u^{n+1} - u_e^{n+1}\right) + \text{[Momentum equation]} \times (n+1)u^n. \tag{2.20}$$

For $n = 0$ equation (2.20) gives[1] the common form of the unsteady Kármán integral relation (see i.e. White [154])

$$\frac{1}{u_e^2}\frac{\partial(u_e\delta^*)}{\partial t} + \frac{\partial\theta}{\partial x} + (2+\frac{\delta^*}{\theta})\frac{\theta}{u_e}\frac{\partial u_e}{\partial x} = \frac{C_f}{2}, \tag{2.21}$$

where (also see appendix (B))

$$\begin{aligned}
\text{Shape factor:} \quad H &= \frac{\delta^*}{\theta},\\
\text{Wall friction coefficient:} \quad C_f &= \frac{\tau_w}{\frac{1}{2}\rho u_e^2},\\
\text{Displacement thickness:} \quad \delta^* &= \int_0^{y_e}\left(1-\frac{u}{u_e}\right)dy,\\
\text{Momentum thickness:} \quad \theta &= \int_0^{y_*}\frac{u}{u_e}\left(1-\frac{u}{u_e}\right)dy.
\end{aligned}$$

Rewriting the unsteady Von Kármán equation using the expression for H

$$\frac{1}{u_e^2}\frac{\partial(u_eH\theta)}{\partial t} + \frac{\partial\theta}{\partial x} + (2+H)\frac{\theta}{u_e}\frac{\partial u_e}{\partial x} = \frac{C_f}{2}, \tag{2.22}$$

or in fully conservative form

$$\frac{2}{u_e^2}\left(\frac{\partial\left(u_e\delta^*\right)}{\partial t} + \frac{\partial\left(u_e^2\theta\right)}{\partial x} + u_e\frac{\partial u_e}{\partial x}\delta^*\right) = C_f. \tag{2.23}$$

A similar procedure as for the momentum integral equation is followed to find a mechanical energy integral relation, using $n = 1$ equation (2.20) results in

$$\frac{1}{u_e}\frac{\partial(\theta+\delta^*)}{\partial t} + 2\frac{\theta}{u_e^2}\frac{\partial u_e}{\partial t} + \frac{1}{u_e^3}\frac{\partial(u_e^3\delta^k)}{\partial x} = C_D, \tag{2.24}$$

where

$$\begin{aligned}
\text{Viscous diffusion} \quad D &= \int_0^{y^*}\tau\frac{\partial u}{\partial y}dy,\\
\text{Viscous diffusion coefficient:} \quad C_D &= \frac{2D}{\rho u_e^3},\\
\text{Kinetic energy thickness:} \quad \delta^k &= \int_0^{y^*}\frac{u}{u_e}\left(1-\frac{u^2}{u_e^2}\right)dy.
\end{aligned}$$

Following the same procedure as for the momentum integral and the kinetic energy integral a third integral can be obtained. Using $n = 2$ equation (2.20) results in

$$\frac{1}{u_e^4}\left(\frac{\partial(u_e^3\delta^k)}{\partial t} + \frac{\partial(u_e^4\delta^{k+})}{\partial x} + u_e^3\frac{\partial\delta^*}{\partial t} - 3u_e^2\frac{\partial u_e}{\partial t}\theta - 3u_e^3\frac{\partial u_e}{\partial x}\theta\right) = 6C_K, \tag{2.25}$$

$$\tag{2.26}$$

where

$$\begin{aligned}
C_K &= 6\frac{\nu}{u_e^4}\int_0^{y^*}u\left(\frac{\partial u}{\partial y}\right)^2dy,\\
\delta^{k+} &= \int_0\frac{u}{u_e}\left(1-\frac{u^3}{u_e^3}\right)dy.
\end{aligned}$$

[1] The unsteady Kármán integral equation can also be found by direct integration,(see i.e. Özdemir[107]).

The reader is referred to appendix (A) for a complete derivation of the IBL equations. Throughout the report equations (2.21), (2.24) and (2.25) will be denoted as the IBL equations.[2]

The IBL equations can be written in the non-conservative form

$$AF_t + BF_x = C, \tag{2.27}$$

where F is the primary variable vector,A and B are coefficient matrices and C is the source vector. The conservative system is written as

$$F_t + f_x = L. \tag{2.28}$$

Independent of which combination of integral equations is chosen this system can not be solved in the current form since there are more unknowns than equations, namely $C_K, C_D, C_f, \theta, \delta^*, \delta^k, \delta^{k+}$, therefore more equations are needed to close the system.

The benefit of the integral boundary formulation compared to the field form of the boundary layer equations is firstly a reduction of order in computational effort. If N, M is the amount of elements in x- and y-direction respectively the field form requires $\sim N \times M$ computations per time step whereas the integral form requires $\sim N \times K$ computations per time step, where K is the amount of closure relations. It is yet unclear how much impact the closure relations will have on the computational efficiency so for the purpose of general comparison the boundary layer equations should also be solved in the field form, this has not be done in the current work, the outline of such a method is given for instance in Cebeci[19], Krainer[77] (also see appendix L). According to Cousteix the Integral Boundary Layer method is one order of magnitude faster than the so-called field method, see e.g. Cousteix[28]. Another clear advantage (as noted by Wirz[158]) is the simplification of the initial condition formulation since there is no dependency on y. Disadvantages are the lack of generality and accuracy since the usability of the IBL equations is very much dependent on the choice of the closure relations which are in practice empirical models. An advantage of using empirical models is that the accuracy for specific situations is comparable to the accuracy obtained by using the field form of the differential equations (see i.e. White[154],Van den Berg[136]).

The closure relations are the subject of the next chapter.

[2] In fact there is also the thermal-energy integral relation in case temperature is not assumed to be constant (see White[154]).

Chapter 3

Overview of Closure Relations

The previous chapter ended with an unclosed system of equations, the purpose of this chapter is to present common methods to close the IBL equations, the presented equations are meant as a reference and will not be discussed in detail. The closure relations are needed to literally close the system of IBL equations, these closure relations are based on empirical data which were obtained for certain test conditions or they are a result of specific solutions of the boundary layer equations, consequently these approximations are valid only in certain regions of the flow. More specifically laminar models are only valid in laminar flow conditions and turbulent flow models are most effective for turbulent flow, also most empirical models have difficulty with seperated flow (laminar or turbulent).To facilitate the use of multiple models, laminar to turbulent transition has to be considered as well as the point of flow separation.

It was shown by Nash (as referenced by i.e. Mughal[98])that there is close resemblance between empirical data for three dimensional and two dimensional boundary layers, provided there is little crossflow, this supports the idea to use a two dimensional model as a means to compare numerical models for three dimensional boundary layers for the case of negligible cross flow effects. In case there is strong cross flow, the hyperbolicity of the system may be affected which directly changes the applied solution method, this is discussed in section(5.6.4).

Most common methods for laminar boundary layers are due to Falkner and Skan, Pohlhausen, Thwaites and others, some of these models will be discussed.
The IBL equations incorporates laminar as well as turbulent flow, this is reflected in different closure relations. Turbulent boundary layer methods for instance due to Heads and Greens, Spaldings, Coles and Swafford will be discussed shortly. For a more detailed discussion on these closure relations see i.e. White [154], Warsi [151] and Schlichting [118].

Since it is not the purpose of this thesis to study and compare closure models in detail the evaluation of these models will be concise. Within this scope the writer aims to find the most generic set of closure relations to describe a boundary layer flow, whether the boundary layer is laminar, turbulent, separated or attached.

In a computational sense empirical relations are the cheapest way to close the momentum and energy integral equations. For implementation, simple substitution in the IBL equations suffices to reduce the number of unknown variables (for instance $\tau_w = f(x)$). It is not uncommon to employ pre-determined empirical boundary layer profiles as did Mughal [98]. The range of applicability for all closure relations hinges on the initial simplifications and assumptions or the specifications of the experimental data, this has to be kept in mind when a closure model is implemented.

The inherent added difficulty of considering separate laminar and turbulent boundary

layers is the fact that a transition point has to be determined. Considerable empirical studies have been performed on this subject, some of the common methods will be presented.
Also a subject of discussion is the separation of the boundary layer, this will be discussed shortly. Subsequently there will be a short discussion on the coupled method which is used to solve separated boundary layer flows. The difficulty of the unsteady

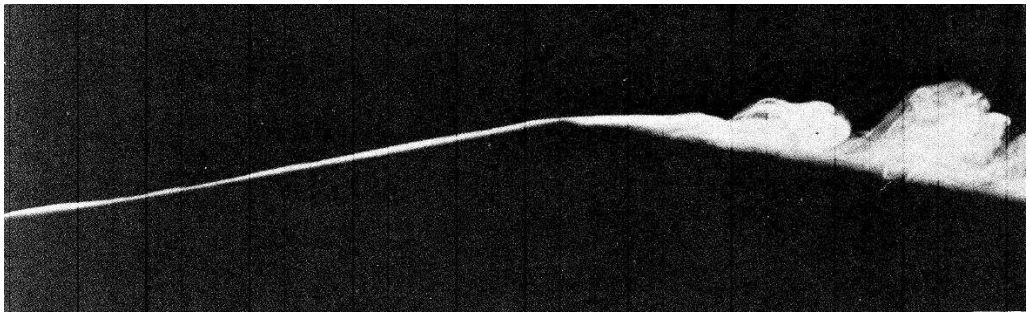

Figure 3.1: Laminar flow over a corner .

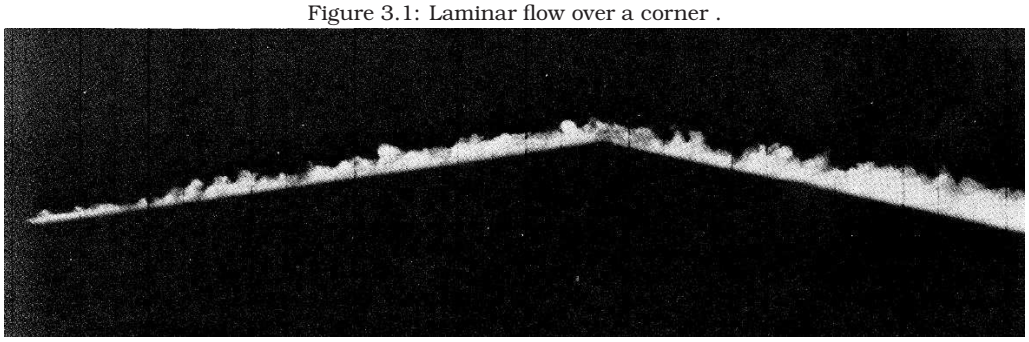

Figure 3.2: Turbulent flow over a corner .

approach comes from the fact that most closure relations are based on steady flows. Unsteady boundary layers are perhaps not as well described as steady boundary layers, most likely measuring unsteady boundary layers was not feasible when most of the basic theories arose and in general some unsteadiness parameter has to be defined like e.g. the unsteady Pohlhausen parameter. Several integral methods for unsteady incompressible boundary layers exist and are due to e.g. (also see Schlichting[118])

- Schuh(1953), Yang(1959), Rozin[116](1960) and Hayasi[61](1962) : guessed velocity profile, two equation one parameter solution method, applied to laminar boundary layers
- Lyrio et al[51](1982), Strickland and Graham[105](1983) : Von Kármán equation in combination with Head's entrainment applied to turbulent boundary layers
- Matsushita[91],[90](1984,1985) : correlation of variables, two and three equation two parameter solution method, applied to laminar boundary layers
- He[62](1993), Hall[58](2001) : Von Kármán equation, kinetic energy integral equation and unsteady lag entrainment

Of these, the methods by Hayasi, Matsushita et al and He and Hall will be discussed in more detail in section (4.2). Also a subject of discussion for the unsteady laminar boundary layer is the steady two equation formulation by Drela(1985), this is written in unsteady form, see section(4.2).

IBL closure relations for unsteady turbulent boundary layers are scarcely available, alternatively steady variants of turbulent models are used(see i.e. Swafford[129]), common turbulent closure relations are due to e.g.

- Head(1958),Green(1977) : entrainment equation and lag entrainment equation
- Swafford et al(1981),Swafford and Whitfield(1985) : full velocity profile description of turbulent boundary layer

Of these models only Head's entrainment method and Green's lag entrainment have been written in unsteady form however the empirical closure is still based on steady boundary layers. Whitfield and Swafford have devised velocity profiles for the entire turbulent boundary layer, including separation.

A quasi-steady approach is also possible, however this confines the range of problems that can be considered. One speaks of quasi-steady boundary layers if it is assumed that the boundary layers adapts to the external flow instantaneously. For a sinusoidal free stream velocity over a flat plate the flow can be considered quasi-steady if (see Moore[96])

$$
\begin{aligned}
&Re_\delta \frac{\delta\, k}{u_{e,0}^2} \ll 1,\\
&\left(Re_\delta \frac{\delta\, k}{u_{e,0}}\right)^2 \frac{u_e^*}{u_{e,0}} \ll 1,\\
&\text{frequency of oscillation:} \quad k,\\
&\text{amplitude of oscillation:} \quad u_e^*,\\
&\text{undisturbed free stream velocity:} \quad u_{e,0}.
\end{aligned}
$$

Very large timescales of the flow perturbations allow for the assumption of quasi-steadiness (see i.e. Schlichting[118]). Moore[96] stated specifically for the unsteady flat plate boundary layer flow that the following non-dimensional parameters should be $\ll 1$ to assume quasi-unsteadiness.

$$
\frac{x}{u_e^2}\frac{\partial u_e}{\partial t}, \quad \frac{x^2}{u_e^3}\frac{\partial^2 u_e}{\partial t^2}, \quad \cdots \frac{x^n}{u_e^{n+1}}\frac{\partial^n u_e}{\partial t^n}.
$$

Whenever it is possible (and appropriate) the actual equations are placed in appendix (E).

3.1 Laminar Boundary Layer

The laminar boundary layers are well described by practical experiments which in turn have led to the development of several different approximation methods. Two main approximative ways to describe the laminar boundary layer are (also see Cebeci [22] and White [154])

- similarity solutions, solution scales with one or more parameters dependent on x, y, t (see chapter 1.2)
- integral methods, velocity profile is assumed or equations are reduced through substitution of correlating primary variables
- Correlation based methods, derive closure relations using analytical, numerical or experimental solutions

Due to their relative mathematical simplicity similarity flows were developed early in the pre-computer era. Blasius presented his flat-plate solution as early as 1908, the more general Falkner-Skan equation was derived later in 1931 by Falkner and Skan.
The first integral method is a combination of the Von Kármán equation and a velocity profile due to Pohlhausen who assumed the velocity profile to be a 4^{th} order polynomial, this was extended to 6^{th} order by Libby [83] for variable viscosity. The most popular (integral) method for laminar boundary layer flow is due to Thwaites and Holstein and Bohlen (see i.e. Schlichting [118]). The latter method, to be called the method of Thwaites, is the most commonly used method for the approximation of the steady laminar boundary layer. This method however is not suitable for unsteady boundary layer flow and there has been no notable effort to change this, although an unsteady version has been found in literature (see section (4.3)). The benefit of the method due to Thwaites is that it does not require the prescription of a velocity profile as does for instance the Von Kármán -Pohlhausen method. The solution methods for steady boundary layers which use both equation (2.21) and equation (2.24) are found to be superior to single equation models, see e.g. Hayasi[61]. For accelerated flow higher order one-parameter polynomial profiles perform comparable to two-parameter methods of the same order, see Libby[83].

3.1.1 Similarity Solutions

Starting from the boundary layer equations it is possible for certain external velocity profiles to write a single ODE or a system of ODE's dependent on one variable usually denoted as $\eta(x, y, t)$. This means that a solution for some η simply scales in any direction for which η is constant, the solution is called self-similar in that direction. The first similarity solution was for a flat-plate boundary layer flow, due to Blasius in 1908. A subset of the similarity solutions are the semi-similarity solutions where the problem variable are reduced to two variables, see i.e. Hayasi[61].
Note that the flat-plate is defined as such through the external velocity profile, i.e. $u_e = Constant$. This should not be confused with the current flat-plat problem where the flat-plate is assumed merely for the ease of using an orthogonal coordinate system. The Falkner-Skan equation represented the similarity solution of the boundary layer equations for a power law velocity distribution $u_e = Constant x^m$ where m ranges from -0.09043 which represents severely stagnation flow to $m > 0$ which represent accelerating flow. To obtain a Falkner-Skan like equation for the unsteady form of the boundary layer equations the time derivative has to be incorporated. Specific unsteady similarity solutions for the impulsively started semi-infinite wedge are given by Nanbu [102], Khan et al (2006)[74] and Philip et al[110].

Matsushita[91] employed the original Falkner-Skan formulation using a slipping wall boundary condition, i.e. $f^{'}(0) = u_{wall}$ and extracted correlations for shape factors and integral variables, see section (4.2.4). Matsushita refers to Tani[133] in stating that the Falkner-Skan profiles are especially suitable for accelerating flows, also see for instance Mughal[99].

Downside of the similarity solutions is their reliance on a velocity prescription $u_e = f(x, t)$, this limits their applicability since an actual unsteady flow can in general not be described through an analytical relation. However for laminar (boundary/wake) flow the velocity distributions produced by the similarity solutions or semi-similarity solutions can be used to create relations for the shape factors. To that end similarity and semi-similarity solutions have been used to specifically approximate accelerating boundary layer flow, decelerating boundary layer flow, stagnating boundary layer flow and wake flow. The Falkner-Skan solution for power-law flow provides a reference for accelerating boundary layer flows. Often used for decelerating flow is the quartic profile due to Tani, the shape factors are tabulated in his paper[132]. For the stagnating boundary layer flow, Matsushita and Akamatsu[90] use a similarity solution by Proudman and Johnson, and Robins and Howarth which they based on the rear stagnation point of a

moving cylinder. For $0 < t < 5$ the shape factors are assumed to be variable, for large t the boundary layer will approach the similarity solution found by Hiemenz (see Proudman[111]).
In case the wake is laminar the semi-similar solution due to Williams[156] can be used. The solution due to Williams was applied by Matsushita et al[91] for $0.2 < m < 1.3$.

As the similarity solutions cannot be applied directly to solve general boundary layer problems, however they can be used to obtain correlations for the integral variables, see section(3.1.3). For more details on the specific (semi-similarity) problems the reader is referred to appendix (C).

The one-parameter integral methods are suitable to be applied directly in generic IBL application , these methods will be discussed in the next section.

3.1.2 One-parameter Integral Methods

The one-parameter integral methods are substitution methods for the IBL equations, the most common substitution is provided by some assumed velocity profile. This approach was first suggested by Pohlhausen in 1921 for steady boundary layer flow, this led to several alternative methods for the unsteady boundary layer flow due to for instance Schuh(1953) and Tani(1954). The benefit of this approach is that once a suitable guessed profile is found the integral parameters can be produced directly through integration without dependence on empirical relations.
The assumed velocity profile for the Pohlhausen method is a 4^{th} order polynomial (see for instance Schlichting[118])

$$f(\eta) = \frac{u}{u_e} = \frac{u(\eta)}{u_e} = a_0 + a_1\eta + a_2\eta^2 + a_3\eta^3 + a_4\eta^4,$$
$$\eta = \frac{y}{\delta},$$

using

$$\begin{aligned} &y = 0, u = 0, \\ &y \to \infty, u = u_e(x), \\ &y \to \infty, \frac{\partial u}{\partial y}, \frac{\partial^2 u}{\partial y^2}, \frac{\partial^3 u}{\partial y^3}, \cdots \to 0, \end{aligned}$$

and using the steady variant of the momentum equation (2.17) at the edge of the boundary layer, the following values for the constants emerge

$$a_0 = 0,\ a_1 = 1 + \frac{\Lambda}{6},\ a_2 = -\frac{\Lambda}{2},\ a_3 = -2 + \frac{\Lambda}{2},\ a_4 = 1 - \frac{\Lambda}{6},$$

where Λ (also known as the Pohlhausen-parameter) is defined as

$$\Lambda = \frac{\delta^2}{\nu}\frac{du_e}{dx}$$

The velocity profile can now be written as

$$\frac{u}{u_e} = \left(2 - 2\eta^2 + \eta^3\right)\eta + \frac{1}{6}\Lambda\eta(1-\eta)^3.$$

The 4^{th} order method by Pohlhausen was dismissed by White[154] as not being very accurate, also it gave less accurate results near seperation points, the latter would later also bother the derived methods (see Libby [83]). Schuh considered the Pohlhausen method with respect to unsteady flow and Libby applied Pohlhausen to the steady compressible IBL equations, see i.e. Libby [83]. The Pohlhausen method can also be extended to three dimensions as was implemented by for example Smith and Young [125].

By differentiating the boundary layer momentum equation more boundary conditions can be found (see i.e. Rosenhead[114])

$$\left.\frac{\partial^3 u}{\partial y^3}\right|_{y=0} = 0, \left.\frac{\partial^4 u}{\partial y^4}\right|_{y=0} = \frac{1}{\nu}\left.\frac{\partial u}{\partial y}\right|_{y=0} \left.\frac{\partial^2 u}{\partial x \partial y}\right|_{y=0}, \cdots$$

The latter boundary condition can be written as

$$\left.\frac{\partial^4 u}{\partial y^4}\right|_{y=0} = \frac{u_e^4}{4\nu^3} C_f \frac{dC_f}{dx}.$$

It is stated by Libby[83] that the polynomial approximation of the velocity profile will be exact for an infinite polynomial order, i.e. if the polynomial distribution satisfies all of the above boundary conditions. Infinitely many profiles can be derived based on different combinations of the boundary conditions, see appendix D.
Several forms of the profile have been suggested which satisfy some set of the above mentioned boundary conditions, the following form is due to Mangler(see Rosenhead[113])

$$\frac{u}{u_e} = 1 - (1-\eta)^n (1 + a_1\eta + a_2\eta^2 + \cdots), \tag{3.1}$$

which satisfies n of the boundary conditions at $\eta = 1$ plus the boundary conditions $f^{'}(0) = 0, f^{''}(0) = -\Lambda$ and $f^{'''}(0) = 0$. The Pohlhausen equation is a form of the Mangler equation. Wieghardt used a two-parameter approach for the equation of Mangler with $n = 8$ so the two-parameter method from Wieghardt satisfies eight of the earlier mentioned boundary conditions at $\eta \to 1$ (see equation (E.1), Rosenhead[113]) Rosenhead notes that the profiles due to Wieghardt may become inadequate in regions of sharply falling pressure. The above methods derived from Mangler can have the unphysical result of $\frac{u}{u_e} > 1$ in case of strong adverse pressure gradient but is more accurate in case of favorable pressure gradients. For Pohlhausen $\frac{u}{u_e} > 1$ will occur at $\Lambda = 12$.
Timman suggested a profile which meets all boundary conditions at $\eta = 1$ and which cannot yield the unphysical result mentioned above (see equation (E.2), Rosenhead[113]). Cooke[27] uses an following adaptation of Timman's profile. The formulation by Cooke however requires the application of two integral equations since both θ and δ are present in the resulting differential equation(s) (see equation (E.3)). Drela[35] has found that the Falkner-Skan similarity solutions are a very good approximation for attached, non-similar flows. Mughal uses an empirical curve fit for solutions of the Falker-Skan equation (see equation (E.4), Mughal[99]). It was reported by Drela[37] that the previous approximation overestimates negative velocities in separated regions. A more recent method involving a two parameter method is due to Thomas and Amminger. For more on steady approximate methods the reader is referred to Rosenhead[113] and Walz[149].
At present the unsteady variant of the momentum equation is considered, which has the following boundary conditions for quasi-steady boundary layer flow

$$\begin{aligned}
&y = 0, u = 0 \\
&\nu \left(\frac{\partial^2 u}{\partial y^2}\right)_0 = -\left(\frac{\partial u_e}{\partial t} + u_e \frac{du_e}{dx}\right), \\
&y \to \infty, u = u_e(x), \\
&y \to \infty, \frac{\partial u}{\partial y}, \frac{\partial^2 u}{\partial y^2}, \frac{\partial^2 u}{\partial y^3}, \cdots \to 0.
\end{aligned}$$

Note that the (instantaneous) velocity distribution is incorporated in Λ and as will be seen later, the approximate profiles are not time-dependent apart from the time-dependency of the external velocity. Applying the boundary conditions leads to the following description of the Pohlhausen parameter

$$\Lambda = \frac{\delta^2}{\nu}\left(\frac{\partial u_e}{\partial x} + \frac{1}{u_e}\frac{\partial u_e}{\partial t}\right) \tag{3.2}$$

here $\frac{\delta^2}{\nu}$ may be regarded as a measure of the time required to diffuse a change through the boundary layer (see i.e.Moore[96]). For application to unsteady flows Schuh, Yang, and Hayasi[61] used the following parameter as a substitute of the original Pohlhausen parameter which will be called the unsteady Thwaites' parameter[62]

$$\Lambda = -\frac{\theta^2}{\nu u_e}\left(\frac{\partial^2 u}{\partial y^2}\right)_w = \frac{\theta^2}{\nu}\left(\frac{\partial u_e}{\partial x} + \frac{1}{u_e}\frac{\partial u_e}{\partial t}\right). \tag{3.3}$$

A direct observation can be made with regard to the unsteadiness of the boundary layer; if $\frac{1}{u_e}\frac{\partial u_e}{\partial t} \ll \frac{\partial u_e}{\partial x}$ then the flow is in effect quasi-steady.
Note that the adapted Pohlhausen parameter contains the integral parameter θ, Hayashi suggested to solve this through the momentum integral equation(2.21) or the mechanic energy integral equation(2.24), see section (4.2.3). The two former methods (Yang, Schuh) perform weakly under decelerating flow, Tani improved the method and came up with a different quartic velocity profile which was more suitable for decelerating flow (see Tani [132]). Tani's method was applied to a separating and reattaching laminar flow by Lees and Reeves (as referenced by Matsushita[91]).
Tani used the following velocity profile

$$\frac{u}{u_e} = \left(6 - 8\eta + 3\eta^2\right)\eta^2 + a\eta(1-\eta)^3. \tag{3.4}$$

Here a is proportional to the square of the momentum thickness, i.e. a is not directly related to the pressure distribution (see Rosenhead[113]). Using two IBL equations (2.21) and (2.24) in combination with the guessed velocity profiles by Tani and Hartree[60], Hayasi[61] concluded that the quartic velocity profile is preferable over the Hartree profile for $\Lambda \leq 0$ and vice versa the Hartree profile is preferable for $\Lambda \geq 0$, i.e. roughly stating Hartree is best for accelerating flows and the quartic velocity profile is best for a decelerating flow. Hayashi finds that the Hartree profile is appropriate for $u_e = ct^\alpha$ with α being being close to 4. It should be mentioned that the Hartree profile is limited to the power-law family of velocity profiles.

Starting from the general polynomial form $\sum_{i=1}^{N} a_i p^i$ alternatives can be found using arbitrary sets for the boundary conditions. It was concluded by Libby et al [83] that increasing the order to 6 leads to an approximation which is comparable in accuracy to a two-parameter integral method of lower order.

3.1.3 Correlation Based Methods

The closure models by Drela, Mughal, Nishida, Matsushita, Head's and others rely on predetermined relations for the shape factors and integral variables.

For turbulent boundary layer flow these predetermined relations are based on empirical data and in all cases these relations are based on steady flow cases.

For laminar boundary layer flow however theoretical (semi-)similarity solutions are employed which assume certain types of velocity distributions like the power law distribution for the Falkner-Skan equation. These solutions are exact within the range of validity for boundary layer theory and provide a realistic foundation for the laminar closure relations. For example it was noted by Drela[35] that given a similar value for the shape factor H the Falkner-Skan profile should be similar to the actual boundary layer profile. Different (semi-)similarity solution families are employed in practice , for instance solution families by Falkner-Skan, Proudman and Johnson, and Williams. These three similarity solution families have specific ranges of applicability, namely accelerated flow, rear-stagnation flow and wake flow. A set of integral variable values by Tani[132] can be used to describe the boundary layer shape factors for retarded flow.This approach of problem specific similarity solutions allows for a dedicated approach for the case of

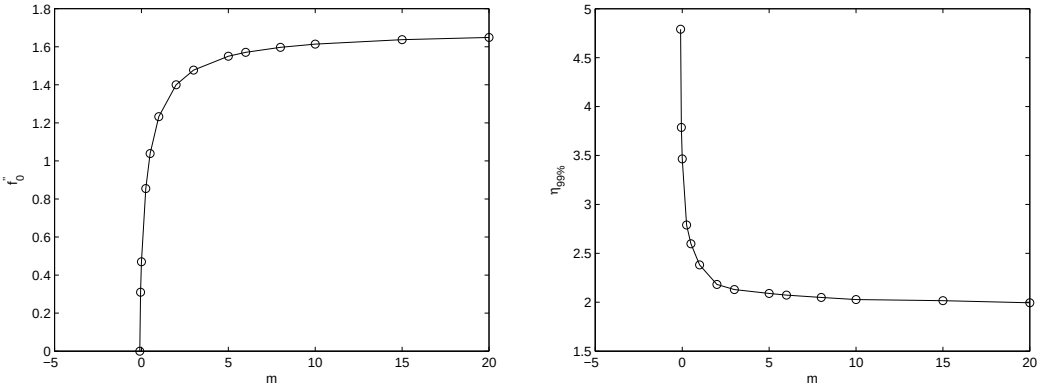

Figure 3.3: Falkner-Skan starting values for different powers,(left) $f_0^{''} - m$,(right) $\eta_{99\%} - m$.

wind turbine flow using either experimental or numerical results.

Now that the general method for laminar boundary layer have been discussed it is time to move on to turbulent boundary layers, or particularly, the transition from a laminar boundary layer to a turbulent boundary layer.

3.2 Laminar to Turbulent Transition

Already in 1921 Prandtl predicted that all types of laminar boundary layers become unstable at finite Reynolds numbers, this was confirmed by Tollmien in 1921. This instability signals the transition of a laminar flow into a turbulent boundary layer which requires a different solution approach. Empirically Cebeci and Smith[24] determined the following criterion for completed transition in a steady flow with an adaptation of Michel's method

$$\begin{aligned} Re_{\theta,tr} &\geq 1.174 \left(1 + \frac{22,400}{Re_{x,tr}}\right) Re_{x,tr}^{0.46}, \\ Re_\theta &= \frac{u_e \theta}{\nu}, \quad Re_x = \frac{u_e\, x}{\nu}, \end{aligned} \tag{3.5}$$

which is similar to

$$Re_{\theta,tr} \geq 2.9 Re_{x,tr}^{0.4} + 208 \exp\left(-\frac{Re_{x,tr}}{22400}\right),$$

where the left terms is Michel's original one-step method, the adaptation should avoid spurious transition soon after stagnation, see Michelsen[93]. Michel's one-step method is robust and relatively simple, therefore this method is applied amply in literature. Alternatively the two-step method by Granville (see equation (E.10), Cebeci and Cousteix[22]) can be used or alternatively for turbulent external flow due to Arnal et al (see equation (E.11), Cebeci and Cousteix[22]). The method due to Arnal is used by Coenen[26] with Coenen also using a relation for the critical Reynolds number to define a transition region (see equation (E.18)). Several other empirical relations for Re_{crit} exist, e.g. due to Drela[35], Drela and Giles[40], and Abu et al[47],[78] (see equations (E.21) - (E.24)). The stability of a steady flow can be related to integral characteristics and the flow Reynolds number, however for the unsteady boundary layers and the subsequent unsteady formulation of the IBL equations there is also the influence of time-history. This is expressed through temporal and spatial amplification of eigenmodes depending on the external velocity and pressure. This complex problem is encompassed in

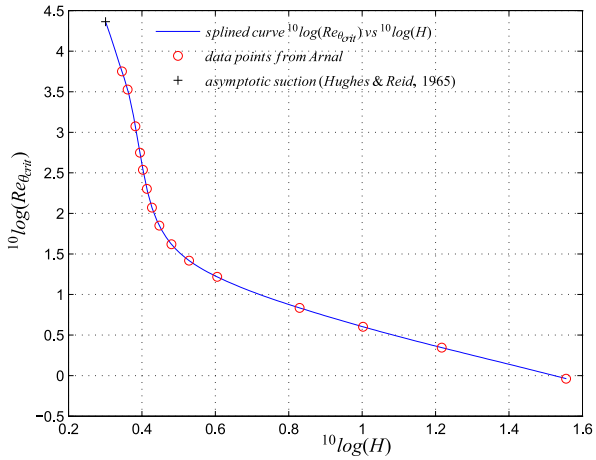

Figure 3.4: The critical Reynolds number Re_{crit} as a function of the shape factor H, see Bongers[14]

the Orr-Sommerfeld equation, which is a reduction of the NS-equations using the assumption that the velocity components can be defined as constant components which are perturbed by small-disturbances. These small disturbances are then described by some complex valued function, commonly known as Tollmien-Schlichting waves, subsequently further simplifications are possible, the result is

$$(u_e - c)(v'' - \alpha^2 v) - u_e'' + \frac{iv}{\alpha}(v'''' - 2\alpha^2 v'' + \alpha^4 v) = 0,$$

where c is the propagation speed of the waves and α is the wave number or frequency, see i.e White[154]. It is usually assumed that all disturbance frequencies within a certain range occur at any given time, the maximum amplitude is then determining for the stability.
For very high Reynolds numbers this results in the Rayleigh equation, see i.e. Schlichting[118]

$$(u_e - c)(v'' - \alpha^2 v) - u_e'' = 0.$$

The e^n envelope method first used by Smith[122] and Van Ingen[139] is based on linear stability theory of the Orr-Sommerfeld equation and uses either spatial or temporal amplification theory. Originally the method was known as the e^9-method where $n = 9$ is the highest exponent of a disturbance relative to the initial amplitude. Later the initial amplitude was replaced by an initial disturbance which introduced the need for a variable value for the highest exponent, this would be called the e^n method, see i.e. and Van Ingen(2008)[138] for an overview. Cebeci and Cousteix give a numerical procedure to solve the Orr-Sommerfeld equation and to estimate the onset of turbulent flow using the e^n method, see [22, ch.7]. The specific code by Cebeci and Cousteix is available and can be implemented in the code for the IBL equations with the notation that it requires a velocity profile in normal direction, this can be obtained from i.e. the Wieghardt or Pohlhausen velocity profiles as was discussed in section(3.1.2).
The e^n envelope method is also used in the popular program XFOIL, which is described in a paper by Drela[36]. The amplification envelopes can be found using an assumed solution, i.e. the Falkner-Skan solution as used by Drela[35]. This can be integrated in a future solver dependent on the computational load, independent of whether the field method or the integral method is used. In 2003 Drela formulated a solution procedure for a full e^n frequency method using a database to fetch the amplitude for a given set of input variables, the method described in this paper is supposedly more accurate for variable shape factors (non-similar flows), this method is used in the solver MSES (see Drela[39]). For the e^n envelope method a database was applied by Johansen and Sørensen[71]. Both the envelope method and the frequency method can be solved as

part of the solution.
Simpler is the $H - R_x$ envelope method by Wazzan et al[152]),the $H - R_x$ method gives a relation for the transitional local Reynolds number $Re_{x,tr}$ based only on the shapefactor H, see equation (E.20). The $H - R_x$ envelope method is limited to accelerated flows and slightly retarded flows. Cebeci[22] notes that the $H - R_x$ method gives reasonable results if there is local similarity in the boundary layer. It should be noted that the relation by Wazzan et al is based on more recent experimental data than the relations by Michel, Cebeci and Smith, and Granville and is preferable for accelerated flows ($u_e = x^m;\ m > \frac{1}{3}$). The Abu-Ghanam/Shaw transition criterion [1] is a so-called bypass method, here transition is induced by turbulence outside the boundary layer. [1]. Modified by Drela[38] this method was successfully applied to a Reynolds Averaged Navier-Stokes simulation of a multistage turbine (see Kraus[65]). Abu-Ghannam/Shaw modified by Drela is given by equation (E.14). The outer turbulence level is incorporated in the transition criterion through a variable critical amplification factor n as used in the e^n method. Different empirical formulas exist that relate the critical and transitional amplification factor to the outer turbulence level , e.g. due to Mack (equation (E.15)), Henkes and Van Ingen[14] (equation (E.16)), Anderson et al (equation (E.17)), also see figure (3.5) for the critical and transitional amplification factor from Henkes and Van Ingen.

Rotational effects are also of importance and most somehow be incorporated in the determination of the critical point and the transition point. Du[41] in reference to Johnston applies the following criterion for the critical displacement thickness

$$Re_{\delta,crit} > \frac{8.8}{\sqrt{Ro_\delta}}, \quad |Ro_\delta| \ll 1,$$

with the rotational parameter

$$Ro_\delta = \frac{2\Omega\delta}{u_e}.$$

If the flow is turbulent there is still the possibility that it becomes laminar, this is

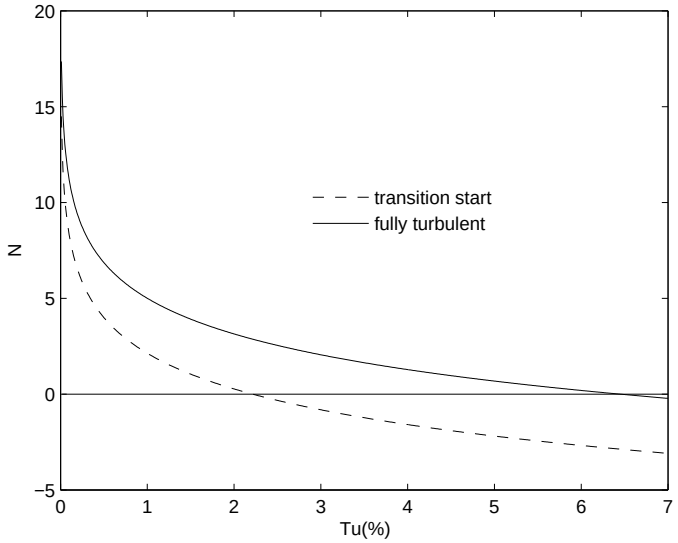

Figure 3.5: Values for the amplification factors in case of bypass turbulence

called relaminarisation (see i.e. Schlichting [118]). This phenomena may occur in

[1]Transition from laminar to turbulent boundary layer flow over rough surfaces and for turbulent outer flow is often referred to as bypass transition

strongly accelerated flow, in reference to Narasimha and Sreenivasan, Schlichting[118] and White[154] state the following criterium

$$\frac{\nu}{u_e^2}\frac{du_e}{dx} \geq K$$
$$\text{Schlichting:} \quad K = 3.5 \cdot 10^{-6},$$
$$\text{White:} \quad K = 3 \cdot 10^{-6}.$$

Besides relaminarisation it might occur that the amplification factor decreases, i.e. after reaching a critical Reynolds number, a favorable pressure gradient may reduce the amplifications of the disturbances.

Literature suggests that laminar boundary layer flow over profiles is quite normal for $Re \sim 100,000$, if only for the first $10\% - 30\%$ of the chord, provided that the outer flow is in fact laminar. However in case the outer flow is turbulent the critical Reynolds number at which the laminar boundary layer flow transitions into a turbulent boundary layer flow decreases with increasing turbulence level, exponentially at high Reynolds numbers ($Re > 500,000$)and linearly at lower Reynolds numbers (see Andersson, Berggren and Henningson[6]). According to the relations which based the transitional amplification factor on the bypass turbulence level it can be assumed that starting from a bypass turbulence of $Tu \approx 2.2\%$ the transition to turbulence starts immediately, also see figure (3.5). The average bypass turbulence for offshore windturbines is about 5% (see figure (3.6)), and thus, disregarding for instance frequency dependency, the boundary layer will start to develop to a turbulent boundary layer immediately.

Early measurement on the flat plate with zero incidence showed a critical Reynolds number of about $3.5\ 10^5 - 5.0\ 10^5$, which was presumably obtained from windtunnel results with a turbulence intensity of about 1%. Later the experiment was repeated by Dryden,Skramstad and Schubauer with a turbulence intensity 50 times lower than the earlier experiment which gave a critical Reynolds number of about $3.9\ 10^6$, more than 10 times(!) larger. This latter value was supposedly the asymptotic value so a lower turbulence level would not increase the critical Reynolds number, see Schlichting[118]. In a later experiment by Wells acoustic disturbances were also removed, this increased the transition point to $4.9\ 10^6$. The above is mentioned because it shows the sensitivity of laminar-to-turbulence transition, not only to the turbulence of the surrounding flow(bypass turbulence) but also to acoustic noise. With regard to the bypass turbulence the following should be noted; The turbulence level in the athmospheric boundary layer is between 5%(off shore) and 40% (see Sicot et al[121]), this means that the critical Reynolds number may be reduced to near zero (see Cowley[31] and Van Ingen[140]) which in turn would mean that a laminar boundary layer over a windturbine profile is rather unlikely.

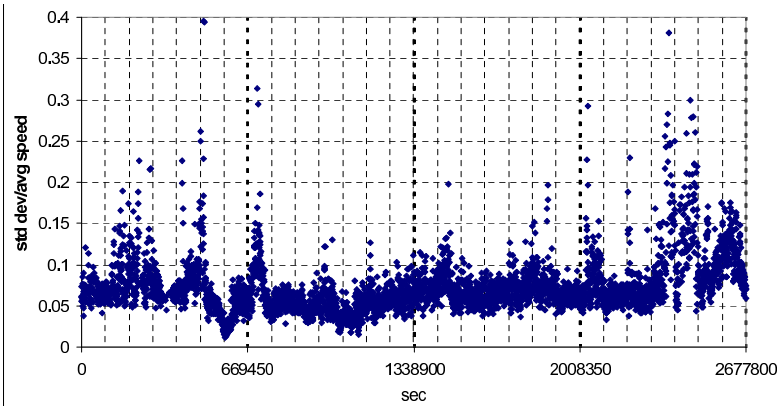

Figure 3.6: Turbulence intensity for off shore farm over long measurement period

Whether a given disturbance grows(unstable), remains constant (neutral) or decays(stable) depends on the frequency of the disturbance, the shape of the velocity profile, the Reynolds number, the amplitude of the disturbance and other more illusive factors like the receptivity of the flow. Therefore the turbulence intensity is not sufficient to determine the decrease in the critical Reynolds number due to turbulence in the outer flow. According to a recent study by Schepers and Van Ingen the turbulence frequency is much lower ($\mathcal{O}(1)\ Hz$) than the frequency at which the critical amplification factor occurs ($\mathcal{O}(3)\ Hz$), which prevents the possibility of interference. This suggests that the e^n amplification method can still be used with confidence to detect transition over wind turbine profiles, however more experimental data is needed to confirm the result.

Disregarding the effect of bypass turbulence on transition, in practice, a fully turbulent boundary layer is often assumed for the three dimensional flow over rotors, mainly because the computational logic for tracking the transition point is difficult to integrate in general flow solvers (see Bak et al[8]). Here it should be noted that for instance Nishida[103] and Milewski[94] use a so-called attachment line within a few steps of the stagnation point, with the additional note that supposedly the major part of the profile is insensitive to the boundary condition at the leading edge. On a side note, recently there has been much interest in applying active flow control through suction/blowing to reduce the friction drag over cars but also lifting surfaces, this increases the stability of the boundary layer and may even cause re-laminarisation. In case suction is applied the transition criterion can be determined with the method by Van Ingen(see Van Ingen[140] and Bongers[14]). A more recent method of controlling the boundary layer uses plasma induced velocity, here a body force is created through two electrodes and a dielectric material. This has the benefit of not inducing drag through bleeding suction air as would occur with suction methods. Beside boundary layer suction or plasma induced velocity, cooling also has a positive effect on the stability of the boundary layer flow(see Wazzan[152]).

Literature on turbulence transition over wind turbine blades is scarce, more research has to be performed to obtain dedicated closure models.

The approaches discussed above are based on steady boundary layer flows when it is clear that time-dependent fluctuations in the external velocity influence the transition requirements (see i.e. Schlichting[118]). The unsteady boundary layer transition including wake effects can be approximated using a method due to Chakka and Schobeiri[119] which uses eddy viscosity with a time-dependent intermittency factor. For three dimensional boundary layer flow, Menter and Langtry[92] provide a method using added differential equations involving the intermittency factor, this recent method is applied in the Ansys CFX solver. The intermittency factor is a measure in which the boundary layer can be considered turbulent, an intermittency factor of near 1 suggests the entire boundary layer is turbulent and a near zero factor indicates a fully laminar boundary layer. To determine what is actually turbulent inside the boundary layer some turbulence criterion has to be given. The transition Reynolds number and the critical Reynolds number form the upper and lower bound for the intermittency. This still necessitates the use of a separate transition model, i.e. Orr-Sommerfeld.

3.2.1 Intermittency Transition Model

In recent years there has been much (renewed) interest in the development of intermittency transport equations to describe the transition from laminar to turbulent. The methods are hinged upon other turbulence methods for the entire flow, i.e. $\kappa-\omega, \kappa-\epsilon, SST$. The transport of the intermittency γ is dependent on the distribution of κ,ϵ and/or ω and thus this can not be implemented as-is. A starting point for practical implementation is the technical report from the Risø institute by Bak [8], in this report the

wall intermittency function by Menter et al[92] is addressed and the missing constants[2] are retreived through wind tunnel experiments. More on turbulence intermittency can be found in Schobieri and Wright[119], Akhter and Ken-Ichi[3] and Elsner et al[78]. The intermittency equation is typically written as

$$\frac{\partial(\rho\gamma)}{\partial t} + \frac{\partial(\rho u_i \gamma)}{\partial x_i} = P_\gamma + \frac{\partial}{\partial x_i}\left[\left(\mu + \frac{\mu_t}{\sigma_\gamma}\right)\frac{\partial \gamma}{\partial x_i}\right],$$

where P_γ is a production term which may be dependent on quantities describing the turbulence of the flow, i.e. ω, k and ϵ. Although the intermittency models are probably more refined in describing the development of turbulence than the e^n amplification theory it is still dependent on empirical models to describe the point where turbulence development begins, i.e. the earlier mentioned Re_{crit}. A local value for the turbulence intensity may be obtained using the following expression given by Elsner et al[78] in reference to Mayle

$$Tu_{local} = 1.93 Tu \sqrt[5]{\frac{\theta}{L_t}}, \quad L_t = \frac{\sqrt{k}}{0.09\omega}.$$

Since the starting point for the intermittency transport function is signaled with conventional correlations for Re_{crit}, since the region where the intermittency is between zero and one is actually quite small and since the computational implementation of the transition does not seem to affect the solution of the turbulent boundary layer (see Drela[35]) it is considered unnecessary to introduce an intermittency transport model for the purpose of capturing the intermittency region. More important in the unsteady case is the transient behaviour of the intermittency region which is missing from the current transition criteria used for the (integral) boundary layer equations. A detailed discussion on this subject can be found in the references already provided above, also see Menter's PhD for a literature review on intermittency[80]. It is advised that the steady transition models are critically assessed for typical wind turbine flow situations and that perhaps a specific transition model is devised which incorporates the main characteristics of the unsteady outer flow. If indeed the transition prediction is inappropriate a transition point needs to be preset.

Once the turbulence boundary layer flow is established the laminar models should be replaced by turbulence models, this is discussed in the next section.

3.3 Turbulent Boundary Layer

With the onset of turbulence specific closure models for turbulent boundary layers need to be employed to ensure the solubility of the boundary layer equations.

It should be noted that most turbulence closure models for the IBL equations assume quasi-steady flow (see e.g. Zhang[160], Swafford[129]), probably due to a limited amount of experimental data (see e.g. Cebeci[22, §9.10]). The same holds for the field form of the boundary layer equations, although several unsteady turbulence models are in existence unsteady closure relations for near wall turbulence were difficult to find, one due to Cebeci is presented in appendix (K).

3.3.1 Velocity Profiles for Turbulent Boundary Layers

The simplest closure model for the integral equations is probably the power law distribution of the velocity which describes the entire boundary layer. The velocity distribution can be described simply by

$$u = u_e \eta^\beta,$$

[2] Menter et al give an almost complete description of their method but forfeit to give two constants due to proprietary reasons

where $\beta = \frac{1}{7}$ is commonly used for boundary layers (see i.e. Warsi[151], Mughal[99]), this was introduced by Prandtl in 1921. The $1/7^{th}$ power law method gives a simple analytical description of the entire boundary layer (see equation (E.25) for the integral variables), however it assumes the turbulent boundary layer can be described by a single profile. As with the closure models for the Reynolds stress it is assumed that the velocity profile has two distinct layers, see figure (3.7). In general the following expressions are

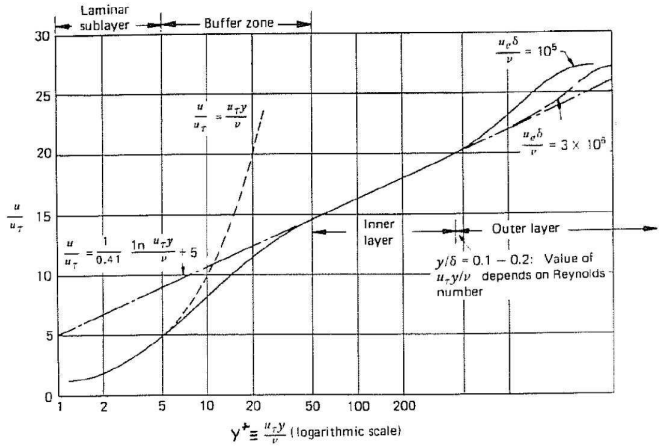

Figure 3.7: Sublayers in turbulent boundary layer,[24].

used (see i.e. Cebeci[22],White[154])

$$\text{Inner layer}: \begin{cases} \text{sublayer} & u^+ = y^+ & y^+ < 5 \\ \text{buffer layer} & u^+ = f_1(y^+) & 5 < y^+ < 50 \\ \text{fully turbulent wall region} & u^+ = \frac{1}{\kappa}\ln y^+ + c & 50\frac{\nu}{u_\tau} < y < 0.15\delta \end{cases},$$

$$\text{Outer layer}: \quad \frac{u_e - u}{u_\tau} = f_2\left(\frac{y}{\delta}\right),$$

where

$$y^+ = \frac{y u_\tau}{\nu}, \quad u_\tau = \sqrt{\frac{\tau_w}{\rho}}, \quad u^+ = \frac{u}{u_\tau}.$$

The separate relations for the inner layer were deduced to a single composite formula by Spalding (see equation (E.26), White[154]). Coles law of the wake is an extension of the log-law of the wall to the outer layer and is given by (see Cebeci and Cousteix[22])

$$u^+ = \frac{1}{\kappa}\ln y^+ + c + \frac{\Pi(x)}{\kappa} f\left(\frac{y}{\delta}\right), \tag{3.6}$$

where $\Pi(x) \approx 0.55$ for $Re_\theta > 5000$, c is set to 5.0 (see White[154]), further White proposes two curve fits, see equation (E.29). Granville proposed a simplification of Coles law (see equation (E.30)), which can be supplemented by a set of relations due to Thompson (see equation (E.31), Cebeci and Cousteix[22]). The parameter Π in equation (3.6) varies strongly with the so-called Rotta-Clauser parameter β (see i.e. White[154, fig:6-27]), which is defined as

$$\beta = \frac{\delta^*}{\tau_w}\frac{dp_e}{dx}.$$

White gives a function $\beta(\Pi)$ with which Π is given implicitly (see equation (E.32)) and an extra function $\beta(\Pi, \theta, H)$ (see equation (E.33)). Using the two relations for β the Rotta-Clauser parameter β, Π can be written as a function of θ and H. Now given θ and H there results an indication for the velocity profile of a turbulent BL, this might be used to complement an integral method which lacks information on the velocity profile as does for

instance the well known procedure by Drela (see sections (I.1.6),(4.2.1)). Near separation of the boundary layer flow the above discussed law of the wake becomes inappropriate as β and Π go to infinity and a specific curve fit was found, the so-called sin-squared wake law (see equation (E.34), e.g. White[154]). Whitfield(1979) devised a composite solution method for the inner and outer layer of the complete turbulent boundary layer using trigonometric formulas, Swafford extended the solution for separated boundary layers. The solution due to Swafford[129] and Whitfield[155] is described by equation (E.27). It is convenient to have one formulation for the complete profile of attached and separated boundary layers, although the above method is somewhat laborious it does not require a separate check for the separation, the above formulation is used by Mughal[99]. Turbulent velocity profiles which incorporate the cross flow angle are given by Cross[32] (see equation (E.28)).

A one-parameter integral method can not be constructed simply because there are at least two parameters for the turbulent velocity profiles, furthermore the different sub layers prevent a direct implementation. The one equation velocity profile by Swafford and Whitfield is very cumbersome and requires multiple steps therefore a multiple parameter integral method analogous to what is discussed in section (3.1.2) will not be considered.

In the following section two semi-empirical methods are discussed, namely the unsteady entrainment equation and the unsteady lag entrainment equation.

3.3.2 Unsteady Entrainment and Shear Stress Lag

Alternatively the so-called entrainment equation can be derived (see Head [63] and Green [57]). The entrainment equation was specifically created to involve the rate at which mass from the boundary layer is mixed with the irrotational external flow. The entrainment is given by

$$\frac{dQ}{dx} = \frac{1}{u_e}\frac{d\left(u_e\theta H_1\right)}{dx} = F(H_1), \tag{3.7}$$

where

$$\text{shape factor} \quad H_1 = \frac{\delta - \delta^*}{\theta},$$
$$\text{boundary mass flow} \quad Q = \int_0^\delta u dy.$$

The above differential equation is still generic, it holds for laminar and turbulent flow. Veldman[145] suggests to take $(H - H_1)_{min}$ as an estimate for the separation. Here F is some empirical function relating the boundary mass to the shape factor. Cebeci and Bradshaw produce several curve fits using Head's empirical data for F and H_1 for turbulent boundary layers (see equation (E.47), e.g. Cebeci and Cousteix [22]). Where the closure relation for H_1 is not appropriate for separating flows (see White[154]). Coenen[26] uses (in reference to Lock and Williams) a closure relation for separated flows which has a minimum value for H_1 at about $H = 2.85$, see equation (E.48). For severe trailing edge separation Coenen uses (in reference to Houwink) yet another closure relation for H_1 which has a minimum of about $H = 2.732$, see equation (E.49). Ferziger et al (see the report by Strickland[105]) rewrite the entrainment method using the shape parameter $\zeta = \frac{\delta^*}{\delta}$, according to White[154] the resulting method is in better agreement in case of adverse pressure gradient but is less satisfactory for favorable pressure gradients. The entrainment method can be rewritten to hold for unsteady flow, consider that the entrainment for boundary layer flow can be written as

$$F(H_1)_{steady} = \frac{\partial\delta}{\partial x} - \frac{v_e}{u_e},$$

if this is explained as the non-dimensional boundary layer growth velocity with respect to the normal velocity of the external flow then the following extension seems natural

$$F(H_1)_{unsteady} = \frac{\partial \delta}{\partial x} + \frac{1}{u_e}\frac{\partial \delta}{\partial t} - \frac{v_e}{u_e}.$$

Given the extra term the entrainment equation has to be rewritten

$$F(H_1)_{steady} + \frac{1}{u_e}\frac{\partial \delta}{\partial t} = \frac{1}{u_e}\frac{\partial \left(u_e \theta H_1\right)}{\partial x}, \tag{3.8}$$

$$F(H_1)_{steady} = \frac{1}{u_e}\frac{\partial \left(u_e \theta H_1\right)}{\partial x} - \frac{1}{u_e}\frac{\partial \left(\theta H_1 + \delta^*\right)}{\partial t}.. \tag{3.9}$$

Although this extension is intuitive formal proof is absent. This was applied by Cousteix[29] in a study on three dimensional turbulent boundary layers.

An extra equation may be formed by the shear stress lag equation due to Green et al[56]. The Green lag-entrainment method gives the following differential equation for the entrainment (see Cebeci and Cousteix[22])

$$\frac{dF}{dx} = \frac{F(F+0.02) + 0.2667 C_{f0}}{\theta(H - H_1)(F + 0.01)}\Pi \tag{3.10}$$

with

$$\Pi = 2.8\left[\sqrt{C_{\tau,eq}} - \sqrt{C_\tau}\right] + \left(\frac{\delta}{u_e}\frac{du_e}{dx}\right)_{eq} - \frac{\delta}{u_e}\frac{du_e}{dx},$$

with equation set (E.52) for the closure (also see Green[57] and Green et al[56]). Here the suffix eq stands for equilibrium boundary layer which is defined as a turbulent boundary layers for which the velocity and shear-stress profiles do not vary in shape with x, equal to similarity flows in laminar boundary layers they scale with some similarity variable. For the lag entrainment method specific relations for C_f and H_1 are used (see equation set (E.53), Green et al[56]). Drela[35] derived a different lag equation using the shear stress coefficient C_τ

$$C_\tau = \frac{1}{u_e^2}(-\overline{u'v'})_{max},$$

where $(-\overline{u'v'})_{max}$ is the maximum Reynolds stress. Drela defined the normal velocity gradient as

$$\frac{\partial u}{\partial \eta} = \frac{1}{L}\sqrt{(-\overline{u'v'})_{max}},$$

where L is the dissipation or mixing length. Substituting $\frac{\partial u}{\partial \eta}$ and C_τ in the Reynolds stress transport equation, neglecting normal convection and keeping only the terms with C_τ Drela finds

$$\frac{\delta}{C_\tau}\frac{\partial C_\tau}{\partial x} = K_c\left(\sqrt{C_{\tau,eq}} - \sqrt{C_\tau}\right), \tag{3.11}$$

which is closed using equation set (E.50). The original value for K_c is 5.6 but Drela reported better results using $K_c = 4.2$ (see Drela[35]). C_τ can be initialized with a formulation used by Nishida[103], see equation (E.51). Drela's assumption that the higher order terms of the lag entrainment equation can be neglected was supported by Bhanderi and Babinksy[10]. The derivation of Drela's altered lag entrainment equation assumed the steady Reynolds stress transport equation, in the unsteady case the lag entrainment equation can be written as (see Hall[58] in reference to Cebeci and Bradshaw)

$$\frac{\delta}{u_e^3 C_\tau U_{max,s}}\frac{\partial\left(u_e^2 C_\tau\right)}{\partial t} + \frac{\delta}{u_e^2 C_\tau}\frac{\partial\left(u_e^2 C_\tau\right)}{\partial x} = K_c\left(\sqrt{C_{\tau,eq}} - \sqrt{C_\tau}\right),$$

here $U_{s,max}$ is the equilibrium slip velocity (see figure (3.8)) at the point of maximum shear stress which is equivalent to the local slip velocity as given by Drela (see Hall[58]). Note that the unsteady variant of Green's lag entrainment equation contains the external

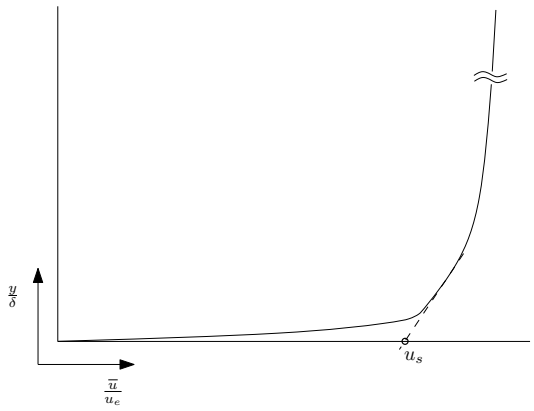

Figure 3.8: Impression of slip velocity

velocity u_e inside the differential terms, also changing the behavior of the lag equation in case of steady flow. Writing out the differential and rearranging, the unsteady lag entrainment equation becomes

$$\frac{\delta}{u_e C_\tau U_{max,s}} \frac{\partial C_\tau}{\partial t} + \frac{\delta}{C_\tau} \frac{\partial C_\tau}{\partial x} = K_c \left(\sqrt{C_{\tau,eq}} - \sqrt{C_\tau} \right) - \frac{2\delta}{u_e^2 U_{max,s}} \frac{\partial u_e}{\partial t} - 2\frac{\delta}{u_e} \frac{\partial u_e}{\partial x}. \quad (3.12)$$

The unsteady lag entrainment equation was written somewhat differently by Fenno et al[50]

$$\frac{\delta}{u_e C_\tau U_{max,s}} \frac{\partial C_\tau}{\partial t} + \frac{\delta}{C_\tau} \frac{\partial C_\tau}{\partial x} = K_c \left(\sqrt{C_{\tau,eq}} - \sqrt{C_\tau} \right) + \left(2\frac{\delta}{u_e} \frac{\partial u_e}{\partial x} \right)_{EQ} - 2\frac{\delta}{u_e} \frac{\partial u_e}{\partial x}, \quad (3.13)$$

where the measure for the diffusion namely $\left(2\frac{\delta}{u_e}\frac{\partial u_e}{\partial x}\right)_{EQ}$ is not ignored. Doing the same for the formulation used by Hall gives the third formulation

$$\frac{\delta}{u_e C_\tau U_{max,s}} \frac{\partial C_\tau}{\partial t} + \frac{\delta}{C_\tau} \frac{\partial C_\tau}{\partial x} = K_c \left(\sqrt{C_{\tau,eq}} - \sqrt{C_\tau} \right) + \left(2\frac{\delta}{u_e} \frac{\partial u_e}{\partial x} \right)_{EQ} - 2\frac{\delta}{u_e} \frac{\partial u_e}{\partial x} - \frac{2\delta}{u_e^2 U_{max,s}} \frac{\partial u_e}{\partial t}. \quad (3.14)$$

Once anyone of the models (3.12), (3.13) or (3.14) above is implemented implementation of the other models is trivial.

3.4 Skin friction coefficient

The skin friction coefficient is perhaps the most important parameter for aerodynamic body design and is therefore well described by empirical data. In this section some of the formulations to obtain the skin friction coefficients are presented. All of the following C_f formulations are for turbulent boundary layer flow unless otherwise noted. The most commonly used relation for the skin friction coefficient is due to Ludwieg and Tillman, which is based on empirical data on turbulent flow over a flat plate, see equation (E.35). According to White[154] the relation by Ludwieg and Tillman is within 10% of the empirical data. With equation (E.37) White[154] gives a correlation which is more accurate. White suggested an approximation for the skin friction coefficient for Karman-based integral methods with a pressure gradient in x-direction, see equation (E.36), White[154] states that this relation fits empirical data within 3%.

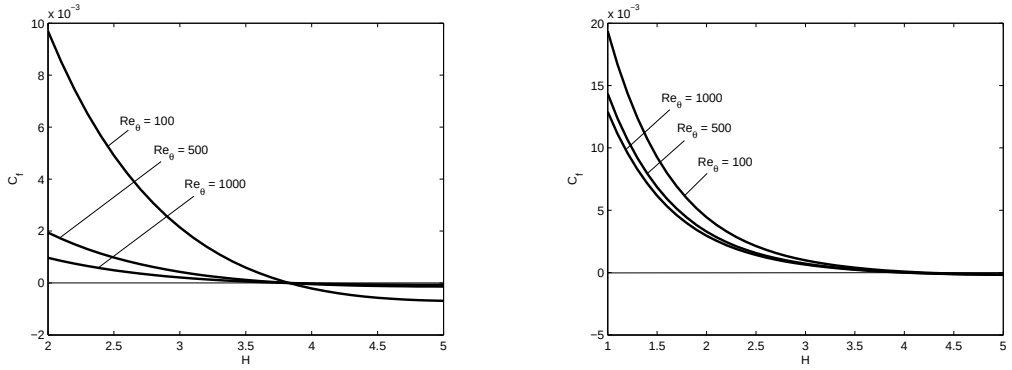

Figure 3.9: Closure relation for friction coefficient C_f, (left) for laminar boundary layer based on equation (E.9), (right) for turbulent boundary layer based on equation (E.41)

The downside of the relations mentioned above is they cannot be negative, as would occur in seperated/separating flows. Green, Ferziger et al, and Swafford provide closure relations which can be negative.
For Green[57] different empirical correlations were used, for both correlations the maximum Reynolds number for a reasonable curve fit is of order 10^5, which is too low for wind turbine applications (see equation (E.38).
Ferziger et al present a solution method for the IBL equations where the friction coefficient is dependent on the so-called blocked factor ζ which is defined as the ratio between the displacement thickness δ^* and the boundary layer thickness δ (i.e. $\zeta = \frac{\delta^*}{\delta}$) (see equation (E.39), White[154]).

This approximation is supposedly good for adverse pressure gradients but not for favorable pressure gradients (see White[154]). For the above method it is assumed that there is 'full' separation for $\zeta = \frac{1}{2}$, see section(3.6).
Lyrio et al (as referenced by Strickland and Graham[105]) give description for the unsteady laminar boundary layer flow based on the blockage factor ζ and the unsteady Thwaites parameter. The closure relations for the equation from Lyrio et al are based on unsteady wedge flow (i.e. an unsteady similarity solution).
Based on solutions of the Falkner-Skan equation, in reference to Drela-Giles to Sekar[120] gives a set of closure relation for the friction coefficient of a laminar boundary layer flow, see equation (E.9). A relation due to Swafford[129] is also able to approximate negative values for the skin friction coefficient. Swafford empirically extended the relation due to White (equation(E.36)) using data on separated flows, see equation (E.41). Swafford claims the relation is a good approximation for both attached and separated boundary layers.
Cousteix and Houdeville[30] used an expression based on Coles log law for an unsteady turbulent boundary layer flow over a flat plate, see (E.42).

Cross flow is incorporated in the formulation by Du and Selig[41] in reference to Lakshiminarayana and Govindan, see equation (E.40). Finally it must be noted that the friction coefficient for separated flow might be fixed to a very small negative number, in reference to Lock and Williams Coenen[26] uses $C_f = -0.00001$.

3.5 Dissipation Coefficient

The dissipation coefficient C_D is the rate at with which energy is dissipated at the wall due to a wall normal gradient in velocity. If either (semi-)similarity solutions or guessed velocity profiles are employed the dissipation coefficient may follow from the profile (see i.e. Matsushita[91], Mughal[99], Swafford[129]). It is also possible to resolve the dis-

sipation coefficient through empirical relations, some of these relations are presented below. Mughal[98] uses a formulation by Whitfield which is based on a numerical inte-

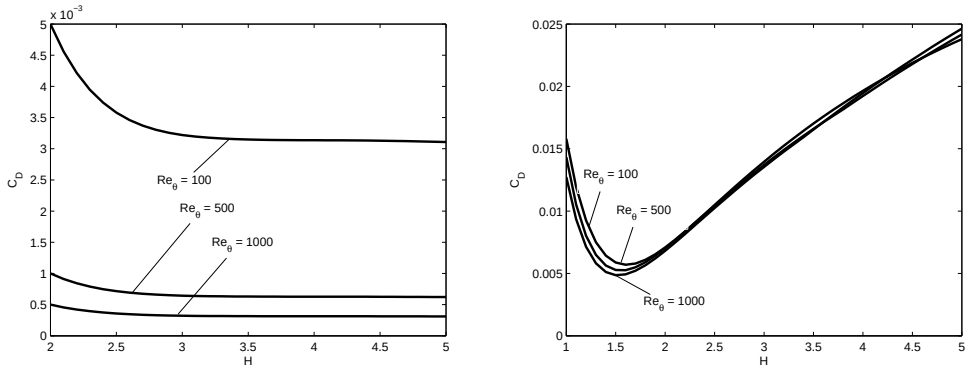

Figure 3.10: Closure relation for diffusion coefficient C_D, (left) for laminar boundary layer based on equation E.5, (right) for turbulent boundary layer based on equation (E.44)

gration of turbulent velocity profiles for the inner and outer layer, see equation (E.43). Drela[35] used a correlation for the laminar boundary layer, following from the Falkner-Skan profiles, see equations (E.5),(E.6). For the equilibrium turbulent boundary layer flow Drela uses equation (E.44) for the dissipation coefficient and equation (E.45) for the kinetic shape factor H^*. These closure relations follow directly from the relations given by Whitfield[155] and Swafford[129], see equation (E.27). Drela also gives an expression for C_D for a non-equilibrium turbulent boundary layer which requires the wall shear stress C_τ, and thus the lag entrainment equation comes into play, see equation (E.46). The third and last coefficient that will be considered is the C_K term in the third integral equation. If the third IBL equation is used C_K can be solved by writing out the integral using a guessed velocity profile or C_K has to be considered as a primary variable in the solution procedure, the latter means that the non-primary variables will have to be (cor)related with C_K which is only possible using either guessed velocity profiles, similarity solutions or numerical solutions of viscous models since this term is not as such empirically described in literature. Matsushita et al ([91], [90]) use several (semi)-similarity solutions for this purpose.

The next section deals with the occurrence of separation.

3.6 Separation Point

Following the flow over a body, pressure gradients may accelerate or decelerate the flow. Acceleration through negative(or favorable) pressure gradients enforces the flow direction of the boundary layer whilst deceleration through positive pressure gradients may cause the flow to reverse direction at some height above the body surface, this initial reversed flow causes an even larger positive pressure gradient cascading into a region of large circulation and low pressure, the flow now becomes detached from the surface, see figure (3.11), i.e. flow separation(which starts in the boundary layer) leads to detached flow. The seperation point is roughly the location where the boundary layer detachment starts, For steady flow it holds that there is a pressure minimum if seperation occurs, vice versa is not necessarily true (see Philip [110]). Also, the presence of $\frac{\partial u}{\partial y} = 0$, i.e. zero friction, in steady flow is usually the indicator that the flow solution will become singular, the so-called Goldstein singularity. This singularity is associated with flow separation because near this point of singularity the boundary layer thickness grows very rapidly and exactly at the point of separation $\frac{d\delta^*}{dx} \rightarrow \infty$, which is of course

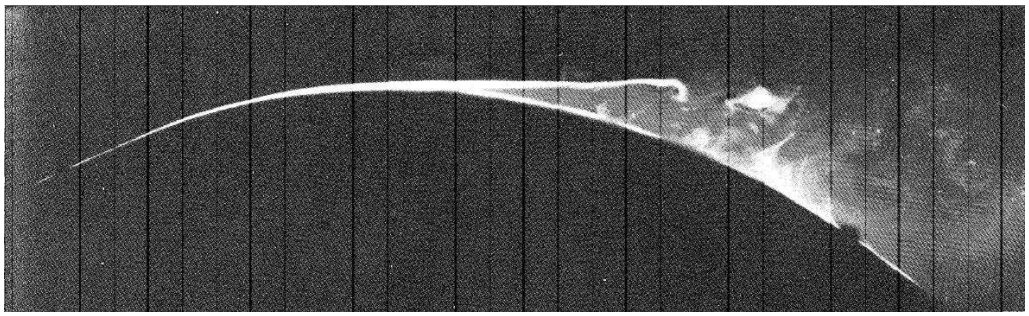

Figure 3.11: Laminar separation

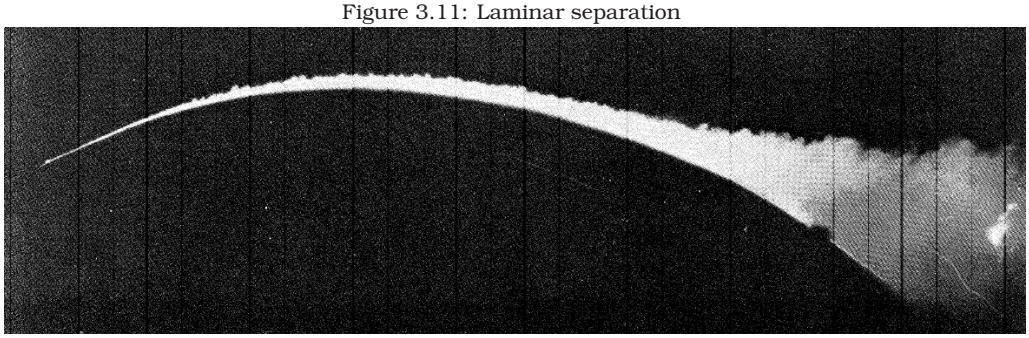

Figure 3.12: Turbulent separation

non-physical and it simply signals the break down of the method. Also used for steady flow is the criterium

$$\text{Thwaites parameter:} \quad \lambda = \frac{\theta^2}{\nu}\frac{du_e}{dx} < -0.09. \tag{3.15}$$

For unsteady flow this is not true except if conditions are locally steady (see Bradshaw[15]), seperation occurs if there is a discontinuity (see e.g. Schlichting[118]) e.g. $\frac{\partial \delta^*}{\partial x} \to \infty$, which is again a mathematical singularity. To recognize this singularity before it actually occurs, there is the so-called MRS-criterion due to Moore, Rott and Sears (see i.e. Schlichting[118]) which states there is separation if

$$u = u_s, \quad \frac{\partial u}{\partial y} = 0,$$

where u_s is the seperation velocity. The separation velocity u_s follows from the displacement of the point where it holds that $\frac{\partial u}{\partial y} = 0$, therefore the MRS criterion is difficult to control computationally, see i.e. Krainer[77]. The MRS-criterion will be used for both laminar and turbulent boundary layers although, admittedly, the added complexity of turbulence is ignored, see i.e. Smith [123]. Heuristically, the MRS criterion may be applied to the mean velocities in a turbulent boundary layer flow.

For methods which do not incorporate the velocity profile in the solution, as do most integral procedures, a different approach has to be used. For turbulent boundary layer flow Veldman suggests to take the minimum of $H - H_1$, which will have to be the first minimum in case of an arbitrary external velocity profile (see Veldman[145]). For unsteady laminar boundary layer flow without velocity profile information the criterion used for steady boundary layer flow, namely zero wall friction, may be used as a crude engineering approach.

If the system of equations is hyperbolic, discontinuities arise through the formation of shocks, which is used by Matsushita et al[91] to predict separation. Methods which do

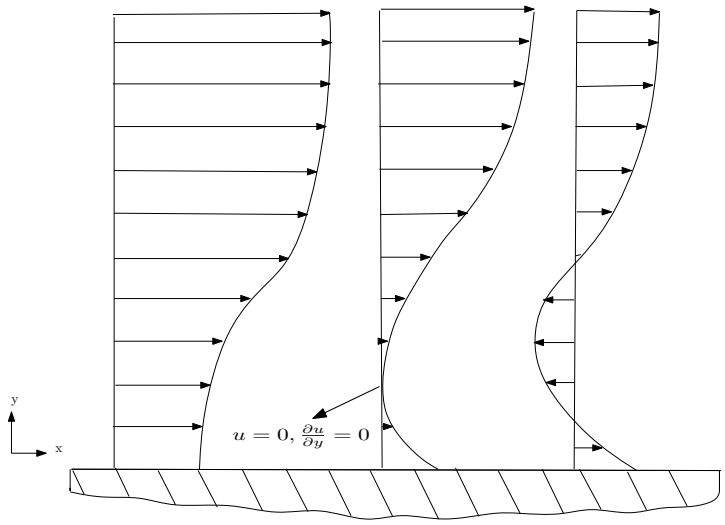

Figure 3.13: Boundary flow seperation according to the MRS-criterion

contain velocity profile information, like i.e. Hayasi[61], allow the monitoring of the zero friction point and thus have a direct way of predicting separation.

Another unsteady separation check was found in a report by Strickland and Graham[105], supposedly it is meant for the detection of intermittent separation, the criterion is directly based on the unsteadiness in the edge velocity,

$$H > \frac{2-\zeta}{1-\zeta}, \tag{3.16}$$

where ζ follows from equation(E.8). Bong-Jin[13] reports that the intermittent separation check actually performs much better to detect separation than the 'full' separation check.

Alternatively, if all else fails, one may resort to an ad hoc procedure, whereby a blow-up of integral variables is the indicator for a singularity, obviously this method requires the storage of at least two time steps. In fact, as can be read in section (4.2.4), a negative value for the momentum thickness signals a break down of the conventional integral methods which contain the shape factor H as a primary variable.

Once separation is detected, the solution procedure can be changed so that the strong interaction between the boundary layer and the outer flow is modelled correctly. This is treated in the next section but will not be included in the code development since it requires a direct integration of the external flow solver, relevant however is the way in which the proposed discretisation schemes lend themselves to applying the inverse method.

3.7 Solution Procedure for Mildly Separated Flow

As said, at flow seperation the IBL equations have to be coupled strongly to the inviscid solution to ensure solvability (see i.e. Cousteix [28], Cebeci et al[23]). The validity of the boundary layer equations is questionable for fully separated flow since the physical boundary layer ceases to exist. In practice it is found that the integral boundary layer equations *can* still be used to resolve the boundary layer for mildly separated flow. The term 'mildly' must be explained, it is suspected that is based on the requirement that the characteristic length scale of the separated bubble is similar to the boundary

layer thickness([142]), no formal definition is given in the referenced papers, although Coenen[26] makes a similar statement. The nearly separated boundary layer flow produces a discontinuity through $\frac{\partial \delta^*}{\partial x} \rightarrow \infty$, which is known as the Goldstein singularity. The singularity is not a physical phenomenon but rather a result of a recurring mismatch between the inviscid outer solution and the viscid inner solution.

Several methods exist to solve the coupled inviscid/viscid problem for separated flow, most notably the inverse, semi-inverse, simultaneous and quasi-simultaneous method (see figure (3.14)). The coupling methods are built around the concept that the external velocity and the displacement thickness are coupled in some way.

When a coupled method is applied to overcome the discontinuity, there may still be a large growth of the boundary layer which signals fully separated flow. It is unclear to what extent of separation the coupled method can be used and how the small scale separation should be discriminated from the large scale separation.

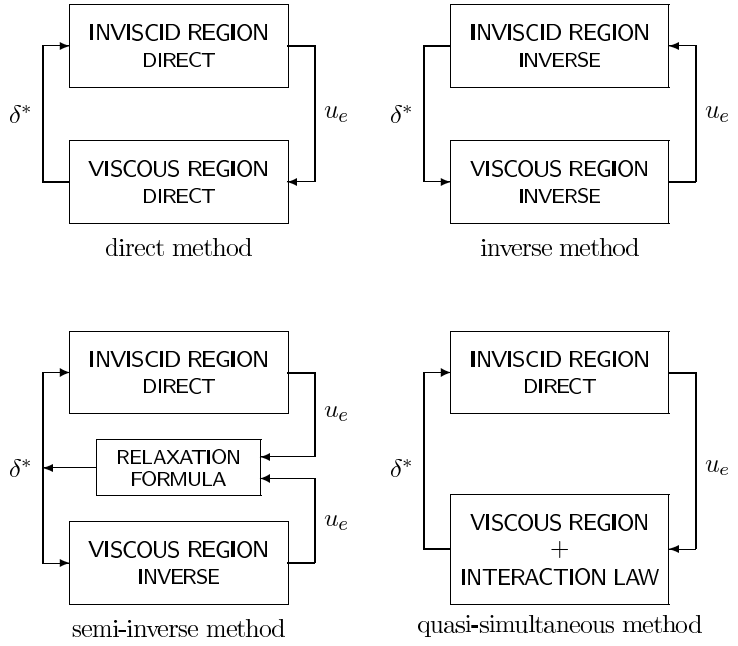

Figure 3.14: Coupling methods, see Veldman[145]

Direct Method

The direct method is the traditional coupling method wherein the velocity at the edge of the boundary layer is given by the inviscid solution. The inviscid velocity distribution forms the input for the IBL equations which produce a displacement thickness which is fed back into the inviscid formulation to give a new velocity distribution, etcetera , this process continues until the displacement thickness and the velocity are converged. Downside of this iteration process is that in case of separation there will be no convergence because one (or more) of the parameters/variables in the IBL equations becomes discontinuous. The direct method is used by e.g. Swafford[130]. The advantage is that it has a straightforward implementation, there are no added requirements except that there is an iteration process to find the converged solution. In general the direct method can only be used when there is weak interaction between the inviscid outer layer and the boundary layer, i.e. when there is a weak coupling between the two layers.

Inverse Method

Literally the inverse of the direct method since the IBL equations and the inviscid solver are treated in an inverse manner, the inverse inviscid solution gives the boundary layer thickness and the inverse IBL solution gives the velocity, again this is solved recursively until the solutions are converged. Downside is that the inverse form of the equations is much more elaborate than the normal form and an inverse form will not always exist.

The (semi-)inverse method will fail for attached flow (e.g. Sekar[120],Edward[44],Howlett[67]) and it is known to converge slowly (see i.e. Veldman[145]).

The (semi-)inverse method seems to perform well for unsteady boundary layer flow (Howlett[67],Zhang[160],Hall[58]).

Semi-inverse method

Here only the IBL equations are solved in inverse form, the resulting velocity is combined with the velocity that results from the inviscid solution to form the update of the displacement thickness through some relaxation parameter. Basically when the two velocities are equal there is convergence. This was applied by e.g. Howlett[67],Edwards[44] and Zhang[160].

Simultaneous

Here the system of IBL equations is directly coupled with the system of equations for the inviscid solution through for instance an adapted continuity equation which incorporates the boundary displacement (see Hall[58]) , a direct normal displacement of the streamline with the boundary thickness (see Drela[35]) or through the concept of wall transpiration (see Nishida[103],Milewski[94] or Mughal[99]).
The advantage of the simultaneous method is that there is no need for an interaction law. The simultaneous method has been applied successfully by for instance Drela[35] for the steady case which involved a coupled system of the steady IBL equations and the steady Euler equations in an iterative manner using a Newton-Rhapson procedure. Hall[58] applied simultaneous coupling successfully for the unsteady case. For the unsteady formulation no iterations are needed per time step, see Hall[58]. Downside is that extra assumptions have to be made to obtain the physical coupling of the boundary layer and the inviscid outer flow.

The (quasi-)simultaneous method may also be used directly for the attached flow, this may well be more robust than an initial attached flow formulation since any separation like phenomenon is then automatically incorporated in the solution and for the unsteady procedure there is no need for an iterative procedure if the fully simultaneous method is used

Quasi-simultaneous

The main idea of the quasi-simultaneous method is that instead of directly coupling the complete inviscid solution to the boundary layer solution some simple approximation for the inviscid solution is used. The difference between the approximation and the actual inviscid solution is handled iteratively. The quasi-simultaneous method has been applied first by Veldman and Houwink[146] and involved the asymptotic solution of the potential problem near the boundary layer. This solution could be described by a finite number of terms, the more terms the better the boundary layer would match the inviscid solution, but the more costly the matrix operations, it was shown that the number of off-diagonals can be reduced to zero, leaving only the diagonal terms, see Veldman[145] and Coenen[26]. Quasi-simultaneous coupling using only the diagonal of the external coefficient matrix leads to a simple and robust coupled method, this was successfully

applied by Coenen[26]. The diagonal simply functions as a relaxation factor for the iteration process. The iteration process does not require the inverse solution of the integral boundary layer equations and the added coupling term is very simple. The advantage is the great simplicity with which the coupling can be formulated, the downside is the large number of iterations needed for convergence (order 100).

The quasi-simultaneous and simultaneous methods should be more suitable to solve strongly coupled problems than the inverse and semi-inverse since the coupling is integral part of the solution procedure, the former methods are called strongly coupled schemes and the latter weakly coupled schemes, see Milewski[94] in reference to Lock and Williams. An approach could be to use the direct method for the attached region and one of the other coupling methods for the separated region, this has merit because of the simplicity of the direct method compared to the other coupling methods. The downside is the requirement that separation has to be monitored, however it is reasonable to assume that separation is also monitored for other purposes. This approach is a necessity if the (semi-)inverse method is applied. The (quasi-)simultaneous methods can be run for both attached and separated flows and thus warrants the option to apply the coupling methods for both the attached and the separated flow.

The methods above assume that the coupling is achieved through the displacement thickness δ^*, as is done in for instance MSES and MISES, another approach could be a coupling through the surface transpiration as is done in e.g. XFOIL and by Hall et al[58]. Using a transpiration velocity is beneficial compared to the displacement thickness in that no grid adaptation is required, the normal outflow boundary condition at the wall is simply adapted, see Jameson et al[69].

3.8 Conclusion

A wide variety of closure models and approximations have been discussed. This serves as the stepping stone to the implementation of several combinations of models to determine the models of choice for the present thesis, this will be done in part II. Once the global solution method has been chosen the numerical methods (FEM,FVM,FDM) are discussed in more detail and specific choices are made, such as the order of discretisation and the choice between implicit and explicit, grid type, stability etc.
Finally in part III the chosen selection(s) of models will be applied to several test cases using the FEM, FVM and FDM implementations.

Part II

Selection of Models and Application of Theory

Chapter 4

Description of Integral Boundary Layer methods

Given the IBL equations and the closure models the integral variables can be approximated numerically. Before the numerical procedures are discussed the previously discussed closure models are considered in actual solution procedures. Several combinations of closure relation have been used to solve for the integral boundary layer equations, some of these methods will be discussed in this section. Starting with the steady Von Kármán equation (2.21) the general solution procedure is discussed together with any implementation issues that may arise, the complexity is increased up to unsteady flow with turbulence and detachment, this incremental approach will help put the previous theory in context and it will serve as the rationale for using the final combination of IBL equations and closure models. The models that will be used are presented at the end of this chapter.

4.1 Steady Flows

The absence of time-dependency significantly simplifies the solution procedure and many writers have simply assumed their usage to be valid through quasi-steady boundary layer behavior. Even flutter cases have been approached by using the steady formulations for the boundary layer (e.g. Zhang[160] or Sekar[120]). In appendix (I.1) some of the steady IBL methods will be elaborated which will subsequently be tested using a Finite Difference Method (FDM) with a fourth order Runge-Kutta integration in space. The steady methods are written in Matlab, especially the methods using guessed velocity profiles rely heavily on the symbolic math toolbox which is not available in Fortran. The tested steady methods are

- Von Kármán equation with Pohlhausen guessed velocity profile,
- Von Kármán equation with higher order guessed velocity profiles,
- Von Kármán equation with Timman velocity profile,
- Von Kármán equation with Wieghardt velocity profile,
- Thwaites' integral method,
- Von Kármán equation, kinetic energy integral equation and Drela's closure relations.

These steady methods were applied to the following cases

- Von Kármán $u_e = x^m$ with several values for m, from retarded flow $m < 0$ to strongly accelerating flow $m > 1$,
- Von Kármán several velocity distributions with steady separation.

The most important result of those test cases involves the boundary condition, this is discussed in the next section, for more details above the steady test cases see appendix (I.2).

4.1.1 Results of Steady Test Cases

More boundary conditions for the guessed velocity profiles is not necessarily a recipe for a more accurate solution. The boundary conditions should not be concentrated on either the edge or the wall, and the order of the velocity profile polynomials is not unlimited due to oscillatory behavior. More advanced guessed velocity profiles such as the profiles due to Wieghardt and Timman do not have much merit over much simpler lower order polynomial guessed velocity profiles and are more difficult to implement.

The use of the boundary layer thickness δ should be done with caution as the value is very sensitive to the definition, i.e. δ will vary strongly if $\frac{u_\delta}{u_e}$ is changed slightly.

As for the boundary conditions the following recommendations are made;

- as a generic initialisation for the laminar boundary layer it is recommended to use Thwaites integral (equation (I.22)),
- for stagnation flow it is recommended to use the values by Nishida (equation (I.27)), Milewsi (equation (I.28)) for laminar flow and Coenen (equation (I.29)) for turbulent flow,
- for non-stagnation flow it is recommened to use flat plate solution e.g. the Blasius solution for laminar flow (equation (I.20)), $1/7^{th}$ power law profile for turbulent flow (equation (E.25)).

Grid refinement is recommended near the stagnation point to suppress influence of the initial wiggle and to improve the initial value obtained with Thwaites' integral.

4.2 Unsteady Flows

Both the method due to Drela and the method using Head's entrainment equation have H and θ as primary variables. If $\delta^* = \theta H$ is used for the unsteady Von Kármán equation together with the steady closure relations an extension to unsteady boundary layers is straightforward for Head's method since no new unknown is added. For Drela's method the energy integral needs to be rewritten to obtain the time dependent shape factor H^*. The system of ordinary differential equations for the steady case is now replaced by one or two partial differential equations which can be solved numerically.
The unsteady formulation due to Hayasi is based on a similar shape factor formulation as the method due to Drela, however Hayasi used a guessed polynomial velocity profile to close the system.
If the guessed velocity profiles using polynomials are extended to the unsteady case two IBL equations are needed to solve for the primary variables C_f and δ, see appendix D. Alternatively if C_f is closed directly through one of the empirical models discussed earlier the primary variables are θ and δ or H and δ.
Finally the method due to Matsushita will be considered, Matsushita uses two and three IBL equations in combination with closure relations via similarity or semi-similarity solutions. Matsushita produces a system of equations which is hyperbolic in nature.
It must be said that using an unsteady model for the turbulent boundary layer might

not be a significant improvement over using a steady model since as already mentioned Howlett[67] and Zhang[160] successfully applied a steady turbulent approach to a coupled unsteady boundary layer problem. Cousteix and Houdeville did extensive research on turbulent BL's over oscillating flat plates and found that the time-mean flow is not affected by a forced oscillation of the external flow, however they also state that even at low reduced frequencies the response of the boundary layer is not quasi-steady and that unsteady effects are present near the wall. They state that a quasi-steady closure relation for the skin friction can be used for reduced frequencies $\frac{\omega x}{u_e}$ lower than 5. Different from the steady methods the unsteady methods will be programmed in Fortran.

4.2.1 Unsteady Von Kármán Equation, Kinetic Energy Integral and Unsteady Lag Entrainment Equation

Starting from the unsteady Von Kármán equation and energy integral equation

$$\begin{aligned} \frac{1}{2}C_f &= \frac{1}{u_e^2}\left(u_e H\frac{\partial\theta}{\partial t} + u_e\theta\frac{\partial H}{\partial t} + \theta H\frac{\partial u_e}{\partial t}\right) + \frac{\partial\theta}{\partial x} + \frac{\theta}{u_e}(2+H)\frac{\partial u_e}{\partial x}, \\ C_D &= \frac{1}{u_e}\frac{\partial\theta}{\partial t} + \frac{1}{u_e}\frac{\partial\delta^*}{\partial t} + 2\frac{\theta}{u_e^2}\frac{\partial u_e}{\partial t} + \frac{3\delta^k}{u_e}\frac{\partial u_e}{\partial x} + \frac{\partial\delta^k}{\partial x}, \end{aligned} \tag{4.1}$$

now dividing the unsteady Von Kármán equation and the energy integral equation by the momentum thickness θ and the energy thickness δ^k respectively and subsequently subtracting the resulting momentum integral from the resulting energy integral equation results in

$$\begin{aligned} \frac{C_D}{H^*\theta} - \frac{1}{2}\frac{C_f}{\theta} = (1-H)\frac{1}{u_e}\frac{\partial u_e}{\partial x} + \frac{1}{H^*}\frac{\partial H^*}{\partial x} + 2\frac{1}{H^* u_e^2}\frac{\partial u_e}{\partial t} \\ - \frac{H}{u_e\theta}\frac{\partial\theta}{\partial t} - \frac{1}{u_e}\frac{\partial H}{\partial t} - \frac{H}{u_e^2}\frac{\partial u_e}{\partial t} + \frac{1}{u_e H^*\theta}\frac{\partial\theta}{\partial t} + \frac{1}{u_e H^*\theta}\left(H\frac{\partial\theta}{\partial t} + \theta\frac{\partial H}{\partial t}\right). \end{aligned} \tag{4.2}$$

where

$$\frac{1}{H^*}\frac{\partial H^*}{\partial x} = \frac{1}{\delta^k}\frac{\partial\delta^k}{\partial x} - \frac{1}{\theta}\frac{\partial\theta}{\partial x}, \quad H^*\theta = \delta^k, \quad H\theta = \delta^*.$$

For the steady case this results in a differential equation with only the shape factors as primary variables, for the unsteady case this is obviously not the case. Making use of the closure relations for H^*, the energy integral equation can be written as

$$C_D = \frac{1}{u_e}(1+H)\frac{\partial\theta}{\partial t} + \frac{\theta}{u_e}\frac{\partial H}{\partial t} + H^*\frac{\partial\theta}{\partial x} + \theta\frac{\partial H^*}{\partial H}\frac{\partial H}{\partial x} + 2\frac{\theta}{u_e^2}\frac{\partial u_e}{\partial t} + 3\frac{H^*\theta}{u_e}\frac{\partial u_e}{\partial x}. \tag{4.3}$$

Equation (4.2) or (4.3) together with the unsteady Von Kármán equation form a system of partial differential equations.

$$\begin{aligned} F_t + KF_x &= L, \\ K &= A^{-1}B, \\ L &= A^{-1}C. \end{aligned}$$

Using (4.2) the coefficient matrices are as follows

$$F = \begin{pmatrix} \theta \\ H \end{pmatrix},$$

$$A = \begin{pmatrix} \frac{H}{u_e} & \frac{\theta}{u_e} \\ \frac{1}{u_e H^* \theta} - \frac{H}{u_e \theta} + \frac{H}{u_e \theta H^*} & \frac{1}{u_e H^*} - \frac{1}{u_e} \end{pmatrix},$$

$$B = \begin{pmatrix} 1 & 0 \\ 0 & \frac{1}{H^*}\frac{dH^*}{dH} \end{pmatrix},$$

$$C = \begin{pmatrix} -\frac{\theta}{u_e}(2+H)\frac{\partial u_e}{\partial x} + \frac{1}{2}C_f - \frac{\theta H}{u_e^2}\frac{\partial u_e}{\partial t} \\ \frac{C_D}{H^*\theta} - \frac{1}{2}\frac{C_f}{\theta} + \frac{H}{u_e^2}\frac{\partial u_e}{\partial t} - \frac{2}{u_e^2 H^*}\frac{\partial u_e}{\partial t} - (1-H)\frac{1}{u_e}\frac{\partial u_e}{\partial x} \end{pmatrix},$$

where K and L are found as

$$K = \begin{pmatrix} (-1+H^*)\,u_e & u_e\theta\frac{dH^*}{dH} \\ -(-1+H\,H^*-H)\,\frac{u_e}{\theta} & -H u_e \frac{dH^*}{dH} \end{pmatrix},$$

$$\begin{aligned} L(1) = {} & \left(-1+H^*\right) u_e \left(-\frac{\theta}{u_e}(2+H)\frac{\partial u_e}{\partial x} + \frac{1}{2}C_f - \theta\frac{H}{u_e^2}\frac{\partial u_e}{\partial t}\right) \\ & + u_e H^* \theta \left(\frac{C_d}{H^*\theta} - \frac{1}{2}\frac{C_f}{\theta} + \frac{H}{u_e^2}\frac{\partial u_e}{\partial t} - \frac{2}{u_e^2 H^*}\frac{\partial u_e}{\partial t} - \frac{1-H}{u_e}\frac{\partial u_e}{\partial x}\right), \\ L(2) = {} & \left(-1+HH^*-H\right)\frac{u_e}{\theta}\left(-\frac{\theta}{u_e}(2+H)\frac{\partial u_e}{\partial x} + \frac{1}{2}C_f - \theta\frac{H}{u_e^2}\frac{\partial u_e}{\partial t}\right) \\ & - u_e H^* H \left(\frac{C_d}{H^*\theta} - \frac{1}{2}\frac{C_f}{\theta} + \frac{H}{u_e^2}\frac{\partial u_e}{\partial t} - \frac{2}{u_e^2 H^*}\frac{\partial u_e}{\partial t} - \frac{1-H}{u_e}\frac{\partial u_e}{\partial x}\right). \end{aligned}$$

Using the closure relation from Drela for the laminar boundary layer gives for $\frac{1}{H^*}\frac{dH^*}{dH}$

$$\frac{1}{H^*}\frac{dH^*}{dH} = \frac{1}{1.515 + \alpha\frac{(H-4)^2}{H}}\left[\alpha 2\frac{H-4}{H} - \alpha\frac{(H-4)^2}{H^2}\right],$$

$$\alpha = \begin{cases} 0.076, H < 4, \\ 0.040, H > 4. \end{cases}$$

The eigenvalues and eigenvectors are found as

$$\lambda_\pm = u_e\left[-\frac{1}{2}H\frac{\partial H^*}{\partial H} - \frac{1}{2} + \frac{1}{2}H^* \pm \frac{1}{2}\sqrt{G}\right],$$

$$\xi_\pm = \begin{pmatrix} 1 \\ \frac{1}{u_e\frac{\partial H^*}{\partial H}\theta}\left[\left(-\frac{1}{2}\frac{\partial H^*}{\partial H}H - \frac{1}{2} - \frac{1}{2}H^* \pm \frac{1}{2}\sqrt{G}\right)u_e + u_e\right] \end{pmatrix},$$

where the root term G is given by

$$G = H^2\left(\frac{\partial H^*}{\partial H}\right)^2 + 2H\frac{\partial H^*}{\partial H} - 2HH^*\frac{\partial H^*}{\partial H} + 1 - 2H^* + {H^*}^2 + 4\frac{\partial H^*}{\partial H}.$$

The eigenvalue is dependent on H,H^* and $\frac{dH^*}{dH}$, this reduces to H using the laminar closure relations for H^* and given the fact that $\frac{dH^*}{dH}$ is directly dependent on H. Using the turbulent closure relations from Drela this would result in H and θ. For the laminar closure G is unconditionally positive, the eigenvalues are plotted using the laminar closure relations by Drela and an external velocity u_e of $100[\frac{m}{s}]$, see figure 4.1. The smallest eigenvalue is smaller than zero for $H > 4$, this corresponds to $C_f = 0$ with the given closure relations (see Drela[35], also see Cousteix and Houdeville[29]).

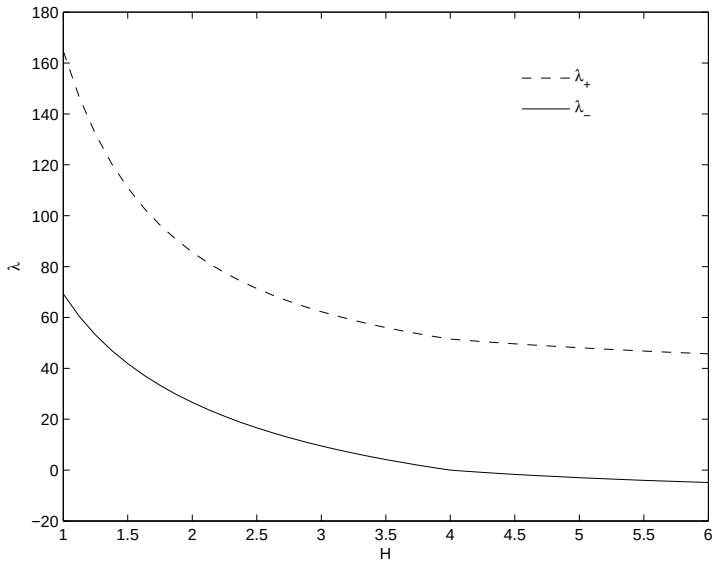

Figure 4.1: eigenvalues for Drela's system, with laminar closure using $u_e = 100$

Hyperbolicity

The hyperbolicity of the system of equations (2.27) is determined by considering the coefficient matrix $K = A^{-1}B$, the system is hyperbolic if (see Wesseling[153])

$$(nB - \lambda A)F = 0 \Rightarrow |K - \lambda| = 0,$$

leads to a full set of linearly independent eigenvectors with real valued eigenvalues. Indeed it is found that there is full set of distinct and real eigenvalues for the coefficient matrix K, this helps to determine the numerical approximation method, see chapter (5).

As was said Drela also formulated closure relations for turbulent boundary layers, in fact, Drela formulated two different turbulent closure relations for the dissipation coefficient. One assumes an equilibrium turbulent BL and the other forfeits this assumption and requires the lag entrainment equation to close the system. The equilibrium turbulent boundary layer closure relations require an adaptation of the coefficient matrix B since it contains the derivative $\frac{1}{H^*}\frac{\partial H^*}{\partial H}$. Writing out $\frac{1}{H^*}\frac{\partial H^*}{\partial H}$

$$\frac{1}{H^*}\frac{\partial H^*}{\partial H} = \begin{cases} \dfrac{\left(0.165-\frac{1.6}{\sqrt{Re_\theta}}\right)\left[1.6\frac{(H_0-H)^{0.6}}{H}-\frac{(H_0-H)^{1.6}}{H^2}\right]}{1.505+\frac{4}{Re_\theta}+\left(0.165-\frac{1.6}{\sqrt{Re_\theta}}\right)\frac{(H_0-H)^{1.6}}{H}}, & H < H_0, \\ \dfrac{2(H-H_0)\left(\frac{0.04}{H}+0.007\frac{\ln(Re_\theta)}{\left(H-H_0+\frac{4}{\ln(Re_\theta)}\right)^2}\right)+(H-H_0)^2\left(-\frac{0.04}{H^2}-0.014\frac{\ln(Re_\theta)}{\left(H-H_0+\frac{4}{\ln(Re_\theta)}\right)^3}\right)}{(H-H_0)^2\left(\frac{0.04}{H}+0.007\frac{\ln(Re_\theta)}{\left(H-H_0+\frac{4}{\ln(Re_\theta)}\right)^2}\right)}, & H > H_0. \end{cases},$$

where

$$H_0 = 3 + \frac{400}{Re_\theta}.$$

If the system is closed using the non-equilibrium closure relations and the lag entrainment equation the coefficient matrices give a singular matrix for K since $A^{-1}B$ contains a zero division. The steady lag entrainment equation is uncoupled from the system and

can thus be taken out of the system to be solved in parallel. However since the steady lag entrainment equation is in principle not suitable for the unsteady problem, an unsteady lag entrainment equation is used, see equation (3.12). Using the unsteady lag entrainment equation the coefficient matrices become

$$F = \begin{pmatrix} \theta \\ H \\ C_\tau \end{pmatrix},$$

$$A = \begin{pmatrix} \frac{H}{u_e} & \frac{\theta}{u_e} & 0 \\ \frac{1}{u_e H^* \theta} - \frac{H}{u_e \theta} + \frac{H}{u_e \theta H^*} & \frac{1}{u_e H^*} - \frac{1}{u_e} & 0 \\ 0 & 0 & \frac{1}{u_e u_s} \end{pmatrix},$$

$$B = \begin{pmatrix} 1 & 0 & 0 \\ 0 & \frac{1}{H^*}\frac{\partial H^*}{\partial H} & 0 \\ 0 & 0 & 1 \end{pmatrix},$$

$$C = \begin{pmatrix} -\frac{\theta}{u_e}(2+H)\frac{\partial u_e}{\partial x} + \frac{1}{2}C_f - \frac{\theta H}{u_e^2}\frac{\partial u_e}{\partial t} \\ \frac{C_D}{H^*\theta} - \frac{1}{2}\frac{C_f}{\theta} + \frac{H}{u_e^2}\frac{\partial u_e}{\partial t} - \frac{2}{u_e^2 H^*}\frac{\partial u_e}{\partial t} - (1-H)\frac{1}{u_e}\frac{\partial u_e}{\partial x} \\ \frac{K_c C_\tau}{\delta}\left(\sqrt{C_{\tau_{eq}}} - \sqrt{C_\tau}\right) - 2\frac{C_\tau}{u_e^2 u_s}\frac{\partial u_e}{\partial t} - 2\frac{C_\tau}{u_e}\frac{\partial u_e}{\partial x} \end{pmatrix},$$

where an extra eigenvalue and eigenvector is produced compared to the equilibrium turbulent closure, namely

$$\lambda_3 = u_s\, u_e, \quad \xi_3 = \begin{pmatrix} 0 \\ 0 \\ 1 \end{pmatrix}.$$

The coefficient matrix K and the coefficient vector L are expanded with

$$K(3,3) = u_s\, u_e,$$
$$L(3) = u_s u_e \left[\frac{K_c C_\tau}{\delta}\left(\sqrt{C_{\tau,eq}} - \sqrt{C_\tau}\right) - 2\frac{C_\tau}{u_e^2 u_s}\frac{\partial u_e}{\partial t} - 2\frac{C_\tau}{u_e}\frac{\partial u_e}{\partial x}\right].$$

The non-conservative system is now given by

$$F_t + KF_x = L, \quad F = \begin{pmatrix} \theta \\ H \\ C_\tau \end{pmatrix},$$

$$K = \begin{pmatrix} (-1+H^*)\,u_e & u_e\theta\frac{dH^*}{dH} & 0 \\ -(-1+H\,H^*-H)\frac{u_e}{\theta} & -Hu_e\frac{dH^*}{dH} & 0 \\ 0 & 0 & u_s u_e \end{pmatrix},$$

$$L(1) = \frac{\theta}{u_e}\frac{\partial u_e}{\partial t}(H-1) + \theta\frac{\partial u_e}{\partial x}\left(H - 3H^* + 2\right) - \frac{u_e}{2}C_f + u_e C_D, \tag{4.4}$$

$$L(2) = \frac{H}{u_e}\frac{\partial u_e}{\partial t}\left(2 - 2HH^* + H\right) + H\frac{\partial u_e}{\partial x}\left(-2HH^* - H^* + H + 3 + \frac{2}{H}\right)$$
$$+ \frac{1}{2}C_f\left(-\frac{u_e}{\theta} + 2\frac{u_e}{\theta}HH^* - H\frac{u_e}{\theta}\right) - \frac{u_e H}{\theta}C_D$$

$$L(3) = u_s u_e \left[\frac{K_c C_\tau}{\delta}\left(\sqrt{C_{\tau,eq}} - \sqrt{C_\tau}\right) - 2\frac{C_\tau}{u_e^2 u_s}\frac{\partial u_e}{\partial t} - 2\frac{C_\tau}{u_e}\frac{\partial u_e}{\partial x}\right].$$

The eigenvalues are plotted in figures (4.2), (4.3) and (4.4), u_e was again set at $100\ [\frac{m}{s}]$ and the kinematic viscosity ν was set at $2\cdot 10^{-4}\ [\frac{kg}{ms}]$, finally the Reynolds number Re_θ is taken as $[100, 5000]$, for $Re_\theta < 100$ the eigenvalues show erratic behavior[1]. It can be seen

[1] From the Falkner-Skan solutions it seems Re_θ is normally well above 100 within 10% of the plate length

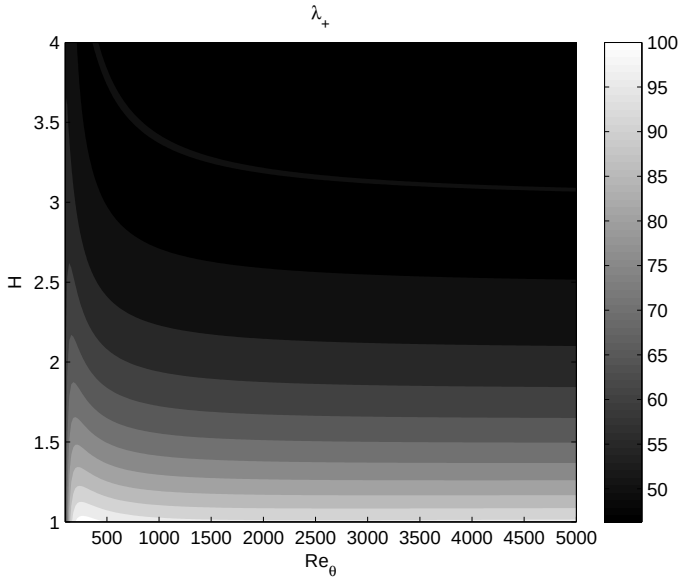

Figure 4.2: Contourplot of eigenvalue λ_+

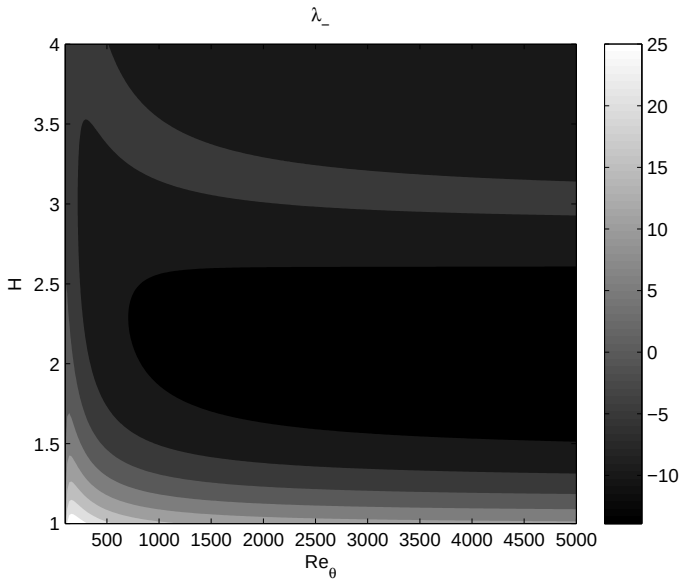

Figure 4.3: Contourplot of eigenvalue λ_-

that λ_- becomes negative for relatively low values of the shape factor H, for decreasing values of the shape factor, λ_- stays positive for increasing values of Re_θ, until it becomes invariably positive at $H \approx 1.3$. The third eigenvalue λ_3 becomes negative for $H > 4$ which means that the slip velocity becomes negative. It must be said that in the original paper by Green et al[56] it is questioned whether the validity of the lag entrainment closure holds for $H > 2.5$, this is related to the range of data considered to relate H_1 and H.

The steady lag entrainment equation is also suitable for turbulent wakes (see Green, Weeks and Brooman[56]) and mild separation (see Drela[35]). For suitability in predicting wake flow, the friction coefficient is set to zero and it is assumed that the dissipation

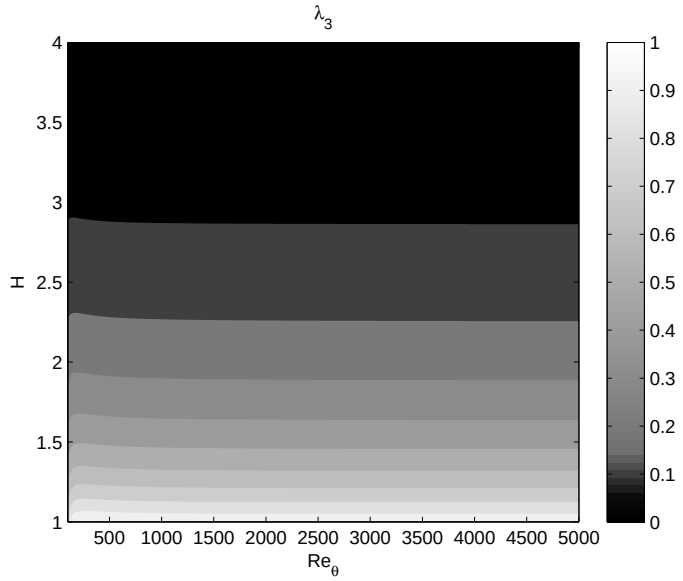

Figure 4.4: Contourplot of eigenvalue λ_3

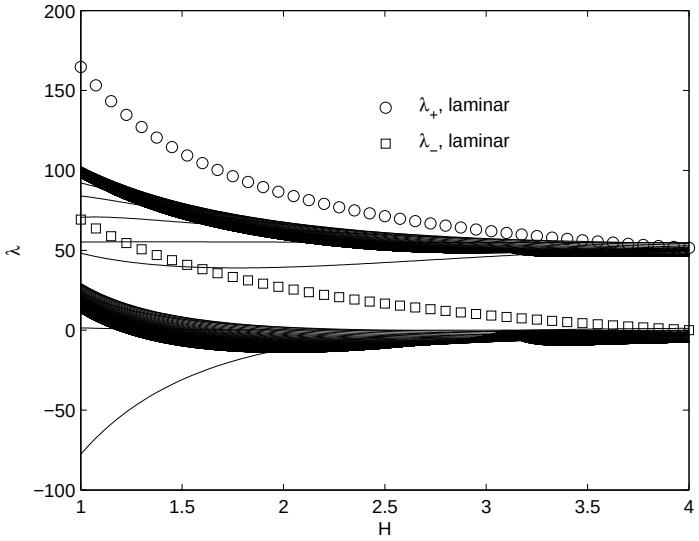

Figure 4.5: Comparison of eigenvalues for laminar and turbulent boundary layer flow, the solid lines represent the turbulent eigenvalues for different values of Re_θ

length scale is doubled (see Green[57]). The latter assumption is based on the presumption that the wake consists of two symmetric parts, one from the upper boundary layer and one from the lower BL. In case the boundary layer thicknesses of the upper and lower boundary layer flows are vastly different this assumption breaks down. The constant K_c in the lag entrainment equation is affected by this change of the dissipation length scale and it is adviced that the best value is determined on a case by case basis. Given some laminar to turbulent transition criterium the entire boundary layer is described including the wake since, following Drela, a laminar wake is unlikely to survive very long since it will be very sensitive to disturbances. More importantly, the transition

point will most likely occur far ahead of the trailing edge, and in fact it is not uncommon to assume a fully turbulent boundary layer as has been mentioned earlier (see i.e. Vermeer et al[147]).
The next methods to be discussed use the entrainment equation and the lag entrainment equation and form a dedicated method for turbulent boundary layers.

4.2.2 Unsteady Entrainment Method

Using the formulation for the steady Head's entrainment method using the closure from Cebeci and Bradshaw in combination with the unsteady Von Kármán equation results in

$$\begin{aligned}
\frac{1}{2}C_f &= \frac{1}{u_e^2}\left(u_e H\frac{\partial\theta}{\partial t} + u_e\theta\frac{\partial H}{\partial t} + \theta H\frac{\partial u_e}{\partial t}\right) + \frac{\partial\theta}{\partial x} + \frac{\theta}{u_e}(2+H)\frac{\partial u_e}{\partial x},\\
\frac{\partial H}{\partial x} &= \frac{1}{\frac{dH_1}{dH}\theta}\left[0.0306\,(H_1-3)^{-0.6169} - H_1\frac{\partial\theta}{\partial x} - \frac{\theta H_1}{u_e}\frac{\partial u_e}{\partial x}\right],\\
H_1 &= \begin{cases} 0.8234(H-1.1)^{-1.287}+3.3, & H<1.6,\\ 1.5501(H-0.6778)^{-3.064}+3.3, & H\geq 1.6.\end{cases}
\end{aligned}$$

The above system of ordinary differential equations cannot be solved numerically. It requires the first two timesteps to be known since the time derivatives do not follow directly from the other derivatives, a direct result from the fact that the entrainment equation is steady. It is not possible to solve directly even if two timesteps are initialised since the individual time derivatives cannot be solved for using the solution values after the initialisation. So Head's method may seem easily extended to unsteady flow, the entrainment equation itself has not been altered which leads to an unsuitable problem formulation. Adding the time-dependent version of the Head's equation will produce a solvable system as will be explained later. Mughal and Nishida use the shear stress lag equation due to Drela, this however requires the use of the energy integral equation. In case the three equation approach due to Matsushita et al is used this method has the advantage that the only change is the replacement of moment-of-moment equation by the simplified shear stress lag equation. It must be noted that the steady lag entrainment equation has been used successfully for the application of an viscid-inviscid solver to unsteady boundary layer flow with separation, see i.e. Zhang and Liu[160] or Howlett[67] and more importantly the unsteady lag entrainment equation has been successfully applied by Hall et al [58].

Applying the unsteady variant of Head's method the entrainment equation is written as

$$\frac{1}{u_e}\frac{\partial\left(u_e\theta H_1\right)}{\partial x} - \frac{1}{u_e}\frac{\partial\left(\theta H_1+\delta^*\right)}{\partial t} = 0.0306\,(H_1-3)^{-0.6169},$$

isolating the differential terms for H and t gives

$$-\frac{\theta}{u_e}(1+\frac{dH_1}{dH})\frac{\partial H}{\partial t} - \frac{H+H_1}{u_e}\frac{\partial\theta}{\partial t} + H_1\frac{\partial\theta}{\partial x} + \theta\frac{dH_1}{dH}\frac{\partial H}{\partial x} = 0.0306\,(H_1-3)^{-0.6169} - \frac{H_1\theta}{u_e}\frac{\partial u_e}{\partial x},$$

with the same relations for H_1 and $\frac{dH_1}{dH}$ as in the steady case. Care must be taken here since the original closure is based on steady turbulent flow. The system of equations is now formed by the unsteady Von Kármán equation and the unsteady entrainment equation

$$\begin{aligned}
F_t + KF_x &= L,\\
K &= A^{-1}B,\\
L &= A^{-1}C,
\end{aligned}$$

with

$$F = \begin{pmatrix} \theta \\ H \end{pmatrix}, A = \begin{pmatrix} \frac{H}{u_e} & \frac{\theta}{u_e} \\ -\frac{H+H_1}{\theta} & -\frac{\theta}{u_e}(1+\frac{dH_1}{dH}) \end{pmatrix}, B = \begin{pmatrix} 1 & 0 \\ H_1 & \theta\frac{dH_1}{dH} \end{pmatrix},$$
$$C = \begin{pmatrix} -\frac{\theta H}{u_e^2}\frac{\partial u_e}{\partial t} - \theta\frac{2+H}{u_e}\frac{\partial u_e}{\partial x} + \frac{1}{2}C_f \\ 0.0306\,(H_1-3)^{-0.6169} - \frac{H_1\theta}{u_e}\frac{\partial u_e}{\partial x} \end{pmatrix}.$$

The procedure is started using initial values for H and θ, these follow from the preceding laminar boundary layer flow solution.
The matrices K and L are found as

$$K = \frac{1}{-\theta H - \theta H\frac{dH_1}{dH} + u_e H + u_e H_1}\begin{pmatrix} -\theta u_e(1+\frac{dH_1}{dH}+\frac{dH_1}{dH}) & -\theta^2\frac{dH_1}{dH}u_e \\ \frac{u_e}{\theta}\left(u_e H + H H_1\theta + u_e H_1\right) & H\theta\frac{dH_1}{dH}u_e \end{pmatrix},$$
$$L(1) = \frac{\theta u_e(1+\frac{dH_1}{dH})}{H\theta + H\theta\frac{dH_1}{dH} - u_e H - u_e H_1}\left(-\frac{\theta H}{u_e^2} - \frac{\theta(2+H)}{u_e}\frac{du_e}{dx} + \frac{1}{2}C_f\right)$$
$$+ \frac{\theta u_e\left(0.0306(H1-3)^{0.6169} - H_1\theta/u_e\frac{du_e}{dx}\right)}{H\theta + H\theta\frac{dH_1}{dH} - u_e H - u_e H_1},$$
$$L(2) = -\frac{(H+H_1)u_e^2}{\theta\left(H\theta + H\theta\frac{dH_1}{dH} - u_e H - u_e H_1\right)}\left(-\frac{\theta H}{u_e^2} - \frac{\theta(2+H)}{u_e}\frac{du_e}{dx} + \frac{1}{2}C_f\right)$$
$$- \frac{H u_e\left(0.0306(H1-3)^{0.6169} - H_1\theta/u_e\frac{du_e}{dx}\right)}{H\theta + H\theta\frac{dH_1}{dH} - u_e H - u_e H_1}.$$

With the eigenvalues and eigenvectors given by

$$\lambda_\pm = -u_e\frac{H\theta\frac{dH_1}{dH} - \theta - \theta\frac{dH_1}{dH} - H_1\theta \pm \sqrt{G}}{2\left(H\theta + H\theta\frac{dH_1}{dH} - u_e H - u_e H_1\right)},$$
$$\xi_\pm = \begin{pmatrix} 1 \\ \frac{1}{2\theta^2\frac{dH_1}{dH}u_e}\left[-\frac{A}{B}u_e H\theta - \frac{A}{B}u_e H\theta\frac{dH_1}{dH} + \frac{A}{B}u_e^2 H + \frac{A}{B}u_e^2 H_1 - u_e\theta - u_e\theta\frac{dH_1}{dH} - u_e H_1\theta\right] \end{pmatrix},$$

with

$$G = H^2\theta^2\frac{dH_1}{dH}^2 + 2H\theta^2\frac{dH_1}{dH} + 2H\theta^2\frac{dH_1}{dH}^2 - 2H\theta^2\frac{dH_1}{dH}H_1 + \theta^2 + 2\theta^2\frac{dH_1}{dH} +$$
$$2H_1\theta^2 + \theta^2\frac{dH_1}{dH}^2 + 2\theta^2\frac{dH_1}{dH}H_1 + H_1^2\theta^2 - 4H\theta\frac{dH_1}{dH}ue - 4\theta\frac{dH_1}{dH}ueH_1,$$

$$A = H\theta\frac{dH_1}{dH} - \theta - \theta\frac{dH_1}{dH} - H_1\theta \pm \sqrt{G},$$
$$B = H\theta + H\theta\frac{dH_1}{dH} - u_e H - u_e H_1.$$

Cousteix and Houdeville[29] found that the system with the unsteady entrainment equation leads to a set of distinct and real eigenvalues and eigenvectors for the coefficient matrix K. Cousteix and Houdeville used a simplified relationship for H_1

$$H_1 = \frac{0.631H^2 + H}{H-1}.$$

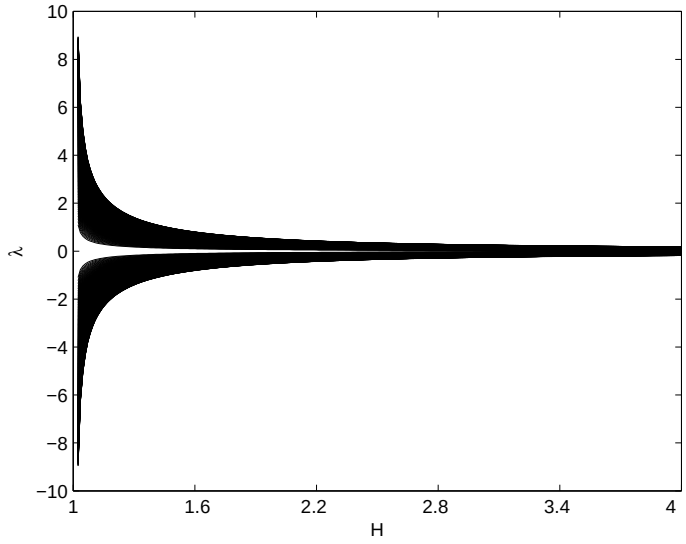

Figure 4.6: Eigenvalues for unsteady Head's entrainment and the Von Kármán equation with Drela's closure for H_1 for several values of Re_θ

Next the unsteady lag entrainment equation is considered. The unsteady lag entrainment equation is used together with the momentum integral equation and the unsteady entrainment equation

$$\frac{1}{2}C_f = \frac{1}{u_e^2}\left(u_e H\frac{\partial\theta}{\partial t} + u_e\theta\frac{\partial H}{\partial t} + \theta H\frac{\partial u_e}{\partial t}\right) + \frac{\partial\theta}{\partial x} + \frac{\theta}{u_e}(2+H)\frac{\partial u_e}{\partial x},$$

$$0.0306\,(H_1-3)^{-0.6169} = -\frac{\theta}{u_e}(1+\frac{dH_1}{dH})\frac{\partial H}{\partial t} - \frac{H+H_1}{u_e}\frac{\partial\theta}{\partial t} + H_1\frac{\partial\theta}{\partial x} + \theta\frac{dH_1}{dH}\frac{\partial H}{\partial x} + \frac{H_1\theta}{u_e}\frac{\partial u_e}{\partial x},$$

$$K_c\left(\sqrt{C_{\tau,eq}} - \sqrt{C_\tau}\right) = 2\frac{\delta}{u_e}\left(\frac{1}{u_e U_{max,s}}\frac{\partial u_e}{\partial t} + \frac{\partial u_e}{\partial x}\right) + \frac{\delta}{u_e C_\tau U_{max,s}}\frac{\partial C_\tau}{\partial t} + \frac{\delta}{C_\tau}\frac{\partial C_\tau}{\partial x} - \left(2\frac{\delta}{u_e}\frac{\partial u_e}{\partial x}\right)_{EQ},$$

where C_f,$C_{\tau,eq}$ and H_1 are closed using the turbulent closure relations suggested by Drela in his PhD thesis[35], also see sections (2) and (4.2.1). The boundary layer thickness δ is then closed using the definition for H_1

$$\delta = (H_1 + H)\,\theta,$$

the measure for diffusion is given by

$$\left(2\frac{\delta}{u_e}\frac{\partial u_e}{\partial x}\right)_{EQ} = 2\,(H_1+H)\left[\frac{C_f}{2} - \left(\frac{H-1}{\alpha H}\right)^2\right]\frac{1}{H\beta},$$

Green,Weeks and Brooman[56]: $\alpha = 6.432, \quad \beta = 0.8,$

and without the entrainment factor

$$\left(2\frac{\delta}{u_e}\frac{\partial u_e}{\partial x}\right)_{EQ} = 2\left[\frac{C_f}{2} - \left(\frac{H-1}{\alpha H}\right)^2\right]\frac{1}{\beta},$$

Drela[35]: $\alpha = 6.7, \quad \beta = 0.75.$

Note that the diffusion term does not incorporate the time-derivative. From the paper by Green et al[56] it can be seen that this equivalent diffusion term is based on the

advection term $u_e \frac{\partial u_e}{\partial x}$. In the unsteady case this would become $\frac{\partial u_e}{\partial t} + u_e \frac{\partial u_e}{\partial x}$ which gives for the equivalent diffusion term

$$\left(2\frac{\delta}{u_e} \left[\frac{1}{u_e} \frac{\partial u_e}{\partial t} + \frac{\partial u_e}{\partial x} \right] \right)_{EQ}.$$

The unsteady lag entrainment equation is implemented in the same manner as described in section (4.2.1). Again an extra eigenvalue and eigenvector is produced compared to the equilibrium turbulent closure, namely

$$\lambda_3 = u_s \, u_e, \quad \xi_3 = \begin{pmatrix} 0 \\ 0 \\ 1 \end{pmatrix}.$$

For the laminar case the shear lag is identically zero and the unsteady laminar method described in section 4.2.1 can be used. Use Green's equations for the turbulent wake flow with zero wall friction C_f, also see Yoshihara[148], Green[57]. Green suggests to use a different definition for the entrainment coefficient in the wake, namely

$$F_{wake} = \beta \, 0.435(H-1)^{0.907} + (1-\beta) 0.0306 \, (H_1 - 3)^{-0.6169},$$

where

$$\beta = 1 - \exp \frac{x_{te} - x}{5\delta_{te}}.$$

The unsteady variants of Head's entrainment method and Green's shear stress lag equation employ empirical relations based on steady flow, or more specifically steady external flow. As has been mentioned earlier, for unsteady turbulent boundary layer flows there are few empirical models and for the integral boundary layer none was found. This suggests that the validity is limited to gradually changing boundary layer flows. Howlett[67] however found that Green's steady lag entrainment equations coupled to a transonic small disturbance potential equation give a good approximation of the viscous effects of an oscillating aileron up to as far 20 Hz at high subsonic velocity ($\kappa = 0.137$). Hall[58] had good results using the lag entrainment equation for a pitching motion around the mean chord with a reduced frequency of $\kappa = 0.85$, where the amplitude is 2°. Using $\kappa = \frac{\omega c}{u_\infty}$ for the reduced frequency and a chord of one meter the frequency is $\omega = \kappa u_\infty$.

4.2.3 Unsteady Integral Method by Hayasi using Guessed Velocity Profiles

Hayasi devised a one-parameter integral method which uses a guessed velocity profile to close the integral equations. The strength of this approach comes from the fact that it is relatively general in nature given a suitable velocity profile, the main limitations are the relative complexity of the formulation of the integral variables and the dependency on δ.

The solution procedure suggested by Hayasi is as follows; first (shape) factors are introduced

$$H = \frac{\delta^*}{\theta}, H^* = \frac{\delta^k}{\theta}, \tag{4.5}$$

$$P = 2\frac{\theta}{u_e} \left. \frac{\partial u}{\partial y} \right|_{y=0}, Q = 4\frac{\delta^k}{u_e^2} \int_0^\delta \left(\frac{\partial u}{\partial y} \right)^2 dy, Z = \frac{\theta^2}{\nu}. \tag{4.6}$$

Following Schuh, a one parameter (to be called γ) velocity profile is assumed, all the shape factors are now a function of this shape factor. In Schuh's original method the Von Kármán equation is rewritten to

$$H\frac{\partial Z}{\partial t} + u_e \frac{\partial Z}{\partial x} + 2\left[\frac{H}{u_e}\frac{\partial u_e}{\partial t} + (2+H)\frac{\partial u_e}{\partial x} + \frac{\partial H}{\partial t} \right] Z = P,$$

and the energy equation

$$(H+1)\frac{\partial Z}{\partial t}+UH^*\frac{\partial Z}{\partial x}+2\left[\frac{2}{u_e}\frac{\partial u_e}{\partial t}+3H^*\frac{\partial u_e}{\partial x}+\frac{\partial H}{\partial t}+u_e\frac{\partial H^*}{\partial x}\right]Z=\frac{Q}{H^*}.$$

Since the shape factors are definite functions of the profile parameter γ, Z can be written as a function of γ. Using either the momentum integral equation or the energy integral equation γ can be retrieved by applying the following expression for Λ

$$\Lambda=Z\left(\frac{\partial u_e}{\partial x}+\frac{1}{u_e}\frac{\partial u_e}{\partial t}\right)=-\frac{\nu Z}{u_e}\left(\frac{\partial^2 u}{\partial y^2}\right)_{y=0}$$

Once γ is known, the shape factors and integral variables follow from the velocity profile. Hayasi transformed the momentum and energy integral equations directly using the fact that $Z=f(\gamma)$ and for the flat plate of the present case $R=\frac{1}{r}\frac{\partial r}{\partial x}\approx 0$,

$$\begin{aligned}H\frac{\partial Z}{\partial t}+u_e\frac{\partial Z}{\partial x}+2Z\frac{dH}{d\gamma}\frac{\partial \gamma}{\partial t}&=P-2\left[\frac{H}{u_e}\frac{\partial u_e}{\partial t}+(2+H)\frac{\partial u_e}{\partial x}\right]Z,\\ (H+1)\frac{\partial Z}{\partial t}+u_eH^*\frac{\partial Z}{\partial x}+2Z\frac{dH}{d\gamma}\frac{\partial \gamma}{\partial t}+2u_eZ\frac{dH^*}{d\gamma}\frac{\partial \gamma}{\partial x}&=\frac{Q}{H^*}-2\left[\frac{2}{u_e}\frac{\partial u_e}{\partial t}+3H^*\frac{\partial u_e}{\partial x}\right]Z.\end{aligned}\tag{4.7}$$

Given a chosen velocity profile the above system of ordinary differential equations can be solved to obtain Z and γ. Before Hayasi can be applied h, h^*, p and Q must be described by a single parameter velocity profile where γ is the parameter, one profile supposedly suitable for retarded flows is due to Tani (see i.e. Hayasi [61], Tani [132]), restating Tani's profile

$$\frac{u}{u_e}=f=\left(6-8\eta+3\eta^2\right)\eta^2+\gamma\eta(1-\eta)^3.\tag{4.8}$$

Tani's profile adheres to the following boundary conditions

$$f(0)=0,\quad f(1)=1,\quad \frac{\partial f}{\partial \eta}=\frac{\partial^2 f}{\partial \eta^2}=0,$$

which means that the velocity profile is independent from the instantaneous velocity distribution at the edge. Alternatives to Tani's profile can be easily found and compared using symbolic mathematical tools, one simply assumes an n^{th} degree polynomial with $n-1$ boundary conditions, the profile parameter is then equal to the floating coefficient. Continuing with Tani's profile the shape factors and integral variables can be written as a function of γ explicitly (also see Tani[132])

$$\begin{aligned}\delta^*&=-\frac{1}{20}\delta\gamma+\frac{2}{5}\delta,\\ \theta&=-\frac{1}{252}\delta\gamma^2+\frac{1}{105}\delta\gamma+\frac{4}{35}\delta,\\ \delta^k&=-\frac{1}{2860}\delta\gamma^3-\frac{23}{5460}\delta\gamma^2+\frac{73}{5005}\delta\gamma+\frac{876}{5005}\delta,\\ H&=63\frac{-8+\gamma}{-12\gamma-144+5\gamma^2},\\ H^*&=\frac{3}{143}\frac{-876\gamma-10512+21\gamma^3+253\gamma^2}{-12\gamma-144+5\gamma^2},\\ P&=2\frac{\theta}{\delta}\gamma,\\ Q&=-\frac{3}{25025}ue\gamma^5-\frac{9}{7007}ue\gamma^4+\frac{376}{75075}ue\gamma^3+\frac{5296}{175175}ue\gamma^2+\frac{168192}{175175}ue.\end{aligned}\tag{4.9}$$

Given Z and γ the boundary layer thickness can be found with the relation for the momentum thickness θ

$$\delta=\frac{\sqrt{\frac{Z}{\nu}}}{-\frac{1}{252}\gamma^2+\frac{1}{105}\gamma+\frac{4}{35}}.$$

Hayasi did not construct a solution method for the general formulation stated above, instead he simplified the differential equations for specific test problems. The general system of non-linear partial differential equations can be written as

$$\begin{aligned} F_t + KF_x &= LF, \\ K &= A^{-1}B, \\ L &= A^{-1}C. \end{aligned} \tag{4.10}$$

with

$$F = \begin{pmatrix} Z \\ \gamma \end{pmatrix},$$

$$A = \begin{pmatrix} H & 2Z\frac{dH}{d\gamma} \\ H+1 & 2Z\frac{dH}{d\gamma} \end{pmatrix},$$

$$B = \begin{pmatrix} u_e & 0 \\ u_e H^* & 2u_e Z\frac{dH^*}{d\gamma} \end{pmatrix},$$

$$C = \begin{pmatrix} -2\left[\frac{H}{u_e}\frac{\partial u_e}{\partial t} + (2+H)\frac{\partial u_e}{\partial x}\right] & \frac{P}{\gamma} \\ -2\left[\frac{2}{u_e}\frac{\partial u_e}{\partial t} + 3H^*\frac{\partial u_e}{\partial x}\right] & \frac{Q}{\gamma H^*} \end{pmatrix}.$$

K and L are found as

$$K = \begin{pmatrix} -u_e + u_e H^* & 2u_e Z\frac{\partial H^*}{\partial \gamma} \\ \frac{1}{2}\frac{H+1}{Z\frac{\partial H}{\partial \gamma}}u_e - \frac{1}{2}\frac{H}{Z\frac{\partial H}{\partial \gamma}}u_e H^* & -\frac{H}{\frac{\partial H}{\partial \gamma}}u_e\frac{\partial H^*}{\partial \gamma} \end{pmatrix},$$

$$L = \begin{pmatrix} 2\frac{H}{u_e}\frac{\partial u_e}{\partial t} + 2(2+H)\frac{\partial u_e}{\partial x} + \frac{1}{2}\frac{P}{\gamma}\frac{H+1}{Z\frac{\partial H}{\partial \gamma}} & -2\frac{H}{u_e}\frac{\partial u_e}{\partial t} - 2(2+H)\frac{\partial u_e}{\partial x} - \frac{1}{2}\frac{P}{\gamma}\frac{H}{Z\frac{\partial H}{\partial \gamma}} \\ \frac{4}{u_e}\frac{\partial u_e}{\partial t} + 6H^*\frac{\partial u_e}{\partial x} + \frac{1}{2}\frac{Q}{\gamma H^*}\frac{H+1}{Z\frac{\partial H}{\partial \gamma}} & -\frac{4}{u_e}\frac{\partial u_e}{\partial t} - 6H^*\frac{\partial u_e}{\partial x} - \frac{1}{2}\frac{Q}{\gamma H^*}\frac{H}{Z\frac{\partial H}{\partial \gamma}} \end{pmatrix}.$$

The above formulation is still generic since it is independent of the velocity profile. Using Tani's velocity profile and freezing the right-hand-side of equation (4.10) the eigenvalues and eigenvectors for K are determined, it has a full set set of eigenvalues and eigenvectors. The eigenvalues $\lambda_{1,2}$ and the accompanying eigenvectors $\xi_{1,2}$ are given by

$$\lambda_{1,2} = \frac{1}{2\frac{\partial H}{\partial \gamma}}\left[H^*\frac{\partial H}{\partial \gamma} - \frac{\partial H^*}{\partial \gamma}H - \frac{\partial H}{\partial \gamma} \pm \sqrt{G}\right]u_e,$$

$$\xi_{1,2} = \begin{pmatrix} 1 - \frac{1}{2u_e Z\frac{\partial H^*}{\partial \gamma}}\left(-\frac{1}{2\frac{\partial H}{\partial \gamma}}\left(-\frac{\partial H^*}{\partial \gamma}H - \frac{\partial H}{\partial \gamma} + H^*\frac{\partial H}{\partial \gamma} + \sqrt{G}\right)u_e - u_e + u_e H^*\right) \end{pmatrix},$$

where the root is given by

$$G = H^{*^2}\left(\frac{\partial H}{\partial \gamma}\right)^2 - 2H^*\frac{\partial H}{\partial \gamma}\frac{\partial H^*}{\partial \gamma}H - 2H^*\left(\frac{\partial H}{\partial \gamma}\right)^2 + \left(\frac{\partial H^*}{\partial \gamma}\right)^2 H^2 + 2\frac{\partial H^*}{\partial \gamma}H\frac{\partial H}{\partial \gamma} + \left(\frac{\partial H}{\partial \gamma}\right)^2 + 4\frac{\partial H}{\partial \gamma}\frac{\partial H^*}{\partial \gamma}.$$

The root in the eigenvalues and eigenvectors has 4 variables, which can be reduced to a single variable γ using the expressions derived earlier for the profile by Tani (see equation (4.9)). The root is written as a quotient where the nominator has two roots meaning there are two poles. The lowest value for γ in the steady case is zero which translates to zero wall friction and the occurrence of separation, in the unsteady case zero wall friction does not necessarily mean separation so the lower value of γ is set

below zero. The considered range of γ is $[-1, 5]$, where the upper limit is taken from Tani[132], where it must be noted that there is a pole at $\gamma = 6.7$. The eigenvalues and eigenvectors are discontinuous at $\gamma = 4$ since both $\frac{\partial H}{\partial \gamma}$ and $\frac{\partial H^*}{\partial \gamma}$ are zero valued, see figure (4.7). For $\gamma > 4$ the root is non-unique, there are two values for γ which produce

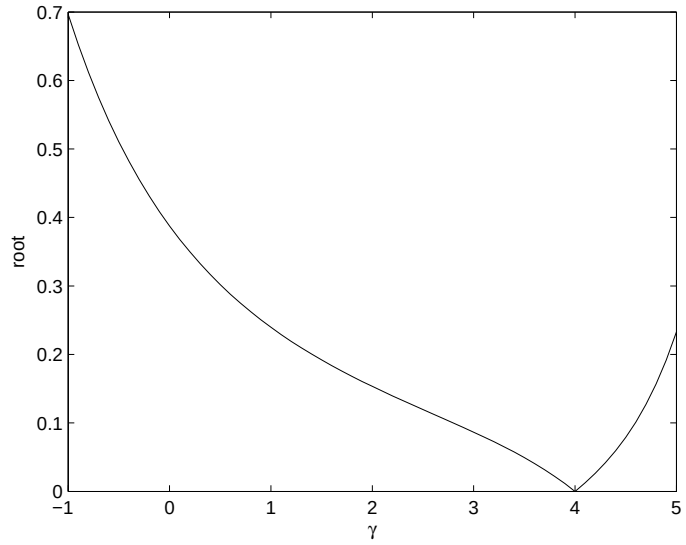

Figure 4.7: Root term in eigenvalues and eigenvectors

the same shape factor relations, subsequently γ is limited to $[-1, 4]$. For this range of γ the eigenvalues are continuous and the eigenvalues are real valued, see figure (4.8).

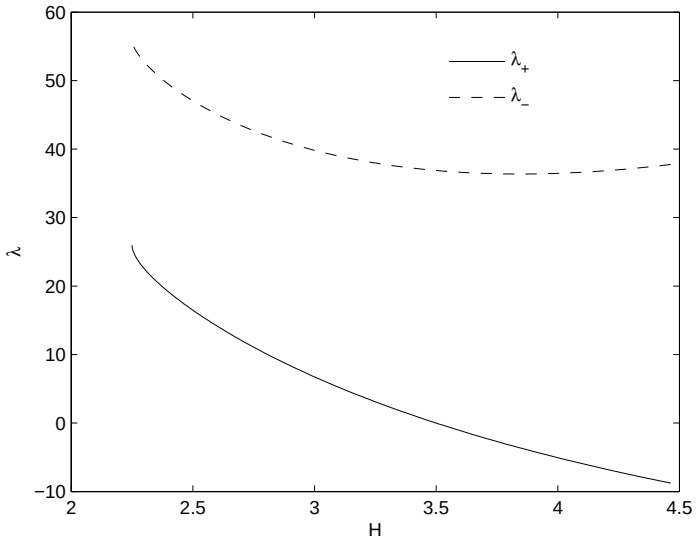

Figure 4.8: Eigenvalues of Hayasi's system using Tani's velocity profile

Unconditionally real eigenvalues with linearly independent eigenvectors give a system of equations which is unconditionally hyperbolic. The general approach to solve hyperbolic systems will be discussed in section (5.1).

Hayasi's method can be seen as an improvement of the method due to Schuh (see Hayasi[61]), giving better results for retarded flows. Tani subsequently employed a two-equation model without the application of a velocity profile, instead Tani found shape factor relations using the Falkner-Skan velocity profile. This work was continued by Matsushita, Murata and Akamatsu resulting in a two and three equation two parameter integral method. Before these methods can be applied the shape factor relations have to be found for different solution families, see section 3.1.3. Strictly the similarity or semi-similarity solutions for the boundary layer equations are only applicable for specific types of velocity distributions which may in fact be far off from the actual flow problem. Therefore it makes sense to apply problem specific velocity distributions, either resulting from the solution procedure or resulting from actual measurements. As was said earlier throughout literature it is assumed implicitly that steady laminar boundary layer profiles are very close to the Falkner-Skan similarity solutions.

The minimum value for H is 2.25 which limits it to equivalent linearly accelerating flows ($u_e = c\,x$), a maximum shapefactor of 4.5 is in line with the focus of this method , namely retarded flows. However it does necessitate the use of a 2^{nd} velocity profile for strongly accelerating flows, Hayasi uses the Hartree profile for this purpose (see Hayasi[61]). In case of turbulence the original system is only useful if a suitable turbulence velocity profile is found which contains the parameter γ, this is not directly available from literature.

4.2.4 Two and Three Equation Model by Matsushita et al

Schuh applied unsteady Pohlhausen to a general class of unsteady boundary layers using only one IBL equation, failing for strong adverse pressure gradients, his method was improved by Tani[132] who applied 2 IBL equations and a different quartic velocity profile. Building on the work of Tani in 1984 Matsushita et al[91] developed a 2 parameter integral method for the unsteady laminar boundary layers which can handle flow seperation.

Starting with the dimensional form of the three IBL equations (2.21), (2.24) and (2.25) Matsushita et al construct a system of equations. First the shape parameters are defined

$$E = \frac{\theta}{\delta^*}, \quad F = \frac{\delta^k}{\delta^*}, \quad G = \frac{\delta^{k+}}{\delta^*},$$
$$B = \frac{2\delta^*\tau_w}{\mu u_e}, \quad S = \frac{2\delta^*}{u_e^2}\frac{D}{\tau}, \quad Q = \frac{2\delta^*}{u_e^3}\int_0^\infty u\left(\frac{\partial u}{\partial y}\right)^2 dy,$$

which are substituted in the IBL equations, the resulting system is

$$\begin{aligned} w_t + f_x &= z, \\ w = \begin{pmatrix} \delta^* \\ (E+1)\delta^* \\ (F+1)\delta^* \end{pmatrix}, f &= \begin{pmatrix} u_e E\delta^* \\ u_e F\delta^* \\ u_e G\delta^* \end{pmatrix}, \\ z = \begin{pmatrix} \frac{B}{2\delta^*} - \frac{\delta^*}{u_e}\frac{\partial u_e}{\partial t} - (E+1)\delta^*\frac{\partial u_e}{\partial x} \\ \frac{S}{\delta^*} - \frac{2E\delta^*}{u_e}\frac{\partial u_e}{\partial t} - 2F\delta^*\frac{\partial u_e}{\partial x} \\ \frac{3Q}{\delta^*} + \frac{3(E-F)\delta_1}{u_e}\frac{\partial u_e}{\partial t} + 3(E-G)\delta^*\frac{\partial u_e}{\partial x} \end{pmatrix}. \end{aligned} \tag{4.11}$$

With the displacement thickness δ^*, the inverse shape factor E and the energy shape factor F as the unknowns. Matsushita considers the laminar boundary layer flow over a cylinder and assumes two regions, a laminar region (attached/detached) over the cylinder and the trailing edge flow aft of the the rear stagnation point. The laminar flow

over the cylinder is approximated using the Falkner-Skan[48] equation with a slipping wall boundary condition $u_w \neq 0$, see equation (C.1). The trailing edge flow is assumed to be semi-similar (2 similarity parameters) which is approximated by a method due to Williams[157]. As pointed out by Drela, the assumption of a laminar wake is not very realistic, any wake is most likely turbulent in nature (see Drela[35]).
Matsushita solves equation (4.11) using a first order upwind scheme for the attached region and a central Lax scheme for the separated region. The quasi-linear system is given by

$$w_t + Aw_x = z^{'}, \quad z^{'} = z - \begin{pmatrix} E\delta^* \frac{\partial u_e}{\partial x} \\ F\delta^* \frac{\partial u_e}{\partial x} \\ G\delta^* \frac{\partial u_e}{\partial x} \end{pmatrix},$$

$$A = u_e \begin{pmatrix} -1 & 1 & 0 \\ -1 & 0 & 1 \\ G - (E+1)\frac{\partial G}{\partial E} - (F+1)\frac{\partial G}{\partial F} & \frac{\partial G}{\partial E} & \frac{\partial G}{\partial F} \end{pmatrix}.$$

This system has distinct real roots and thus it is hyperbolic, subsequently this system can be solved using a Riemann-like solver, Matsushita and Akamatsu[90] use the Steger-Warming Flux Vector Splitting scheme (see sections (5.1.1) and (6.1.1)). For $H = 3.5$ the wall shear stress vanishes and for $H > 3.5$ a reversed flow starts to develop (see Matsushita and Akamatsu [90]). This confirms the correct implementation of the method by Hayasi which has negative eigenvalues for $H > 3.5$.

Summarising, Matsushita et al use three momentum integrals, the earlier derived IBL equations, together with functional relations based on two shape parameters E and F and the displacement thickness δ^*. Matsushita et al assume a self-similar laminar boundary layer flow which is approximated using the Falkner-Skan equation with slipping wall. Matsushita et al approximate the wake profile with a semi-similar solution due to Williams.

Some time later Matsushita and Akamatsu use a two equation and one parameter model and multiple (semi-)similarity solutions to determine shape factor relations; Falkner-Skan for accelerating flow[60], Tani[132] for decelerating low and Proudman and Johnson[111] for the rear stagnation flow, and as was already mentioned they employ the Steger-Warming Riemann solver for the solution procedure. The solution method due to Matsushita and Akamatsu also allows separation. Which may be attributed to the fact that the inverse shape factor E is used which gives that near separation E goes through zero where otherwise the shape factor H would go to infinity. Note that starting from the original formulation by Matsushita et al the solution method is generic, the subsequent choice of the closure relations confines the range of applicability in this case. Most interesting is the assertion that this method can handle separated flows which avoids the need to use an (semi-)inverse solution procedure and may possibly lower the amount of iterations needed for the quasi-simultaneous method. However since the separation can be identified from the convergence of characteristics one is free to apply a coupled method (inverse or with some interaction law). Also, Matsushita et al use specific similarity solutions which are suitable for (nearly) separated flow and with that give closure for large values of the shape factors which is not the case for say Drela's closure.
For the converging characteristics Matsushita and Akamatsu found that together with the singularity in the integral variables the wall friction becomes zero for the steady boundary layer flow. A similar result was also found by Cousteix and Houdeville[29].

As was said the solution method is generic and thus empirical closure relations for turbulent boundary layers can be used to relate H,F and δ^* to the other shape factors and integral variables, the shape factor G requires the use of a velocity profile of the turbulent boundary layer like Coles law of the wake (see section (3.3)). To close the shape factors other approximate methods can be used, for instance the earlier discussed methods due to Drela,Head's and Green. For this thesis the system of Matsushita will

be used together with closure relations from Drela. The closure relations for C_k and H^{**} can be obtained from the Falkner-Skan equation for the laminar profile, the turbulent profile is more difficult to close. For practical purposes another approximative method may be employed which does not require C_k and H^{**}, then using one of the turbulent velocity profiles in section (3.3.1) C_k and H^{**} can be retrieved. Alternatively Swafford's turbulent velocity profile can be used to together with a definition for C_f and the integral definitions for δ^{k+} and θ, this can be solved implicitly (see i.e. Drela[35]). The laminar closure relations are obtained by solving the Falkner-skan equation using the shooting method, also see figure (4.9)

$$H^{**} = -0.049H^3 + 0.57H^2 - 2.2H + 4.7$$
$$\frac{C_k Re_\theta}{H} = 96{H^*}^3 - 450{H^*}^2 + 700H^* - 360$$

From the paper by Matsushita and Akamatsu correlations can be extracted which

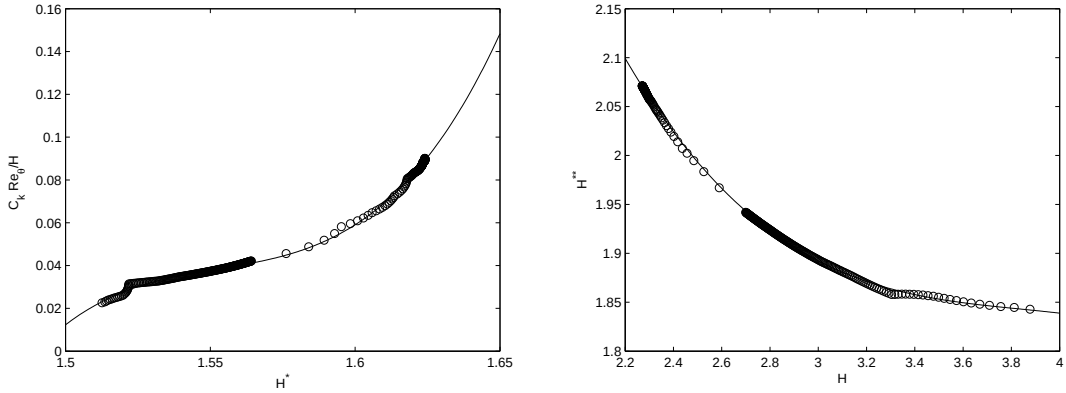

Figure 4.9: Falkner-Skan correlations

are suitable for separating flow through the earlier mentioned combination of Tani's data, Falkner-Skan's similarity solution and Proudman and Johnsons semi-similarity solution, see figure (4.10). The interpolation plots in figure (4.10) are given by

$$B : \begin{cases} B_{left} = -225.86E^3 - 3016.6E^2 - 208.68E - 17.915 & , E < -0.0616 \\ B_{middle} = \frac{B_{left}+B_{right}}{2} & , -0.0616 < E < -0.0395 \\ B_{right} = 131.9E^3 - 167.32E^2 + 76.642E - 11.068 & , E > -0.0395 \end{cases} , \tag{4.12}$$

$$F = 4.8274E^4 - 5.9816E^3 + 4.0274E^2 + 0.23247E + 0.15174, \tag{4.13}$$

$$S : \begin{cases} S_{left} = 451.55E^3 + 2010E^2 + 138.96E + 11.296 & , E < -0.0582 \\ S_{middle} = \frac{S_{left}+S_{right}}{2} & , -0.0582 < E < -0.042 \\ S_{right} = -96.739E^3 + 117.74E^2 - 46.432E + 6.8074 & , E > -0.042 \end{cases} , \tag{4.14}$$

where

$$E = \frac{1}{H}, \quad F = \frac{H^*}{H}, \quad B = C_f Re_{\delta^*}, \quad S = C_d Re_{\delta^*}.$$

The sets of third order interpolations are favored over single fifth or higher order interpolations due to the computer accuracy. The third and fourth order of the interpolations may still give numbers which are not in range of the numerical accuracy for very small values of E. The values are also added to the algorithm with tables, intermediate values are extracted using interpolation. Especially near separation this will most likely produce better results than the closure relations based on the Falkner-Skan

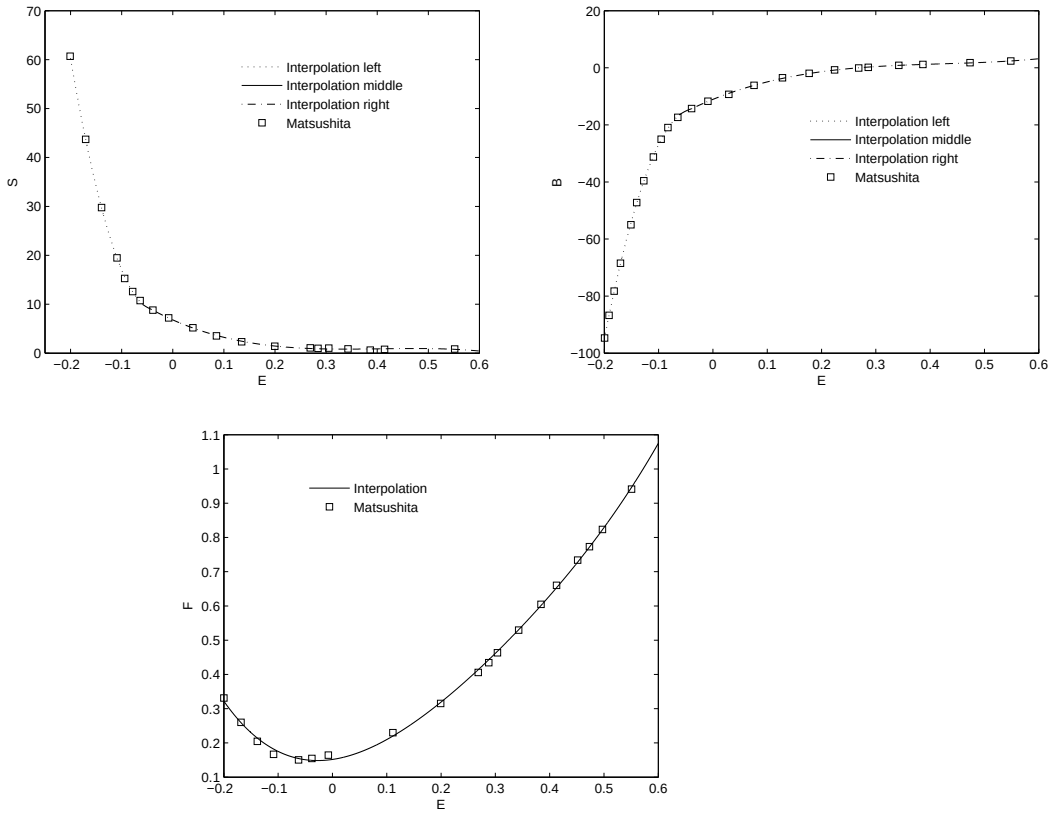

Figure 4.10: Matsushita and Akamatsu's closure correlations obtained for this Thesis

equations (without slip). The strength of Matsushita et al's choice of parameters lies in the fact that E can become negative continuously, which will occur for strong separation since the momentum thickness can become negative in a continuous fashion. The weakness of e.g. Drela's system is that the shape factor becomes negative in a discontinuous manner. In fact the shape factor becomes very large near separation as the momentum thickness goes through zero and the displacement thickness becomes very large(analytically $\delta^* \rightarrow \infty$) , i.e. the sign of the shape factor changes discontinuously whereas with E as a primary variable the change would be continuous from positive to negative.
Concluding, the above correlation functions with E will likely produce better results near separation than the Falkner-Skan derived closure relations as used by i.e. Drela. However when the momentum thickness becomes negative the shape factor changes abruptly from very large positive to very large negative. Separated flow to the extent that the momentum thickness becomes negative would require the use of a coupled solver or a different set of primary variables which can handle the change in sign continuously.
Together with the shape factor H also the kinetic shape factor H^* switches sign from large positive to large negative, starting from the equations (2.22),(2.23) and (2.25) a system can be written which contains E and δ^* as primary variables, note that $\theta = \delta^* E$

$$\frac{1}{2}C_f E = \frac{1}{u_e^2}\left[u_e \frac{\partial(\delta^* E)}{\partial t} - u_e \delta^* \frac{\partial E}{\partial t} + \theta \frac{\partial u_e}{\partial t}\right] + E\frac{\partial(\delta^* E)}{\partial x} + \frac{\theta}{u_e}(2E+1)\frac{\partial u_e}{\partial x},$$

$$C_D = \frac{1}{u_e}\frac{\partial(\delta^* E)}{\partial t} + \frac{1}{u_e}\frac{\partial \delta^*}{\partial t} + 2\frac{\delta^* E}{u_e^2}\frac{\partial u_e}{\partial t} + \frac{\partial(F\delta^*)}{\partial x} + 3\frac{F\delta^*}{u_e}\frac{\partial u_e}{\partial x}.$$

For laminar boundary layer flow the above formulation should give results equal to the results by Matsushita and Akamatsu, for turbulent boundary layer flow the typical turbulent closure models used by i.e. Drela, Nishida and Milewski may be used with the note that a negative shape factor is in general not within the range of application for any empirical turbulence model (Oudheusden [142]). The downside of the above set of equations is that a conservative formulation requires a division by $\frac{1}{E}$, the original system from Matsushita does not have this issue.

Applying the closure relations provided by equations (4.12),(4.13) and (4.14) should already be an improvement for laminar separated flow compared with the Falkner-Skan closure relations which are typically used for laminar BL's.

Assuming the two-equation system by Matsushita and Akamatsu is solved using a FVM or FEM the Jacobian needs to be written out explicitly. For the laminar case this is trivial, for the turbulent case the derivative $\frac{\partial F}{\partial E}$ needs some elaboration. Given turbulent closure relations which are most often written in terms of the Reynolds momentum thickness Re_θ and the shape factor H. Writing out the derivative in terms of the shape factor and the kinetic shape factor gives

$$\begin{aligned}
\frac{\partial F}{\partial E} &= \frac{\partial \left(\frac{H^*}{H}\right)}{\partial \left(\frac{1}{H}\right)}, \\
\frac{\partial F}{\partial E} &= -H^2 \frac{\partial \left(\frac{H^*}{H}\right)}{\partial H}, \\
\frac{\partial F}{\partial E} &= -H \frac{\partial H^*}{\partial H} + H^*,
\end{aligned}$$

which can be readily written out with the presented turbulent closure relations for H^*.

4.3 Unsteady Thwaites

An unsteady method was found in a paper by He and Denton[62] using Thwaites' integral, the unsteady Von Kármán equation and the unsteady Thwaites parameter they arrive at

$$\frac{\partial(\theta^2 u_e^6)}{\partial x} = \left[0.45 - \frac{2\theta}{\nu u_e}\left(u_e \frac{\partial \delta^*}{\partial t} + \theta \frac{\partial u_e}{\partial t}\right)\right] \nu u_e^5.$$

They use the correlations based on the steady Thwaites' parameter i.e., quasi-unsteadiness is assumed which automatically limits the method to low reduced frequencies. Unsteady Thwaites' will not be considered beyond this point simply because of the inherent quasi-unsteadiness.

4.4 Laminar-to-Turbulence Transition

Using the Falkner-Skan profile family Drela[35] produced spatial amplification curve envelopes. Drela gives the following solution procedure to determine the amplification factor

$$\begin{aligned}
\frac{d\tilde{n}}{dx} &= \frac{d\tilde{n}}{dRe_\theta}\frac{m+1}{2}\frac{l}{\theta}, \\
l &= \frac{6.54H - 14.07}{H^2}, \\
m &= \frac{1}{l}\left(0.058\frac{(H-4)^2}{H-1} - 0.068\right), \\
\tilde{n} &= \int_{x_{crit}}^{x} \frac{d\tilde{n}}{dx}dx,
\end{aligned} \tag{4.15}$$

$$\text{Drela[35]:} \quad \frac{d\tilde{n}}{dRe_\theta} = 0.01\sqrt{\left(2.4H - 3.7 + 2.5\tanh\left[1.5(H-3.1)\right]\right)^2 + 0.25},$$

$$\text{Drela and Giles:} \quad \frac{d\tilde{n}}{dRe_\theta} = 0.028\,(H-1) - \frac{0.0345}{\exp\left[-\left(\frac{3.87}{H-1} - 2.52\right)^2\right]}. \tag{4.16}$$

The integration for $\tilde{n}$ can take place when $Re_\theta \geq Re_{\theta,crit}$, where the critical Reynolds number $Re_{\theta,crit}$ is given by equations (E.20), (E.21), (E.22) and (E.23). The transitional Reynolds number can be determined in a variety of ways, most noteworthy is the criterion by Michel, see equation (3.5). The first fulfilment of the critical or transitional criteria based on equations (E.20), (E.21), (E.22), (E.23) and the criterion by Michel[2] will be used as the starting point for integrating the differential equation 4.15.

The transition criterion ranges between $\tilde{n}_{tr} = 7$ and $\tilde{n}_{tr} = 11$, commonly used is $\tilde{n}_{tr} = 9$. In combination with the Falkner-Skan based transition method by Drela this leads to a hybrid method, one combining free transition and bypass transition. It must be noted that White[154] gives a different validity range namely $0.07\% < Tu < 2.98\%$. The empirical formulation indicates the obvious, for higher external turbulence levels transition occurs sooner(at lower amplification levels). The differential equation defined above can be solved together with the integral variables, once $\tilde{n}$ reaches the transition criterion the amplification differential is dropped from the solution procedure.
Once the transition criterion has been met, a certain transition boundary layer is in effect. Drela uses the following averaging method for the integral variables

$$val = (1 - \gamma_{tr})val_{lam} + \gamma_{tr}val_{turb},$$

where γ_{tr} follows from

$$\gamma_{tr} = \frac{\tilde{n}_{turb} - \tilde{n}_{tr}}{\frac{d\tilde{n}}{dx}}\frac{1}{x_{turb} - x_{lam}},$$

where $\tilde{n}_{tr}$ is the transition criterion. Drela assumed laminar to turbulent transition in one step , in reality there will be a transition region. Drela set the shear stress coefficient C_τ to be $0.7C_{\tau,eq}$ at the transition point.
Stock and Haase compared several transitional length models and produced the followed modified model (see Stock and Haase[127])

$$Re_{\Delta x} = 4.6Re_{\delta^*_{tr}}^{\frac{3}{2}}.$$

In reference to Chen and Thyson Johansen and Sørensen[70] used a different transition region

$$\gamma_{tr} = 1 - \exp\left[\left(-\frac{u_e^3}{\nu^2 G_{\gamma_{tr}}}\right)Re_{x_{tr}}^{-1.34}(x - x_{tr})\int_{x_{tr}}^{x}\frac{1}{u_e}dx\right],$$

where Johansen and Sørensen use an expression for $G_{\gamma_{tr}}$ adapted by Cebeci(see Johansen and Sørensen[70])

$$G_{\gamma_{tr}} = 213\frac{\log\left(Re_{x_{tr}}\right) - 4.732}{3}.$$

[2]Although admittedly the criterion from Michel is meant for the transition value of the momentum thickness Reynolds number

γ_{tr} will become one for large x, a prescribed transitional length may still be required depending on the length of the profile. Lian and Shyy[82] suggest an intermittency function for low-Reynolds number flow (Re$\sim 10^5 - 10^6$) which also incorporates the separation point.

Alternatively the intermittency factor γ_{tr} is based on the amplification factor directly; two main options are considered

1. Starting from the critical Reynolds number, base the intermittency factor on the current amplification factor in relation to the transition amplification number, this is to be called pre-transition model
2. Starting from the transition point, base the intermittency factor on the current amplification factor in relation to a reference amplification number , this is to be called post-transition model

The pre-transition model has the requirement that $\gamma_{tr} = 0$ for $\tilde{n} = 0$, and $\gamma_{tr} = 1$ for $\tilde{n} \geq \tilde{n}_{tr}$. The post-transition model has the requirement that $\gamma_{tr} = 0$ for $\tilde{n} = \tilde{n}_{tr}$, and $\gamma_{tr} = 1$ for $\tilde{n} \geq \tilde{n}_{ref}$ where $\tilde{n}_{ref}$ is the value for the amplification factor at which the entire boundary layer is assumed to be turbulent.
There are several ways to meet the above requirement using some continuous function, for this thesis, roughly a convex and a concave function is constructed. The convex function is formed by an exponential and the concave function by a polynomial of arbitrary degree, see equation (4.17) and figure (4.11).

$$\begin{aligned} \text{exponential:} \quad \gamma &= \begin{cases} \dfrac{\exp\left(\frac{-1}{c\chi}\right)}{\exp\left(-\frac{1}{c}\right)} & \text{pre-transition} \\ \dfrac{\exp\left(\frac{-1}{c\chi(\chi-1)}\right)}{\exp\left(-\frac{1}{c(\chi_{ref}-1)}\right)} & \text{post-transition} \end{cases}, \\ \text{polynomial:} \quad \gamma &= \begin{cases} 1-(1-\chi)^c & \text{pre-transition} \\ \frac{(\chi-1)\chi^c}{(\chi_{ref}-1)\chi_{ref}^c} & \text{post-transition} \end{cases}, \end{aligned} \tag{4.17}$$

where

$$\chi = \left(\frac{\tilde{n}}{\tilde{n}_{tr}}\right), \quad \chi_{ref} = \left(\frac{\tilde{n}_{ref}}{\tilde{n}_{tr}}\right).$$

It should be exemplified that the pre- and post-transition models of figure (4.11) are

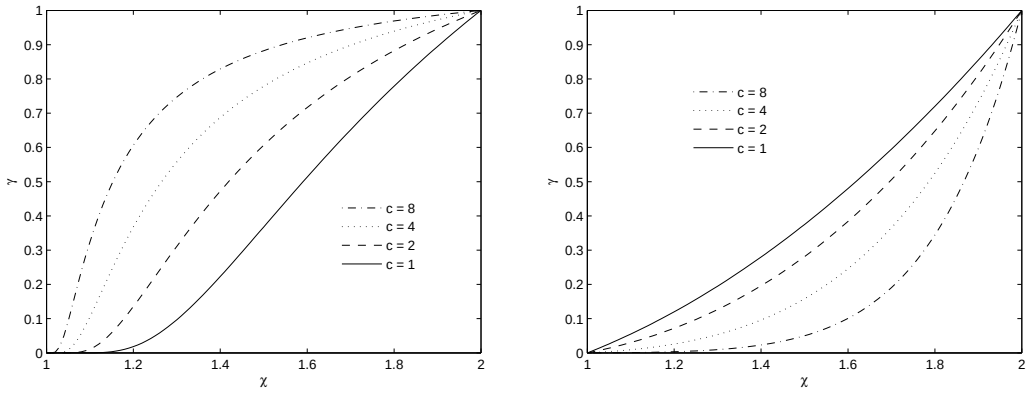

Figure 4.11: Intermittency function with $\chi_{ref} = 2$, post-transition model, (left) exponential, (right) polynomial.

not based on actual empirical data other than the observation that there *is* a transition region. The transition amplification factor, the reference amplification factor and

the shape constant c are settable by the user. The above treatment of the transition assumes that the intermittency is only a spatial variable and thus it assumes that the transition is an instantaneous event. Obviously this is not true, the turbulence transition may occur within a small time-scale it will still take time to propagate over the profile, nevertheless, for this thesis it is assumed that the transition is instantaneous, which is in line with using a steady transition method. The separation of the boundary layer in a laminar, a transitional and a turbulent part can perhaps be reduced to a transitional part and a turbulent part by using a suitable intermittency function, in line with the intermittency transport relations by Menter and Langtry, however relying on some empirical function instead of (semi-empirical) differential equations, to experiment with this idea the critical Reynolds number can be set to zero and subsequently a suitable value for $\tilde{n}_{ref}$ can be chosen to fit the reference results.

Sekar[120] uses data from Schubauer and Klebanoff to validate the e^n method for the steady, the same will be done for the present case, see section(7.1.1).

4.5 Conservative Formulation

To be able to apply the FVM and FEM consistently (without any corrective measures) one needs a conservative system of equations.

The methods due to Matsushita et al and Matsushita and Akamatsu are already written in conservative form by default, this leaves the unsteady method derived from Drela, the unsteady entrainment method and the method by Hayasi.

Unsteady Von Kármán Equation, Kinetic Energy Integral and Unsteady Lag Entrainment Equation

Starting with equation set (4.1) a conservative formulation is already provided since this was derived in section(2), see equations (2.23) and (2.24). Equation (3.12) which represents the lag entrainment poses a slight problem since the flux component $u_s\frac{\partial C_\tau}{\partial x}$ is non-conservative. If it is assumed that $\frac{\partial u_s}{\partial x} = 0$ locally it holds that $u_s\frac{\partial C_\tau}{\partial x} = \frac{\partial (C_\tau u_s)}{\partial x}$. The following conservative formulation emerges

$$
\begin{aligned}
&F_t + u_e f_x = u_e B,\\
&F = \begin{pmatrix} \delta^* \\ \theta + \delta^* \\ C_\tau \end{pmatrix}, \quad f = \begin{pmatrix} \theta \\ H^*\theta \\ u_s C_\tau \end{pmatrix},\\
&B = \begin{pmatrix} \frac{1}{2}C_f - \frac{\theta}{u_e}(2+H)\frac{\partial u_e}{\partial x} - \frac{\delta^*}{u_e^2}\frac{\partial u_e}{\partial t} \\ C_D - \left(\frac{2\theta}{u_e^2}\frac{\partial u_e}{\partial t} + 3\frac{H^*\theta}{u_e}\frac{\partial u_e}{\partial x}\right) \\ \frac{K_c C_\tau u_s}{\delta}\left(\sqrt{C_{\tau_{eq}}} - \sqrt{C_\tau}\right) - 2\frac{C_\tau}{u_e^2}\frac{\partial u_e}{\partial t} - 2\frac{C_\tau u_s}{u_e}\frac{\partial u_e}{\partial x} \end{pmatrix},
\end{aligned}
\tag{4.18}
$$

of course one of the other unsteady lag entrainment formulations can be chosen, see equations (3.12), (3.13), (3.14). So with relative ease the unsteady system from Drela can be written in a conservative form where the characteristics have already been derived from the non-conservative form earlier, the above system is used by Hall[58] and Fenno et al[50]. The quasi-linear form of the above system requires the Jacobian matrix which is given by

$$
K = u_e \begin{pmatrix} 0 & \frac{\partial \theta}{\partial(\theta+\delta^*)} & 0 \\ \theta\frac{\partial H^*}{\partial \delta^*} & \frac{\partial H^*\theta}{\partial(\theta+\delta^*)} & 0 \\ C_\tau\frac{\partial u_s}{\partial \delta^*} & C_\tau\frac{\partial u_s}{\partial(\theta+\delta^*)} & u_s \end{pmatrix},
$$

where the composed differential terms can be written as

$$\frac{\partial f(\delta^*,\theta)}{\partial(\theta+\delta^*)} = \frac{\partial f(\delta^*,\theta)}{\partial\theta}\frac{\partial\theta}{\partial(\theta+\delta^*)} + \frac{\partial f(\delta^*,\theta)}{\partial\delta^*}\frac{\partial\delta^*}{\partial(\theta+\delta^*)},$$

now using $\frac{\partial\delta^*}{\partial(\theta+\delta^*)} = \frac{\partial\theta}{\partial(\theta+\delta^*)} = 1$ the Jacobian can be written as

$$K = u_e \begin{pmatrix} 0 & 1 & 0 \\ \theta\frac{\partial H^*}{\partial\delta^*} & H^* + \theta\left(\frac{\partial H^*}{\partial\theta} + \frac{\partial H^*}{\partial\delta^*}\right) & 0 \\ C_\tau\frac{\partial u_s}{\partial\delta^*} & C_\tau\left(\frac{\partial u_s}{\partial\theta} + \frac{\partial u_s}{\partial\delta^*}\right) & u_s \end{pmatrix},$$

which can be written out explicitly in terms of the primary variables since, at least for the closure relations in this thesis, H^* and u_s are functions of θ and δ^*.

Unsteady Entrainment Method

Using $H_1\theta = \delta - \delta^*$ equation (3.9) is written as

$$\frac{1}{u_e}\frac{\partial\delta}{\partial t} - \frac{1}{u_e}\frac{\partial u_e\theta H_1}{\partial x} = -0.0306\left(H_1-3\right)^{-0.6169},$$

which can be added to system (4.18). The combined system has, as far as could be found in literature, not yet been applied in practice.

The combined system would become

$$F = \begin{pmatrix} \delta^* \\ \theta+\delta^* \\ C_\tau \\ \delta \end{pmatrix}, \quad f = \begin{pmatrix} \theta \\ H^*\theta \\ u_s C_\tau \\ -\theta H_1 \end{pmatrix},$$
$$B = \begin{pmatrix} \frac{1}{2}C_f - \frac{\theta}{u_e}(2+H)\frac{\partial u_e}{\partial x} - \frac{\delta^*}{u_e^2}\frac{\partial u_e}{\partial t} \\ C_D - \left(\frac{2\theta}{u_e^2}\frac{\partial u_e}{\partial t} + 3\frac{H^*\theta}{u_e}\frac{\partial u_e}{\partial x}\right) \\ \frac{K_c C_\tau u_s}{\delta}\left(\sqrt{C_{\tau_{eq}}} - \sqrt{C_\tau}\right) - 2\frac{C_\tau}{u_e^2}\frac{\partial u_e}{\partial t} - 2\frac{C_\tau u_s}{u_e}\frac{\partial u_e}{\partial x} \\ -0.0306u_e\left(H_1-3\right)^{-0.6169} + \theta H_1\frac{\partial u_e}{\partial x} \end{pmatrix}, \tag{4.19}$$

with the Jacobian

$$K = u_e \begin{pmatrix} 0 & 1 & 0 & 0 \\ \theta\frac{\partial H^*}{\partial\delta^*} & H^* + \theta\left(\frac{\partial H^*}{\partial\theta} + \frac{\partial H^*}{\partial\delta^*}\right) & 0 & 0 \\ C_\tau\frac{\partial u_s}{\partial\delta^*} & C_\tau\left(\frac{\partial u_s}{\partial\theta} + \frac{\partial u_s}{\partial\delta^*}\right) & u_s & 0 \\ 1 & 1 & 0 & -1 \end{pmatrix}.$$

Hayasi's Method

The system from Hayasi can be written in conservative form if the coefficient matrix K can be integrated with the primary variables, i.e. $\int K\partial F$ leads to an analytical solution. Given that the shape factors lead to simple quotients with γ as the main variable analytical integrals are sure to exist. The flux vector can be written as

$$f = \begin{pmatrix} \left(-u_e + u_e H^*\right)Z + 2u_e Z H^* \\ \frac{1}{2}u_e Z\frac{H+1}{Z\frac{\partial H}{\partial\gamma}} - \frac{1}{2}\int u_e\frac{HH^*}{Z\frac{\partial H}{\partial\gamma}}d\gamma - \int u_e\frac{H}{\frac{\partial H}{\partial\gamma}}\frac{\partial H^*}{\partial\gamma}d\gamma \end{pmatrix},$$

where the remaining integrals are dependent on the description of the velocity profiles, therefore the system by Hayashi is not suitable for general applications.

The unsteady Green's lag entrainment equation and the unsteady Head's entrainment need to be applied only for turbulent boundary layer flow.

4.5.1 Hyperbolicity of the Conservative Systems

The hyperbolicity of the system by Matsushita et al is given and system(4.7) by Hayasi is not considered beyond this point, this leaves system (4.18). For the determination of the hyperbolicity first the eigenvalues of the Jacobian matrix are determined algebraically, then any set of closure relations can be used to obtain the eigenvalues as functions of the primary variables.

The eigenvalues are

$$\lambda_\pm = (\frac{1}{2}H^* + \frac{1}{2}\theta\frac{\partial H^*}{\partial\theta} + \frac{1}{2}\theta\frac{\partial H^*}{\partial\delta^*} \pm \frac{1}{2}\sqrt{G})u_e,$$
$$\lambda_3 = u_e u_s,$$
$$G = (H^*)^2 + 2H^*\theta\frac{\partial H^*}{\partial\theta} + 2H^*\theta\frac{\partial H^*}{\partial\delta^*} + \theta^2\left(\frac{\partial H^*}{\partial\theta}\right)^2 + 2\theta^2\frac{\partial H^*}{\partial\theta}\frac{\partial H^*}{\partial\delta^*} + \theta^2\left(\frac{\partial H^*}{\partial\delta^*}\right)^2 + 4\theta\frac{\partial H^*}{\partial\delta^*},$$

where the term $u_e u_s$ has already been treated in section (4.2.1). The eigenvectors are given by

$$\xi_\pm(1) = 1,$$
$$\xi_\pm(2) = \frac{1}{2}H^* + \frac{1}{2}\theta\frac{\partial H^*}{\partial\theta} + \frac{1}{2}\theta\frac{\partial H^*}{\partial\delta^*} \pm \frac{1}{2}\sqrt{G},$$
$$\xi_\pm(3) = -C_\tau\frac{\xi_\pm(2)}{\theta\frac{\partial H^*}{\partial\delta^*}\left(-\xi_\pm(2)u_e + u_e\, u_s\right)}T$$
$$T = \xi_\pm(2)u_e\frac{\partial u_s}{\partial\delta^*} + \frac{\partial u_s}{\partial\theta}u_e\theta\frac{\partial H^*}{\partial\delta^*} - u_e H^*\frac{\partial u_s}{\partial\delta^*} - u_e\theta\frac{\partial H^*}{\partial\theta}\frac{\partial u_s}{\partial\delta^*},$$
$$\xi_3 = \begin{pmatrix} 0 \\ 0 \\ 1 \end{pmatrix}.$$

To get representative values for the root term G and the eigenvalues the laminar closure relations from equations (4.12),(4.13) and (4.14) are applied and for the turbulent closure relations equations (E.41), (E.44), (E.45) and (E.46).

The derivatives $\frac{\partial H^*}{\partial\theta}$, $\frac{\partial H^*}{\partial\delta^*}$ are written as follows for the laminar boundary layer

$$\frac{\partial H^*}{\partial\theta} = \frac{1}{\theta}\left(3aE^3 + 2bE^2 + cE - eH\right),$$
$$\frac{\partial H^*}{\partial\delta^*} = \frac{1}{\theta}\left(-3aE^4 - 2bE^3 - cE^2 + e\right),$$

where the coefficients are given as

$$a = 4.8274, \quad b = -5.9816, \quad c = 4.0274, \quad e = 0.15174.$$

The derivatives $\frac{\partial u_s}{\partial\theta}$, $\frac{\partial u_s}{\partial\delta^*}$ are written as follows for the turbulent boundary layer

$$\frac{\partial u_s}{\partial\theta} = \frac{1}{6}\frac{\partial H^*}{\partial\theta}\left(\frac{4}{H} - 1\right) + \frac{2}{3}\frac{H^*}{\delta^*},$$
$$\frac{\partial u_s}{\partial\delta^*} = \frac{1}{6}\frac{\partial H^*}{\partial\delta^*}\left(\frac{4}{H} - 1\right) + \frac{2}{3}H^*\theta.$$

The derivative $\frac{\partial H^*}{\partial\theta}$ for the turbulent boundary layer is given by

$$H < H_0: \quad \frac{\partial H^*}{\partial \theta} = -\frac{4}{\theta Re_\theta} + \frac{0.8}{\theta\sqrt{Re_\theta}}\left(\frac{H_0 - H}{H}\right)^{1.6} + \frac{4.8}{\delta^*}\left(0.165 - \frac{1.6}{\sqrt{Re_\theta}}\right)\left(\frac{H_0 - H}{H}\right)^{0.6},$$

$$H > H_0: \quad \frac{\partial H^*}{\partial \theta} = -\frac{4}{\theta Re_\theta} + 2(H - H_0)\left(-\frac{H}{\theta} + \frac{400}{\theta Re_\theta}\right)\left(\frac{0.04}{H} + 0.007\frac{\ln(Re_\theta)}{\left(H - H_0 + \frac{4}{\ln(Re_\theta)}\right)^2}\right)$$

$$+ (H - H_0)^2\left(\frac{0.04}{\delta^*} + 0.007\frac{\frac{1}{\theta}\left(H - H_0 + \frac{4}{\ln(Re_\theta)}\right)^2 - 2\ln(Re_\theta)\left(H - H_0 + \frac{4}{\ln(Re_\theta)}\right)\left(-\frac{H}{\theta} + \frac{400}{\theta Re_\theta} - \frac{4}{\theta\left(\ln(Re_\theta)\right)^2}\right)}{\left(H - H_0 + \frac{4}{\ln(Re_\theta)}\right)^4}\right),$$

where

$$H_0 = \min\left(3 + \frac{400}{Re_\theta}, 4\right).$$

The derivative $\frac{\partial H^*}{\partial \delta^*}$ for the turbulent boundary layer is given by

$$H < H_0: \quad \frac{\partial H^*}{\partial \delta^*} = \left(0.165 - \frac{1.6}{\sqrt{Re_\theta}}\right)\left(\frac{-1.6(H_0 - H)^{0.6}H - (H_0 - H)^{1.6}}{\delta^* H}\right),$$

$$H > H_0: \quad \frac{\partial H^*}{\partial \delta^*} = 2\frac{H - H_0}{\theta}\left(\frac{0.04}{H} + 0.007\frac{\ln(Re_\theta)}{\left(H - H_0 + \frac{4}{\ln(Re_\theta)}\right)^2}\right) +$$

$$(H - H_0)^2\left(-\frac{0.04}{\delta^* H} - 0.014\frac{\ln(Re_\theta)}{\theta\left(H - H_0 + \frac{4}{\ln(Re_\theta)}\right)^3}\right).$$

The following value ranges are used to test the hyperbolicity

$$\begin{aligned} \text{Laminar:} \quad & H = [2, 10], \quad Re_\theta = [0, 10000], \\ \text{Turbulent:} \quad & H = [1, 5], \quad Re_\theta = [0, 20000], \end{aligned}$$

with $\nu = 2 \cdot e - 5 \ \left[\frac{kg}{ms}\right], \quad u_e = 50 \ \left[\frac{m}{s}\right]$.

The results are plotted in figure (4.12), λ_- for the laminar closure relations goes through zero for $H \approx 3.44$ which is close to the value 3.5 found by Hayasi and Matsushita and Akamatsu. For the turbulent closure relations λ_- goes through zero for $H = 4$ at a Reynolds momentum thickness of 100 and decreases to about 3 for a Reynolds momentum thickness of 10000. This corresponds with the minimum value of $H^*(H)$ for different values of the Reynolds momentum thickness. Most importantly, the hyperbolicity of the conservative system (4.18) is confirmed for a realistic range of the problem parameters/variables.

4.6 Overview of Unsteady Integral Boundary Layer Methods in Literature

Schuh, Hayasi[61], Yang and others apply a guessed velocity profile for laminar boundary layer flow which they substitute in the unsteady Von Kármán equation and the unsteady kinetic energy integral equation. These methods have the benefit that the velocity profile information is also known.

Daneshyar and Mugglestone, and after that, Smith[123],Strickland[105], Bong[13], He and Denton[62] and Lyrio et al use the unsteady Von Kármán equation in combination with the steady Head's method for the turbulent boundary layer flow. He and

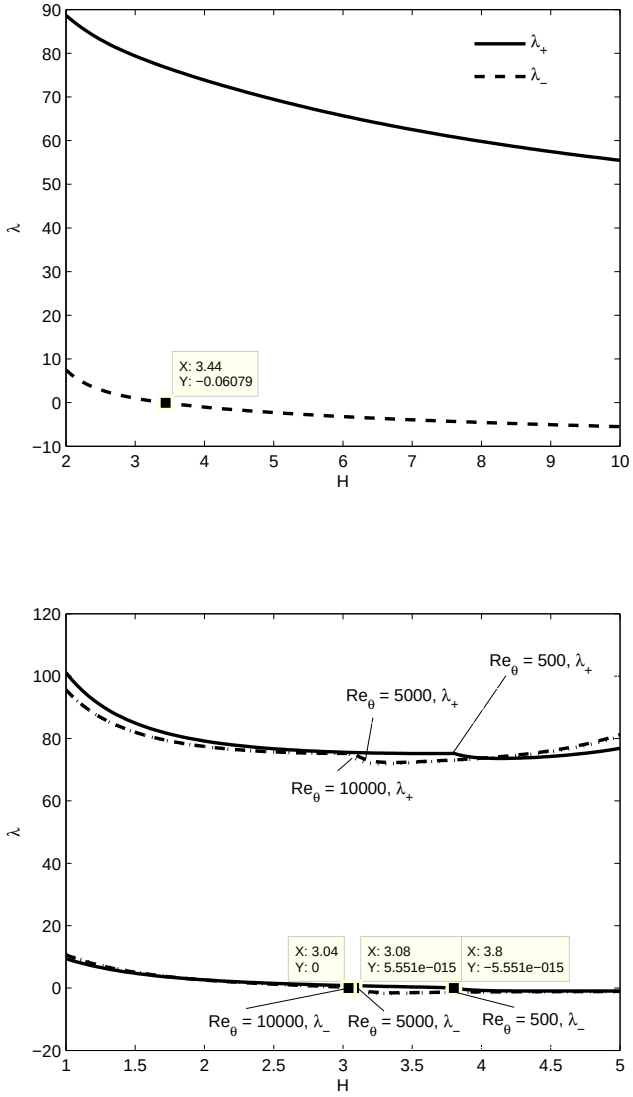

Figure 4.12: Eigenvalues λ_- and λ_+ (top) for the laminar closure relations, (bottom) for the turbulent closure relations

Denton, and Strickland apply the unsteady Thwaites parameter to the unsteady Von Kármán equation. This method is limited to low reduced frequencies of unsteadiness.

Matsushita et al[91][90] use the unsteady Von Kármán equation and the kinetic energy integral equation plus a third equation. Matsushita et al use closure relations for laminar flow based on specific semi-similarity solutions of accelerating, stagnating an separating flow. They apply an upwind finite difference scheme for the attached boundary layer flow and a Lax finite difference scheme for the separated boundary layer flow. Very interesting is the approach of using inverted shape factors as primary variables/parameters.

Swafford and Whitfield[129][128][130] apply the Von Kármán and the kinetic energy integral equations to three-dimensional compressible flow boundary layer flow. They use

an FDM and incorporate the geometry of the profile directly in the differential terms. Swafford and Whitfield use a central differencing scheme with numerical smoothing and an upwind difference scheme without smoothing.

Hall[58] applies system (4.18) together with Drela's e^n envelope method, for the coupling he uses source terms and the continuity equation in defect form. Fenno et al[50] apply the semi-inverse coupling method with the displacement thickness as the connecting variable. Fenno et al apply both the equilibrium and non-equilibrium closure for the diffusion coefficient C_D.

Mughal[99] discusses the hyperbolicity of the unsteady IBL equations and suggests to enforce the hyperbolicity through the eigenvalues, the benefit is that it guarantees the validity of the solution method but also influences the closure relations to an unpredictable degree. Mughal[99] has a particular approach for the closure relations, he chooses to use guessed velocity profiles to obtain the integral equation through numerical quadrature, both for the laminar as for the turbulent boundary layer.

Although this thesis deals specifically with the unsteady integral boundary layer equations for the purpose of e.g. aeroelastic simulations in literature there are several (recent) examples of aeroelastic simulations with the steady integral boundary layer equations. See Zhang[160], Howlett[67], Edwards[44][45] and Sekar[120].

4.7 Selection of Models

The main choice is now between the system by Matsushita et al and the unsteady Von Kármán equation plus the unsteady kinetic energy integral equation, both systems can be augmented with the unsteady lag entrainment and the unsteady entrainment equation. Assuming for each given point that the gradient in x-direction is very small, the boundary layer flow is likely to show a distribution close to some self-similar profile. As was noted, Falkner-Skan similarity profiles supposedly give a good approximation for steady laminar boundary layers for given shape factors. Thus using Falker-Skan based closure relations in combination with shape factors as primary variables is likely to produce good results for steady laminar boundary layers. Hayasi produces a system of equations which is conditionally hyperbolic, this significantly increases the complexity of the solution procedure and it will require an iterative procedure in case the system becomes non-hyperbolic. The method due to Hayasi was not found in any applications by other writers and Hayasi himself only applied his method for special cases, the benefit of using Hayasi is that the velocity profile is part of the solution which allows for a relatively straightforward prediction of separation. A different approach might be found by simply extending the guessed velocity profile to the unsteady case which would give C_f and δ as primary variables, see appendix (D).

The extension of the steady solution method by Drela to unsteady is likely to be comparable to the two equation method by Matsushita and Akamatsu, in the latter case multiple profiles are used to provide the closure relations with one parameter (the shape factor H), whereas the former method uses one profile to provide two-parameter(H and the momentum thickness θ) closure relations. It is likely that using the two parameter two equation approach by Drela in combination with multiple profiles as do Matsushita and Akamatsu provides a more robust approach than using a one parameter method, also it must be noted that Drela's approach gives excellent results for Falkner-Skan like flows. The turbulent closure by Swafford[129] (see equation(E.27)) requires the shape factor and the momentum thickness to equate the integral variables, this is compatible with i.e. the two equation model by Drela and the two equation model by Matsushita et al which would avoid the use of a third differential equation. The two and three equation models by Matsuhita et al are hyperbolic and can handle mildly separated laminar boundary layer flow. This is made possible first by the closure relations which cover

separating flow and second because the inverse shape factor is used which avoids the discontinuity in the shape factor when the momentum thickness goes through zero. The handling of separated flow is not necessarily an argument pro since it is already clear that a viscid-inviscid interation method will be employed at separation. However it is clear that if one can continue to use the direct method without blow-up of the solution it is very much preferable over the other coupling methods which require extra computations (e.g. an iteration procedure) for matching the solutions. This is certainly worth an investigation, the set of laminar closure models is already given by Matsushita et al and the turbulence closure models might be extracted in a similar way as did Matsushita et al by using separate models for different flow situations.

It was noted that Green's steady lag entrainment equation and Head's steady entrainment equation have been used successfully for an viscid-inviscid solution procedure applied to unsteady problems. This was also done for the unsteady lag entrainment equation. The (un)steady lag entrainment equation has been used successfully without Head's entrainment equation by Drela, Hall, Fenno et al.

Based on the previous considerations, the following choices are made; Either the conservative system (4.18) or the non-conservative system (4.4) will be applied and the system by Matsushita et al(see system 4.11) is advised for future research. [3] Furthermore the unsteady lag entrainment method is employed and an employment of unsteady Head's entrainment equation is advised for future implementation.

The linear amplification method as used by Drela[35] (see equation (4.15) in his PhD thesis will also be employed in the present case although the more advanced full transition criterion is supposedly more accurate. The mere simplicity of the envelope method and the fact that it seems to produce good results (see Drela[35], Hall[58], Sekar[120]) is reason to use it for this thesis. The effect of unsteadiness on the laminar-to-turbulence transition is ignored, this approach is also used by Hall[58]. Somewhat easier methods which do not entail an extra differential term are the methods due to Michel and Wazzan as discussed in chapter(2), these may be used for comparison.

Following the discussion in this chapter and the previous chapter the following combination of models will be used for the implementation, see table 4.1.

problem	**approach**
initialisation	Rayleigh solution (first Stokes problem)
equations used	Von Kármán equation, kinetic energy integral equation, unsteady Green's lag entrainment [58]
laminar closure	Matsushita et al [91]
turbulent closure	equilibrium and non-equilibrium boundary layer closure, see Drela[35]
transition	e^n, amplification envelope method following from Falkner-Skan profiles[35]
separation	all discussed methods ($\lambda, H_1(H)_{min}$,shock formation, etc.)

Table 4.1: Selection of models

[3] Although the elaboration of the numerical methods is generic the non-conservative system is erroneously approximated with a FVM,FEM, this will be explained later

The specific closure relations that are implemented are given in table (4.2).

case	**approach**
laminar	equations (E.6), (E.9), (E.5), (4.14), (4.13), (4.12)
turbulent	equations (E.41), (E.45), (non-equilibrium) (E.46), (E.50), (equilibrium) (E.44)
transition	equations (4.15), (E.21), (E.22), (E.23), (3.5), (E.20), (4.17)

Table 4.2: Relevant equations

Chapter 5

Application of Unsteady Integral Methods

5.1 Solution Procedures for Unsteady Integral methods

Given the system of equations and the closure relations the problem can be solved. In the previous chapter several systems of equations were investigated in terms of hyperbolicity.

Since the system of equations is hyperbolic characteristic directions might be determined. Assume M contains the eigenvectors as columns, dividing equation (2.27) with the coefficient matrix A and multiplying with M^{-1} gives

$$M^{-1}F_t + (M^{-1}K\,M)M^{-1}F_x = M^{-1}L,$$

where $K = A^{-1}B$ and $L = A^{-1}C$, here $M^{-1}K\,M$ is a diagonal matrix containing the eigenvalues of K, now the problem is divided into a dimension number of uncoupled non-linear ordinary differential equations. The importance for the numerical implementation lies in the fact that the solution propagates in the directions of the characteristics.

Mughal[98] uses the characteristic directions, as defined by the eigenvectors, to help determine whether the closure relations are coherent. Mughal elucidates that the characteristics should be contained within the boundary layer, the directions should be comparable to the external streamline. In a more practical sense the characteristic directions will determine the direction of upwinding for the finite difference schemes, it allows for certain boundary conditions and the eigenvalues will be of importance for the stability requirement.

5.1.1 Hyperbolic System

Solution methods for hyperbolic systems rely on the eigenvalues and eigenvectors to determine the flux over the cell faces (for FVM's and FEM's) or through the nodal points (for FDM's) and to determine the direction of upwinding. Several methods can be applied, two general approaches for an arbitrary direction of the characteristics are the flux vector splitting and the flux difference scheme and for each approach several methods are in existence. For the present case the Steger-Warming scheme, the Roe scheme and the Kurganov-Tadmor scheme will be considered. The Steger-Warming scheme because it is applied with success to the integral boundary layer equations by Matsushita and Akamatsu[90]. The Roe-scheme because it is well known from gasdynamics to be accurate near discontinuities, also it is likely to produce less numerical diffusion than the Steger-Warming scheme. The Steger-Warming scheme is an FDM to solve hyperbolic conservation laws, the Roe scheme is known as an approximate FVM Riemann

solver with the original intent to solve the Euler equations. The Kurganov-Tadmor finite volume scheme is added because of it's relative simplicity. For the DG approach one is free to choose either the Roe-scheme or the Kurganov-Tadmor scheme.

In addition several scalar(-based) FDM's are implemented.

More on the numerical procedure can be found in section (6).

5.1.2 Method of Lines

Before a numerical method can be defined a general approach has to be outlined. The general approach to solve the system of equations is the method of lines. The method of lines treats all but one dimension in a discrete manner which results in a semi-discrete approach.

Using the method of lines Swafford and Whitfield[131],[129] solve the system

$$A\frac{\partial f}{\partial t} + B\frac{\partial f}{\partial x} = C,$$

which in their case is written as

$$A\frac{\partial f}{\partial t} = b, \quad b = C - B\frac{\partial f}{\partial x},$$

where the right-hand-side vector contain the spatial derivatives. In this thesis, the system is written as

$$\frac{\partial f}{\partial t} = b, \quad b = L - K\frac{\partial f}{\partial x},$$

An important aspect is that the temporal integration is separated from the spatial integration , this allows for more flexibility in the choice of a temporal and spatial integrator. Also important, the method of lines allows for a vector-based implementation. For the time-integration a one to fourth order Runge-Kutta method will be implemented. A Runge-Kutta integration with adaptive timestep is possible (e.g. Runge-Kutta-Fehlberg) but requires at least ten evaluations of the spatial difference vector. It was noted by Swafford and Whitfield[131] that applying the CFL condition already provided the necessary stability, therefore the adaptive Runge-Kutta method is not considered for this thesis.

Using the method of lines, the approach is as follows, initially the entire profile is considered laminar, the relevant closure models are then applied using the initial values for the primary variables, now given the initial distribution the turbulence transition point is detected, the current timestep is redone for the transition/turbulent region of the profile and finally the values at the next timelevel are found through integration. For the following timesteps a similar procedure is followed, however (see figure(5.1)). The transition model by Drela[35] is based on the Falkner-Skan equation which is steady, this means that each consideration of the transition takes place with no reflection of the history of the transition point. The treatment of the transition point underlines that the assumption of a fully turbulent boundary layer is perhaps not only physically more robust but it will also simplify the computation. For the test cases both a transition check will be used as well as an assumed fully laminar and fully turbulent boundary layer.

5.1.3 Physical Interpretation of Hyperbolicity

The equations from which the integral boundary layer originate are parabolic which means that the single eigenvalue is directly dependent on time, any change in the outer conditions propagates in the normal direction through a diffusive process and the change in the tangential direction is propagated through a convection process. Now

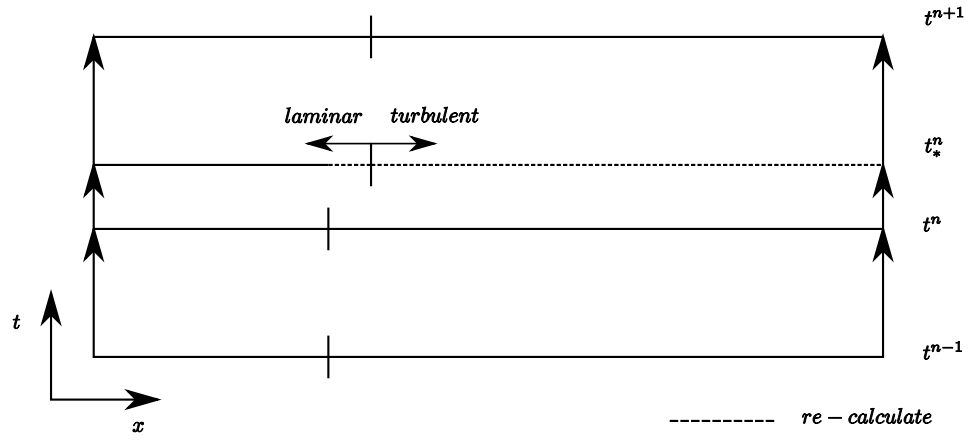

Figure 5.1: Algorithmic logic for moving transition point

if the y-dependent differential terms are removed a one-dimensional (non-linear) convection equation is yielded, similar to the equation in section (5.4), which is hyperbolic. The integration of the diffusion term in the boundary layer equation results in a first order dependency, i.e. the advection in space-time is the direct result of the integration of the second order diffusion term. This is effectively what happens in constructing the integral boundary layer equations. To construct the integral equations the y-dependency[1] is removed from the differential terms, now through pre-multiplication with suitable variables a set of differential equations is obtained with different factors but with unchanged differential order, not surprisingly the resulting system is purely convective in nature. Heuristically the hyperbolicity of the system is a direct result of the hyperbolicity of the initial field form in case y-dependency is removed.

Physically the hyperbolicity of the integral boundary layer equations relates to the convection of disturbances, in the two dimensional field form of the boundary layer equations this is simply a change in tangential velocity which is convected downstream and for the integral boundary layer equations this relates to the less intuitive integral variables which change as a result of the change in distribution $u(y)$ upstream.

A practical proof comes from the instantaneously moved semi-infinite flat plate; the solution domain has separate regions based on the signal transfer from the disturbance at the plate nose, based on the value of $\frac{u_e t}{x}$ as would be expected since the speed with which the disturbance propagates should be equal to the eigenvalue (see Lighthill[84], Stewartson[126], Smith[124], Riley[112]) which is u_e initially.

5.2 Initialisation and Boundary Conditions

A crucial step in any numerical simulation is the definition of the boundary conditions and the initialisation of the numerical solution, these will be treated separately.

5.2.1 Initialisation

The previous treatment of the initialisation was based on a steady formulation of the IBL equations and required a special treatment to get the shape factors and integral variables at the most forward point. This difficulty was caused in part by the fact that a steady solution implicitly assumes the boundary layer to have been developed already.

[1] More general would be; the profile normal dependency

The unsteady solution simply starts at the point where there is no boundary layer whatsoever, this simplifies the initialisation. This is not trivial as the shape factors are non-zero regardless of the zero-valued integral variables, the shape factors will require a separate treatment.
A full Dirichlet approach may be suitable for the initial step, depending on the coefficient matrices. In case the coefficient matrices rely heavily on the shape factors the steady solution approach is more suitable compared to a Dirichlet approach since the shape factors will be non-zero instantaneously, then any isolated integral variables may be set to zero. The former is the case with the solution methods presented earlier (Drela, Hayasi, etc.).

As an example consider the method by Hayasi, see equation (4.10). First it is assumed that the integral variable $Z = \frac{\theta^2}{\nu}$ is zero, then if the stagnation point is fixed in space $\frac{\partial u_e}{\partial t}$ can be set to zero also and the following equation emerges

$$H^* (H + 1) P = HQ,$$

the above leads to an equations from with γ as the only variable, once γ has been retrieved the eigenvalues and eigenvectors are known and the solution can be started.
Matsushita and Akamatsu[90] assume for an impulsively started cyilinder that initially there is a boundary layer of the Rayleigh type which effectively means that each point on the cylinder is considered to be a point on an infinitely long impulsively moved flat plate (also see Cebeci and Bradshaw[20] and Cowley[31]). For small time this is probably a good approximation since the variance of the external velocity in spatial direction has not yet influenced the neighboring points, i.e. all convective terms are negligible. The initial time-step has to be chosen such that the information of the grid points upstream has not yet reached the local grid point (also see Lighthill[84]). From the field form of the conservative boundary layer equation it can be seen that for small t the equation behaves like a diffusion equation since $u \ll 1$ and therefore $\frac{\partial^2 u}{\partial y^2} \sim \frac{\partial u}{\partial t} \gg u\frac{\partial u}{\partial x}$ (also see Cowley[31], Telionis and Tsahalis[134]). Also, this flat-plate assumption is (obviously) limited to profiles with a negligible curvature $\frac{\partial r}{\partial x} \ll 1$. Ideally the velocity gradient in time is also taken into account with the initialisation, this can be done with Duhamel's folding integral (see equation (I.33), however this function is very cumbersome to solve and requires the external velocity at two points in time. If Rayleigh's solution (see equation (I.32) for the instantaneously moving infinite flat plate is used, the initial values for the boundary layer velocity follow from

$$u(x, y, t) = u_e(x, t)\text{erf}(\eta), \quad \eta = \frac{y}{2\sqrt{\nu\Delta t}}.$$

For $\eta = 1.83$ the boundary layer velocity is 99% of the external velocity, hence y can be limited to $[0, 3.66\sqrt{\nu\Delta t}]$, where the initial timestep Δt follows from the requirement that for each point on the profile $\Delta t u_e(x, 0) < \Delta x$. Applying the definition for the displacement thickness with the error function gives

$$\delta^* = \delta - \frac{1}{\sqrt{\pi}}\sqrt{\Delta t\nu}\left[-2 + 2\exp\left(-\frac{1}{4\Delta t\nu}\delta^2\right) + \frac{1}{\sqrt{\Delta t\nu}}\delta\sqrt{\pi}erf\left(\frac{1}{2\sqrt{\Delta t\nu}}\delta\right)\right], \quad \delta = 3.66\sqrt{\nu\Delta t}$$

unfortunately no explicit integral was found for the momentum thickness, applying the 11^{th} order polynomial fit that was also used for the Timman profile leads to an extremely cumbersome expression so a 4^{th} order polynomial fit is chosen which is almost completely within plotting accuracy.

The initialisation using the Rayleigh solution assumes some instantaneously moving profile which would be the case for most applications. A true zero initialisation, where the profile is assumed static initially, would lead to the added difficulty of plate wise zero divisions and it begs to differ whether the integral boundary layer equations would produce meaningful results for near zero velocities (and thus very low Reynolds numbers).

Cousteix and Houdeville[30] discuss the unsteady boundary layer and IBL equations in relation to unsteady turbulent flow and suggest to use a steady solution as the initialisation. Cousteix and Houdeville also raise the point that for oscillating airfoils the stagnation point will change position, for low reduced frequencies they suggest to use a quasi-steady value, otherwise they use experimental data to extract a boundary condition, for more detailed solutions Cousteix and Houdeville refer to a paper by Cebeci and Carr[21]. Hall et al[58] apply a similarity solution from Cebeci and Bradshaw[19] to relate the stagnation displacement thickness to the edge velocity.

5.2.2 Boundary Conditions

The eigenvectors indicate the direction in which perturbations are propagated into the solution domain, that being said; if the incoming characteristics are initialised the problem is fully defined and thus the outgoing characteristics do not need to be defined at the flow exit, conversely the solution is insensitive to the value at the outer bound. The value of the incoming characteristic is determined by the stagnation value. A useful assumption is to consider the forward stagnation value to be instantaneously equal to the steady stagnation value. This can be justified by considering that the stagnation point is the immediate and local representation of the stagnation flow upstream. With this assumption the approach to approximate the stagnation point value for the steady case can be directly applied to the unsteady case. A problem arises when this BC is applied; since the initial values of the profile are independent of the boundary value, thus at the boundary, going from the BC to next point on the profile, there is a, possibly very large, flux which is directly dependent on the stepsize. In reference to Cebeci and Bradshaw, Hall et al [58] employ an analytical similarity solution for the initial points. Swafford[130] applies a clamped boundary layer with success, he however sets the initial primary values over the entire profile to be equal to the boundary value, which prevents the initial high flux at the boundary, this is however unphysical and should not be used for transient solutions. Both methods will be implemented.

Specifically, for the stagnation flows the following solutions are implemented

- laminar stagnation value by Nishida[103]
- laminar stagnation value by Milewski[94]
- the first step of Thwaites integral
- turbulent stagnation value by Coenen[26]

and for the flat plat (like) boundary layer flow

- the first step of Thwaites integral, at from $x = 0$ to $x = \Delta x$
- Blasius solution at $x = \Delta x$ for laminar flow
- Rayleigh solution at $x = \Delta x$
- 1/7th power law for turbulent flow at $x = \Delta x$

The boundary condition for the right side of the profile/plate is left open, no solution is imposed there. Thus the boundary value on the right side most follow from the left neighboring points, or more correctly all information needed for the right boundary value comes from the inner solution.

For the specific numerical application of the boundary conditions the reader is referred to chapter (6).

5.3 Stability Considerations

To be able to transport the perturbations through the solution domain it is required that the grid (in time-space) has the correct relative grid size. For more details see section (6.5).A general remark can be made about the stability of the numerical scheme in case an explicit discretisation is used in time; the direction in which the information is carried determines the direction in which the upwind differencing should take place. Suppose that from some point two or more different characteristics are emanated, meaning two or more different information carriers with information about the same point, these characteristics diverge since they travel with different velocities. Since each point emanates these characteristics there are intersections of characteristics, these intersections allow the solution to be solved exactly if the invariants (the initial solutions which are carried with the characteristics) are known. The basic requirement is that given characteristics moving in the positive x-direction, backward-differencing is required to be able to use the correct characteristic information. If forward differencing is used one basically applies information that is physically unavailable. Central differencing will cause wiggles and has a stricter stability requirement, the positive side is that these wiggles directly convey information on the solution quality and there is no artificial diffusion. The FDM flux solvers are basically either upwind differencing schemes or central differencing schemes, the FVM and FEM flux solvers will use a mixed formulation based on the direction of the individual eigenvectors. The characteristics give a first requirement on the grid resolution since it constraints the relative grid size to $\frac{\Delta x}{\Delta t} < \min(\lambda)$, this guarantees that all characteristics have passed the next grid point downstream of the current point. As was said, this applies to explicit time-marching schemes only, if the condition is too restrictive an implicit scheme should be considered. For different time-integration schemes the condition changes based on the stability of the specific time-integration scheme, in general the following applies for the local stability requirement

$$\left(\frac{\Delta t}{\Delta x}\right)_{local} \leq \frac{CFL}{\rho(K)}, \quad \text{spectral radius:} \quad \rho(K) = max(|\lambda|) \tag{5.1}$$

where the CFL-number, after the inventors Courant-Friedrich-Lewy, is dependent on the time-integration scheme. The global stability (in case of a spatially constant time-step) then follows from

$$\frac{\Delta t}{\Delta x} \leq \min\left(\left(\frac{\Delta t}{\Delta x}\right)_{local}\right), \tag{5.2}$$

which will be relatively slow compared to adaptive methods e.g. a local timestep, if the higher gradients are confined locally. The approach is to first determine the distance steps Δx based on the gradients of the integral variables, then base the timestep Δt on the relative grid size requirements stemming from the CFL-condition which has to be based on the specific time-integration scheme.

. It must be kept in mind that the effect of numerical diffusion increases for decreasing relative grid size, therefore the largest possible relative grid size should be applied. Also see Mughal[99] who discusses the region of influence for three-dimensional unsteady boundary layer flow.

Where for the left boundary it was assumed that only the incoming characteristics determine the solution, for the right boundary the same is assumed for the outgoing characteristics. Whereas this approach requires an imposed value for the left boundary condition, the right boundary condition can be left open, the outgoing characteristics simply follow from the solution. To facilitate this open right boundary condition, a backward difference scheme is enforced. This approach is taken by for instance Smith[124] who assumes that information convects downstream for the entire profile.

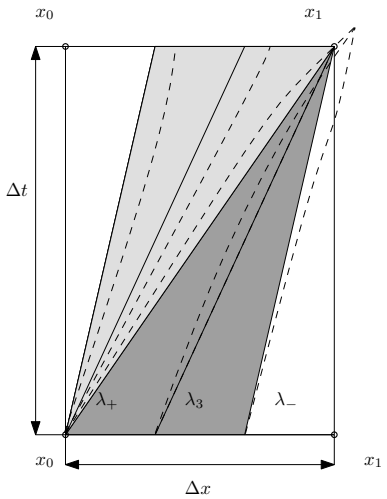

Figure 5.2: Dark area: domain of dependence of x_1 at new time level, Light area: domain of influence of x_0 at old time level, dashed lines indicate actual characteristics which may be curved in $x - t$

5.4 Predicting Separation using Converging Characteristics

As has been confirmed by several writers the convergence of characteristics signals the onset of separation. This can be explained directly by the simple notion that through the coalescence of characteristics there is a discontinuity over which the eigenvalues, and thus the solution, change instantaneously, the coalesced characteristics will be referred to as a shock, a term also used by Shen and Nenni(see Cousteix[28]).

In reference to Shen Matsushita and Akamatsu [90] state that these singularities, i.e. $\frac{\partial \delta^*}{\partial x} \rightarrow \infty$, are reducible to the formation of a shock-like formation of the characteristics.

To predict the formation of a shock and thus the onset of separation, some measure for the coalescence of characteristics is defined as the separation indicator. Depending on whether forward or backward differencing is used the shock indicator I_{sep} in a point in some spatial direction is defined as the difference in characteristic velocity in the direction opposite to the direction of the characteristic , relative to the cell velocity $\frac{\Delta x}{\Delta t}$. For a one-dimensional advection problem this becomes

$$\begin{aligned} \text{a} > 0\text{, backward differencing :} \quad & I_{sep,1D} = \frac{\Delta t}{2\Delta x}\left(a_{j,i-1} - a_{j,i+1}\right), \\ \text{a} < 0\text{, forward differencing :} \quad & I_{sep,1D} = \frac{\Delta t}{2\Delta x}\left(a_{j,i+1} - a_{j,i-1}\right), \end{aligned}$$

where a is the characteristic velocity. Now the critical value for the separation indicator I_{sep} is user dependent. The separation indicator is positive for shocks and negative for expansion fans[2], both can be discriminated from the normal solution merely by the magnitude of the indicator for shocks/expansions relative to the average magnitude of the indicator. The relative shock indicator is denoted as $J_{sep} = \frac{I_{sep}}{\overline{I_{sep}}}$, here $\overline{I_{sep}}$ is based on the values of the previous timestep.
Assuming a finite thickness the discontinuity is strongest perpendicular to the shock, especially in numerical sense since the thickness is at least the size of one distance step. To optimize the separation prediction one can resort to using older values for increasing

[2](centrally) diverging characteristics

speed of the characteristic, effectively increasing the angle with respect to the shock, the downside is that at least two timesteps are required to determine the shock indicator and the detection is off by at least one timestep (see figure 5.3).

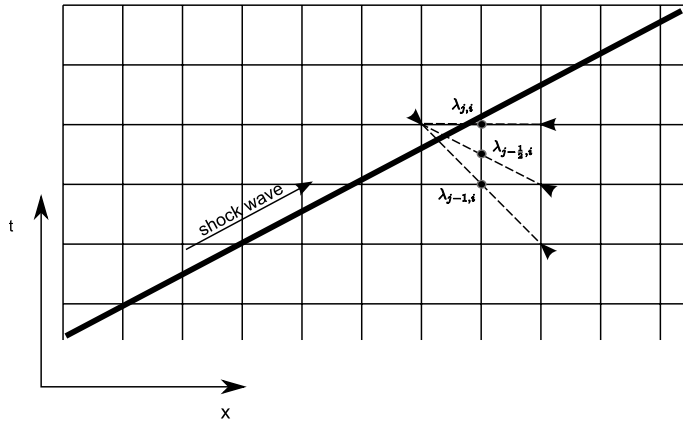

Figure 5.3: Detection of shock using neighbouring eigenvalues

To get an idea of the relative shock indicator value a non-linear one-dimensional advection problem is formulated and solved for a given initial distribution, the initial distribution is then varied to investigate the magnitude of the relative shock indicator. The non-linear one-dimensional advection problem shock indicator is defined by

$$u_t + u\,u_x = 0,$$

and is solved using forward Euler for the time integration and backward differencing for the flux determination. As an initial distribution consider the following

$$\text{Distribution A:} \quad u = \begin{cases} \sin(\pi x), & 0 \le x < 1, \\ 1.5, & 1 \le x < 1.5, \\ \sin(\pi(x-1.5), & 1.5 \le x < 2.5, \\ 1.5, & 2.5 \le x \le 3. \end{cases}$$

$$\text{Distribution B:} \quad u = \begin{cases} x, & 0 \le x < 1, \\ 1.5, & 1 \le x < 2.5, \\ 0.5(x-1.5), & 1.5 \le x < 2.5, \\ 1.5, & 2.5 \le x \le 3. \end{cases}$$

Using the following relation the exact intersection point of the characteristics can be determined for distribution (A)

$$\begin{aligned} t_{shock} &= -\frac{1}{\left(\frac{\partial a}{\partial x}\right)_{min}}, \\ x_{shock} &= t_{shock} a_{\left(\frac{\partial a}{\partial x}\right)_{min}}. \end{aligned} \tag{5.3}$$

See figures (5.4) and (6.10), these figures were produced using 600 elements in x-direction and 400 elements in t-direction. Using equation (5.3) the shocks for velocity distribution (A) should start forming at

$$\begin{aligned} x &= \frac{3}{2\pi} + 1,\ t = \frac{1}{\pi}, \\ x &= \frac{3}{2\pi} + \frac{3}{2},\ t = \frac{1}{\pi}. \end{aligned}$$

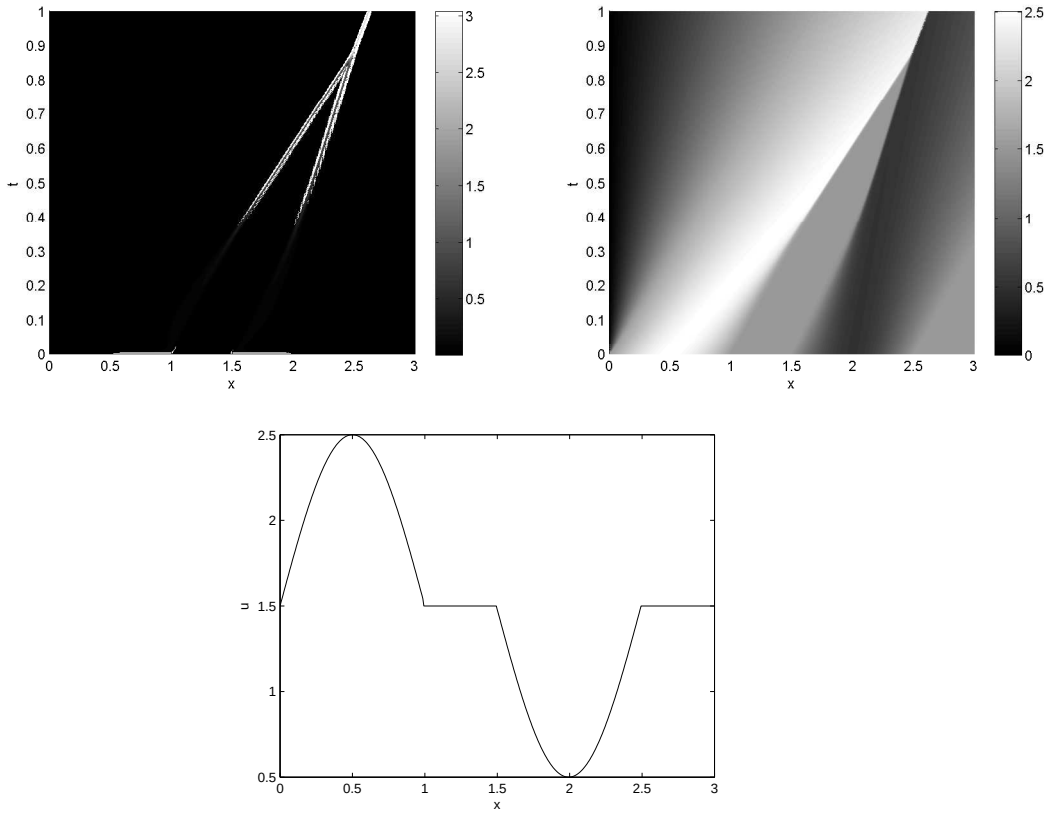

Figure 5.4: non-linear advection equation with double sin velocity distribution, (left) J_{sep} distribution, (right) u distribution, (bottom) initial velocity.

Plotting the separation indicator in the above points the shock is clearly visible, see figure (5.6). It seems that for shocks and expansions the relative magnitude is in the order of at least order ten. The relative shock indicator magnitude is proportional to the perturbation magnitude, To remove this dependency the relative shock indicator can be divided by the max difference in successive eigenvalues, in other words the relative shock indicator is normalized with the jump over the strongest shock. This however leads to an overprediction over the shock strength since normalization has the effect that in time levels with a small maximum velocity gradient in x-direction even small velocity differences appear to be large. A test will have to be done for the final system of integral boundary layer equations using known separation problems to establish typical magnitudes of the separation indicator.

The apparant downside of this approach is that the separation indicator needs to be calculated and stored. For the integral boundary layer equations this becomes in general

$$\begin{aligned} \lambda_{j,i} > 0: \quad J_{sep} &= \frac{\Delta t}{\Delta x}\frac{\lambda_{j,i-1} - \lambda_{j,i+1}}{N\overline{\lambda}}, \\ \lambda_{j,i} < 0: \quad J_{sep} &= \frac{\Delta t}{\Delta x}\frac{\lambda_{j,i+1} - \lambda_{j,i-1}}{N\overline{\lambda}}, \\ \overline{\lambda}_j &= \frac{\sum_{i=1}^{N}\lambda_{j,i}}{N}. \end{aligned} \tag{5.4}$$

Alternatively, instead of dividing by the averaged eigenvalues one can also divide by the

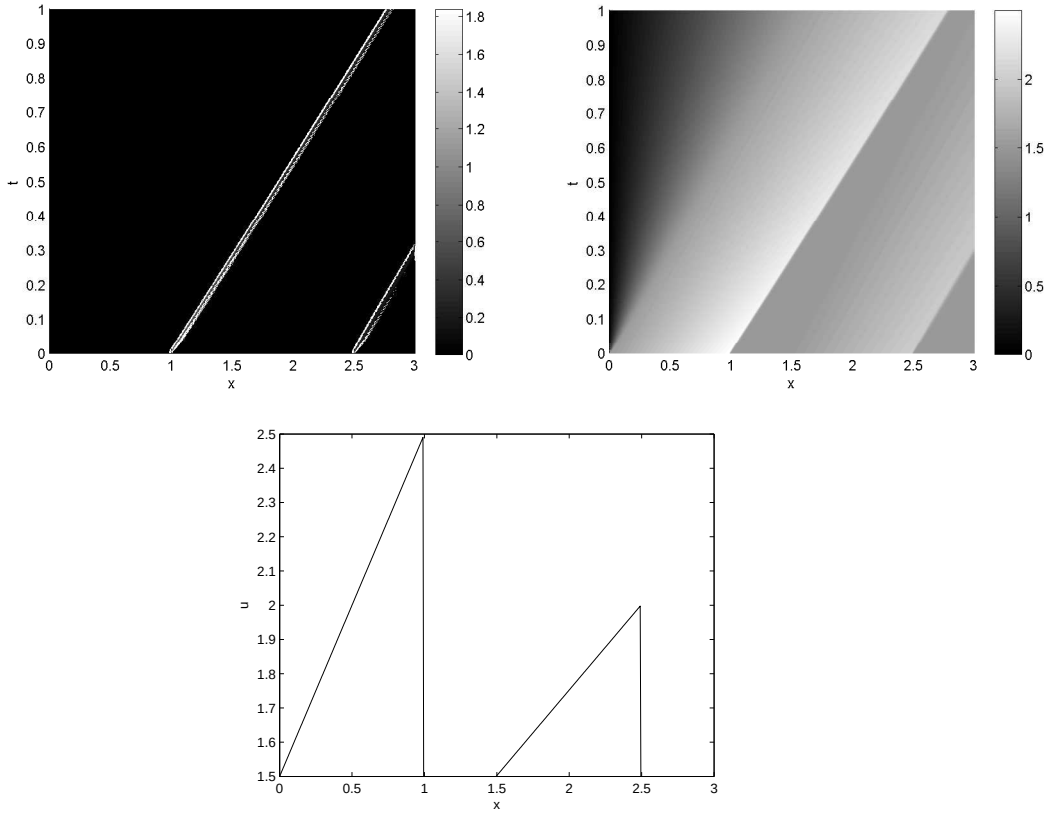

Figure 5.5: non-linear advection equation with double linear velocity distribution, (left) J_{sep} distribution, (right) u distribution, (bottom) initial velocity.

average difference of the eigenvalues, this however cannot detect the presence of shock since the maximum value will be the same for a given problem regardless of any shocks.

According to the triple deck model, the transition to the small scale separation should take place within $\mathcal{O}(Re^{-\frac{3}{8}})\ [m]$ (see i.e. Veldman[145]), this may be an indication of the required resolution to identify separation.

The above described method suffers a flaw, the left boundary will form the first (and maybe the largest) discontinuity for non-stagnation flow due to inevitable mismatching between the boundary value and the inner solution, obfuscating the presence of any discontinuity in the 'inner' solution. For the stagnation flow the separation indicator may form a useful prediction tool.

Alternatively the paths of the characteristics can be monitored and therefore any intersection of characteristics can be predicted, (see figure(5.7). On the same chord one can use the motion of the zero friction point to predict the point of seperation by estimating if and where the zero friction point comes to a halt. The benefit of the current separation indicator is that the strength of the shock is monitored, the next step would be to relate this shock strength to the degree of separation, that is however outside the scope of this thesis.

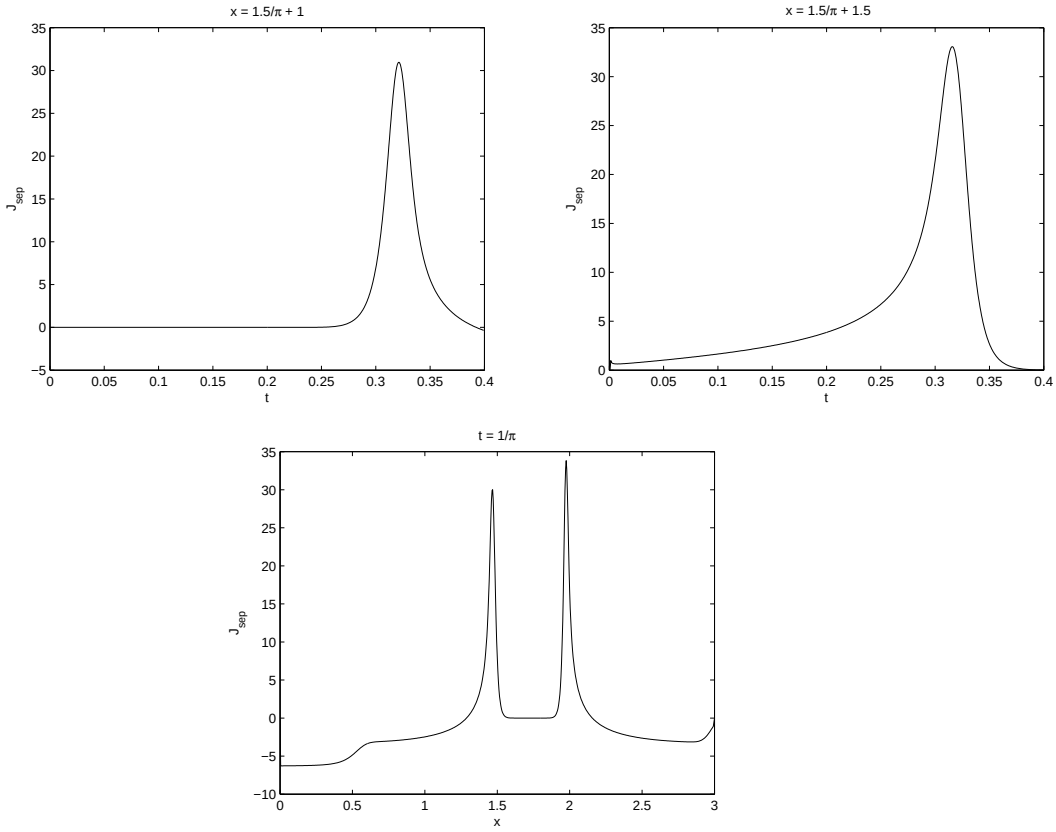

Figure 5.6: J_{sep} distribution for non-linear advection equation with double sin velocity distribution, (left) t, J_{sep} for $x = \frac{3}{2\pi} + 1$, (right) t, J_{sep} for $x = \frac{3}{2\pi} + \frac{3}{2}$,(bottom) x, J_{sep} for $t = \frac{1}{\pi}$.

5.5 Adaptive Grid

The integral boundary layer method is primarily of interest because the reduction of the problem dimension significantly decreases the amount of computations needed to resolve the integral variables. To further optimize the computational efficiency an adaptive grid may be employed. The adaptive grid might be initialised using a uniform spatial grid, subsequently the spatial grid distribution follows from the integral variables in the previous timestep. Only the time step or the distance step can be refined at each time step, whereby the other step size follows directly from the stability requirements. Per time step, because there is nothing preventing an alternating grid adaptation.
The adaptiveness can be global, which relates the new overall step size to the maxima of the space-derivatives so basically a new grid is created at each time step but with the same relative distances, or it can be local where the local space-derivatives determine the step size. The major issue with spatial grid adaptation is that the sum of all the distance steps must be constant, which means that when the grid is refined, more points need to be created and conversely points to be removed if the grid is coarsened. For uniform grids this is trivial and non-uniform grids with global adaptation only require treatment at the edge of the grid. Locally adaptive grids require points to be created and removed from between other points, this is not trivial. Also, for locally adaptive grids there may be the issue of conflicting adaptations between coarsening the grid and

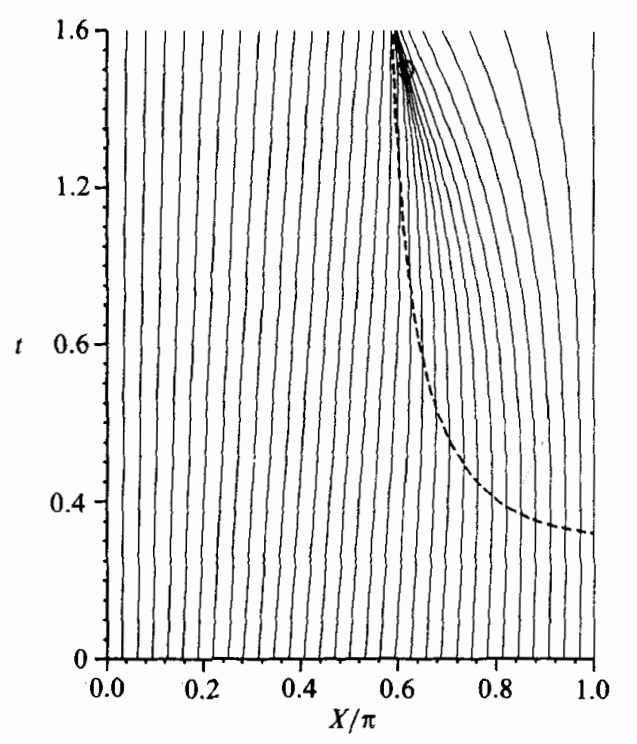

Figure 5.7: Converging characteristics of a quasi-linear IBL system for a flow over a cylinder, see Matsushita [91]

refining the grid. A typical grid refinement correlation is given by

$$\Delta x \propto \left[C_1 \frac{\partial I}{\partial x} \right]_{max}^{m},$$

here C_1, C_2 and m will have to be determined by trial-and-error, I is some integral variable. Conceptually the easiest grid adaptation follows from the use of the local eigenvalues to, given a certain timestep, reconstruct the grid completely. So starting from the left boundary one marches to the right with the distance which follows from the eigenvalue and the timestep. After a new grid is obtained the values of the previous grid is projected onto the current grid. Whether global or local spatial grid adaptation is used interpolation is required to extract the values at the new grid points and thus requires the storage of results over two time steps. Furthermore in the final approach, the IBL equations will be coupled to an external solver which completely defines the grid points over the profile. This means that the IBL result on the refined grid needs to be interpolated again to get the values on the external grid points, i.e. there are two interpolation steps. For these reasons local adaptiveness of the distance step will not be considered for this thesis.

To ensure stability the CFL criterion will be used to determine the required value for the global time step, the global time step at some time level n is given by

$$\Delta t^n \leq \Delta x_{local} \left[\frac{CFL}{|\lambda|_{max}} \right]_{min}^{n}. \tag{5.5}$$

A local time stepping method is completely different from the spatial grid refinement in that there is no need for interpolation while the solution convergence for the IBL equa-

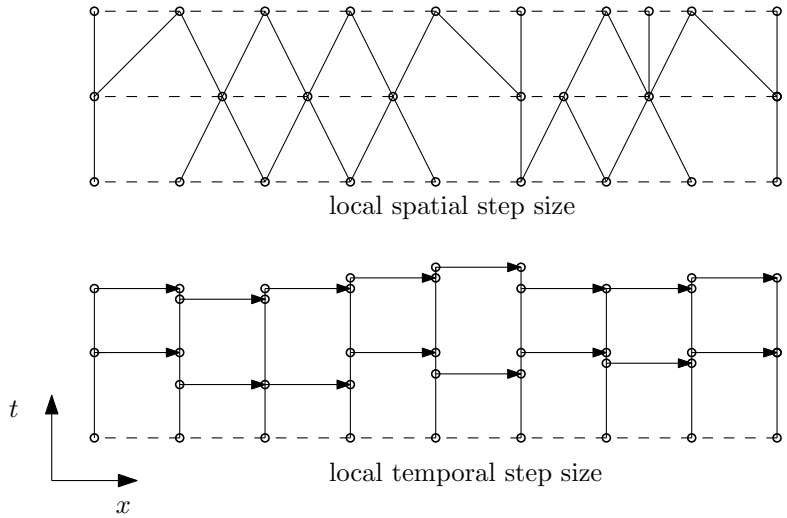

Figure 5.8: One-dimensional grid with local step size

tions is indeed accelerated, see i.e. Swafford[130], Jameson[68]. Local time stepping is however primarily used to accelerate the convergence for problems with a definite steady state solution (see e.g. Anderson et al[4, p.301]) as it produces an unphysical transient solution: each point/cell marches with a local time step, at the next time level the adjacent values are used for the flux although these values represent a different time level thus giving unphysical values for the flux, see e.g. Jameson[68]. To make the local time stepping method physical one may apply extrapolation and interpolation to obtain newer values and intermediate values respectively, however for smooth problems it is questionable whether the added work of finding extrapolated/interpolated values outweighs the gain in performance, not to mention the loss in accuracy due to the extrapolation/interpolation. It is possible to use local time-stepping for transient solutions by means of a space-time method for the DG-FEM, see Klaij[75], Gassner[87] and then naturally also for the FVM since that is basically a DG with zeroeth order basis functions, see section (6.3), for the FDM there is the so-called FDTDM (or finite difference time domain method) but a local time stepping method could not be found.

Whether global or local time stepping is chosen depends on the application. If the IBL equations are to be used in a coupled time-dependent method, as is the case, the transient solution of the IBL equations should be synchronous to the external flow solution. The time steps used to integrate the IBL equations should be smaller than or equal to the time steps used by the external solver but preferably of course the time steps are as close as possible to the time step of the external solver. Assuming that each global time step has preferably only one time step for the IBL equations an implicit time integration scheme must be used if the time step required for the IBL equations is lower than the time step for the external solver.

Local Order Refinement

The purpose of local order refinement is that local higher order phenomena in the problem are captured more accurately without increasing the number of grid points. This prevents the need for interpolation/extrapolation as is required for an adaptive spatial grid.
The downside of the finite difference method and the finite volume method is that to increase the order of accuracy the stencil size needs to be increased. Which means that the approximation of the flux through/over a point/cell requires information from

more neighboring points/volumes. Also, higher order finite difference and finite volume schemes cannot be arbitrarily generated, they need to be hard coded.
For the DG method local order refinement is straightforward since each control volume has their own order of accuracy which is given by the maximum (polynomial) order of the basis function, this is described in section (6.7.2).

5.6 Extensions

The IBL equations can be extended, firstly of course by adding a dimension, secondly by adding physical effects which are related to the three-dimensionality and thirdly by adding effects related to the specific problem that is considered.

5.6.1 Three Dimensionality

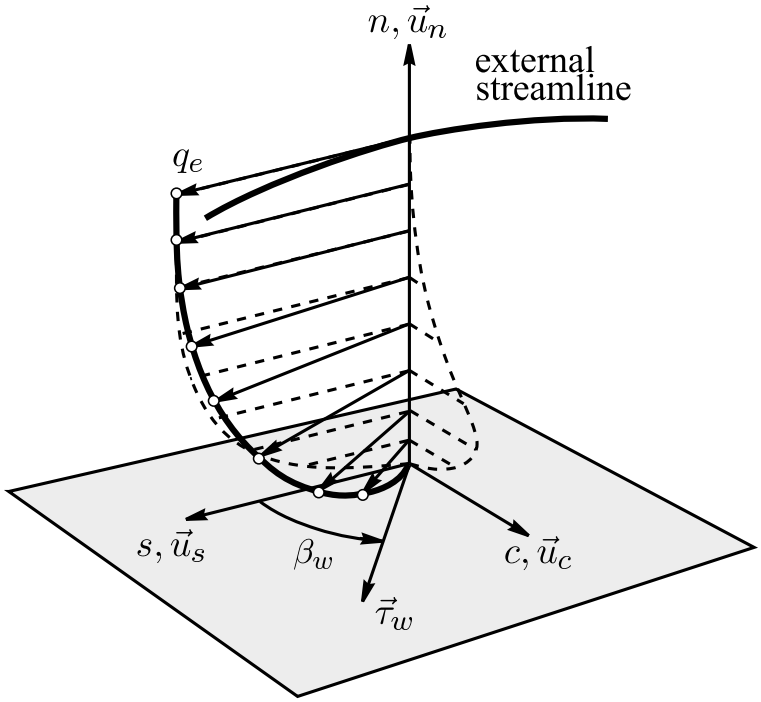

Figure 5.9: three dimensional boundary layer

Going from two to three dimensions requires the addition of one momentum equation and extra differential terms to account for the added dimension, see e.g. Mughal[99].Also, the closure relations have to account for the effect of crossflow effects, for negligible cross flow two-dimensional behavior is assumed in stream wise direction[99]. The detection of separation and transition becomes more complex, whereas for two dimensions there is a point of separation and a point of transition three dimensions requires the consideration of a separation and transition line. Often transition is assumed after a small percentage of the chord length, then a transition line is imposed on the solution, this is forced transition. Natural transition through transition detection requires the consideration of the direction in which the transition occurs. For separation coalesc-

ing streamlines can form a separation line which should be comparable to the lines of vanishing wall shear stress[3].

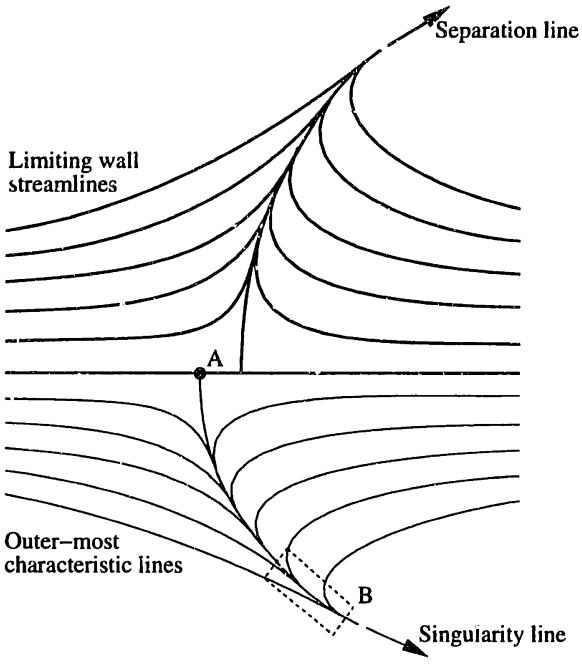

Figure 5.10: The separation line is determined by the coalescing streamlines, see Mughal[99]

[3]for the steady case coalesced streamlines and lines of vanishing wall shear stress should coincide

5.6.2 Addition of Body Forces for Wind Turbines

To apply the two-dimensional system to an inherently three dimensional problem like a rotating profile the most important added forces should be incorporated somehow. Assuming a quasi-steady rotational velocity and a rigid blade the centrifugal force follows directly from the radius and the rotational velocity of the blade.

$$\rho \overline{f}_1 = -\rho \overline{\Omega} \times \left(\overline{\Omega} \times \overline{r} \right). \tag{5.6}$$

Given the centrifugal force, there will be an induced crossflow which in turn will induce a Coriolis force, which directly affects the effective pressure gradient over the profile in chordwise direction.

$$\rho \overline{f}_2 = -2\rho \left(\overline{\Omega} \times \overline{u} \right). \tag{5.7}$$

A contribution for the case of a HAWT(Horizontal Axis Wind Turbine) rotor is the periodically changing direction of gravity which directly influences the magnitude of the pressure gradient in chordwise direction and thus acts to enforce/counteract the centrifugal force and the Coriolis force depending on the azimuth angle of the blade. Suppose the magnitude of the gravitational acceleration is only dependent on time and the frequency with which the blade rotates, then assuming the rotation frequency is constant

$$f_{grav} = \pm g_0 \sin(\omega t)$$

Where the sign depends on the rotation direction and the direction of the axes in three dimensions, for the present two dimensional case the sign will be assumed positive. This term can easily be added to the integral equations since it is independent of the boundary layer thickness. Unfortunately this requires an alteration of the two and three equations models that have been presented earlier, however this will not affect the characteristics of the problem formulation, i.e. the hyperbolicity is unaffected since the gravity term is not dependent on the primary variables. The time dependent force term due to gravity can also be added to the field form of the boundary layer equations which allows for a numerical reference result

If the time-dependency of the angular velocity is considered an extra force vector is added namely

$$\rho \overline{f}_3 = -\rho \frac{\partial \overline{\Omega}}{\partial t} \times \overline{r}, \tag{5.8}$$

which will also not affect the hyperbolicity directly. Finally, in case three-dimensional boundary layer flow is considered the twist of the blade in radial direction will induce a crossflow component. Whereas the body forces are easily added as they do not affect the integral formulation, the profile induced crossflow requires special closure relations, i.e. due to Stock for laminar and Mager or Johnston for turbulent boundary layer (see Van Garrel[52]). The closure models for the crossflow are however based on flows over rotationally static profiles (i.e. conventional aircraft wings, flat plates etcetera), a dedicated closure model for windturbines, with significant contributions of the above mentioned fictitious forces, has yet to be derived. The separation point is slightly delayed due to rotational effects, mostly because of the effect of the centrifugal force and the coriolis force (see e.g. Du and Selig[42], [41]). Some clues may be derived from early experiments with rotating discs with laminar boundary layer flow (see e.g. Banks and Gadd [9]), or from numerical tests (see e.g. Miller[95]), however more research is needed to determine a complete set of closure relations which incorporate all the rotational effects.

5.6.3 Compressibility

Drela devised a correction term for the varying density based on the Mach number, this correction can be readily substituted in the current formulation (see Drela [35],

Sekar[120] in reference to Drela and Giles, and Wolles). The correction enters the system of equations through an extra shapefactor. In case the compressibility becomes negligible the extra shapefactor becomes equal to the shapefactor for incompressible flow and the extra terms in the partial differential equations drop out or become unity, this ensures a continuous solution and avoids the need for extra logic.

5.6.4 Effects on Hyperbolicity

The addition of cross flow, the Coriolis force and compressibility will affect the hyperbolicity of the IBL equations. To evaluate the effect a three dimensional boundary layer flow is assumed with the addition of fictitious body forces and crossflow. Compressibility is considered negligible since the Mach number will be at most ~ 0.3 and only near the edge of the rotor blade. Starting with the two-dimensional IBL equations one can already introduce the fictitious forces assuming a given radius, rotational speed and crossflow velocity, this is done in RFOIL for the steady case using the chord/radius ratio.
As said, only the cross flow and the Coriolis force directly affect the hyperbolicity, however the fictitious forces will likely also affect the hyperbolicity indirectly through a contribution to the closure relations. Again, this will have to be investigated further through numerical or experimental studies.

Chapter 6

Description of Numerical Methods

Using an finite difference method (FDM) for a three-dimensional boundary layer might come at premium cost compared to the finite volume method (FVM) and the finite element method (FEM) to account for the grid transformation and the cross flow angle. Furthermore, the fact that the differential equations need to be adapted to accommodate the local geometry requires on the fly changes in the code and finally certain transformation terms in the differential equations might grow excessively large for large angles. In general the following qualitative statements can be made

- FDM
  - – Conservation is not maintained automatically
  - – Limited to smooth shapes
  - – Higher order requires increase of resolution
  - + easy to implement for simple geometries
- FVM
  - – Higher order requires increase of resolution
  - – difficult to apply to three dimensional geometries in order higher than two
  - + Conservation is maintained
  - + easy to implement for simple geometries
- FEM
  - – Ill-formed formed matrices
  - – Selection of weight functions
  - + Conservation is maintained
  - + Can handle complex geometries
  - + Order can be increased more easily

All presented numerical methods use the method of lines and the time integration will be done explicitly using a one to fourth order Runge-Kutta scheme, see section (5.1.2). For stability of higher order schemes smoothing may be applied and/or a so-called flux/slope limiter. For expediency the methods will be described using a uniform spatial grid. The flux/slope limiter basically selects and/or modifies the fluxes at the cell faces in order to preserve monotonicity. The method is only suitable for the FVM and FEM, FDM may require smoothing for the central difference schemes(see Swafford[128]). For the FVM and FEM A so-called Total Variation Diminishing(or TVD) scheme for the

spatial discretisation combined with a TVD preserving Runge-Kutta temporal scheme (or Strong Stability Preserving-RK) should lead to a suppression of wiggles or spurious modes (see e.g. Hesthaven[64],Cockburn[25] or Naber[101]), this should take away the need for smoothing. Following Cockburn and Shu, Naber employs a minmod limiter in combination with the SSP-RK integration to preserve monotonicity. The higher order flux discretisations for the FVM and FEM can be found through Monotone Upwind Schemes for Conservation Laws (or MUSCL), see Hesthaven[64],Cockburn[25]. Starting with the FDM the basics of numerical approximations will be discussed, then naturally followed by the FVM and finally the FEM followed by a discussion on the time integration and stability considerations.

For the FDM's the non-conservative system is used, see system (4.4). For the FVM's and the FEM the conservative system should be used, see system (4.18).

6.1 Finite Difference Method

The discretisation methods will be elaborated for the following exemplary non-conservative partial differential equation (PDE)

$$F_t + KF_x,$$

which should not be confused with the quasi-linear form of the conservative PDE's.

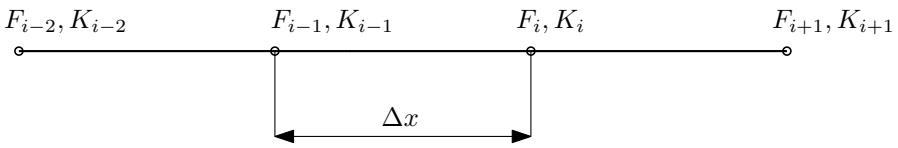

Figure 6.1: Representation of discretision for the FDM

6.1.1 General Descriptions

The first and most obvious way to discretise the differential equation is to consider numerical approximations of the differential terms e.g. using Taylor expansions. Consider the expansions around the point x

$$\begin{aligned}
F(x+\Delta x) &= F(x) + \Delta x\frac{dF}{dx} + \frac{\Delta x^2}{2}\frac{d^2F}{dx^2} + \mathcal{O}(\Delta x^3),\\
F(x-\Delta x) &= F(x) - \Delta x\frac{dF}{dx} + \frac{\Delta x^2}{2}\frac{d^2F}{dx^2} + \mathcal{O}(\Delta x^3),\\
&\vdots\\
F(x\pm n\Delta x) &= F(x) \pm n\Delta x\frac{dF}{dx} + n^2\frac{\Delta x^2}{2}\frac{d^2F}{dx^2} + \mathcal{O}(n^3\Delta x^3),
\end{aligned}$$

with combinations of these approximations the differential terms $\frac{d^nF}{dx^n}$ can be approximated to various orders of accuracy. Using more points and higher order expansions higher order approximations can be found for the differential terms. The approximation is consistent if in the limit $\Delta x \to 0$ it becomes equal to the exact differential terms. This consistency holds surrounding the nodal points at which the differential equations are considered. Many combinations are possible to obtain different schemes, the following well known finite difference schemes are implemented

- First, Second, Third order upwinding and Quadratic Upstream Interpolation for Convective Kinematics(QUICK)

- Second and Fourth order central differencing
- single step Lax-Wendroff scheme and MacCormack scheme

First, Second, Third order Upwinding and QUICK Differencing Schemes

An important (and wellknown) downside of using upwinding is the introduction of artificial diffusion; in upwind discretisation the neighboring nodes are used with directional bias, this asymmetry causes the first even differential term (i.e. $\frac{\partial^2 F}{\partial x^2}$) to be present in the approximation for the first order differential term (i.e. $\frac{\partial F}{\partial x}$). The importance of this first even differential term is directly dependent on the grid resolution, the importance decreases for increasing order of upwinding. The asymmetry (i.e. the directional bias) is also present due to the forward explicit time integration.

If one has to solve for problems with a very small timestep the distance step is necessarily lowered to prevent artificial diffusion from polluting the solution, i.e. the CFL-number is maintained (see sections (5.3), (6.5)). This however requires a very fine grid to be solved for very small time steps. Inversely, given a spatial discretisation the time step is limited due to stability considerations.

In case of central differencing the artificial diffusion is not present and the distance step size Δx can be maintained (lowering the CFL number) without the addition of diffusion or any other even order effect. However odd order effects remain present for central differencing and it is clear that for hyperbolic problems upwind differencing produces more stable solutions provided that the direction of upwinding corresponds roughly with the average direction of the characteristics, see the next section. The first order upwind differencing scheme is written as

$$\text{Forward differencing: a<0} \quad F_x = \frac{F_{i+1} - F_i}{\Delta x} + \mathcal{O}(\Delta x^2),$$
$$\text{Backward differencing: a>0} \quad F_x = \frac{F_i - F_{i-1}}{\Delta x} + \mathcal{O}(\Delta x^2),$$

and a popular second order upwind differencing scheme is given by

$$\text{Forward differencing} \quad F_x = \frac{-F_{i+2} + 4F_{i+1} - 3F_i}{2\Delta x} + \mathcal{O}(\Delta x^3),$$
$$\text{Backward differencing} \quad F_x = \frac{F_{i-2} - 4F_{i-1} + 3F_i}{2\Delta x} + \mathcal{O}(\Delta x^3).$$

The above choice between forward and backward differencing is implemented with a switch which uses the sign function to discriminate between the predominant direction of the information flow. Predominant because for this thesis a system is solved with not one but three directions in which information travels. The predominant direction for this thesis is determined simply by considering the sign of the averaged eigenvalue[1]. Alternatively one can choose the sign of the largest eigenvalue, then the overall direction of information travel is assumed to be equal to the direction of the characteristic which accompanies the largest eigenvalue.

When the characteristics do not travel in the same direction selecting one direction of upwinding will effectively cause downwind discretisation for one or more of the characteristics. Since downwind discretisation is unconditionally unstable stability issues are expected for upwind differencing. This may not be a problem if the downwind discretisation takes places for the characteristic which has a relatively small eigenvalue.

$$\text{Forward differencing:} \quad \frac{1}{2}\left[1 - sign(\lambda_{i,max})\right]\Delta_x,$$
$$\text{Backward differencing:} \quad \frac{1}{2}\left[1 + sign(\lambda_{i,max})\right]\nabla_x,$$

[1] i.e. the sign of the sum of the eigenvalues

where Δ_x and ∇_x are commonly used to denote the forward and backward differencing operator respectively.

In the absence of diffusion the central differencing scheme is prone to oscillatory behavior due to odd-even decoupling, to alleviate this a discretised third derivative is added to the solution, see e.g. Gerritsma[53]

$$\begin{aligned} \text{Forward: K<0} \quad F_x &= \frac{F_{i+1} - F_{i-1}}{2\Delta x} - \lambda \frac{F_{i-1} - 3F_i + 3F_{i+1} - F_{i+2}}{\Delta x} + \tau, \\ \text{Backward: K>0} \quad F_x &= \frac{F_{i+1} - F_{i-1}}{2\Delta x} - \lambda \frac{F_{i+1} - 3F_i + 3F_{i-1} - F_{i-2}}{\Delta x} + \tau. \end{aligned}$$

where

$$\tau = \Delta x^2 \left(\lambda - \frac{1}{6} \right) \frac{\partial^3 u}{\partial x^3} + \mathcal{O}(\Delta x^4).$$

now depending on the value of λ different schemes emerge, $\lambda = \frac{1}{6}$ gives a third order upwind discretisation and $\lambda = \frac{1}{8}$ gives the QUICK scheme which, if applied to a FVM would amount to upwind/downwind quadratic interpolation for the face values.

Second and Fourth Order Central Differencing Schemes

Previously the differential term $\frac{\partial F}{\partial x}$ was approximated by taking the nodes predominantly in one direction based on the sign of the average eigenvalue. For central differencing schemes no such distinction is made, the neighboring nodes are used equally, this reduces the spatial numerical diffusion. However, the forward differencing in time indirectly causes negative diffusion and this negative diffusion term causes errors to growth unbounded, the forward in time, central in space scheme is unconditionally unstable (see Gerritsma[53]). For this reason smoothing or added artificial diffusion is usually required to maintain stability. The second order accurate central differencing scheme is given by

$$F_x = \frac{F_{i+1} - F_{i-1}}{2\Delta x} + \mathcal{O}(\Delta x^3),$$

and for the fourth order central differencing, from Veldman[143]

$$F_x = \frac{-F_{i+2} + 8F_{i+1} - 8F_{i-1} + F_{i-2}}{24\Delta x} + \mathcal{O}(\Delta x^5).$$

Lax-Friedrich, Single step Lax-Wendroff and MacCormack Difference Schemes

The differencing schemes to be discussed now are basically of mixed composition in that they combine upwinding, central differencing and multiple time steps, to obtain better properties in terms of accuracy and/or stability.

As said the forward in time central in space schemes are unconditionally unstable, one way to solve this is to add artifical diffusion which is done for the Lax-Friedrich scheme and the Lax-Wendroff scheme. The Lax-Friedrich scheme adds the following diffusion term to the central differencing scheme

$$\frac{\Delta x^2}{2\Delta t} \frac{F_{i+1} - 2F_i + F_{i-1}}{\Delta x^2}.$$

For the single step Lax-Wendroff scheme a different diffusion term is added. Originally the Lax-Wendroff scheme is meant for scalar advection equations, this scalar value can be approximated by the spectral radius of the coefficient matrix which gives

$$\rho^2(K) \frac{\Delta t}{2\Delta x^2} \frac{F_{i+1} - 2F_i + F_{i-1}}{\Delta x^2},$$

where $\rho(K)$ is the spectral radius of the (Jacobian) coefficient matrix K, alternatively the full coefficient matrix K can be used which gives a matrix-vector multiplication.

The MacCormack scheme consists of two steps, namely a predictor and a corrector step, the predictor step uses either forward or backward differencing and the corrector step uses the opposite scheme. For this thesis a method of lines approach is taken so a semi-discrete formulation is used.

$$\text{Predictor, forward:} \quad \frac{\partial F}{\partial t} = -\frac{K}{\Delta x}(F_{i+1} - F_i) + L, \quad \rightarrow F^{\overline{n+1}},$$
$$\text{Corrector, backward:} \quad \frac{\partial F}{\partial t} = -\frac{K}{2\Delta x}(F_i^{\overline{n+1}} - F_{i-1}^{\overline{n+1}}) + \frac{L}{2}, \quad \rightarrow F^{\overline{\overline{n+1}}},$$

The next time step is then given by

$$F^{n+1} = F^{\overline{\overline{n+1}}} + F^n - \frac{F^{\overline{n+1}}}{2}.$$

In the current implementation the MacCormack scheme can be part of a higher order Runge-Kutta time integration.

Steger-Warming Flux Vector Splitting Scheme

Matsushita and Akamatsu[90] use a second order differencing scheme applied to a set of conservative IBL equations

$$F_t + f_x = L,$$

The approach of Matsushita and Akamatsu consists of two distinct parts, one being the first order scheme and the other the required extension to obtain second order differencing. For the Steger-Warming scheme the left and the right flux are split in a positive and a negative direction and what results is basically an eigenvalue based upwind scheme. The first order differencing scheme is defined by

$$F_i^{\overline{n+1}} = F_i^n - \frac{\Delta t}{\Delta x}\left(f_i^{+,n} - f_{i-1}^{+,n} + f_{i+1}^{-,n} - f_i^{-,n}\right) + \Delta t L_i^n,$$

The second order differencing scheme is then defined by

$$\begin{aligned} F_i^{n+1} = \frac{1}{2}\left(F_i^n + F_i^{\overline{n+1}}\right) \\ - \frac{\Delta t}{2\Delta x}\Big[f_i^{+,n} - 2f_{i-1}^{+,n} + f_{i-2}^{+,n} - f_i^{-,n} + 2f_{i+1}^{-,n} - f_{i+2}^{-,n} \\ + f_i^{+,\overline{n+1}} - f_{i-1}^{+,\overline{n+1}} + f_{i+1}^{-,\overline{n+1}} - f_i^{-,\overline{n+1}}\Big] + \frac{1}{2}\Delta t L_i^{\overline{n+1}}, \end{aligned}$$

where

$$f^{\pm} = K^{\pm} F, \tag{6.1}$$
$$K^{\pm} = M\Lambda^{\pm}M^{-1}, \tag{6.2}$$

with M containing the right-eigenvectors $\xi_{1,2}$ and Λ^+ and Λ^- containing the eigenvalues λ_+ and λ_- which are defined by

$$\lambda_{\pm} = \frac{1}{2}\left(\lambda \pm |\lambda|\right).$$

Note that the overbar values indicate the values at the new timestep of the first order solution. The above scheme is basically a Lax-Wendroff time-step combined with a first and a second order Steger-Warming scheme. Since for this thesis the method of lines is used the time derivative needs to be written explicitly, the first order step is then

$$\left(\frac{\partial F}{\partial t}\right)^{\overline{n}} = -\frac{1}{\Delta x}\left(f_i^{+,n} - f_{i-1}^{+,n} + f_{i+1}^{-,n} - f_i^{-,n}\right) + L_i^n,$$

and the second order scheme

$$\frac{\partial F}{\partial t} = \frac{1}{2}\frac{\partial F^{\overline{n}}}{\partial t} - \frac{1}{2\Delta x}\Big[f_i^{+,n} - 2f_{i-1}^{+,n} + f_{i-2}^{+,n} - f_i^{-,n} + 2f_{i+1}^{-,n} - f_{i+2}^{-,n} + f_i^{+,\overline{n+1}} - f_{i-1}^{+,\overline{n+1}} + f_{i+1}^{-,\overline{n+1}} - f_i^{-,\overline{n+1}}\Big] + \frac{1}{2}L_i^{\overline{n+1}}.$$

If a one-step approach is taken instead of a two-step approach the semi-discrete second order scheme can be written directly as

$$\frac{\partial F}{\partial t} = L_i^n - \frac{1}{2\Delta x}\left(3f_i^{+,n} - 4f_{i-1}^{+,n} + f_{i-2}^{+,n} + 3f_i^{-,n} - 4f_{i+1}^{-,n} + f_{i+2}^{-,n}\right),$$

and analogously, the standard 3^{rd} order scheme is written as

$$\frac{\partial F}{\partial t} = L_i^n - \frac{1}{6\Delta x}\left(3f_i^{+,n} - 6f_{i-1}^{+,n} + f_{i-2}^{+,n} + 2f_{i+1}^{+,n} + 3f_i^{-,n} - 6f_{i+1}^{-,n} + f_{i+2}^{-,n} + 2f_{i-1}^{-,n}\right),$$

which can be added easily since it does not require an increase of the stencil size.

6.1.2 Boundary Conditions

The numerical treatment of the left and the right boundary condition depend on the numerical scheme that is used to approximate the inner solution. For any higher order FD scheme the first step(s) at the left boundary are based on lower order backward schemes of successively higher order accuracy with each next step until the final higher order accuracy is reached, see figure (6.2) For the right boundary a backward differ-

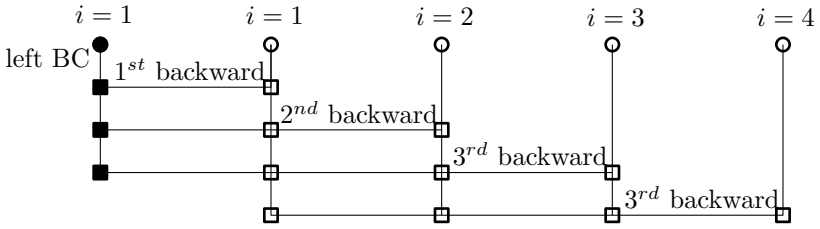

Figure 6.2: Left boundary condition for higher order FDM

encing scheme is used, preferably of the same order as the scheme for the inner approximation. For the Steger-Warming scheme the right BC is left open using backward differencing, although one can also choose to ignore the negative flux vector f^- which represents left travelling characteristics.

6.2 Finite Volume Method

The finite volume discretisation and the finite element discretisation will be elaborated for the following exemplary set of conservative partial differential equations (PDE)

$$F_t + f_x = L,$$

and in quasi-linear form

$$F_t + KF_x = L.$$

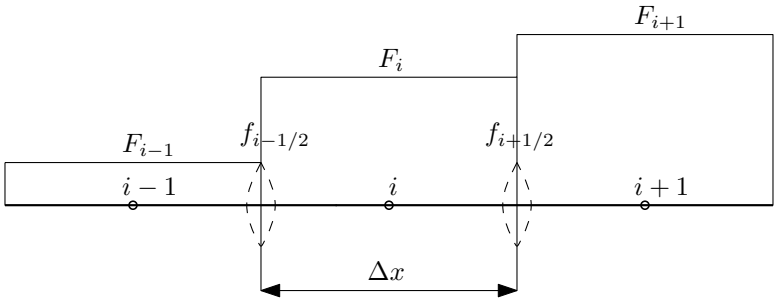

Figure 6.3: Definition of control volumes for the FVM

6.2.1 General Description

The FVM is currently the most popular discretisation method for fluid mechanics due to the relative ease, the intuitiveness of the implementation compared to other method, and the automatic conservation of variables. FVM is considered intuitive because the control volume is physically significant as are the derived conservation relations. In terms of the implementation the FVM's and the FDM's are almost identical for one-dimensional problems, the only appreciable difference is that the FVM's will make use of eigenvalues/eigenvectors of the coefficient matrix K and the flux difference is considered instead of nodal differences as with the FDM's. For the finite volume scheme the domain is divided in non-overlapping control volumes. The conservative form of the differential equations is now integrated over the control volume and rewritten using the divergence theorem

$$\int F_t d\Omega = \int L d\Omega - \oint f \cdot n d\Gamma,$$

which is taken discretely over the control volume. To allow non-zero integration of the

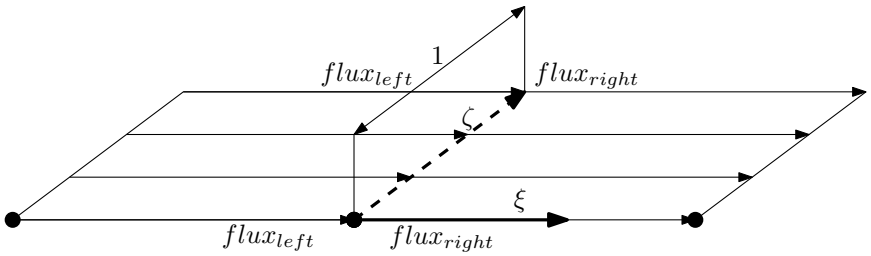

Figure 6.4: Dummy dimension ζ to allow integration

boundary integral a dummy dimension ζ is introduced, the profile will be assumed to be of length one in this direction, see image (6.4). The surface and line integrals for the one dimensional case are simply the length of the one dimensional element and a point respectively, multiplying these with a unit length width gives a surface area and a length respectively. Assuming the solution is piecewise constant per control volume this results for the one-dimensional case in

$$F_t \Delta x = L \Delta x - (f_R - f_L),$$

and the semi-discrete system becomes

$$F_t = L - \frac{1}{\Delta x}(f_R - f_L).$$

The resulting schemes in FVM are based on space and time averaged values, whereas the FDM are based on nodal values, the FEM can use both. Consider the Jacobian of

the conservative system,

$$K_{ij} = \frac{\partial f_i}{\partial F_j},$$

now the flux over the cell faces can be found by integration. Consider the flux over the right face, the flux is estimated first by integrating the Jacobian from the left volume to the right volume

$$\left(\tilde{f}_i\right)_L = (f_i)_L + \int_{F_L}^{F_R} (K_{ij})_L \, dF_j,$$

then from the right to the left volume

$$\left(\tilde{f}_i\right)_R = (f_i)_R - \int_{F_L}^{F_R} (K_{ij})_R \, dF_j,$$

taking a linear approximation for the Jacobian

$$\frac{1}{2}\left[\left(\tilde{f}_i\right)_R + \left(\tilde{f}_i\right)_L\right] = \frac{1}{2}\left((f_i)_L + (f_i)_R\right) - \frac{1}{2}\left((K_{ij})_R - (K_{ij})_L\right)\Delta F_j,$$

which, written in scalars, boils down to the following approximation for the differential term

$$\frac{\partial g}{\partial x} \approx \frac{\Delta(\int_{F_l}^{F_r} K dF)}{\Delta x}.$$

This approximation shows the basic components of the flux difference schemes, the actual flux difference term ΔF_j is used in different way for different flux schemes, one of the most used schemes is the Roe-scheme.

Roe Flux Differencing Scheme

The semi-discrete Roe scheme is written as (see Wesseling[153])

$$\frac{\partial F}{\partial t} = L_i - \frac{1}{\Delta x}\left(f_{i+\frac{1}{2}} - f_{i-\frac{1}{2}}\right),$$

where

$$f_{i\pm\frac{1}{2}} = \frac{1}{2}\left(f_i + f_{i\pm1}\right) - \frac{1}{2}\left|K_{i\pm\frac{1}{2}}\right|\left(\pm F_{i\pm1} \mp F_i\right),$$

and instead of Roe-averaging, the coefficient matrices are initially averaged solely based on the grid spacing

$$K_{i\pm\frac{1}{2}} = \frac{h_i K_{i\pm1} + h_{i\pm1} K_i}{h_i + h_{i\pm1}},$$

or simply $K_{i\pm\frac{1}{2}} = \frac{K_{i\pm1}+K_i}{2}$ for a uniform grid. The requirement that needs to be fulfilled by the Riemann flux is that

$$K_{i\pm\frac{1}{2}}\left(\pm F_{i\pm1} \mp F_i\right) = \pm f_{i\pm1} \mp f_i,$$

suppose the average coefficient matrix is constructed as follows

$$K_{i\pm\frac{1}{2}} = \begin{pmatrix} k_{11}^{\frac{1}{2}} & k_{12}^{\frac{1}{2}} & k_{13}^{\frac{1}{2}} \\ k_{21}^{\frac{1}{2}} & k_{22}^{\frac{1}{2}} & k_{23}^{\frac{1}{2}} \\ k_{31}^{\frac{1}{2}} & k_{32}^{\frac{1}{2}} & k_{33}^{\frac{1}{2}} \end{pmatrix}, \quad K_{i\pm1} = \begin{pmatrix} k_{11}^{\pm1} & k_{12}^{\pm1} & k_{13}^{\pm1} \\ k_{21}^{\pm1} & k_{22}^{\pm1} & k_{23}^{\pm1} \\ k_{31}^{\pm1} & k_{32}^{\pm1} & k_{33}^{\pm1} \end{pmatrix},$$

then based on the requirement each element is given by

$$\begin{aligned} i+\frac{1}{2}: \quad k_{nm}^{\frac{1}{2}} &= \frac{k_{nm}^{+1}F(m)_{i+1} - k_{nm}F(m)_i}{F(m)_{i+1} - F(m)_i}, \\ i-\frac{1}{2}: \quad k_{nm}^{\frac{1}{2}} &= \frac{k_{nm}F(m)_i - k_{nm}^{-1}F(m)_{i-1}}{F(m)_i - F(m)_{i-1}}, \end{aligned} \tag{6.3}$$

which needs to be constructed for each cell face. Obviously the averaged coefficient matrix does not fulfill the requirement. The problem of the above reconstruction method is that for e.g. a flat plate problem there will be locations on the plate where $F(m)_i - F(m)_{i-1} = 0$ leading to zero divisions[2] , fortunately exactly in these situations there is no flux over the cell boundaries, it does however impose the requirement that the flux is set to zero where the difference of successive primary variables is zero. In general the initialisation is independent of the location on the plate, i.e. this cannot be discarded as an artificial problem related to specific theoretical test cases.

The Roe scheme originally has problems if some eigenvalue becomes zero, this is corrected by the so-called sonic entropy fix.
The entropy fix was proposed by Harten in 1984 and is described by (see Wesseling[153])

$$|\tilde{\lambda}_p| = \frac{1}{2}\left(\frac{\lambda}{\epsilon} + \epsilon\right), \quad |\tilde{\lambda}_p| < \epsilon, \quad p = 1, \ldots 3,$$

where ϵ is a small number. If this occurs, the Jacobian coefficient matrix needs to be retrieved through equation (6.2).

Kurganov - Tadmor Scheme

The Kurganov-Tadmor scheme uses a scalar value instead of the Roe-averaged Jacobian, the scalar value is equal to the maximum of the spectral radii of the , i.e.

$$k_{i\pm 1/2} = \max\left(\rho(K_L), \rho(K_R)\right),$$

where the flux over e.g. the right cell face is given by

$$f_{i+1/2} = \frac{1}{2}(f_i + f_{i+1}) - k_{i+1/2}\Delta F_{i+1/2}.$$

Specifically for the Roe scheme the change of the flux over the cell face is approximated linearly using the Roe-average Jacobian matrix and for the Kurganov-Tadmor scheme this is done with the maximum spectral radius.

The implementation of the discussed FVM's is almost identical to the FDM due to the one-dimensionality, except that the grid transformation can take place a posteriori as discussed in the introduction.
The benefit of the Roe-scheme compared to the Kurganov-Tadmor scheme is that it is not necessary to employ eigenvalues or eigenvectors as long as $|\lambda| > 0$. Higher order Roe-schemes can be obtained through monotone upwind schemes for conservation laws (MUSCL), which uses extrapolated states left and right to determine the flux vector, see section (6.6).

6.2.2 Boundary Conditions

The boundary conditions for the FVM schemes are not so straightforward as for the FDM schemes. The different nature of the FVM requires a somewhat different treatment of

[2] at all points, except the first point near the left boundary point, and at $x > \max\left(\int \lambda_+\, dt, \int \lambda_-\, dt, \int \lambda_3\, dt\right)$

the boundaries. As is clear from the problem definition the left boundary condition is fixed and information should only travel away from the boundary condition and the right boundary condition should basically float based on the inner solution where it should not have any influence on the inner solution. This suggests the use of the characteristics as a means to control the directionality of the information. For the Roe scheme this can be incorporated by using a ghost cell on the right boundary, the left neighboring cell then uses only the right travelling characteristics to ensure that the right BC does not influence the cells to the left. The left boundary value fills up the first FV, the right neighboring cell only uses the positive valued eigenvalues to determine the flux over the left face. A basis approach is depicted in figure (6.5), The ghost cell for the Roe scheme

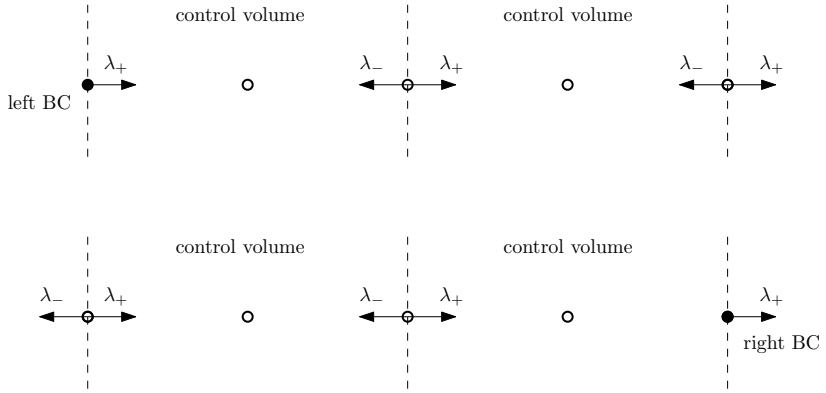

Figure 6.5: Boundary conditions for the FVM

is arbitrary since it does not influence the inner solution, to have a smooth outflow a Von Neumann BC is chosen.

6.3 Finite Element Method

The finite element discretisation and the finite element discretisation will be elaborated for the following exemplary set of conservative partial differential equations (PDE)

$$F_t + f_x = L,$$

and in quasi-linear form

$$F_t + KF_x = L.$$

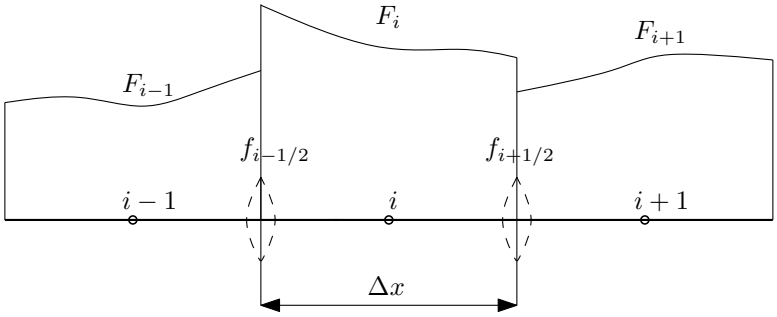

Figure 6.6: Control volumes for the Discontinous Galerkin method

6.3.1 General Description

Discontinuous Galerkin(DG) was the first FEM which could be applied to hyperbolic systems, the conventional (or continuous) Galerkin method assumed continuity on the interfaces of control volumes. In FEM the general idea is to use functionals in combination with a minimisation formulation to find the closest approximation to the exact solution. The conservative formulation allows for a consideration of control elements much like the control volume of the FVM, in fact the first order DG scheme is equivalent to the first order FV scheme.

The discontinuous Galerkin scheme was developed for the purpose of solving hyperbolic equations and has been in use for over 30 years. Benefits in comparison with Continuous Galerkin are the suitability for parallel processing, the geometric flexibility, the possibility of local h refinement and local p refinement, and the invertibility of the mass matrices which allows for explicit time integration. The control volumes are now control elements, these elements may have nodal points in case of a nodal expansion base, the points determine the order of the approximation which is given by a summation of the approximations over the element. In an element centered expansion base the basis functions form the approximation surrounding the cell center, the local values in the control element simply follow from there location with respect to the cell center. The latter approach will be used for this thesis.[3] The elements are tied together through shared element boundaries, this immediately allows for an easy implementation of the boundary conditions since the nodal points lie directly on the boundary. For this hyperbolic problem the nodal points are merely used for the flux determination over the cell faces and in that way the elements are connected. The control elements can be of arbitrary shape as long as the nodal points can be connected to neighboring points. This allows for geometrical flexibility but has the inherent downside of being inefficient in terms of matrix indexing, see figure (6.7). Likewise for the continuous Galerkin method this leads to a large bandwidth of the global mass matrix.
In the following text about DG several indices will be used, see table for the nomenclature of these indices.

name	index
maximum order of basis functions/time-integration	p
polynomial order	i,j
element index/Runge-Kutta step	k
neighboring element index	l
Runge-Kutta substep	m
time step	n
dimension	d

Table 6.1: FEM indices

The solution somewhere in the control element is defined as the sum of the separate values of the different (polynomial) orders of the basis functions $\psi_i(x)$ times a different weight factor for each polynomial order i

$$\hat{F}^k(x) = \sum_{i=1}^{p} W_i \psi_i(x), \quad x \in D^k, \tag{6.4}$$

where k is the k^{th} element, D^k is the space of the k^{th} element, W_i is the i^{th} weight factor and p is the maximum (polynomial) order. For polynomial basis functions the approximation with respect to the center point of the finite element is similar to a series solution approximation surround the center point, i.e. a Taylor expansion, see e.g. Naber[101].

For each cell this gives p number of unknowns versus p equations since the summation is simply a linear combination, i.e. each contribution can be considered separately

[3] has the immediate but inconsequential downside that the solution approximation at the cell faces is least accurate, which of course is exactly where the numerical flux is approximated.

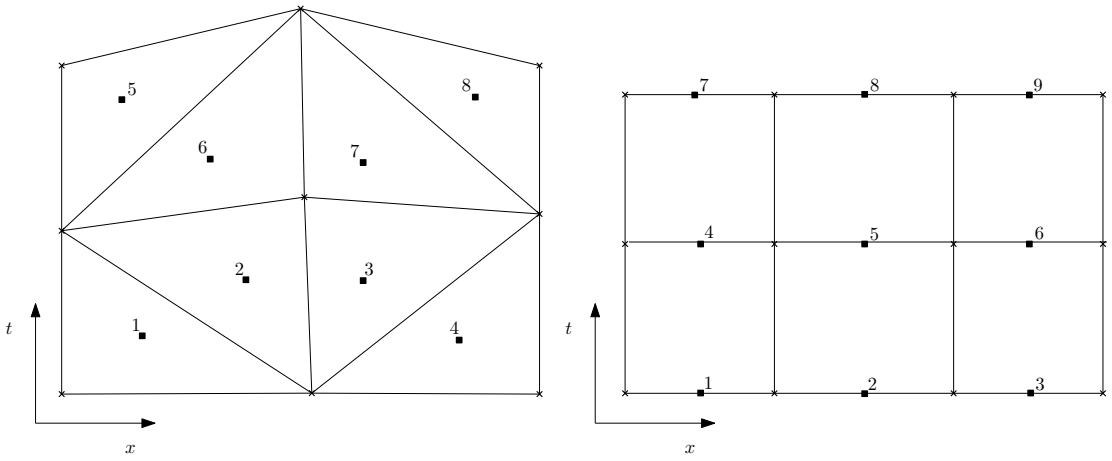

Figure 6.7: Space-time FEM grid (left),Space FEM grid (right)

leading to a different equation for each order/part of the basis function, the summation of which gives the solution in a given point. In general there can be p-refinement, which increases the order of the approximation but also h-refinement which refines the grid resolution, i.e. more or less control elements.

The weight factors will serve as the height of the nodal points and the scaling factors for the global approximation. Given some set of basis functions and weight factors, a solution procedure has to be formulated. To formulate the solution procedure the relevant equations need to be considered, in conservative form the IBL equations are given by

$$F_t + f_x = L,$$

this differential equation should hold over the entire solution domain, so

$$\begin{aligned} \text{Space FEM: } & \int_\Omega \left(\frac{\partial F}{\partial t} + \frac{\partial f}{\partial x} - L \right) dx = 0, \\ \text{Space-Time FEM: } & \int_\Omega \left(\frac{\partial F}{\partial t} + \frac{\partial f}{\partial x} - L \right) dx dt = 0. \end{aligned} \tag{6.5}$$

If space-time Galerkin is used the basis functions should be dependent on x and t whereas the space Galerkin approach only has space dependency, see for instance Klaij who applies space-time DG in his thesis[75]. The space-time formulation will allow for an arbitrarily accurate time-discretisation and a natural extension to local time-stepping. However since higher order time-discretisation is not deemed necessary given the approximative nature of the IBL equations, given the relative newness of space-time DG and given time-constraints only a Runge-Kutta Discontinuous Galerkin method will be used for the FEM. Interesting from the viewpoint of performance optimisation is the possibility to use a $p-level$ multigrid approach with parallel implementation (see Luo et al[88]).

Continuing with the space-FEM, since the bracketed term in equation (6.5) is identically zero it can be multiplied with an arbitrary function $\phi(x)$ which will be called the test function,

$$\int_\Omega \left(\frac{\partial F}{\partial t} + \frac{\partial f}{\partial x} - L \right) \phi(x) dx = 0.$$

Using the approximations this is written as

$$\int_\Omega \left(\frac{\partial \hat{F}}{\partial t} + \frac{\partial \hat{f}}{\partial x} - \hat{L} \right) \hat{\phi}(x) dx = 0, \tag{6.6}$$

where the hat indicates the approximated value. To obtain the continuous Galerkin formulation the test functions ϕ and the basis functions ψ are assumed to span the same space. Given the following definition of the inner product

$$\langle \phi(x), \psi(x) \rangle \equiv \int_{\mathbb{R}} \phi(x)\psi(x)dx = 0,$$

this means that the residual is orthogonal to the basis function, i.e. the approximation is orthogonal to the error of the approximation which is beneficial for stability and convergence. The test functions are written as

$$\hat{\phi}^k(x) = \sum_{i=1}^{p} V_i \psi_i(x), \quad x \in D^k,$$

which is only different from the basis functions through the different weight factors. The integral is rewritten using integration by parts

$$\int_\Omega \frac{\partial \hat{F}}{\partial t}\hat{\phi}d\Omega + \int_\Gamma \tilde{f} \cdot \overline{n}\hat{\phi}d\Gamma - \int_\Omega \nabla\hat{\phi} \cdot \hat{f}d\Omega - \int_\Omega \hat{L}\hat{\phi}d\Omega = 0,$$

where the integral over the boundary is a definite integral, this requires an approximation for the flux on the boundary, this is called the numerical flux, hence the difference in notation for the two flux terms.

Note that using $\hat{\phi} = 1$ would result in a FVM. If the approximations are applied directly in the above formulation of the integral the continuous Galerkin method emerges with some global mass and stiffness matrix. The Discontinuous Galerkin method applies the integral element wise with the alteration that the variables at each node are duplicates so as to ensure that each element has a local description, this effectively means there are two times more variables compared to continuous Galerkin.

The resulting difference over the nodes leads to a flux which needs to be treated separately, this numerical flux is the only means to connect the elements with each other, otherwise the elements are isolated.

Following Özdemir[106] it will be assumed that the solution is separable in space and time and since the basis functions are considered in space only it holds for any element that

$$\hat{F}^k(x,t) = \hat{F}_i^k(t) W_i \psi_i^k(x), \tag{6.7}$$

where the Einstein notation is used for the summation, here $i = 0 \ldots p$. For higher dimensions the separability is assumed for each dimension so (also see Naber[101])

$$\hat{F}^k(x,y,t) = \hat{F}^k_{i_1,i_2}(t) W_{i_1,i_2} \psi^k_{i_1,i_2}(x) \chi^k_{i_1,i_2}(y),$$

where i_1 and i_2 indicate the polynomial order of the basis functions in x and y direction respectively, for these orders it should hold that given a selected order of spatial accuracy p, i_d is limited by

$$\frac{1}{d!} \prod_{s=1}^{d} (p+s),$$

where d is the spatial dimension, this is to ensure that the combined polynomial order of the basisfunctions does no exceed the pre-selected polynomial order.

If Gaussian quadrature is chosen the approximations can be integrated exactly if monomial or polynomial basis functions are used, a computationally cheaper way to integrate is to expand the source term $\hat{L}^k$ and the flux $\hat{f}^k$ in terms of the basis functions (see e.g. Atkins and Shu[7])

$$\hat{f}^k_d = \hat{f}^k_{di}(t)\psi^k_i(x), \quad \hat{L}^k = \hat{L}^k_i(t)\psi^k_i(x),$$

here the terms $\hat{f}^k_{di}$ and $\hat{L}^k_i$ are the flux vector and the source vector based on the primary variable vector $\hat{F}^k_i$. Substituting the approximation in the integral and using Einstein

notation gives for some finite element

$$\int_{\Omega_k} \frac{\partial \hat{F}_i^k(t)}{\partial t} V_i^k W_j^k \hat{\psi}_i^k \hat{\psi}_j^k d\Omega + \int_{\Gamma_k} \tilde{f}_d^k n_d^k V_i^k \hat{\psi}_j^k d\Gamma - \int_{\Omega_k} V_i^k \hat{f}_{di}^k \hat{\psi}_i^k \frac{\partial \hat{\psi}_j^k}{\partial x_d} d\Omega - \int_{\Omega_k} \hat{L}_i^k \hat{\psi}_i^k \hat{\psi}_j^k d\Omega = 0.$$

From the above formulation a final discretisation cannot yet be derived, first the flux terms have to be treated and the surface areas of the elements have to be determined. The weight functions are simply set to 1 and thus $\hat{\psi}_i^k = \hat{\phi}_i^k$.

Coordinate transformation in the one dimensional case is rather trivial as there is only a single angle transformation possible. For higher dimensional problems the Jacobian of the local coordinate system with the global coordinates system has to be applied, the integral terms are affected through the dimensionality of the surface areas, the boundary line segment and the basis functions. Basically the formulation of the problem is based in the computational domain (η, ξ) whereas the solution is sought in the physical domain (x, y), see figure(6.8). The Jacobian for the two dimensional problem is given by

$$J = \begin{bmatrix} \frac{\partial x}{\partial \eta} & \frac{\partial y}{\partial \xi} \\ \frac{\partial y}{\partial \eta} & \frac{\partial x}{\partial \xi} \end{bmatrix},$$

and the derivatives follow from the chain rule

$$\begin{bmatrix} \frac{\partial}{\partial x} \\ \frac{\partial}{\partial y} \end{bmatrix} = \begin{bmatrix} \frac{\partial \eta}{\partial x}\frac{\partial}{\partial \eta} + \frac{\partial \xi}{\partial x}\frac{\partial}{\partial \xi} \\ \frac{\partial \xi}{\partial y}\frac{\partial}{\partial \xi} + \frac{\partial \eta}{\partial y}\frac{\partial}{\partial \eta} \end{bmatrix},$$

which can be written as (also see i.e. Özdemir[106],De Maerschalk[34])

$$\begin{bmatrix} \frac{\partial}{\partial x} \\ \frac{\partial}{\partial y} \end{bmatrix} = \begin{bmatrix} R_{11}\frac{\partial}{\partial \eta} + R_{21}\frac{\partial}{\partial \xi} \\ R_{12}\frac{\partial}{\partial \xi} + R_{22}\frac{\partial}{\partial \eta} \end{bmatrix}, \quad R = |J|^{-1}.$$

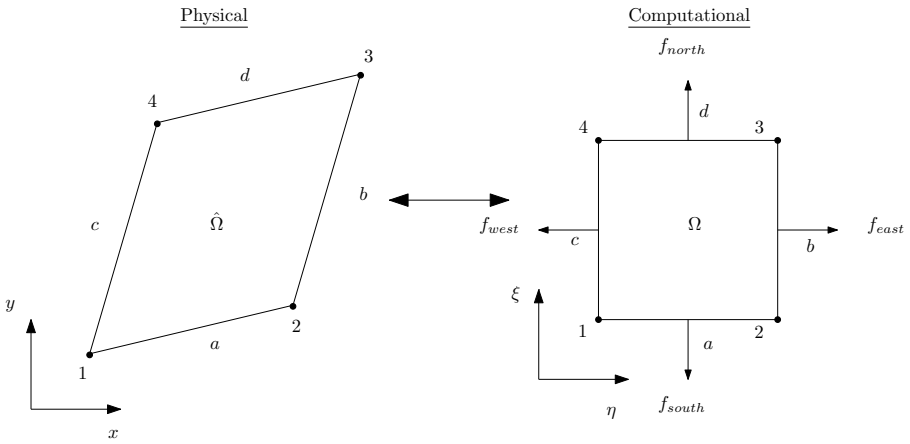

Figure 6.8: Quadrilateral Element transformation for two dimensional problem

The transformation through the Jacobian is placed directly in the integration formula-

tion, writing out the individual integral terms(see Özdemir [106])

$$\int_{\hat{\Omega}_k} \frac{d\hat{F}_i^k(t)}{dt}\hat{\psi}_i^k\hat{\psi}_j^k|J_k|\hat{\Omega},$$
$$\int_{\hat{\Gamma}_k} h_d^k|J_k|\hat{\psi}_j^k d\hat{\Gamma},$$
$$\int_{\hat{\Omega}_k} \hat{f}_{di}^k(t)\left(J_k^{-T}\right)_{dl}|J_k|\hat{\psi}_i^k\left(\frac{\partial\hat{\psi}_j^k}{\partial\xi_d}\right)_l d\hat{\Omega},$$
$$\int_{\hat{\Omega}_k} \hat{L}_i^k(t)\hat{\psi}_i^k\hat{\psi}_j^k|J_k|d\hat{\Omega}.$$

where the flux h_d^k is given by

$$h_d^k = \tilde{f}_d^k n_d^k,$$

where n_d^k is the d^{th} component of the unit outward normal vector on $\partial\hat{\Omega}_k$. For the two-

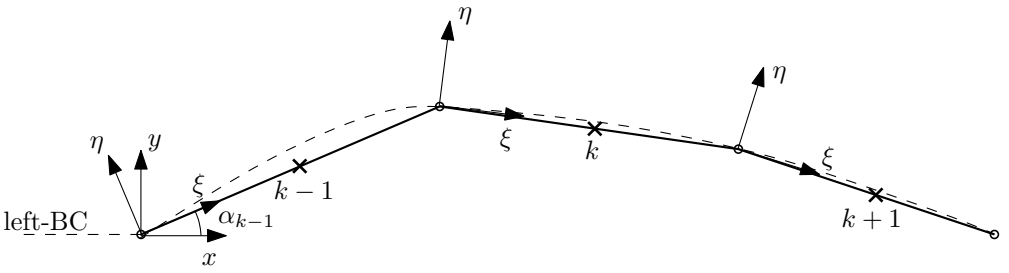

Figure 6.9: three 1D-elements representing some profile

dimensional IBL equations the problem is effectively one-dimensional and therefore the elements are not transformable. In the physical domain however the one-dimensional line segments represent actual segments of a profile segment but this can obviously not affect any direction since there is only one dimension, yet it will affect the magnitude of say the flux, the Jacobian for the (effectively) one-dimensional case will simply be a scalar. The Jacobian can be moved in front of the integrals if it is assumed constant per cell, it makes sense to apply the geometric information of the profile to generate an analytic expression for the direction of the local profile aligned axes (both for the two-dimensional as for the three-dimensional IBL equations). Also, the time derivative can be moved out of the integral since it was assumed that the solution is separable in space and time, also noting that the Jacobian term $|J_k|$ can be divided out of the equation, using the expansion in basis functions for the source vector and flux vector the integral terms are now written as

$$(a)_1 \quad \frac{d\hat{F}_i^k(t)}{dt}\int_{\hat{\Omega}_k}\hat{\psi}_i^k\hat{\psi}_j^k\hat{\Omega},$$
$$(b)_1 \quad \int_{\hat{\Gamma}_k} h_d^k\hat{\psi}_j^k d\hat{\Gamma},$$
$$(c)_1 \quad \left(J_k^{-T}\right)_{dl}\hat{f}_{di}^k(t)\int_{\hat{\Omega}_k}\hat{\psi}_i^k\left(\frac{\partial\hat{\psi}_j^k}{\partial\xi_d}\right)_l d\hat{\Omega},$$
$$(d)_1 \quad \hat{L}_i^k(t)\int_{\hat{\Omega}_k}\hat{\psi}_i^k\hat{\psi}_j^k d\hat{\Omega}.$$

where the source term $\hat{L}^k$ and the flux term f_{di}^k are written in terms of the basis functions, the latter assumption also allows to write the unknowns outside the integrals. This means that mass matrices, i.e. $\int_{\hat{\Omega}_k}\hat{\psi}_i^k\hat{\psi}_j^k\hat{\Omega}$ and $\int_{\hat{\Omega}_k}\hat{\psi}_i^k\frac{\partial\hat{\psi}_j^k}{\partial\xi_l}d\hat{\Omega}$, can be constructed a

priori which avoids the need to integrate over elements at each time level. Expanding the source vector and the flux vector in terms of the basis functions limits the application to a flux vector and a source vector which are linearly dependent on the primary variable vector in the sense that a linear dependency conserves the accuracy of the primary variable vector. In case the Jacobian transformation matrix is not constant over the element an expansion in basis functions can also be applied to the Jacobian, more details on this can be found in Özdemir[106], this is not relevant for the one-dimensional case.

The above formulation was used originally to simulate aeroacoustic with the Linearized Euler Equations, see Özdemir[106] and Blom[12], in these theses the coefficient matrices for the perturbations can be considered constant. In the current thesis the coefficient matrix, the source vector and the flux vector consist of the primary variables and can thus not be assumed constant and in fact, looking at section(4.2),they are not linearly dependent on the primary variables. To account for this non-linearity in the integration completely, the non-linear terms must be contained within the integral. The most accurate form is simply given by the full form

$$
\begin{aligned}
(a)_2 \quad & \frac{d\hat{F}_i^k(t)}{dt} \int_{\hat{\Omega}_k} \hat{\psi}_i^k \hat{\psi}_j^k \hat{\Omega}, \\
(b)_2 \quad & \int_{\hat{\Gamma}_k} h_d^k \hat{\psi}_j^k d\hat{\Gamma}, \\
(c)_2 \quad & \left(J_k^{-T}\right)_{dl} \int_{\hat{\Omega}_k} \hat{f}^k \left(\frac{\partial \hat{\psi}_j^k}{\partial \xi_d}\right)_l d\hat{\Omega}, \\
(d)_2 \quad & \int_{\hat{\Omega}_k} L^k \hat{\psi}_j^k d\hat{\Omega},
\end{aligned}
$$

which requires a quadrature rule for integrating the flux term $(c)_2$ and the source term $(d)_2$.

For the expansion in basis functions (formulation 1) it should be noted that the expansion is centered around the midpoint of the element, also, the expansion of the source vector and the flux vector has automatically the same order as the expansion of the primary variable vector. Thus a higher than linear primary variable dependency of the source term and the flux term will increase the order of the truncation error since the approximation is of lower order, i.e. on top of the error in the primary variable vector an extra error is introduced because of the polynomial mismatch, so even if the primary variable would be known exactly an error would result from the assumed linear dependence of the source/flux term on the primary variable vector. However, if the polynomial order is increased the added error due to the non-linearity of the source/flux term will be of increasingly higher order, thus $p-$refinement is useful despite the non-linearity.

For Gaussian quadrature (formulation 2) there is the immediate benefit that the number of quadrature points for the source vector and the flux vector are independent from the polynomial order of the basis functions so the difference in dependency of the source/flux term on the primary variable can be accounted for by using a different number of roots and weights. For this thesis a linear dependency will be assumed for the GQR implementation.

Both the expansion in basis functions and the GQR will be applied and compared.

Gaussian Quadrature Rule

Numerical Quadrature refers to the numerical integration of functions. To numerically integrate a function one can use direct rules like the Trapezodial rule or Simpson's rule, which are basically different ways of summating the function value at discrete steps on the integration interval. A more efficient rule, and the rule which will be implemented for this thesis, is the Gaussian Quadrature Rule (GQR). The GQR uses specific points with specific weights for the summation which can give an exact value for the integration

depending on the polynomial order and the number of nodes. The number of points required to produce an exact integration of an p^{th} order polynomial is equal to $2p-1$. The basic approach using the GQR is as follows

$$\int_{-1}^{1} f(\xi)d\xi = \sum_{i=1}^{2p-1} = c_i f(\xi_i),$$

where c_i and x_i are the weights and the nodes respectively. For GQR the Gauss-Legendre coordinates are used for the weights and node locations. To get the weights and the nodes for the quadrature rule e.g. the Golub−Welsch algorithm can be used. Calling this algorithm on the fly in case of $p-$refinement is not necessary and it would be expensive, given that the polynomial order will most likely not exceed a number $\mathcal{O}(1)$ the values for the weights and the nodes can be tabulated a priori up to a high order. The flux Term (c) requires a $4p+1$ number of nodes because of the tensor product and the source term (d) requires a $2p+1$ number of nodes. The downside of using Gaussian quadrature as opposed to an expansion in basis functions is apparent, the number of nodes for a two-dimensional problem (like the three-dimensional IBL equations) becomes $4p+1$ for the source term (d) and $8p+1$ for the flux term (c). For this reason, the expansion in basis functions is a viable option, although accuracy will be lost, the gain in computational efficiency is substantial; the difference lies only in integral terms (c) and (d). For a constant uniform or non-uniform grid the expansion in basis functions requires either only one evaluation to obtain the general mass/stiffness matrix or $2 \times N$-number of evaluations respectively whereas the GQR requires $2 \times N$-number of evaluations for each time step, also per evaluation of the integrals (c) and (d) the GQR requires $6p+1$ or $12p+1$ evaluations of the flux and source vector versus only p for the expansion in basis functions.

Expansion in Basis Functions

As said the expansion in basis functions is beneficial from the viewpoint of computational efficiency and should be investigated further for application. The application of the expansion in basis functions is straightforward, both the flux vector in term $(c)_1$ and the source vector in $(d)_1$ are written as functions of the weights for the approximation $\hat{F}^k$. For each order of the approximation of $\hat{F}$ there is basically a separate differential equation, considering the final formulation (see equation (6.10))

$$\begin{aligned}
\frac{d\hat{F}_0^k(t)}{dt} &= \cdots + \left(\mathbb{M}_{ij}^k\right)^{-1} \mathbb{S}_{ji}^k \hat{f}_0^k + \hat{L}_0^k, \\
\frac{d\hat{F}_1^k(t)}{dt} &= \cdots + \left(\mathbb{M}_{ij}^k\right)^{-1} \mathbb{S}_{ji}^k \hat{f}_1^k + \hat{L}_1^k, \\
&\vdots \\
\frac{d\hat{F}_p^k(t)}{dt} &= \cdots + \left(\mathbb{M}_{ij}^k\right)^{-1} \mathbb{S}_{ji}^k \hat{f}_p^k + \hat{L}_p^k,
\end{aligned}$$

where $\hat{f}_i^k, \hat{L}_i^k$ are formed by substituting the i^{th} weight $\hat{F}_i^k$ in the relations for f and L from the original conservative formulation of the IBL equations (see e.g. equations (4.18), (4.11)). A problem now arises: The relations for f and L contain closure relations based on the primary variables in $\hat{F}_i^k$, however the weights $\hat{F}_i^k$ for $i > 0$ are not confined to the applicable value ranges of the closure relations and so the flux and the source vector for these weights will produce erratic numbers causing instability and in any case unpredictability.

In general no physical meaning can be attributed to the weights of the expansion and this collides with the inherent physical representation of the closure relations which are

based on either empirical data or exact analytic solutions. If the exact range of applicability of the closure relations is determined and subsequently extended with smooth well-behaved functions the expansion in basis functions may well be stable and smooth. However, heuristically, the non-physical values would make the solution inconsistent.

Given the heuristic nature of the argument and the importance of the expansion in basis functions for the performance of the DG method a test should be performed comparing both the expansion in basis functions and the Gaussian quadrature. In terms of solution quality for one and second in terms of the actual computational efficiency.

For this reason both approaches will be elaborated.

Basis Functions

Given the final form of the discretisation the basis functions have to be chosen. Polynomial basis functions of arbitrary order can be used in the following form

$$\text{Normalised Monomial:} \quad \psi^k = \sum_{i=0}^{p} \xi^i \sqrt{\frac{2}{2i+1}},$$

$$\text{Lagrange:} \quad \psi^k = l(x) \sum_{i=0}^{p} \frac{w_i}{\xi}, \quad w_i = \frac{1}{\Pi_{i=k,k\neq i}^{p}(x_i - x_k)},$$

$$\text{Legendre:} \quad \psi^k = \sum_{i=0}^{p} P_i^k, \quad P_i^k = \sum_{j=0}^{p} (-1)^j \frac{(2i-2j)!}{2^i j!(i-j)!(i-2j)!} \xi^{i-2j} \sqrt{\frac{2}{2i+1}},$$

with

$$\xi = \frac{2(x - x_k)}{\Delta x_k} \rightarrow \xi = [-1, 1]$$

where the monomials and the Legendre polynomials are L^2-orthogonal which allows to write

$$\int \psi^k(x)\chi^k(y)d\Omega = \int \psi^k(x)dx \int \chi^k(y)dy,$$

which simplifies a future two dimensional implementation of the DG FEM. The Lagrangian polynomials require a nodal expansion base. If high order polynomials are chosen for the approximation the so-called spectral DG-FEM or the p-version DG-FEM emerge for Lagrange and Legendre polynomials respectively. The nodal expansion base of the Lagrangian polynomials is then applied using for instance Gauss-Lobatto-Legendre roots, see i.e. [34],[137]. The usefulness of employing a spectral method for the space-discretisation is questionable if the flux determination is not of similar order, also, the accuracy is limited by the accuracy of the time integration. Furthermore, the coefficients of the Legendre polynomials will become excessively large for higher order, to the extent that starting from about 4^{th} order computer accuracy may not suffice, especially for the inner products of these basis functions (see e.g.Özdemir[108]). The monomials merely have the weight factors as the coefficients and thus do not suffer the above problem, also, the Legendre polynomials can be constructed by a linear combination of monomials (see Blom[12] in reference to Råde and Westergren).

As was mentioned an equivalent first-order time accurate scheme can be constructed with higher order spatial accuracy, for a higher equivalent time accuracy one must resort to using a space-time formulation.
It must be noted that non-normalized monomials give badly conditioned mass matrices which means that numerical precision becomes an issue for higher order monomials, a problem which can be avoided by using normalised monomials as is done for this thesis, see Hesthaven[64], Blom[12].

For the above reasons normalised monomials are chosen as basis functions, the order will be implemented as a free parameter.

Riemann Solver

The numerical flux h needs to be considered in more detail, for some element the flux over the edges is given by

$$\int_{\hat{\Gamma}_k} h_d^k \hat{\psi}_j^k d\hat{\Gamma},$$

where for the one-dimensional case for some element k the flux is given by [4] (see i.e. Cockburn[25],Blom[12],Özdemir[106])

$$\begin{aligned}
\text{local Lax-Friedrich:} \quad & \left(h_1^k\right)_R = \frac{1}{2}\Big[f^k(\xi=1) + f^{k+1}(\xi=-1) - \\
& \theta|\lambda_d|_{max,R}\left(F^{k+1}(\xi=-1) - F^k(\xi=1)\right)\Big], \theta \geq 0, \\
\text{Characteristics based:} \quad & \left(h_1^k\right)_R = \frac{1}{2}\Big[f^k(\xi=1) + f^{k+1}(\xi=-1) - \\
& \theta\overline{K}_d\left(F^{k+1}(\xi=-1) - F^k(\xi=1)\right)\Big], \theta \geq 0,
\end{aligned}$$

where the maximum eigenvalue $|\lambda_d|_{max}$ may be determined from the average of the eigenvalues of the two neighboring elements or by taking the maximum eigenvalues of the two neighboring elements.

For the characteristics based flux the total flux through the element over the edges is given by

$$\begin{aligned}
\int_{\hat{\Gamma}_k} h_d^k \hat{\psi}_j^k d\hat{\Gamma} = \sum^{N_{edges}} \Bigg[\int_{\partial\Omega_{kl}} \frac{1}{2}\Big\{ & \left(\hat{f}^k n_{kd} + \hat{f}^l n_{kd}\right) \\
& -\theta\frac{1}{2}\left[K_d^k n_{kd} + K_d^l n_{ld}\right]\left(F_i^k - F_i^l\right)\Big\}\hat{\psi}_j^k d\Gamma\Bigg],
\end{aligned} \tag{6.8}$$

where the coefficient matrix $\overline{K}_d$ is simply taken as the average of the Jacobian matrices left and right from the edge based on averaged eigenvalues or through equation (6.3). For the present one-dimensional case integral drops out and the flux values $\hat{f}^k$ and $\hat{f}^l$ can be obtained directly from filling in the exact cell faces of $\hat{F}$ in the formulation for f. For higher dimensions Gaussian quadrature has to be applied to obtain the integral.

Blom[12],Özdemir[106] base the numerical flux on the centered values, i.e. they only account for the zeroth order approximation. Cockburn[25] and Naber[101] use the higher order terms but apply a conventional Godunov type Riemann solver. The approximate Riemann solver to obtain the flux values is not of arbitrary order like the approximation of the solution inside in the finite element. However using a multi-stage time integrator in combination with a first order Riemann solver leads to equivalent accuracy as would be obtained using a single stage integrator with a higher order Riemann solver (see e.g. Naber[101]), i.e. the time accuracy is limited to first order for arbitrary order approximations. A generalized Riemann solver can also be used to obtained higher order accurate flux approximations but this is not considered for this thesis. A generalised Riemann solver which accounts for the non-linearity of the flux is arguably not necessary to obtain higher order accuracy, the procedures for the generalised Riemann solver as described in Castro and Toro([18]) are somewhat similar to the procedure described above in equation (6.8). Castro and Toro make use of polynomial expansions to express the non-linearity within one cell as opposed to using interpolated cell face values for conventional Riemann problems and the cell face values are expanded in time (also see Toro and Titarev[135]). The non-linearity in this case is represented by higher order basis functions and the non-linearity in time is accounted for by applying a multi-stage time integrator (also see Naber[101]).

[4] note that the local Lax-Friedrich scheme is also known as the Kurganov and Tadmor central scheme

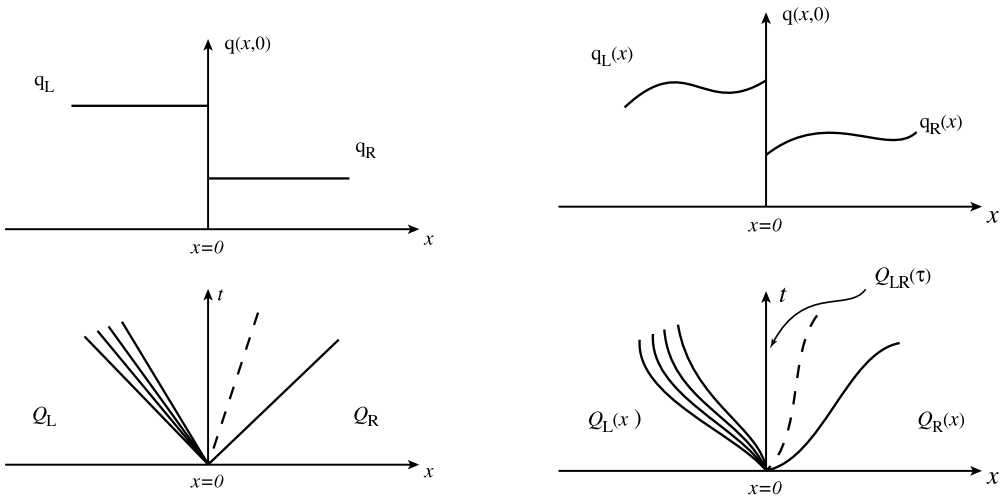

Figure 6.10: non-linear advection equation with double linear velocity distribution, (left) classical Riemann problem, (right) derivative Riemann problem.

Solution Procedure

At each time level there are p equations per element and given a total of N elements, there are a total of $p \times N$ equations. The equations are formed by the discrete representation of the weak formulation (see equation 6.6) for each order of the basis functions. For clarity the weak formulation is written out, first only using the test functions, then the basis functions are introduced, for this explanation one-dimensionality is assumed and Einstein notation is dropped

$$\int_\Omega \frac{\partial \hat{F}^k}{\partial t}\hat{\psi}_j^k d\Omega + \int_\Gamma \tilde{f}^k \cdot \overline{n}\hat{\psi}_j^k d\Gamma - \int_\Omega \frac{\partial \hat{\psi}_j^k}{\partial \xi} \cdot \hat{f}^k d\Omega - \int_\Omega \hat{L}^k \hat{\psi}_j^k d\Omega = 0,$$

here there are $p+1$ equations, given by $\hat{\psi}_j^k, \quad j = 0, \dots p$, noting that the test functions are immediately assumed equal to the basis functions with unity weight factors. The primary variable vector is written as a summation of $p+1$ basis functions and weights which are separable in space and time, considering the integral with the time derivative

$$\begin{aligned}
\int_\Omega \frac{\partial \hat{F}^k}{\partial t}\hat{\psi}_j^k d\Omega &= \sum_{i=0}^{p} \frac{\partial \hat{F}_i^k}{\partial t} \int_\Omega \hat{\psi}_i \hat{\psi}_j \Omega, \quad j = 0, \dots p \\
&= \begin{pmatrix} \frac{\partial \hat{F}_0^k}{\partial t}\int_\Omega \hat{\psi}_0\hat{\psi}_0 d\Omega + \dots + \frac{\partial \hat{F}_p^k}{\partial t}\int_\Omega \hat{\psi}_p\hat{\psi}_0 d\Omega \\ \frac{\partial \hat{F}_0^k}{\partial t}\int_\Omega \hat{\psi}_0\hat{\psi}_1 d\Omega + \dots + \frac{\partial \hat{F}_p^k}{\partial t}\int_\Omega \hat{\psi}_p\hat{\psi}_1 d\Omega \\ \vdots \\ \frac{\partial \hat{F}_0^k}{\partial t}\int_\Omega \hat{\psi}_0\hat{\psi}_p d\Omega + \dots + \frac{\partial \hat{F}_p^k}{\partial t}\int_\Omega \hat{\psi}_p\hat{\psi}_p d\Omega \end{pmatrix}, \\
&= \mathbb{M}_{ji}^k \frac{\partial}{\partial t}\begin{pmatrix} \hat{F}_0 \\ \vdots \\ \hat{F}_p \end{pmatrix} = \mathbb{M}_{ij}^k \frac{\partial}{\partial t}\begin{pmatrix} \hat{F}_0 \\ \vdots \\ \hat{F}_p \end{pmatrix}
\end{aligned}$$

where the mass matrix $\mathbb{M}_{ij}^k$ is given by

$$\mathbb{M}_{ij}^k = \begin{bmatrix} \int_\Omega \hat{\psi}_0 \hat{\psi}_0 d\Omega & \cdots & \int_\Omega \hat{\psi}_p \hat{\psi}_0 d\Omega \\ \vdots & \ddots & \vdots \\ \int_\Omega \hat{\psi}_0 \hat{\psi}_p d\Omega & \cdots & \int_\Omega \hat{\psi}_p \hat{\psi}_p d\Omega \end{bmatrix},$$

i.e. for every time step there is an explicit equation for $\hat{F}_i^k, \quad i = 0, \dots p$ if the remaining terms are divided by the mass matrix $\mathbb{M}^k$. Now the Runge-Kutta integration scheme can be applied to the resulting $p+1$ ordinary differential equations, this results in the following semi-discrete formulation for the multidimensional case

$$\begin{aligned} \frac{d\hat{F}^k(t)}{dt} = & \underbrace{- \left(\mathbb{M}_{ij}^k\right)^{-1} \int_{\hat{\Gamma}_k} h_d^k \hat{\psi}_j^k d\hat{\Gamma}}_{\text{(a)}} \\ & \underbrace{+ \left(\mathbb{M}_{ij}^k\right)^{-1} \left(J_k^{-T}\right)_{dl} \int_{\hat{\Omega}_k} K_d^k \hat{\psi}_i^k \left(\frac{\partial \hat{\psi}_j^k}{\partial \xi_d}\right)_l d\hat{\Omega}\, \hat{F}^k(t)}_{\text{(b)}} + \underbrace{\left(\mathbb{M}_{ij}^k\right)^{-1} \int_{\hat{\Omega}_k} \hat{L}^k \hat{\psi}_j^k d\hat{\Omega}}_{\text{(c)}}, \end{aligned}$$

which for the one-dimensional case can be written as follows for the general case

$$\begin{aligned} \text{formulation A:} \quad \frac{d\hat{F}^k(t)}{dt} = & - \left(\mathbb{M}_{ij}^k\right)^{-1} \int_{\hat{\Gamma}_k} h^k \hat{\psi}_j^k d\hat{\Gamma} + \left(\mathbb{M}_{ij}^k\right)^{-1} \int_{\hat{\Omega}_k} \hat{f}^k \frac{\partial \hat{\psi}_j^k}{\partial \xi} d\hat{\Omega} \\ & + \left(\mathbb{M}_{ij}^k\right)^{-1} \int_{\hat{\Omega}_k} L^k \hat{\psi}_j^k d\hat{\Omega}, \end{aligned} \tag{6.9}$$

and if the expansion in basis functions is applied to source vector and the flux vector

$$\text{formulation B:} \quad \frac{d\hat{F}^k(t)}{dt} = - \left(\mathbb{M}_{ij}^k\right)^{-1} \int_{\hat{\Gamma}_k} h^k \hat{\psi}_j^k d\hat{\Gamma} + \left(\mathbb{M}_{ij}^k\right)^{-1} \mathbb{S}_{ji}^k \hat{f}^k + \hat{L}^k, \tag{6.10}$$

where formulation B uses the expansion in basis functions for the source term and the flux term. The stiffness matrix is given by

$$\mathbb{S}_{ji}^k = \int_{\hat{\Omega}_k} \hat{\psi}_i^k \frac{\partial \hat{\psi}_j^k}{\partial \xi} d\hat{\Omega},$$

$$\mathbb{S}_{ji}^k = \begin{bmatrix} \int_{\hat{\Omega}_k} \psi_0 \frac{\partial \psi_0}{\partial \xi} d\Omega & \cdots & \int_{\hat{\Omega}_k} \psi_p \frac{\partial \psi_0}{\partial \xi} d\Omega \\ \vdots & \ddots & \vdots \\ \int_{\hat{\Omega}_k} \psi_0 \frac{\partial \psi_p}{\partial \xi} d\Omega & \cdots & \int_{\hat{\Omega}_k} \psi_p \frac{\partial \psi_p}{\partial \xi} d\Omega \end{bmatrix}.$$

Using monomials[5] and assuming a uniform grid the mass matrix and the stiffness matrix can be written as

[5] non-normalised for expediency

$$\mathbb{M}^k_{ij} = \Delta x \begin{bmatrix} [\xi]^1_{-1} & \frac{1}{2}\left[\xi^2\right]^1_{-1} & \cdots & \frac{1}{p+1}\left[\xi^{p+1}\right]^1_{-1} \\ \frac{1}{2}\left[\xi^2\right]^1_{-1} & \frac{1}{3}\left[\xi^3\right]^1_{-1} & \cdots & \frac{1}{p+2}\left[\xi^{p+2}\right]^1_{-1} \\ \vdots & \vdots & \ddots & \vdots \\ \frac{1}{p+1}\left[\xi^{p+1}\right]^1_{-1} & \cdots & \cdots & \frac{1}{2p+1}\left[\xi^{2p+1}\right]^1_{-1} \end{bmatrix},$$

$$\mathbb{S}^k_{ji} = \Delta x \begin{bmatrix} 0 & \cdots & \cdots & 0 \\ [\xi]^1_{-1} & \frac{1}{2}\left[\xi^2\right]^1_{-1} & \cdots & \frac{1}{p+1}\left[\xi^{p+1}\right]^1_{-1} \\ \vdots & \vdots & \ddots & \vdots \\ \xi^p \frac{p}{p+1}\left[\xi^{p+1}\right]^1_{-1} & \cdots & \cdots & \frac{p}{p+p}\left[\xi^{p+p}\right]^1_{-1} \end{bmatrix},$$

where Δx should be placed inside the matrices for a non-uniform grid spacing. This can be written directly as

$$\mathbb{M}_{ij} = \frac{\Delta x}{2}\frac{1}{i+j+1}\left[1-(-1)^{i+j+1}\right], \quad \mathbb{S}_{ji} = \frac{\Delta x}{2}\frac{j}{i+j}\left[1-(-1)^{i+j}\right], \quad i,j = 0,\dots p,$$

and using the normalised basis functions (also see Blom[12])

$$\mathbb{M}_{ij} = \Delta x\sqrt{\frac{1}{2i+1}}\sqrt{\frac{1}{2j+1}}\frac{1}{i+j+1}\left[1-(-1)^{i+j+1}\right],$$
$$\mathbb{S}_{ji} = \Delta x\sqrt{\frac{1}{2i+1}}\sqrt{\frac{1}{2j+1}}\frac{j}{i+j}\left[1-(-1)^{i+j}\right], \quad i,j = 0,\dots p.$$

Formulations A and B are constructed with the assumption that the angle α is zero for all elements (see figure 6.9), i.e. a flat plate. The mass matrix and the stiffness matrix are only dependent on the basis functions, given that the unknowns are placed outside the integral the integral can be determined beforehand for all elements. For formulation A the two integral terms (c) and (d) can be found using Gaussian quadrature given the elementwise distribution of the primary variables for the current timestep. For formulation B the terms (c) and (d) contain the predetermined mass and stiffness matrices multiplied by the weight factors of the flux expansion and the source expansion respectively. The numerical flux integral (equation(6.8)), term (b), is expanded as follows if the expansion in basis function is applied

$$\begin{aligned}
\int_{\hat{\Gamma}_k} h^k \hat{\psi}^k_j d\hat{\Gamma} &= \left(\int_0^1 h^k \hat{\psi}^k_j d\zeta\right)_{left} + \left(\int_0^1 h^k \hat{\psi}^k_j d\zeta\right)_{right} \\
&= \frac{1}{2}\sum_{i=1}^{p}\left\{\left[\left(\hat{f}^k_i\right)_{\xi=-1} + \left(\hat{f}^{k-1}_i\right)_{\xi=1}\right]\right. \\
&\quad \left. -\frac{1}{2}\theta\left[K^k_{\xi=-1} + K^{k-1}_{\xi=1}\right]\left(\left(F^k_i\hat{\psi}^k_i\right)_{\xi=-1} - \left(F^{k-1}_i\hat{\psi}^{k-1}_i\right)_{\xi=1}\right)\right\}\hat{\psi}^k_j(\xi=-1) \qquad (6.11) \\
&\quad + \frac{1}{2}\sum_{i=1}^{p}\left\{\left[\left(\hat{f}^k_i\right)_{\xi=1} + \left(\hat{f}^{k+1}_i\right)_{\xi=-1}\right]\right. \\
&\quad \left. -\frac{1}{2}\theta\left[K^k_{\xi=1} + K^{k+1}_{\xi=-1}\right]\left(\left(F^{k+1}_i\hat{\psi}^{k+1}_i\right)_{\xi=-1} - \left(F^k_i\hat{\psi}^k_i\right)_{\xi=1}\right)\right\}\hat{\psi}^k_j(\xi=1),
\end{aligned}$$

and if Gaussian quadrature is used for the flux and the source term

$$\begin{aligned}
\int_{\hat{\Gamma}_k} h^k \hat{\psi}_j^k d\hat{\Gamma} &= \left(\int_0^1 h^k \hat{\psi}_j^k d\zeta\right)_{left} + \left(\int_0^1 h^k \hat{\psi}_j^k d\zeta\right)_{right} \\
&= \frac{1}{2}\left\{\left[\left(\hat{f}^k\right)_{\xi=-1} + \left(\hat{f}^{k-1}\right)_{\xi=1}\right]\right. \\
&\quad \left. -\frac{1}{2}\theta\sum_{i=1}^{p}\left[K^k_{\xi=-1} + K^{k-1}_{\xi=1}\right]\left(\left(F_i^k\hat{\psi}_i^k\right)_{\xi=-1} - \left(F_i^{k-1}\hat{\psi}_i^{k-1}\right)_{\xi=1}\right)\right\}\hat{\psi}_j^k(\xi=-1) \qquad (6.12) \\
&\quad + \frac{1}{2}\left\{\left[\left(\hat{f}^k\right)_{\xi=1} + \left(\hat{f}^{k+1}\right)_{\xi=-1}\right]\right. \\
&\quad \left. -\frac{1}{2}\theta\sum_{i=1}^{p}\left[K^k_{\xi=1} + K^{k+1}_{\xi=-1}\right]\left(\left(F_i^{k+1}\hat{\psi}_i^{k+1}\right)_{\xi=-1} - \left(F_i^k\hat{\psi}_i^k\right)_{\xi=1}\right)\right\}\hat{\psi}_j^k(\xi=1).
\end{aligned}$$

Given an initialisation of the primary variables and a value for the flux at the left boundary the solution at the following time levels is found by applying the Runge-Kutta scheme(equations (6.14),(6.16)). Directly after the initialisation the solution is described as a constant in each element, this means that only the weight for the zeroth order basis function is non-zero. Through the flux term the basis function weights for the higher order terms become non-zero at the next time level.

The solution is naturally taken as the center values of the finite elements, i.e. as the zeroth order weight factors, these values are used for the transition check and the separation check.

6.3.2 Boundary Conditions

In principle the same applies for DG as for the FVM, to guarantee that the control volume only receives information from the inner domain the flux vectors should be splitted as is done for the Steger-Warming scheme.

6.3.3 Cubic Spline and Matrix Inversion

For the DG method information of the edge velocity profile is required at the faces of the control elements. For the final implementation most likely the center points of the control elements will be used as the coupling points between the external (edge) velocity profile and the boundary layer. Therefore the values of the edge velocity must be acquired through interpolation. To interpolate the external velocity profile the well known cubic spline method is applied. The cubic spline algorithm is described in Burden and Faires[16, p.146].

The matrix inversion is obtained by a pivoting method, the credits for the algorithm go to Aswith J. Rego. It should be stressed here that the matrix inversion process is not optimal, for large matrices e.g. LU-decomposition is often used as well as Cholesky factorisation.

Note that if the polynomial order as well as the length (or surface for three-dimensional IBL equation) is the same for all elements the mass matrix only has to be determined once which obviously takes away the need for optimising the inversion process given the small computational size of the IBL problem.

6.4 Time Integration

Once the semi-discrete form is obtained the question remains how the solution is updated, following for instance Cockburn[25], Naber[101] and Özdemir[106] a multi-stage explicit Runge-Kutta approach is chosen to obtain (at least) a first order accurate solution in time.

Explicit Time Integration

For the integration first the time derivative is written as

$$\frac{d\hat{F}}{dt} = \mathbb{L}(\hat{F}).$$

The general Runge-Kutta schemes are written as

$$\begin{aligned} \hat{F}^{n+1} &= \hat{F}^n + \Delta t \sum_{i=1}^{p} b_i k_i. \\ k_i &= \mathbb{L}(\hat{F}^n + \Delta t \sum_{j=1}^{p} a_{ij} k_j). \end{aligned} \tag{6.13}$$

The table with coefficients a_{ij}, b_j is the called the Butcher-tableau, see table (6.2) with the Butcher tableau of the well known fourth order Runge-Kutta scheme in brackets. For $j < i$ the Runge-Kutta scheme is explicit.

0				
$\sum_{j=1}^{1} a_{ij}$	$a_{21}\left(\frac{1}{2}\right)$			
$\sum_{j=1}^{2} a_{ij}$	$a_{31}(0)$	$a_{32}\left(\frac{1}{2}\right)$		
$\sum_{j=1}^{3} a_{ij}$	$a_{41}(0)$	$a_{42}(0)$	$a_{43}(1)$	
	$b_1(\frac{1}{6})$	$b_2(\frac{1}{3})$	$b_3(\frac{1}{3})$	$b_4(\frac{1}{6})$

Table 6.2: Butcher Tableau for Runge-Kutta scheme

The multi-stage RK-integrator applied to DG is usually written as (see Cockburn[25] in reference to Shu and Osher)

$$\begin{aligned} \hat{F}_0 &= \hat{F}^{n-1}, \\ \hat{F}_k &= \sum_{m=0}^{k-1} \alpha_{km} w^{km}, \quad w^{km} = \hat{F}_m + \frac{\beta_{km}}{\alpha_{km}} \Delta t_n \mathbb{L}(\hat{F}_m), \quad k = 1 \ldots, p, \\ \hat{F}^{n+1} &= \hat{F}_p^n. \end{aligned} \tag{6.14}$$

The coefficients α_{km} and β_{km} are given in table (6.3) (see Gottlieb and Shu[54]). The RK coefficients give a Total Variation Diminishing(TVD) scheme which means that oscillatory behavior near discontinuities is suppressed which increases the overall stability, also see Cockburn and Shu[25]. The coefficients of table (6.3) can be directly applied to the Runge-Kutta scheme (6.14) with the exception that for the negative values of β the linear operator should be adapted. For negative β's the scheme should be stable backward in time which requires a linear operator which solves the hyperbolic equation backward in time in TVD, i.e. analogously for the spatial discretisation a reversed upwind direction should be employed. In case of DGFEM (or FVM) in combination with a Roe scheme this linear operator, to be called $\tilde{\mathbb{L}}$ follows directly from negating the eigenvalues of the Jacobian since this directly determines the direction of upwinding. Likewise for FDM the direction of upwinding is determined directly by the sign of the eigenvalues and thus allows for a simple determination of the adapted linear operator.

Order	α_{km}	β_{km}
2	$\begin{array}{cc} 1 & - \\ \frac{1}{2} & \frac{1}{2} \end{array}$	$\begin{array}{cc} 1 & - \\ 0 & \frac{1}{2} \end{array}$
3	$\begin{array}{ccc} 1 & - & - \\ \frac{3}{4} & \frac{1}{4} & - \\ \frac{1}{3} & 0 & \frac{2}{3} \end{array}$	$\begin{array}{ccc} 1 & - & - \\ 0 & \frac{1}{4} & - \\ 0 & 0 & \frac{2}{3} \end{array}$
4	$\begin{array}{cccc} 1 & - & - & - \\ \frac{649}{1600} & \frac{951}{1600} & - & - \\ \frac{53989}{25e5} & \frac{4806213}{2e7} & \frac{23619}{32e3} & - \\ \frac{1}{5} & \frac{6127}{3e4} & \frac{7873}{1e4} & \frac{1}{3} \end{array}$	$\begin{array}{cccc} \frac{1}{2} & - & - & - \\ -\frac{10890423}{25193600} & \frac{5e3}{7873} & - & - \\ -\frac{102261}{5e6} & -\frac{5121}{2e4} & \frac{7873}{1e4} & - \\ \frac{1}{10} & \frac{1}{6} & 0 & \frac{1}{6} \end{array}$

Table 6.3: Runge-Kutta coefficients

Alternatively, a fourth order TVDRK scheme without the presence of negative valued coefficients can be obtained by introducing an extra stage, see Hesthaven and Warburton[64, p.158]. A TVD Low storage Runge-Kutta scheme(LSRK) was found in Gottlieb et al[55] for third order accuracy with $CFL = 0.32$, Ketcheson and Robinson[73] derived a third order LSRK with $CFL = 0.838$, allowing a time step which is more than two times larger. If TVD is deemed unnecessary or if third order accuracy is sufficient the LSRK can be considered which has the advantage that less primary variable vectors have to be stored at each stage. In the paper by Gottlieb et al the following two-register(i.e. two vectors are stored per step) scheme is used for the LSRK

$$\begin{aligned} \hat{F}_0 &= \hat{F}^n, dF_0 = 0 \\ \left.\begin{aligned} dF_k &= \alpha_k dF_{k-1} + \Delta t_n \mathbb{L}\left(\hat{F}_{k-1}\right) \\ \hat{F}_k &= \hat{F}_{k-1} + \beta_k dF_k \end{aligned}\right\} & \quad k = 1, \ldots, p, \\ \hat{F}^{n+1} &= \hat{F}_p, \end{aligned} \tag{6.15}$$

which is a specific form of scheme (6.14) where only the diagonal terms for α and β are maintained. Several LSRK schemes can be found in an ICASE report by Kennedy et al[72], for the two-register scheme they effectively use the same scheme. The coefficients for the two-register LSRK scheme are given in table 1 of their report. A fourth order LSRK scheme was applied by Blom[12] and Özdemir[106]. The LSRK scheme used by Blom and Özdemir is given by

$$\begin{aligned} \hat{F}_0 &= \hat{F}^n, \\ \hat{F}_k &= \hat{F}_0 + \gamma_k \Delta t_n \mathbb{L}\left(\hat{F}_{k-1}\right), \quad k = 1, \ldots, p, \\ \hat{F}^{n+1} &= \hat{F}_p, \end{aligned} \tag{6.16}$$

where for a N-stage scheme the coefficients are given by $\gamma_i = \frac{1}{N+1-i} \quad i = 1, \ldots N$, which is most applicable for linear Jacobians. For this thesis the SSPRK and the two-register LSRK schemes are implemented but not tested, note that the LSRK schemes are simply assumed to be non-TVD since they were not devised with TVD in mind, thus the availability of this property would be fortuitous. A benefit of an SSPRK-scheme is that it allows for a direct extension of the stability requirement for the first order Euler time-integration(6.5) and for non-linear systems it will be stable for higher CFL numbers. Ketcheson observes that non-TVD RK schemes can still preserve monotonicity if the CFL is lowered (well) below the maximum CFL, this should be kept in mind when comparing the LSRK with the SSPRK. If monotonicity for non-TVD RK schemes is indeed preserved it is advisable to apply higher order LSRK schemes as can be found in the report by Kennedy et al[72], or the simple LSRK scheme from Blom. Clearly for the stability preserving time integration scheme as the order of the time-integration increases

it becomes increasingly tedious to extract the Runge-Kutta coefficients and therefore the order of integration is practically limited.

The simple LSRK-scheme used by Blom [12] and Özdemir[106] allows for arbitrary orders of accuracy, has relatively low memory requirements and can be applied for non-linear problems problems while maintaining strong stability[73].

For the finite difference and the finite volume scheme the standard Butcher tableau for Runge-Kutta will be used up till 4^{th} order. For the DG method the LSRK-scheme by Blom and Özdemir is implemented as well as the SSP preserving schemes discussed above[6].

Suggested by e.g. Kennedy et al[72] and Gottlieb et al[55] is the use of a multi-step time integration scheme,

$$\hat{F}^{n+1} = \sum_{k=1}^{p} \left(\alpha_k \hat{F}^{n+1-k} + \Delta t \beta_k \mathbb{L} \left(\hat{F}^{n+1-k} \right) \right), \quad \alpha_k \geq 0, \quad \sum_{k=1}^{p} \alpha_k = 1,$$

where the simulation is started with a single step, with each new time-level the number is of steps is increased by one until the maximum number of steps is reached. A table with multi-step schemes until 5^{th} order is given in Gottlieb et al[55].

Implicit Time Integration

In the time integration methods discussed above explicitness was assumed, this will turn out to be very restrictive for the maximum time step. A larger time step is possible if an implicit time integration scheme is chosen, therefore implicit time integration will be discussed shortly.

The time derivative of the primary variable vector is determined implicitly by

$$\left(\frac{\partial F}{\partial t} \right)^n = (L - f_x)^{n+1}, \tag{6.17}$$

and using a first order approximation in time this gives

$$\left(\frac{\Delta F}{\Delta t} \right)^n = (L - f_x)^n + \frac{\partial (L - f_x)}{\partial F} \left(\frac{\Delta F}{\Delta t} \right)^n \Delta t + \mathcal{O}(\Delta t^2),$$

solving this for F^{n+1} gives the linearised backward Euler scheme

$$F^{n+1} = \left(\frac{\mathbb{I}}{\Delta t} - \frac{\partial L}{\partial F} + \frac{\partial^2 f}{\partial x \partial F} \right)^{-1} \left(L^n - f_x^n \right) + F^n.$$

The immediate downside of this implicit scheme is the inverse term and the fact that $\frac{\partial L}{\partial F}$ and $\frac{\partial^2 f}{\partial x \partial F}$ have to be determined per node/element which excludes the method of lines for the general solution procedure. This above implicit scheme is first order accurate in time, for higher order accuracy the inverse term becomes more involved. The most efficient method for treating the inverse term is to solve the matrix algebraically a priori, during each time step the inverse can be found immediately. Using the Jacobian $K = \frac{\partial f}{\partial F}$ the inverted term is written as

$$\frac{\mathbb{I}}{\Delta t} - \frac{\partial L}{\partial F} + \frac{\partial K}{\partial x},$$

where $\frac{\partial K}{\partial x}$ has to be determined numerically. This time-integration scheme can be applied directly to all the presented finite difference schemes, for the FVM and the DG method the inverted term can be obtained with the cell-centered values.

[6] only the LSRK-scheme is tested

Using a first order backward Euler scheme with a Newton-Rhapson iteration process the updated value F^{n+1} can be obtained through

$$F^{i+1} = F^i - \frac{\Delta t \left(L - f_x\right)^i + F^n - F^i}{\Delta t \left(\frac{\partial L}{\partial F} - \frac{\partial K}{\partial x}\right)^i},$$

where i is the iteration count, for the first iteration F^i is a guessed value following from the value(s) for the previous time step(s). The iteration can be stopped when $\frac{F^{i+1}-F^i}{F^i}$ drops below a preset value. See Gottlieb et al[55] for implicit Runge-Kutta and multi-step schemes who state that implicit higher order Strong Stability Preserving time-integration is not possible.

Persson and Peraire[109] performed a study on low memory iterative solvers for DG applied to the time-dependent compressible Navier-Stokes equations and advise the restarted generalised minimal residual method (GMRES) for general use. GMRES and restarted GMRES are matrix based iterative solvers for which algorithms are freely available, see e.g. Saad and Schultz[117] for a GMRES algorithm and e.g. Erhel et al[46] and Morgan[97] for a restarted GMRES algorithm.

For any multi-stage or multi-step scheme the linear operator $\mathbb{L}$ requires a different edge velocity for each stage/step since each stage/step represents a different time-level. To fulfill this requirement in the current implementation is trivial since there is an exact algebraic representation of the edge velocity. For the final coupled method this is dependent on the exact implementation of the coupling procedure and whether implicit or explicit time integration is used. It is likely that in case explicit time integration is used the IBL equations have to solved in a nested fashion since the time step will be very small, in the order of $\mathcal{O}\left(\frac{\Delta x}{\rho(K)}\right)$, which is likely to make any intermediate change in edge velocity negligible.

6.5 Stability

Although the CFL-criterion, as discussed in section (5.3) will be applied with a conservative value for the CFL-number, a more detailed stability consideration cannot be omitted.

6.5.1 Hyperbolic Problems

The stability of hyperbolic systems was shortly discussed in section (5.3), now a short numeric explanation will be given, see Van Kan et al[141].
The system at hand can be written simply as

$$\frac{\partial F}{\partial t} = C\,F + L, \tag{6.18}$$

where C is the spatial difference operator defined by the coefficient matrix K and the spatial discretisation scheme. For a source vector which is independent of the primary variables this leads to the error equation

$$\frac{\partial \epsilon}{\partial t} = C\epsilon, \tag{6.19}$$

and this leads to the numerical solution

$$\epsilon^{n+1} = G(C\,\Delta t \epsilon^n, \tag{6.20}$$

where G is the amplification matrix which is dependent on the time integration scheme, now there is a stable solution if all eigenvalues of the amplification matrix are smaller

than one in absolute sense. Solving this gives in general

$$\Delta t < \frac{CFL}{|\lambda|_{max}}, \rightarrow \Delta t < \frac{CFL}{\rho} \tag{6.21}$$

where ρ is the spectral radius of the discrete difference operator C, the CFL number depends on the amplification matrix. Assuming a first order Runge-Kutta time integration,i.e. forward Euler, the stability can be determined for the different spatial discretisation schemes. The amplification matrix is given by

$$G = I + \Delta t C.$$

The added difficulty is that the source vector is actually directly dependent on the primary variable vector, i.e. $L = f(U)$, and should thus be part of the stability analysis. Rewriting equation (6.20)

$$\epsilon^{n+1} = G(C\,\Delta t)\epsilon^n + \Delta t L(\epsilon^n), \tag{6.22}$$

which can be treated as follows; separate the flux term and the source term and independently determine the stability requirements, the stability range is now formed by the overlapping requirements, this has the assumption that the stability requirements of the flux vector and the source vector are independent. The above method describes global stability as the discrete operator contains the coefficient for all nodes, i.e. one has to determine the eigenvalues of the global system, of course there is the benefit that this global stability can be calculated once per timestep. For DG the spatial difference operator is considered per element.

For the local stability analysis the method by Von Neumann is often used. Standard Von Neumann analysis starts by assuming an harmonic error solution $\epsilon_k^n = \hat{\epsilon}^n \exp ki\theta, \quad k = \Delta x j$ which is substituted in the system of equations This does not necessarily lead to any difficulties except for finding the eigenvalues of the amplification matrix, the source vector however is riddled with empirical closure relations which are not likely solvable in an analytical manner. A coarse remedy may be formed by polynomially approximating the closure relations with respect to the primary variables so that the terms which are dependent on the primary variables can be added to the spatial difference operator. The Von Neumann stability analysis applies to equi-space rectangular grids with constant coefficients. To be able to find a solution for a non-linear (or quasilinear) system valid on the global domain one must conservatively assume values for the coefficients so as to establish a stability criterion which is valid throughout the domain.

The Von Neumann stability analysis can be performed for the individual characteristics

$$M_1^{-1}F_t + \lambda_1 M_1^{-1}F_x = M_1^{-1}L, \tag{6.23}$$
$$M_2^{-1}F_t + \lambda_2 M_2^{-1}F_x = M_2^{-1}L, \tag{6.24}$$
$$M_3^{-1}F_t + \lambda_3 M_3^{-1}F_x = M_3^{-1}L, \tag{6.25}$$
$$\tag{6.26}$$

with M being the matrix containing the right eigenvectors as columns. The least rigorous approach is formed by taking the scalar advection equation for the different spatial schemes and substituting the largest expected eigenvalue, i.e. $F_t + |\lambda|_{max}F_x = 0$, where the source term is ignored. Applying the assumed harmonic error solution will lead to an amplification factor of which the squared modulus should be smaller than one.

For the Shu & Osher formulation of the Runge-Kutta method (see system (6.14)), the following holds for strong stability preserving RK schemes (see Cockburn and Shu[25], Kubatko et al[79])

$$\Delta \leq \kappa \Delta t_{FE}, \quad \kappa = \min\left(\frac{\alpha_{km}}{|\beta_{km}|}\right),$$

where Δt_{FE} is the stability condition for a forward Euler time-integration scheme, i.e. one only has to determine the stability criterion for a forward Euler time-integration scheme. Likewise for a multi-step time integration scheme

$$\Delta \leq \kappa \Delta t_{FE}, \quad \kappa = \min\left(\frac{\alpha_k}{|\beta_k|}\right).$$

Due to the large number of schemes a scheme dependent stability analysis will not be performed, rather the CFL-number will be set conservatively for all tests.

6.5.2 Discontinuous Galerkin

Again the stability is mostly dependent on the CFL number which for the specific case of a degree p order basis function and a $p+1$ order Explicit Runge-Kutta time integration is approximated by (see i.e. Cockburn and Shu[25], Kubatko et al[79])

$$c\frac{\Delta t}{\Delta x} \leq \frac{1}{2p+1},$$

where c is formed by the spectral radius of the Jacobian matrix K, this estimate for the stability is exact for $p = 0$ and $p = 1$ and is within 5% for $p \geq 2$ (see Kubatko[79]). Obviously the above criterion is very restrictive for higher polynomials orders.

6.6 Flux Limiter

It was already mentioned in section (5.4) that separation is announced by a convergence of characteristics and leads to what can be considered a shock. Another case in which a discontinuity might arise is when due to transition the closure relations are suddenly switched, this effectively gives rise to a discontinuity. For higher order Riemann schemes spurious wiggles will occur around discontinuities, to prevent this from happening the values at faces are altered so that the flux is monotonously increasing or decreasing over each cell.

In general a limited flux consist of part higher order flux and a part lower order flux. The limiter function ϕ determines to what degree the higher order approximation should be incorporated based on a non-linearity parameter r which is defined as

$$r_i = \frac{F_i - F_{i-1}}{F_{i+1} - F_i}, \quad i = \text{element index}$$

where r_i is close to one for a smooth solution since the successive gradients are equal and for r_i close to zero the next gradient is much larger than the previous gradient which is caused by a local discontinuity.

For the limiter function many options exist, where the general division is between continuous (e.g. the Albada limiter) and discontinuous limiters (e.g. the minmod limiter), symmetric and asymmetric[7]. Considering

$$F_t = -\frac{1}{\Delta x}\left(f_{i+1/2} - f_{1-1/2}\right),$$

the general flux limited values are given by

$$f_{i+1/2} = f^{low}_{i+1/2} - \phi(r_i)\left(f^{low}_{i+1/2} - f^{high}_{i+1/2}\right),$$
$$f_{i-1/2} = f^{low}_{i-1/2} - \phi(r_{i-1})\left(f^{low}_{i-1/2} - f^{high}_{i-1/2}\right).$$

Flux limiters for the FVM are often incorporated in the Monotone Upstream-centered Schemes for Conservation Laws (MUSCL) scheme which is second order accurate through

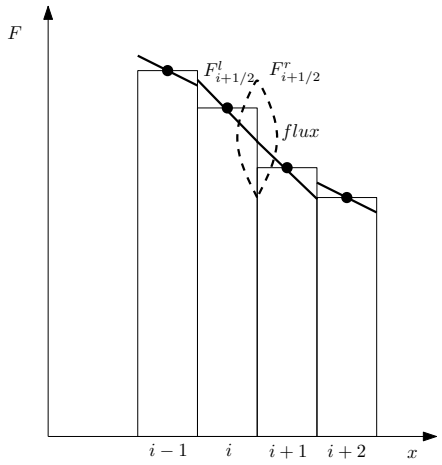

Figure 6.11: MUSCL extrapolation for FVM

linear interpolation of the cell centered values, see figure (6.11). In the MUSCL scheme the flux limiter acts directly on the face values

$$\begin{aligned} F^L_{i-1/2} &= F_{i-1} + \frac{1}{2}\phi(r_{i-1})\left(F_i - F_{i-1}\right), \quad F^R_{i-1/2} = F_i - \frac{1}{2}\phi(r_i)\left(F_{i+1} - F_i\right), \\ F^L_{i+1/2} &= F_i + \frac{1}{2}\phi(r_i)\left(F_{i+1} - F_i\right), \quad F^R_{i+1/2} = F_{i+1} - \frac{1}{2}\phi(r_{i+1})\left(F_{i+2} - F_{i+1}\right). \end{aligned} \tag{6.27}$$

MUSCL is intended for FVM's in that there is no accountancy for the location in the cell for the determination of the extrapolation and the limited values. To apply MUSCL to DG one simply has to realise that instead of centered values in neighboring elements one takes the higher order coefficients of the approximations in the directly neighboring cells (see e.g. Naber[101], Cockburn and Shu[25], Hesthaven[64])[8]. One such scheme is the generalised minmod limiter which is given by (see e.g. Cockburn and Shu[25] in reference to Osher) two steps; first the limited cell face values (denoted with $*$) are determined using

$$\begin{aligned} F^*_{i-1/2} &= F_i - \frac{1}{2} minmod\left(2(F_i - F_{i-1/2}), F_{i+1} - F_i, F_i - F_{i-1}\right), \\ F^*_{i+1/2} &= F_i + \frac{1}{2} minmod\left(2(F_{i+1/2} - F_i), F_{i+1} - F_i, F_i - F_{i-1}\right), \end{aligned} \tag{6.28}$$

where $F_{i\pm1/2}$ are the exact cell face values i.e. including all basis functions. The $minmod$ function is given as (from Cockburn and Shu[25])

$$minmod(a_1, a_2, a_3) = \begin{cases} s = min|a_n|, & \text{if} \quad s = sign(a_1) = sign(a_2) = sign(a_3) \\ 0 & otherwise \end{cases}. \tag{6.29}$$

Now if $F^*_{i+1/2} = F_{i+1/2}$ and if $F^*_{i-1/2} = F_{i-1/2}$, the original values for F are maintained, if not, a limiter is applied. Cockburn and Shu then use the following limiter

$$\begin{aligned} F^*_i &= F_i + \xi \hat{F}^{i*}_1 \\ \hat{F}^{i*}_1 &= minmod(\hat{F}^i_1, F_{i+1} - F_i, F_i - F_{i-1}), \end{aligned} \tag{6.30}$$

where $\hat{F}^i_1$ is the weight factor for the first order basis function for element i, i.e. only the first order basis function is changed and all higher order basis functions are ignored, this reduces the accuracy to second order in case limiting is applied. If higher than

[7] if the limiter works the same in all directions it is symmetric

[8] Of course one can apply the center values of the neighboring elements but this undermines the locality of the DG method.

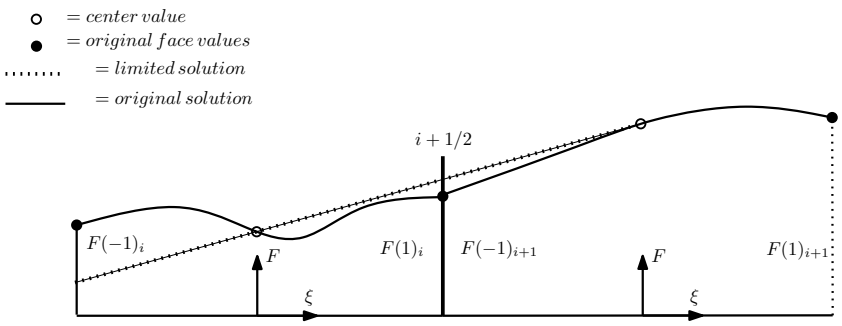

Figure 6.12: Limiter applied to cell face $i + 1/2$

second order accuracy is required Cockburn and Shu suggest a scheme which is Total Variation Bounded in the Mean (TVBM), which means that local non-monotonicity is allowed. Key to their scheme is an adapted minmod routine which contains the constant M which represents "an upper bound of the absolute value of the second order derivative of the solution at local extrema". Finding the value for M in the TVBM method is considered impractical (see Cockburn and Shu[25], Hesthaven[64], Naber[101]) and negatively affects the robustness of the method since M is problem dependent.

An alternative limiter which is higher order accurate is given by Biswas et al[11]. Biswas et al, conditionally applies a limiter to all orders of the basis functions by limiting solution moments. Biswas et al use Legendre polynomials for the solution moments, in this case monomials are used. The solution moments for the monomials are given by (see Biswas[11])

$$\int_{-1}^{1} \hat{F}^k \xi^i d\xi = \int_{-1}^{1} \left(\sum_{j=0}^{p} \hat{F}_j^k \xi^j \right) \xi^i d\xi,$$

here i and j are the order of the basis functions and k is the element index. Since the monomials are L2-orthogonal the integral is given by

$$\int_{-1}^{1} \hat{F}^k \xi^i d\xi = \hat{F}_i^k \frac{2}{2i+1}, \quad i = 0, \ldots p.$$

Since the solution moment is now only dependent on the element varying weights the solution moment can thus be made monotonous through the weights. Biswas et al proceed as follows, starting from the highest order the following minmod-limiter is applied

$$F_{i+1}^{k*} = minmod \left(\hat{F}_{i+1}^k, \frac{\hat{F}_i^{k+1} - \hat{F}_i^k}{2i+1}, \frac{\hat{F}_i^k - \hat{F}_i^{k-1}}{2i+1} \right),$$

once all orders are limited, the higher orders are limited again with the previous limited weights.

Combining this arbitrary order flux limiter in combination with an arbitrary order time integrator gives a solution strategy which is of arbitrary order of accuracy in time and space.

The downside of the arbitary order limiter from Biswas et al is that there is no stability criterium.

The flux limiter must be applied at each stage/step of the time integration scheme, see Hesthaven[64]. Strictly speaking, according to Godunov's barrier theorem (see e.g. Wesseling[153]) *any* higher order Riemann solver is non-TVD, i.e. monotonicity is not preserved. This non-TVD characteristic becomes relevant when discontinuities appear, non-physical spurious wiggles may be introduced. Thus preferably the limiter should

not be applied at all unless it is certain that a discontinuity appears. It will be clear from the transition test case that this is purely a local requirement.

At present the flux limiters are implemented but untested.

6.7 Grid Non-Uniformity and Geometry

6.7.1 Grid Non-uniformity

As was already discussed for the steady stagnation flows grid refinement will help to estimate the correct stagnation value, also any wiggles or discontinuities may be confined to a smaller region. The refinement grid will start with a grid size s times smaller than the standard grid size Δx_{def}, then the grid size is successively increased by the factor f. The grid size is then given by

$$\Delta x_i = \frac{\Delta x_{def}}{s} f \, \Delta x_{i-1},$$

both s and f are user settable in the parameter file. For the stagnation boundary layer problem the must smaller spatial step size does not lead to a much smaller overall temporal step size due the fact that the eigenvalues are close to zero near the stagnation point. For a non-stagnation boundary condition the decreased spatial step size may lead to an overly conservative temporal step size. When the grid is considered to be non-uniform, the numerical approximations for the differential terms are usually adapted. Conventionally the so-called weighted averages are used to directly incorporate the stretching of the grid in scaling the nodal values. Already in 1986 Manteuffel and White showed that the unweighed averaged scheme produce good convergence for low grid resolution. This mimetic type of discretisations also applies to the time integration which would require an implicit scheme of some sort. See Manteuffel and White[89],Gerritsma[53] and Veldman[143].

6.7.2 Adaptive Polynomial Order

How to implement the p-adaptiveness? Firstly it is based on at least the local value of the spectral radius since that remains in the stability requirement, secondly it must be related to reference values of the initial polynomial order and basically all solution values on which the local polynomial order is based. The p-adaptation is effectively a change in local spatial accuracy and should therefore also be based on the rate of change of the primary variables. This rate of change is directly reflected in the eigenvalues of the Jacobian matrix K of which the spectral radius is the largest in absolute sense, therefore it suffices to use the spectral radius as the measure for the polynomial order. Given the spectral radius from the initial solution a suitable correlation needs to be chosen to relate the spectral radius to the polynomial order. Suppose there is the following correlation for the local polynomial order

$$ceiling \left[p_{ref} \left(\frac{|\rho|}{|\rho_{ref}|} \right)^n \right] = p,$$

where n is a free parameter which determines the rate the change of the polynomial order with changing value of the spectral radius compared to the initial spectral radius. To implement p-adaptiveness either Δt or Δx needs to be adaptive also to continuously adhere to the stability requirement. This stability requirement is very restrictive for the application of an adaptive polynomial order since a global time step is used. Based on the time step one might as well apply global polynomial refinement based on the largest spectral radius. For the above reasons an adaptive local polynomial order for the space-DG with global time stepping is ill-adviced. Further consideration of a local adaptive polynomial order is therefore omitted, although, as was mentioned in section (5.5) local time stepping might accelerate convergence for steady state problems.

6.7.3 Geometry

In literature often the profile geometry plays a role in constructing the solution method for the integral boundary layer equations. The way in which the geometry enters the solution formulation differs per numerical method. Drela[35], Mughal[98] and Coenen[26] who use a FVM consider the transformation through an ad hoc transformation, first the system is solved, then the transformation takes place. Mughal[99] Nishida[103] and Milewski[94] who employ a FEM, apply a metric Jacobian to account for the rotation in all directions. Myring[100], Swafford and Whitfield[131], and Cousteix[28] who employ an FDM apply the transformation directly to the differential equations, this is typical for the FDM. For the flat plate assumption and indeed the overall boundary layer equations it is required that the curvature effect is negligible since stream normal pressure gradients are neglected. If this assumption holds and if the tangential velocity distribution over the profile is given it is not necessary to include geometric curvature terms if the boundary layer is considered in local profile coordinates. If local profile coordinates are used, following the profile is effectively equal to following the x-axis in the profile coordinate system, i.e. a quasi-flat plate. Once the primary variables are known in the local profile coordinates the global coordinate values can be retrieved for the two dimensional case with

$$\begin{aligned} C_{f,X} = C_{f,x}\cos\alpha(x), \quad \delta^*_X = \delta^*_x\cos\alpha(x), \quad \theta^*_X = \theta_x\cos^2\alpha(x), \\ \delta^k_X = \delta^k_x\cos^3\alpha(x), \quad \delta^{k+}_X = \delta^{k+}_x\cos^4\alpha(x), \end{aligned} \tag{6.31}$$

where α is the local angle of the profile coordinate system with the global coordinate system. Also since the largest rate of curvature occurs at the leading edge where the friction drag and the displacement thickness are of minor importance it might be argued that the transformation can be omitted from the boundary layer and IBL equations with the exception that the crossflow angle should be accounted for in three-dimensional boundary layer flow.
For the coupled procedure Veldman[144] suggests to include streamline curvature through a pressure jump between boundary layer and the inviscid flow.

6.8 Convergence

Following Lax' theorem convergence should be guaranteed given a stable and consistent discretisation. This is important for the validity of the comparison of the numerical methods. The aim is to compare the methods for similar levels of convergence. To check convergence of the system the results will be compared to the Blasius solution for different grid sizes. This convergence test can be used to the verify that higher order schemes indeed convergence in accordance with their respective order of accuracy. The L2-error norm is used as the convergence indicator. The L2-error norm is defined as

$$L_2 = \sqrt{\frac{\sum(F_{exact} - F^*)^2}{\sum F^2_{exact}}},$$

the error norm is taken over the common points of the successive grids. The exact values of the Blasius solution at any $x-$station are repeated here

$$\theta = \frac{0.664x}{\sqrt{Re_x}}, \quad \delta^* = \frac{1.7208x}{\sqrt{Re_x}}, \quad C_f = \frac{0.664}{\sqrt{Re_x}}.$$

The laminar flat plate is chosen as the only convergence test case for the simple reason that the closure relations should give an exact representation of the boundary layer since the relations are based on the Falkner-Skan solution. The convergence test will be done for a small selection of schemes to draw qualitative conclusions.

For general cases the convergence is monitored using the L2-norm of the current values in relation to the L2-norm of the previous values, the metric is denoted by $C2$

$$C2 = \frac{|L_{2,new} - L_{2,old}|}{L_{2,old}}, \tag{6.32}$$

unless otherwise noted $C2_{min}$ is set to $1e-13$.

6.9 Why the Jacobian is not just some coefficient matrix, a lesson learned

Although the FVM and the FEM descriptions clearly assume a conservative set of differential equations the author used the non-conservative formulation for the actual implementation. Little adaptation of the code is required due to the modular set-up, however it remains a monumental mistake.
The confusion was mainly caused by misinterpreting the paper from Matsushita and Akamatsu. Matsushita and Akamatsu used a quasi-linear form of a conservative system of equations and using the Jacobian they stated $f = Aw$ (i.e. $\frac{\partial f}{\partial w}\frac{\partial w}{\partial x} = \frac{\partial\left(\frac{\partial f}{\partial w}w\right)}{\partial x}$), which was directly translated by the author as $f = KF$, hence the flux terms $f_{i\pm1}$ in the FVM and FEM schemes were mistakingly taken as $f_{i\pm1} = K_{i\pm1}F_{i\pm1}$. Furthermore, initially extensive used was made of the PhD-theses of Blom and Özdemir for the DG implementation, these theses however deal with DG applied to the linearized Euler equation where the quasi-linear form *is* the final system. The quasi-linear form assumes a constant Jacobian which is not the case for the non-conservative system. The conservative form is already given in equations (4.18). The current approximation leads to the following

Originally used system: $F_t + KF_x = L$,
Conservative system: $F_t + f_x = L$,
Actual approximated system: $F_t + (KF)_x = L$,
Correction to regain consistency: $F_t + (KF)_x - FK_x = L$,

For the test cases the correction term $-FK_x$ is added to the FVM and the DG scheme for the sake of testing the implementation. What was actually happening, the vector f is defined by

$$K\frac{\partial F}{\partial x} = \frac{\partial f}{\partial F}\frac{\partial F}{\partial x} \rightarrow f = \int K\partial F,$$

writing out the integration

$$f = \begin{pmatrix} \int K_{11}\partial F_1 + \int K_{12}\partial F_2 + \int K_{13}\partial F_3 + C_1 \\ \int K_{21}\partial F_1 + \int K_{22}\partial F_2 + \int K_{23}\partial F_3 + C_2 \\ \int K_{31}\partial F_1 + \int K_{32}\partial F_2 + \int K_{33}\partial F_3 + C_3 \end{pmatrix}, \tag{6.33}$$

which cannot be done symbolically a priori since the turbulent boundary closure models do not allow an analytical integration of the coefficient matrix. Alternatively the flux vector can be approximated by numerical integration

$$f = f_0 + \begin{pmatrix} \frac{\partial f_1}{\partial F_1}\Delta F_1 + \frac{\partial f_1}{\partial F_2}\Delta F_2 + \frac{\partial f_1}{\partial F_3}\Delta F_3 \\ \frac{\partial f_2}{\partial F_1}\Delta F_1 + \frac{\partial f_2}{\partial F_2}\Delta F_2 + \frac{\partial f_2}{\partial F_3}\Delta F_3 \\ \frac{\partial f_3}{\partial F_1}\Delta F_1 + \frac{\partial f_3}{\partial F_2}\Delta F_2 + \frac{\partial f_3}{\partial F_3}\Delta F_3 \end{pmatrix}. \tag{6.34}$$

this however assumes a constant coefficient matrix which is not the case here, also f_0 is not known, therefore to go from a non-conservative system to a conservative system the Jacobian must be integrated exactly. This is very difficult in general and it is specifically

Module	Subroutine	Module	Subroutine
$PROG\_Main$	$SUBR\_Boundary$	MOD_Gauss	$SUBR\_BasisFunction$
$MOD\_Closure$	$SUBR\_charOutput$		$SUBR\_CSplineCoeff$
$MOD\_Declare$	$SUBR\_ConvergenceCheck$		$SUBR\_FINDInv$ [9]
$MOD\_External$	$SUBR\_Flux$		$SUBR\_FluxLimiter$
	$SUBR\_GridGen$		$SUBR\_FluxLimiterHO$
	$SUBR\_Init$		$SUBR\_FluxLimiterMinMod$
	$SUBR\_Integrator$		$SUBR\_MSmatrix$
	$SUBR\_KL$		$SUBR\_NumFluxVector$
	$SUBR\_Output$		$SUBR\_SourceAndFluxVector$
	$SUBR\_Parameters$		
	$SUBR\_SeparationCheck$		
	$SUBR\_TransitionCheck$		

Table 6.4: Overview of subroutines and modules, (left) for the FDM/FVM algorithms (right) and the extra routines for the DG algorithm

hard for this case, it would be considerably easier to differentiate the flux vector to obtain the Jacobian, therefore one should in general start with the conservative form. To at least test the current implementation a fix will be introduced , the term $-F\frac{\partial K}{\partial x}$ is approximated by the following discretisation

$$\text{FVM:} \quad F_i(K_x)_i = \frac{F_i}{2}\left(K_{i+1} - K_{i-1}\right),$$

$$\text{FEM:} \quad F_i(K_x)_i = \frac{F_{i-1/2} + F_{i+1/2}}{4}\left(K_{i+1} + K_{i+1/2} - K_{i-1/2} - K_{i-1}\right).$$

The only test case considered for the FVM and the FEM scheme is the impulsively moved flat plate, see section(7.1.1).

6.10 Numerical Smoothing

Numerical smoothing is applied over the transition region, i.e. the region where the intermittency is valued between 0 and 1, and basically whenever the numerical simulation is unstable and lowering the CFL-number does not relieve the problem. Smoothing is attained by the simple averaging procedure

$$F_i = \frac{F_{i-1} + F_{i+1}}{2}.$$

6.11 Code Development for Integral Boundary Layers

To facilitate the further development of the code and the final implementation in the full three dimensional solver an overview of the basic programming logic is given. Also, a there is a short discussion on performance optimisation. Since the code development is intrinsically related to the performance of a numerical scheme this cannot be omitted. The basic outline is given in figure 6.13

The parameters module in figure (6.13) may well be linked directly to all other modules as all modules may offer the possibility of user specified settings, by linking it to the central integrator module this general linkage is satisfied.

6.11.1 Program Elements

Shortly the program elements are discussed, the functionality and , the program elements are given in table (6.4). The main program $PROG\_Main$ contains the main loop, connects all the routines , updates the primary variables and calls output routine

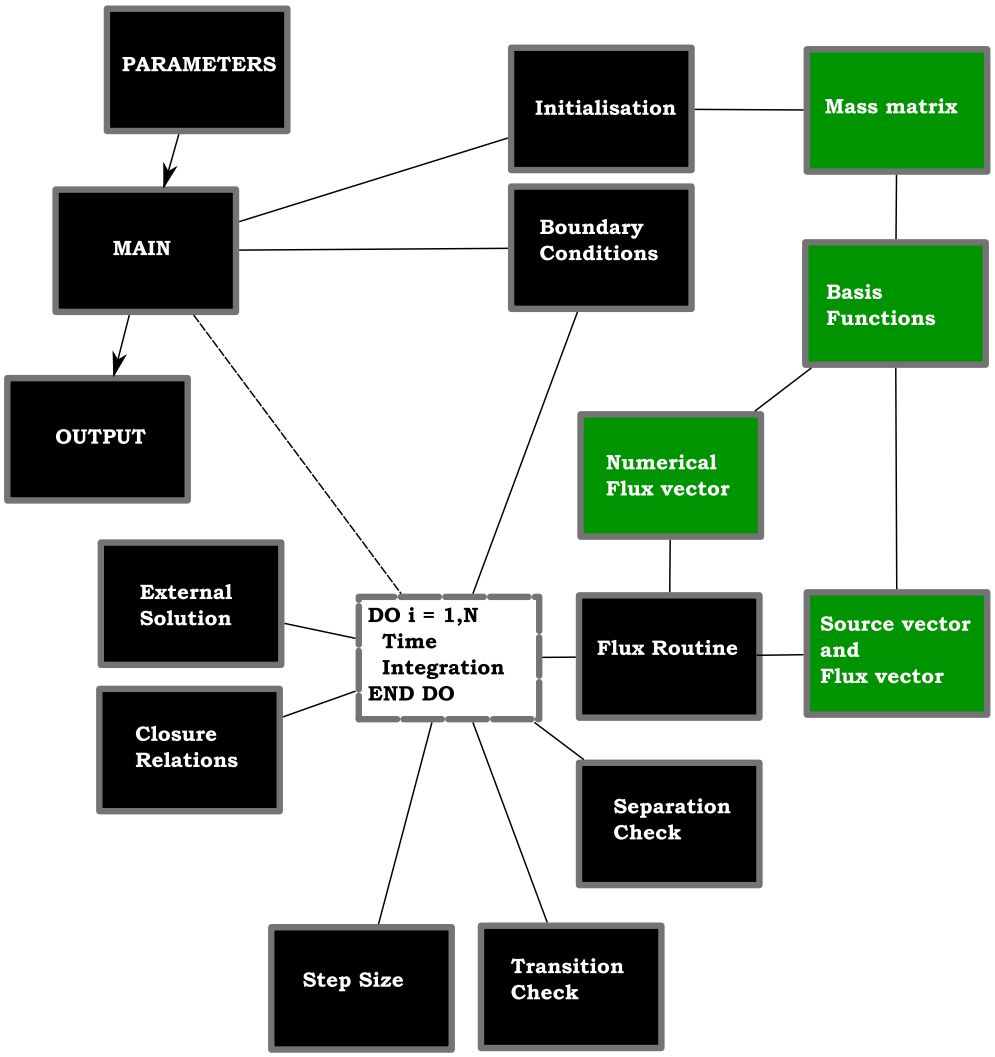

Figure 6.13: Functional logic outline, the green functional blocks represent the extra logic introduced for the DG algorithm

$SUBR\_Output$. For the DG algorithm, at every time step in the main loop, the cubic spline coefficients are generated for the edge velocity distribution.

The module $MOD\_Declare$ declares the common variables and the parameters.

The module $MOD\_Closure$ contains the closure relations and the relations for the eigenvectors and the eigenvalues.

The module $MOD\_External$ generates the velocity profile including the spatial and the temporal derivative.

The subroutine $SUBR\_Boundary$ generates the left boundary condition.

The subroutine $SUBR\_charOutput$ supports the subroutine $SUBR\_Output$, it generates file name prefixes for the output files, credits to H.Özdemir.

The subroutine $SUBR\_ConvergenceCheck$ generates the convergence parameter $C2$ (see equation (6.32)), if the convergence parameter meets the convergence requirement the main loop in $PROG\_Main$ is aborted.

The subroutine $SUBR\_Flux$ generates the temporal flux $\frac{\partial F}{\partial t}$, this subroutine is called by subroutine $SUBR\_Integrator$.

The subroutine $SUBR\_Gridgen$ generates the new timestep based on the eigenvalues, for the DG algorithm this subroutine also contains the code for the adaptive polynomial order.

The subroutine $SUBR\_Init$ first generates the grid, then allocates the variables with the appropriate size (based on the number of grid points) and then assigns the initial values, this subroutine is called by $PROG\_Main$.

The subroutine $SUBR\_Integrator$ uses on of the Runge-Kutta time integration schemes and the temporal flux subroutine $SUBR\_Flux$ to obtain the primary variables for the new time level.

The subroutine $SUBR\_KL$ generates the Jacobian matrix and the source vector, for the DG algorithm a cubic splines function is added to obtain the interpolated value for the velocity at the cell face.

The subroutine $SUBR\_Output$ is called from the main program and prints out all the data files and the plot files, created with assistance from H.Özdemir.

The subroutine $SUBR\_Parameters$ processes the parameter file, the parameter file can be found in appendix (H).

The subroutine $SUBR\_SeparationCheck$ applies the separation indicator based on the shock strength (see equation (5.4)) and several of the discussed separation indicators (see equations (3.16), (3.15)) , also the zero friction point is monitored.

The subroutine $SUBR\_TransitionCheck$ applies the theory of section (5.4) to detect the point where the boundary layer becomes critical up to the point where the boundary layer transitions from laminar to turbulent. In this subroutine the so-called intermittency vector is created, this vector contains for each point a value between 0 and 1 to indicate the degree of turbulence. This intermittency vector can be pre-set in the parameter file.

Specifically for the DG method several extra subroutines are created.

The subroutine $SUBR\_CSplineCoeff$ creates cubic spline coefficients, in this case for the vector containing the edge velocity values.

The subroutine $SUBR\_FINDInv$ finds the inverse matrix, in this case of the mass matrix, this subroutine is called in the initialisation subroutine $SUBR\_Init$ and should also be called in $SUBR\_GridGen$ if an adaptive stepsize or an adaptive polynomial order is used.

The subroutines $SUBR\_FluxLimiter$, $SUBR\_FluxLimiterHO$ and $SUBR\_FluxLimiterMinMod$ determine the flux limited cell face values, using conventional limiters, the higher order limiter and the minmod limiter from Cockburn and Shu[25] respectively (see section (6.6)). These subroutines are called in the subroutine $SUBR\_NumFluxVector$ which determines the numerical flux over the cell faces.

The subroutine $SUBR\_SourceAndFluxVector$ generates the flux vector and the source vector i.e. the last two terms of equations (6.9) and (6.10).

6.11.2 Vectors or Scalars

In the code a scalar approach is taken in general and where easily implemented a vector approach is taken. For example,

```
K(1:currSteps,1) = (-1.0d0+Hstar)*ue
```

and not

```
DO i=1,currSteps
K(i,1) = (-1.0d0+Hstar(i))*ue(i)
END DO
```

The following code snippet is an example of what is considered too 'complex' to implement in vectorised form

```
DO i=3,currSteps-2
   Fl(i,1) = 0.5d0 * (sum(K(i,1:3)*Flocal(i,1:3))+sum(K(i-1,1:3)*Flocal(i-1,1:3))) &
             -0.5d0*sum(abs(Ksl(i,1:3))*(Flocal(i,1:3)-Flocal(i-1,1:3)))
...
END DO
```

Most compilers are optimised for vector-based operations and irrespective of that, in most cases a vector-based operation has less overhead than a scalar-based operation for the simple reason that with each vector call an entire range of memory locations are processed in one go whereas for a scalar based approach each memory location is processed separately. Vector optimised compilers will for instance make sure that the memory locations are sequential.This means considerable gain can be achieved by writing out the algorithms in terms of vectors, irrespective of the compiler used.

Vectorisation in DG will require more effort due to the added nested loops for the polynomial orders.

6.11.3 Boolean Operators

The closure models of have defined ranges which need to be checked using boolean operators, this not only causes overhead in the loops it also prevents the use of a full vector-based approach since the vectors have to be broken. For optimisation the closure models should thus be made continuous over the range of applicability.

Part III

Application of Selected Models to Test Cases and Comparison of Results

Chapter 7

Test Cases

Using a combination of numerical results and experimental data the results from the current IBL system can be verified, the unsteady test cases are

- Impulsively started flat plate,
- Impulsively started cylinder,
- Oscillating infinite flat plate,

and other test cases are possible, see e.g. Sekar[120] for several flutter cases using a coupled approach for the IBL equations (also see appendix(I.4)). The logic behind the selection of test cases is as follows; with the flat plate case both the laminar and the turbulent closure models are verified and the transition criterium is tested. With the cylinder case the simulation of transient behavior and the robustness for separating flow are tested. The oscillating flat plate for the turbulent case contains a velocity distribution which is both time and location dependent, this may verify that the system can properly handle simultaneous time and location changing outer velocity.

This list is by no means exhaustive, several topics can be addressed considering the numerical techniques that have been discussed. In the chapter on the numerical methods several time integration methods have been discussed. This leaves out several time integration schemes which supposedly have better stability properties. Also the subject of flux limiters will not be tested, indeed the first question that needs to be answered is if flux limiters are really necessary at all. Stability in general will not be treated and differences in numerical schemes will not be investigated in any detail due to time constraints.

The values of constants used in the test cases differ per test case and will thus be indicated per test case.

For all test cases appendix (J) contains more plots which do not fit the body text.

7.1 Flow over a Flat Plate

The initial and most obvious testcase is the original flat plat flow with constant external velocity. The flat plate flow with constant external velocity is well described, analytically and empirically. This basic problem can be solved analytically and thus forms an excellent test case for the unsteady flow solver. Based on the impulsively started flat plate an exact solution can be derived for infinite flat plates with arbitrary prescribed

velocity. A more challenging problem is given by the impulsively moved semi-infinite flat plate which can be approximated algebraically for small and large times. Treating this problem with the IBL equations requires that the reference frame is fixed to the plate since zero boundary conditions were used for the wall surface. See appendix(I.4.3) for background information on the laminar flow over a flat plate.

7.1.1 Impulsively Moved Flat Plate

The first test case assumes the flat plate with a uniform velocity distribution which changes in time. The assumption of a flat plate removes the necessity to apply coordinate transformations and should thus level out the performance of the FDM's, FVM's and the FEM, this will be the base comparison. Two subcases will be considered, a periodically changing velocity and an impulsively moved flat plate. These subcases can be compared directly to the earlier discussed limit cases where the only appreciable difference should be the presence of a wake which may also affect the boundary layer before the plate-end.

Laminar Flow, $Re = 100,000$

The first test case that is performed is the laminar flow over a flat plate in which only the steady state solutions are considered. For the global parameters see table(7.1). The

parameter	value	unit
plate length	1.0	$[m]$
run time	convergence	$[s]$
temporal scheme	Runge-Kutta 2/4	$[n/a]$
refinement	none	$[n/a]$
kinematic viscosity	1.5e-5	$[\frac{kg}{ms}]$
edge velocity	1.5	$[\frac{m}{s}]$

Table 7.1: Global variables for laminar flow over impulsively moved flat plate

upwind schemes were tested for several grid resolutions and show grid convergence as should be expected(see e.g. figure(7.2)).

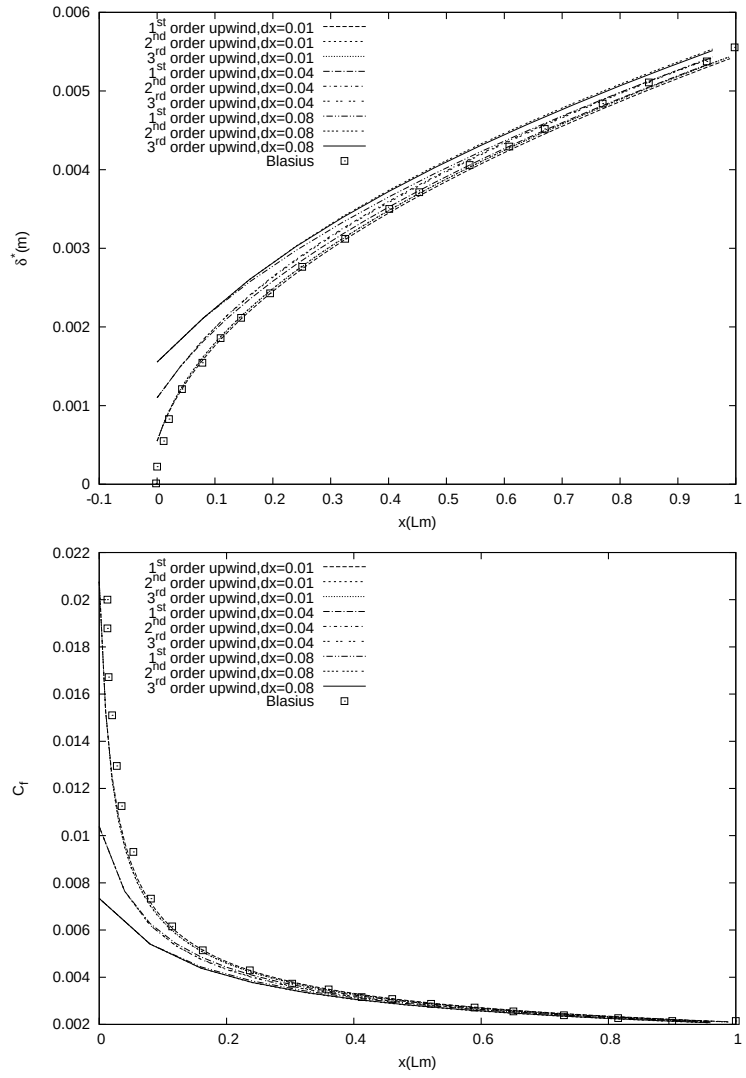

Figure 7.1: Comparison of result for the upwind schemes applied to laminar flow over a flat plate,$RK = 2$,$CFL = 0.5$ at $t = 4.5\ (s)$ at various grid resolutions, (top) Displacement thickness, (bottom) Friction coefficient

The remaining finite difference schemes behave in a similar fashion, no significant issues arose, see figure (7.2). All finite difference schemes produced good results being very close to the reference solution, this indicates that the laminar closure models have been implemented correctly. Now considering the results obtained with the DG scheme, the Roe scheme and the Kurganov-Tadmor scheme, see figure(7.3). Figure (7.3) shows the results for the corrected and the uncorrected schemes, this has been explained in section(6.2). For the DG scheme the three-point Gaussian quadrature was used with linear basis functions, the use of the expansion in basis functions does not work at present. The results for the Steger-Warming schemes were found to be in good agreement with the exact solution, however this was obtained by dividing the spatial flux by four. This artificial fix was maintained in the code.

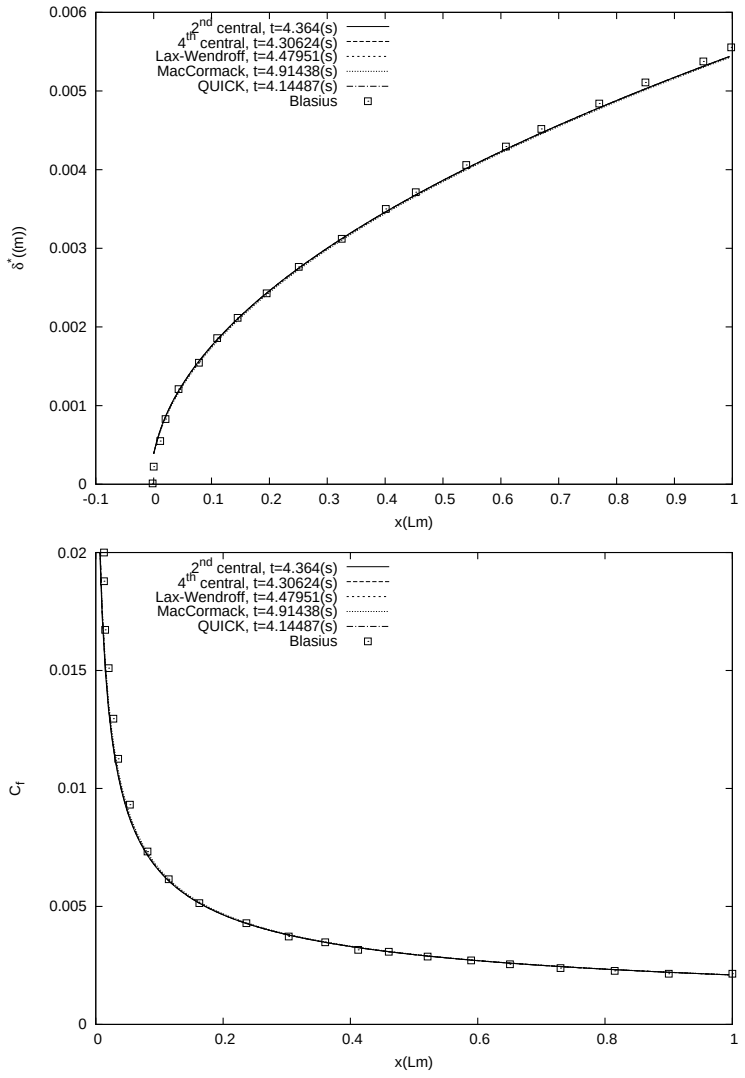

Figure 7.2: Comparison of the steady state result for various schemes applied to laminar flow over a flat plate, $RK = 2$,$CFL = 0.5$, (top) Displacement thickness, (bottom) Friction coefficient

A convergence check with the L_2-norm shows that all schemes converge with a 1^{st} order convergence rate (see figure(7.5)), this may be due to the first order accuracy at the left boundary which pollutes the rest of the solution domain, this remains a guess however. No smoothing was necessary for stability. When smoothing was applied the solution quality deteriorated significantly. It was already stated in the theory section that the steady state should be reached within four seconds based on the reference results (see (I.4.3)), indeed for finer grids the convergence of the finite difference schemes is reached in about four seconds, see figure (7.4).

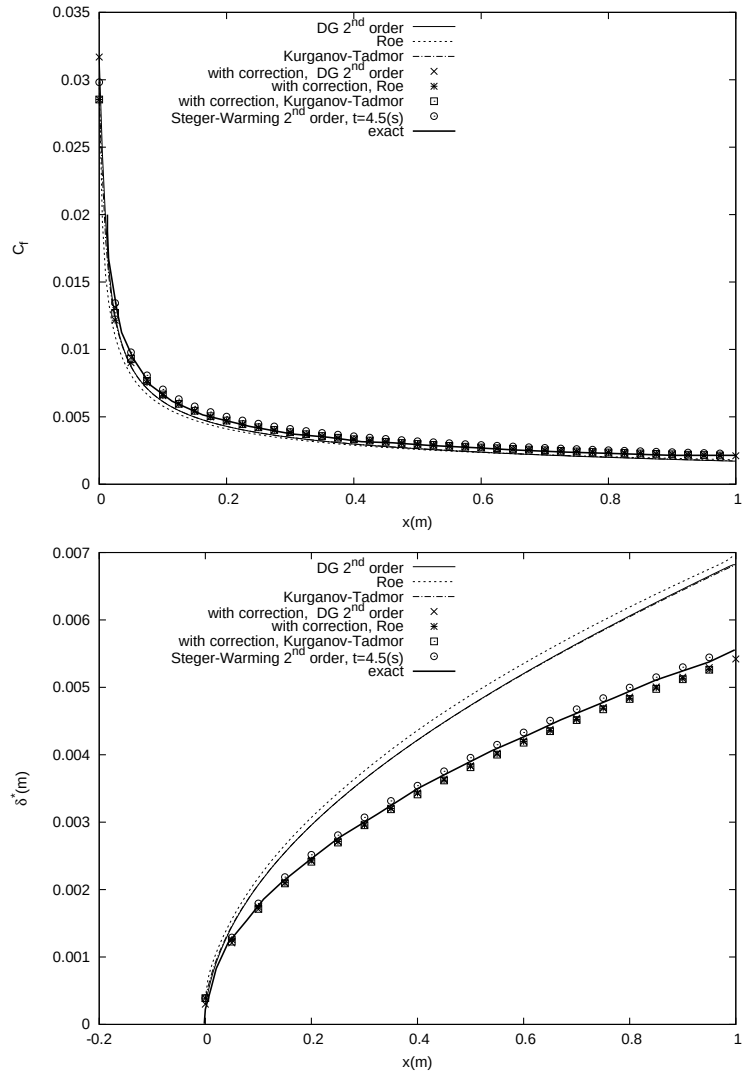

Figure 7.3: Comparison of result using the DG, Roe, Kurganov-Tadmor schemes applied to laminar flow over a flat plate (top) friction coefficient C_f , (bottom) displacement thickness δ^*

Turbulent Flow, $Re = 10,000,000$

This test case involves a fully turbulent boundary layer over a flat plate, again only the steady state solutions are considered, for the global parameters see table(7.2). The flat plate produces an equilibrium boundary layer so as could be expected the results with the equilibrium closure model compare well with the reference results, using the non-equilibrium closure model leads to different quantitative results which still compare well with the reference results. The non-equilibrium model produces a slightly less stable solution, however no additional stability measures are needed for $t = [0, 0.01]$. For $t = [0.01, 0.1]$ stability issues arise both using the non-equilibrium model and the equilibrium model: no finite difference scheme is stable for $CFL = 0.5$ with first order Runge-Kutta time integration and for higher order Runge-Kutta time integration the first and second order upwind scheme and the MacCormack scheme remain unstable. The upwind schemes are less stable if the eigenvalues are of mixed sign which is the

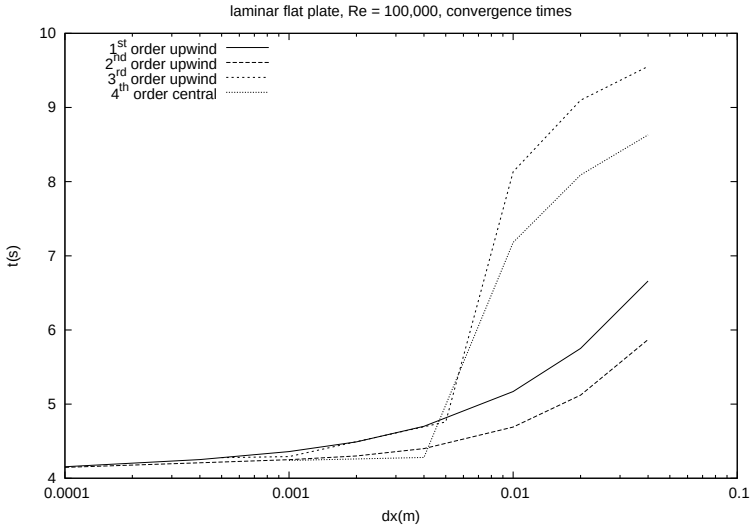

Figure 7.4: Convergence times for differential spatial discretisation schemes

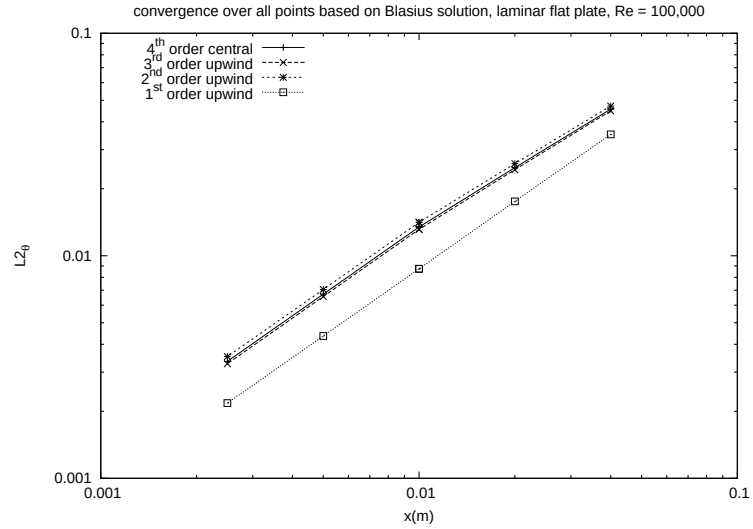

Figure 7.5: L_2 norm over all points

case for high Reynolds turbulent flow. In this case the third order upwind scheme is more stable than the lower order upwind schemes maybe due to the fact that it uses nodes from both sides. The application of smoothing stabilised all schemes and did not significantly affect the steady state result, see figure (7.7).

The $(1/7)^{th}$ power law distribution formed a suitable left boundary condition together with the adapted Rayleigh solution as the initial condition. Suitable in the sense that a steady state solution could be attained, however the shape factor was qualitatively different from the reference value. This was presumably caused by the initial condition over the plate, the Rayleigh solution used in this thesis was not based on empirical data and was merely meant as a quick fix to be able to attain a converged solution, i.e. the transient result should not be considered as physical. A comparison between a smoothed and a non-smoothed solution is shown in figure (7.7), clearly the smoothing has some effect at the boundary but otherwise the solutions overlap. If indeed a tur-

parameter	value	unit
plate length	1.0	$[m]$
run time	0.01	$[s]$
temporal scheme	Runge-Kutta 4	$[n/a]$
refinement	none	$[n/a]$
kinematic viscosity	1.5e-5	$\left[\frac{kg}{ms}\right]$
edge velocity	150	$\left[\frac{m}{s}\right]$

Table 7.2: Global variables for turbulent flow over impulsively moved flat plate

bulent initial boundary layer is considered at all, it should be investigated whether an adapted $(1/7^{th})$ power law condition can be used for the fully turbulent layer, this $(1/7^{th})$ power law distribution should be initialised using the time derivative of the Rayleigh solution for $t = \Delta t$ multiplied with some factor to account for the higher mixing rate of the turbulent boundary layer (and thus the shorter development time and likely larger time derivative). Overall, applying the non-equilibrium closure relation decreased the numerical stability for all schemes. Smoothing was needed for the 2^{nd} order upwinding scheme, even for the equilibrium turbulent boundary layer, however this did not affect the solution quality significantly as it did for the laminar case.

It is concluded here that the current implementation of the IBL equations can handle both laminar and turbulent boundary layer flows.

Transitional Flow, $Re = 6,250,000$

Now the transition criterium will be tested using a steady flat plate transition flow. For the global parameters see table(7.3). The steady results are shown in figure (7.8) and

parameter	value	unit
plate length	3.75	$[m]$
run time	1.0	$[s]$
temporal scheme	Runge-Kutta 1	$[n/a]$
refinement	none	$[n/a]$
left boundary condition	Thwaites	$[n/a]$
kinematic viscosity	1.5e-5	$\left[\frac{kg}{ms}\right]$
edge velocity	25	$\left[\frac{m}{s}\right]$
Δx	0.01	$[m]$

Table 7.3: Global variables for laminar/turbulent flow over an impulsively moved flat plate

are quite satisfactory, the non-equilibrium closure uses a maximum amplification factor of 8.9 and a reference amplification factor of 9.1 so starting from amplification factor 8.9 the intermittency is increased until the amplification factor is equal to the reference amplification factor[1]. It was found that the difference between the maximum amplification factor and the reference amplification factor cannot be larger than about ≈ 0.3. The mechanism for turbulence transition is devised for steady boundary layer flow in that there is no description of transient behavior locked inside the transition models, this was the reason for considering the intermittency transport function. A major assumption with the current implementation is that upon establishing transition in a certain point the points downwind are considered to be fully turbulent, this is followed by checking the assumed turbulent boundary layer for relaminarisation. Thus directly after transition, the following time step contains the intermittency distribution following from the transition check of the previous time step and at the same time the primary variables which are used to determine the new flux vector are still laminar; the boundary layer is considered turbulent after the transition point, yet the primary variables

[1] an exponential post-intermittency function was used here

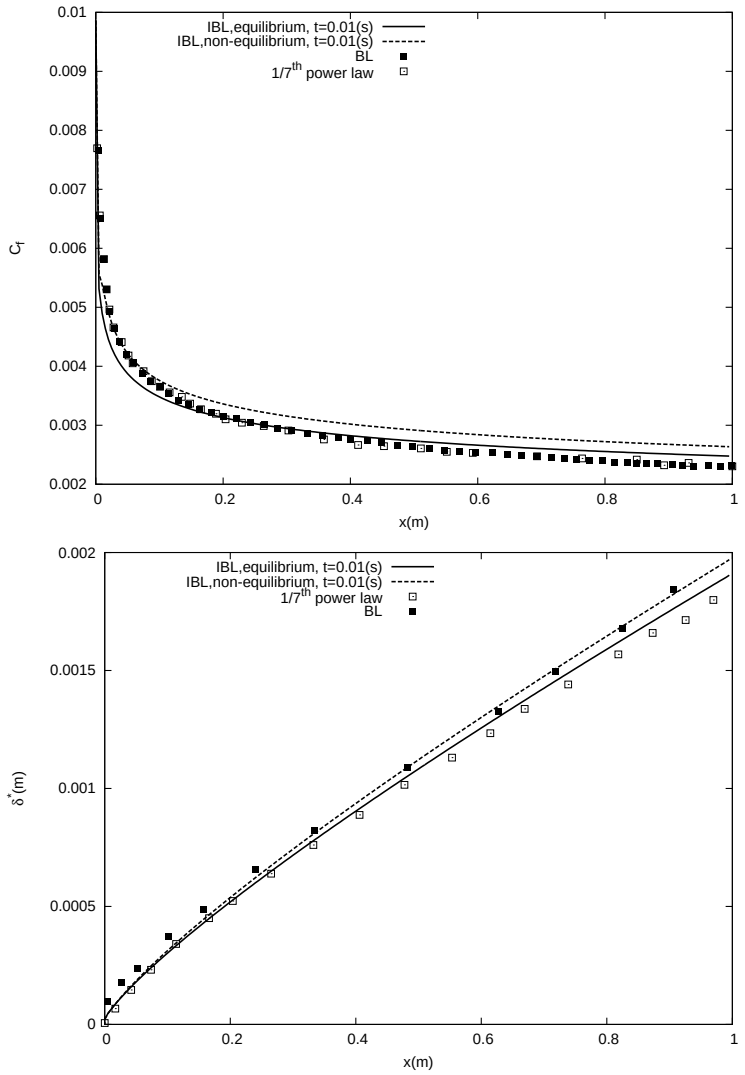

Figure 7.6: MacCormack spatial discretisation scheme with RK4 time integration scheme applied to turbulent flow over a flat plate (top) friction coefficient C_f, (bottom) displacement thickness δ^*

are still laminar at the time, this causes problems because the laminar values for the primary variables are not suitable for the turbulent closure relations, i.e. it will generate unphysical values. This was demonstrated by the travelling disturbance following the transition for the non-equilibrium boundary layer flow, see figure(7.9).

A more realistic approach would be to consider a simplified version of the intermittency transport function , in which the intermittency is continuously dependent on the flow (integral) variables both in time and space, this would avoid the mentioned unphysical behavior at transition. So the obvious problem of the current formulation is that the transition is instantaneous in time, although continuous in space, the main question is how this time dependency is integrated in such a way that the intermittency behaves in a physically correct manner and yet can be fitted in the IBL approach.Secondarily, the shock indicators produced a clear spike at transition which was due to the eigenvalues changing value discontinuously upon transition, in light of the earlier discussion this is likely unphysical, see figure(7.10). The discontinuous change in eigenvalues supports

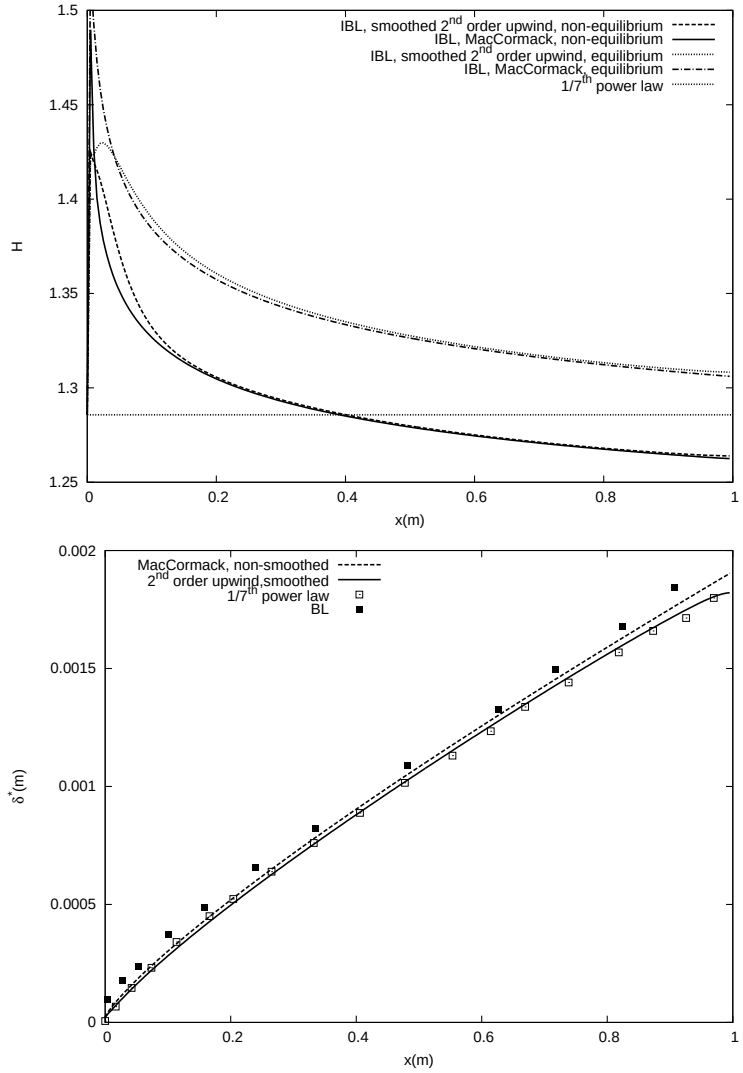

Figure 7.7: Comparison of effect of numerical smoothing for second order upwind scheme applied to turbulent flow over a flat plate, (top) Shapefactor H at $0.01(s)$,$\Delta x = 0.005(m)$, with RK4 time integration, (bottom) Displacement thickness δ^* for a smoothed and a non-smoothed solution

the idea to implement a flux limiter for higher order conservative schemes, at the same time the flux limitation can be limited to a very small region. Exactly the region of transition is indicated by the intermittency being valued between 0 and 1. Based on this result higher order conservative schemes can be implemented without flux limitation. Another situation in which discontinuities may arise is the case of separation, see section (5.4). The friction coefficient for the non-equilibrium boundary layer has a slight overshoot compared to the equilibrium boundary layer, this is comparable to the results by Fenno et al[50][2].

[2]although in their case there was also a shock which may have amplified any existing differences

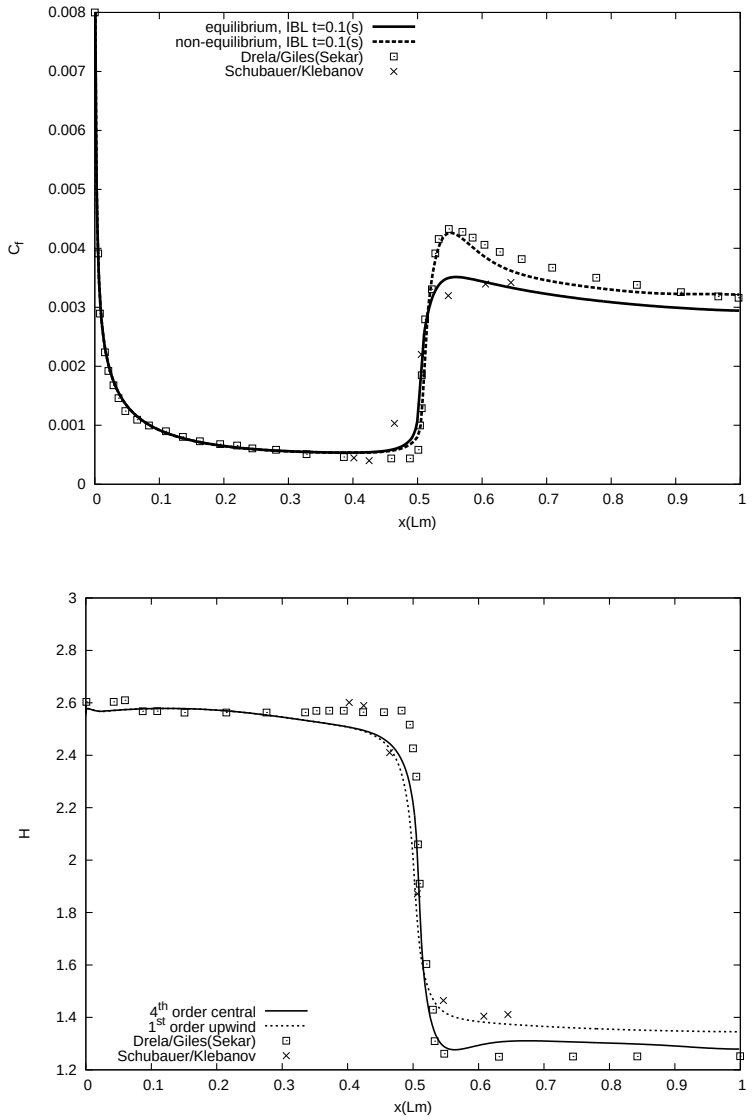

Figure 7.8: Comparison of results for the transition simulation obtained with a 4^{th} order central differencing scheme with $RK1$ time integration, (top) friction coefficient C_f (bottom) shape factor H

7.1.2 Oscillatory Moving Flat Plate

The following test case will cover both an edge velocity gradient in the spatial direction and in the temporal direction and will thus cover the extent of the terms in the Jacobian matrix K and the source vector L. First a laminar boundary layer flow over an oscillating flat plate is considered with only a temporal edge velocity gradient, then the turbulent boundary layer flow over an oscillating flat plate is considered, now with inclusion of spatial edge velocity gradient.

Laminar Flow

The basis comparison for the oscillating flat plate is formed by the analytic solution of the second Stokes problem. The second Stokes problem describes an infinitely long flat

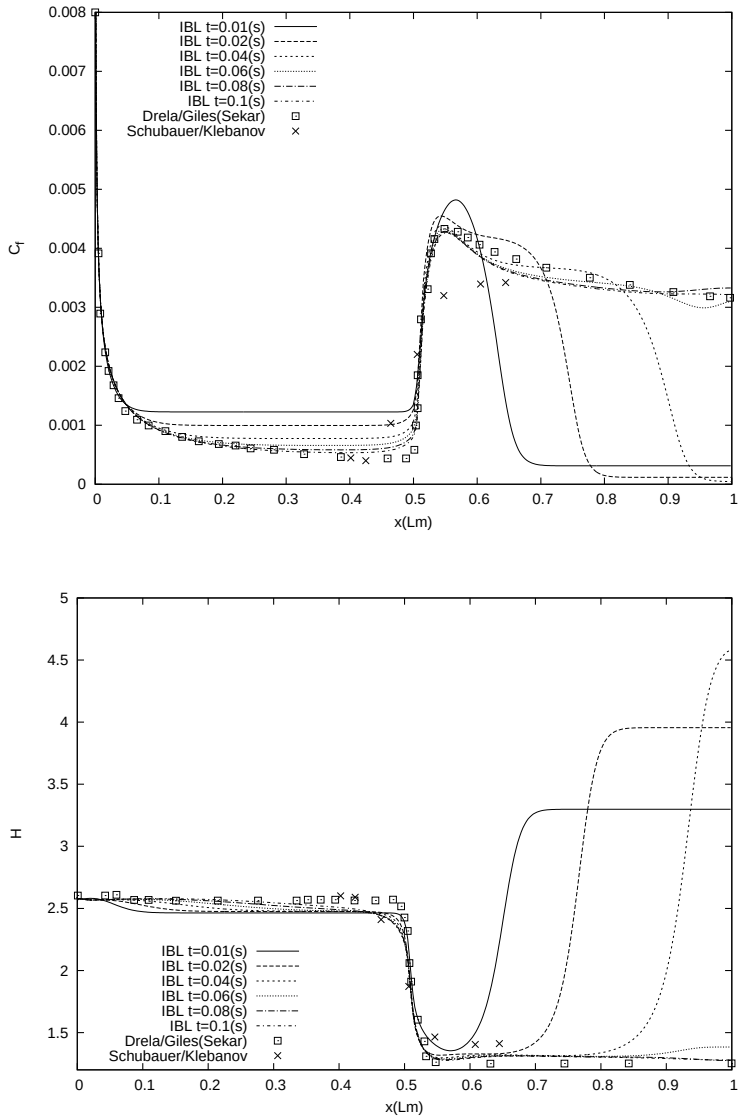

Figure 7.9: Comparison of results for non-equilibrium transition flow, obtained with 4^{th} order central differencing scheme, (top) friction coefficient C_f, (bottom) shape factor H

plate which is undergoing an oscillatory motion. For this thesis the plate is of finite length with no wake influence, furthermore for the boundary conditions it was assumed that the flow direction at the boundaries is unchanged, this limits the comparison. First of all the result can only be compared for the points which are unaffected by the boundaries, secondly the edge velocity can not be negative at the left boundary therefore the time cannot exceed a quarter period. The velocity distribution is given by (see appendix(I.4.3))

$$\frac{u}{u_e} = 1 - \frac{e^{-\eta}\cos(\omega t - \eta)}{\cos(\omega t)}, \quad u_e = u_0\cos(\omega t), \tag{7.1}$$

with $\omega = 2\pi f$ and $\eta = \sqrt{\frac{\omega}{2\nu}}y$, where f is the frequency from the velocity distribution it follows that the friction coefficient is described by

$$C_f = 2\frac{\nu}{u_o}\sqrt{\frac{\omega}{2\nu}}(\cos(\omega t) - \sin(\omega t)) \equiv 2\frac{\nu}{u_o}\sqrt{\frac{\omega}{2\nu}}\cos(\omega t + \frac{1}{4}\pi). \tag{7.2}$$

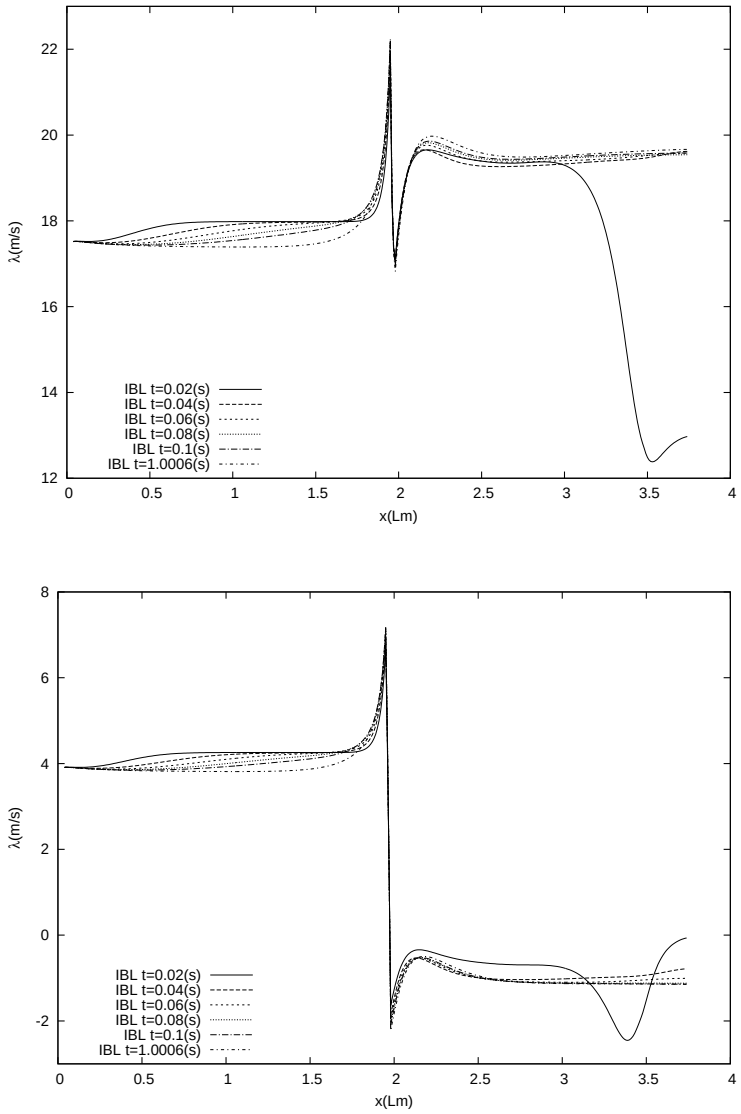

Figure 7.10: Eigenvalues for the transition flow over a flat plate, obtained with 4^{th} order central, with RK1 time integration,(top) λ_+, (bottom) λ_-

So the friction coefficient C_f is ahead of the velocity distribution by $\frac{1}{4}\pi$ ° and thus already for time $t = \frac{1}{8}T$, where $T = \frac{1}{f}$, the friction coefficient becomes negative, therefore the time should be limited to $t < \frac{1}{8}T$. Assuming that the disturbance of the left boundary propagates to the right with the initial velocity of the plate and using the global parameters from table(7.4) the undisturbed reference point is $x > \frac{1}{8}Tu_e$.
This specific test only involves the source vector since it is assumed that the boundaries do not affect the reference point. The boundary layer velocity distribution of the second Stokes problem allows for algebraic integration of the integral variables. The closure relations used for the laminar boundary layer are based on the boundary layer thickness $\delta_{99\%}$ where $\frac{u(\delta)}{u_e} = 99\%$, to facilitate this the boundary layer thickness is determined for each time level, see figure (7.13). The most suitable initialisation of this problem is of course formed by the analytical solution of the second Stokes problem. There are now four cases using the Rayleigh solution or the Stokes solution as initialisation and either the closure relations used by Drela or the closure relations used by Matsushita et al.

parameter	value	unit
plate length	3.0	$[m]$
run time	$\frac{1}{8}T$	$[s]$
frequency of oscillation	5,50	$[\frac{1}{s}]$
reference point	1.5	$[m]$
CFL number	0.25	$[-]$
spatial scheme	indifferent[3]	$[n/a]$
temporal scheme	Runge-Kutta 4	$[n/a]$
refinement	none	$[n/a]$
left boundary condition	Thwaites	$[n/a]$
kinematic viscosity	1.5e-5	$[\frac{kg}{m.s}]$
edge velocity	1	$[\frac{m}{s}]$

Table 7.4: Global variables for the laminar flow over an oscillating flat plate

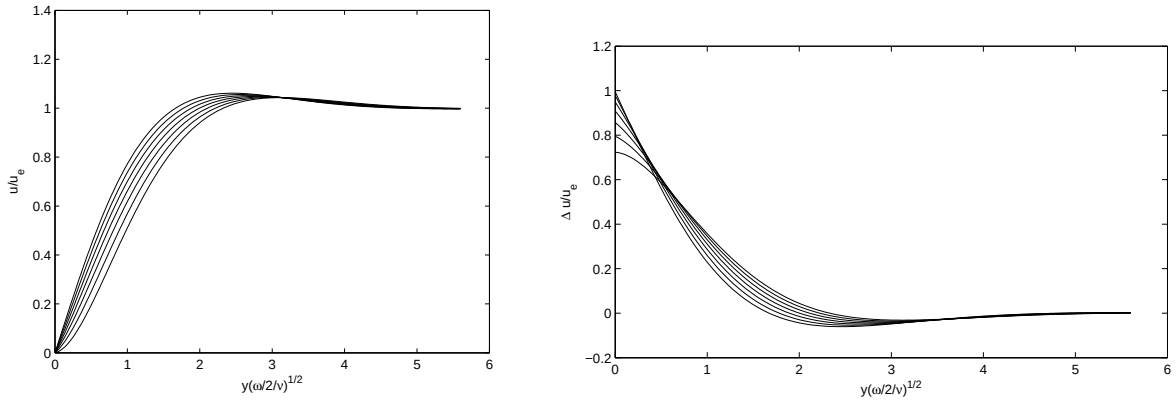

Figure 7.11: 2^{nd} Stokes problem, (left) relative velocity distribution,(right) relative velocity difference with edge velocity

In appendix J.4, the plots for δ^*, θ and C_f are shown for $\delta_{100\%}$, it seems that the relations for the friction coefficient fail for small times where there is not even a qualitative similarity with the exact solution. The displacement thickness is approximated very well, the momentum thickness is overestimated throughout the domain which may be caused by the overestimation of the friction coefficient.

It is clear from experiments(see e.g. Lighthill[84]) and from the Stokes velocity distribution that the velocity increase from the plate to the edge is not monotonous, based on the velocity overshoot the upper layer is lagging behind the lower layer. It is suspected that the effect of this lagging behavior of the upper layer is completely removed by considering only the region of monotonous velocity increase (i.e. the first 99%). The degree of unsteadiness of the entire velocity distribution is limited by the assumption in boundary layer theory that neither convection nor diffusion dominate as the transport phenomenon. As was shown by Lighthill[84] the boundary layer will show an increasing phase lag for increasing frequency, this is caused by the fact that due to inertia the boundary layer is dominated by convection in the upper part and by diffusion in the lower part. Suffice to say that for high frequencies the assumption of similar convection and diffusion is no longer valid and more general, the velocity distribution in the flow can no longer be represented by general approximations since phase lag within the boundary layer cannot be predicted with the integral formulation. At a certain degree of unsteadiness (as measured by for instance the reduced frequency), the closure relations should take the unsteadiness into account e.g. by incorporating the unsteady Thwaites/Pohlhausen parameter. The above test case was also performed using the

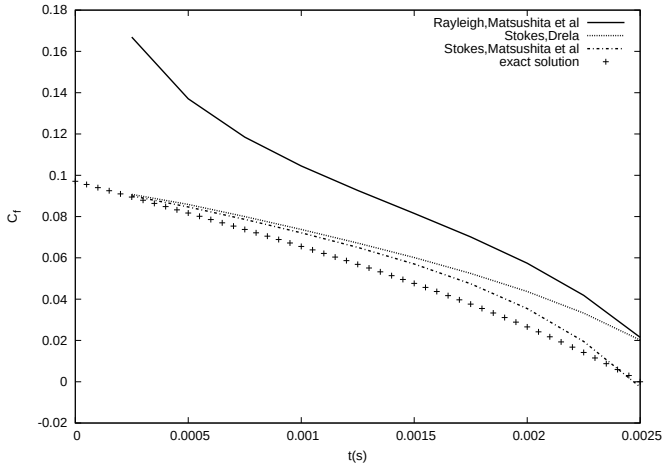

Figure 7.12: 2^{nd} Stokes problem for frequency $f = 50\ Hz$, time history of friction coefficient C_f

friction closure relation by Strickland[105] (see section3.4), which was based on the unsteady wedge flow, unfortunately no overall improvement was noticed, it showed better similarity for $t < 0.01(s)$ but it was in worse agreement for longer times. The closure relation from Strickland contains the unsteady Pohlhausen parameter which was encountered already in section (3.1.2), applying this parameter to the guessed velocity profiles from Wieghardt, Pohlhausen and Falkner-Skan approximation from Drela some indication may be given regarding the suitability of the guessed velocity profiles for unsteady boundary layer flow. Figure (7.14) shows that the guessed velocity profiles with unsteady [4] Pohlhausen parameter does not produce similar velocity profiles to the exact solution. This may be due to the aforementioned difference between the upper and the lower layer, the result is somewhat disappointing nonetheless since the viscous sublayer *should* still be well captured by boundary layer theory. Recall that for the laminar IBL the closure relations due to Drela are implemented, these are based on solutions of the Falkner-Skan equations. Considering the poor resemblance of the Falkner-Skan profiles in figure (7.14) the reasonable results that were obtained using the Falkner-Skan based closure relations might be considered as fortuitous.

Turbulent Flow

The turbulent reference case by Fan et al will be considered next, see equation (7.3). The specific reference result by Fan et al[49] contains phase and amplitude values for the friction coefficient C_f and the displacement thickness δ^*, to obtain these values some post-processing is required. Fan et al apply a $k - \epsilon$ turbulence model to the boundary layer equations.

The flat plate velocity is described by the following function

$$u_e(x,t) = u_0 \left[1 + A(x)\sin\left\{\omega t + \psi(x)\right\}\right], \tag{7.3}$$

[4] using θ or δ^* instead of δ did not produce significantly different results

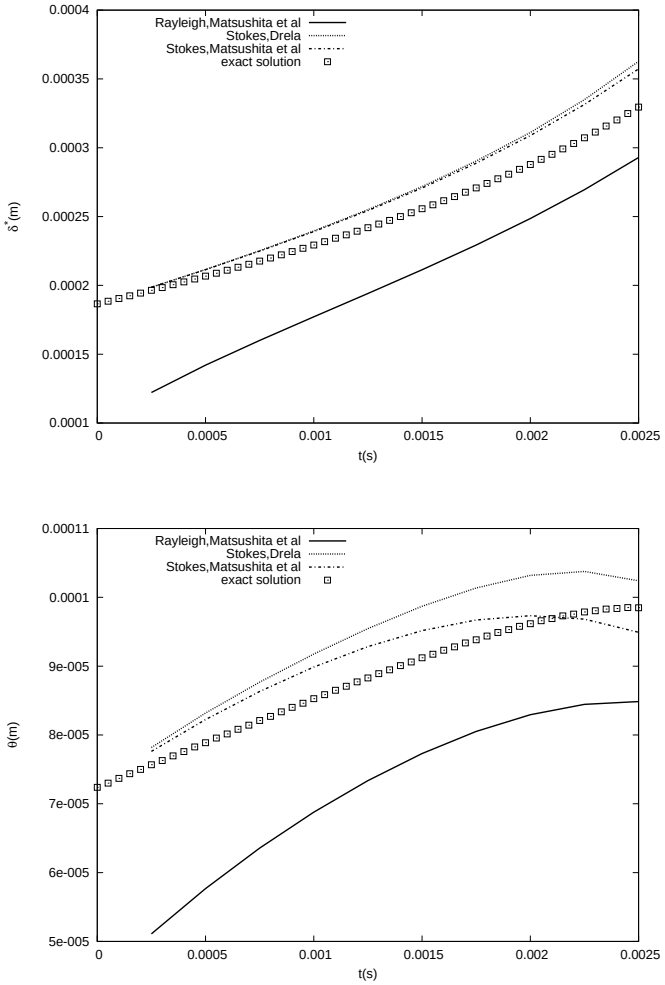

Figure 7.13: 2^{nd} Stokes problem for frequency $f = 50\ Hz$, time histories of (top) displacement thickness δ^*,(bottom) momentum thickness θ

with two cases

$$\text{low frequency:} \quad u_0 = 21.9\ [\frac{m}{s}], \quad f = 38Hz, \quad \omega = 2\pi f$$
$$A(x) = 0.152 - 0.0743(x - 0.047), \quad \psi(x) = 0.1326(x - 0.047),$$
$$\text{high frequency:} \quad u_0 = 16.8\ [\frac{m}{s}], \quad f = 62Hz,$$
$$A(x) = 0.118 - 0.114(x - 0.047), \quad \psi(x) = 1.55(x - 0.047)^2 + 0.116(x - 0.047).$$

This test case has been performed with IBL equations by Cousteix and Houdeville in 1983 which showed that the result is heavily damped for values of $\frac{\omega x}{u_0} > 5$, see Cousteix[28] or Cousteix and Houdeville[30]. For more unsteady turbulent test cases see Cousteix and Houdeville[30] and Carr[17]. The following quantities need to be retrieved

- $amp(\delta^*)$: amplitude of first Fourier component
- $phase(\delta^*)$: phase angle of first Fourier component

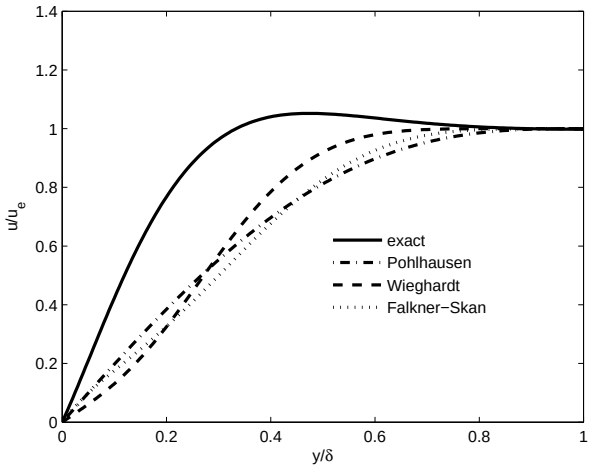

Figure 7.14: Comparison of different guessed velocity profiles for the second Stokes problem using the unsteady Pohlhausen parameter

The Fourier series for arbitrary domains are based on the frequency of the edge velocity[5] , using only the first component the a and b coefficients are defined as follows

$$a_0 = \int_0^{nT} \delta^* dt^{'}, \quad a_1 = (-1)^n \frac{\omega}{\pi} \int_0^{nT} \delta^* \cos(\omega t) dt,$$
$$b_1 = (-1)^n \frac{\omega}{\pi} \int_0^{nT} \delta^* \sin(\omega t) dt, \quad \tilde{\delta}^* = \overline{\delta^*} + A_{\delta^*} \cos(\omega t + \phi_{\delta^*}), \quad \overline{\delta^*} = \frac{a_0}{2}$$

the amplitude and phase angles are then given by

$$A = \sqrt{a_1^2 + b_1^2}, \quad \phi = \arctan\left(\frac{a_1}{b_1}\right).$$

The coefficients a_1, b_1 are found by first order Euler integration over 26 periods based on the frequency ω of the edge velocity. The edge velocity is written as

$$u_e = u_0 + u_0 A_{u_e} \cos(\omega t + \phi_{u_e v} - \frac{\pi}{2}).$$

The comparison requires the following quantities.

$$\zeta_{\delta^*} = \phi_{\delta^*} - \phi_{u_e} + \pi, \quad \xi_{\delta^*} = \frac{A_{\delta^*} \sqrt{\overline{\delta^*}}}{A_{u_e}/u_0}.$$

The test has the following global variables, see table(7.5).

Low Frequency Oscillating Flate Plate

The edge velocity distribution is plotted in figure (7.15). The low frequency case is simulated using the QUICK scheme with a second order Runge-Kutta time integration and a CFL number of 0.25. The momentum thickness over about ten periods of the edge velocity oscillation is shown in figure (J.19).

High Frequency Oscillating Flate Plate

For the high frequency case significant wiggles were present(see figure(7.19)), these wiggles seemed to be neutral in amplitude. For the friction coefficient a different closure

[5] this was not mentioned in the paper by Fan et al[49] and had to be derived from comments by Cousteix[28]

parameter	value	unit
plate length	$17\frac{\omega x}{u_0}$	$[-]$
run time	$\frac{26}{f}$	$[s]$
CFL number	0.25	$[-]$
spatial scheme	QUICK	$[n/a]$
temporal scheme	Runge-Kutta 2	$[n/a]$
refinement	time	$[n/a]$
kinematic viscosity	1.4717	$[\frac{kg}{ms}]$

Table 7.5: Global variables for turbulent flow over oscillating flat plate

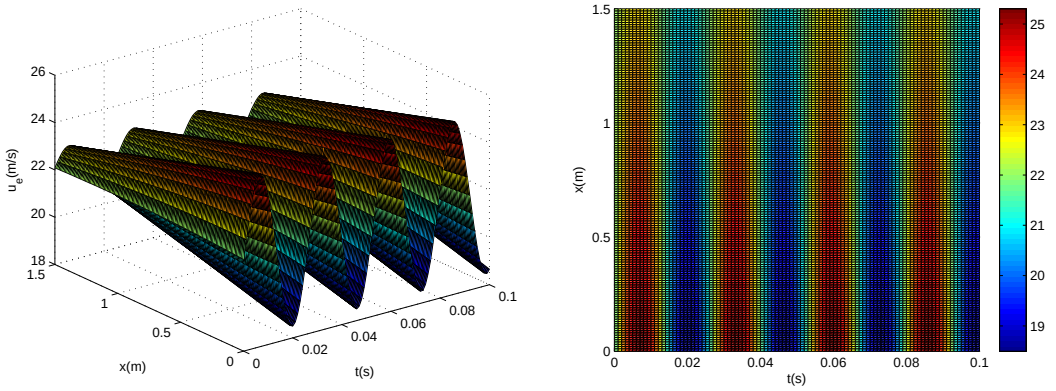

Figure 7.15: $x-t$ edge velocity distribution for low-frequency unsteady flat plate

relation due to Cousteix and Houdeville is tested which should hold for a reduced frequency $\omega x/u_0 < 5$, see section(3.4), no significant improvement was noted, it did however allow a finer grid resolution ($\Delta x = 0.002$), the results using this closure relation for C_f are presented in (7.20). Despite the wiggles the amplitude and the phase values are only affected in higher order, the results are again in reasonable agreement with the experimental data and the result from Fan et al who use a $k-\epsilon$ turbulence model in combination with the boundary layer equations. The low frequency case was close to the theoretical and experimental results, the plots for the displacement thickness seemed a bit displaced in $x-$direction with respect to the $k-\epsilon$ result from Fan et al[49]. For a reduced frequency $\frac{\omega x}{u_0} < 8$ the solution from the current IBL system is in good agreement with the $k-\epsilon$ results from Fan et al. In all cases the current IBL system is in better agreement with the experimental data and the $k-\epsilon$ result.
For the high frequency case the oscillating turbulent flat plate showed wiggles for all schemes, however these wiggles did not diverge. Smoothing removed the wiggles but also damped the solution, to the extent that the oscillatory behavior of the amplitude and the phase quickly dissipated. The wiggles are presumably caused by an unsuitable left boundary condition for the turbulent flat plate. The wiggles do not change if more periods are used for the integration of the coefficients, this suggests that either the wiggles are static or the frequency of the wiggles is a multiple of the disturbance frequency. For the high frequency case the IBL equation with the equilibrium closure relations produces a result close to the result obtained by Cousteix and Houdeville who also use IBL formulation. The non-equilibrium closure relations give better results being in good agreement with the experimental and theoretical reference values.

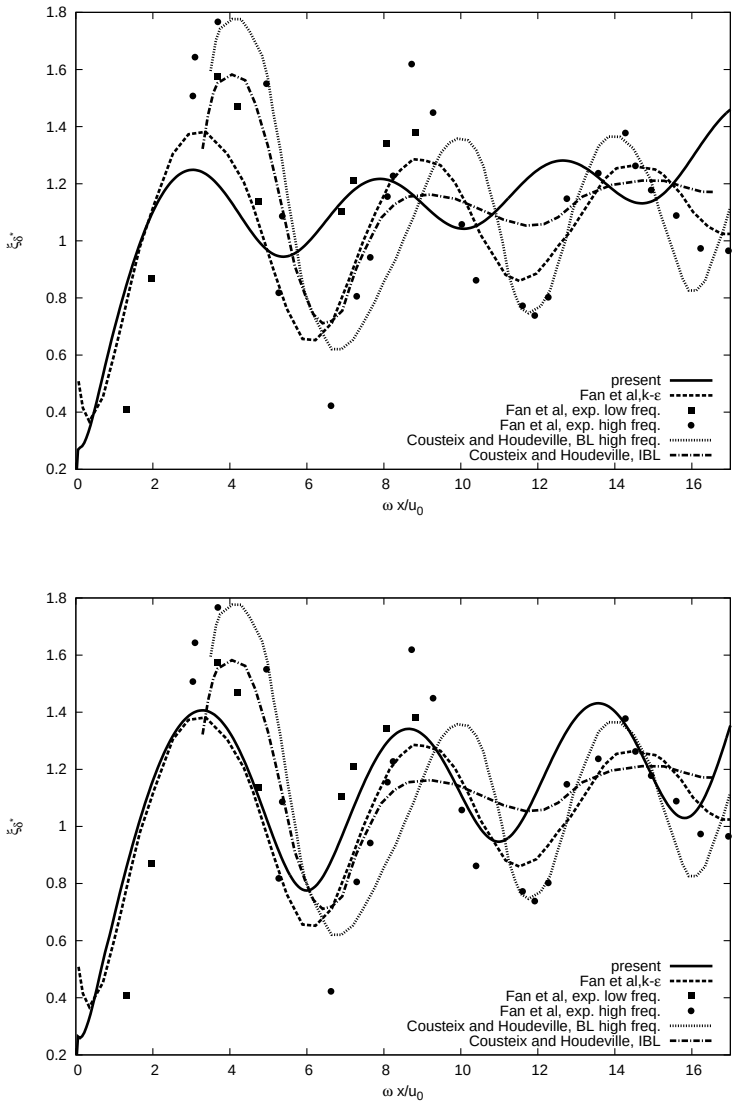

Figure 7.16: Ratio of relative amplitudes of displacement thickness δ^*,(top) using equilibrium closure, (bottom) using non-equilibrium closure

7.2 Impulsively Moved Cylinder

The impulsively moved cylinder is a widely used test case for flow solvers and is well documented by experimental data. Being a well documented example of a flow with a strong adverse pressure gradient and a known location for unsteady laminar separation it forms an interesting test case for this thesis.

7.2.1 Laminar Flow

A cylinder is moved instantaneously with constant velocity u_0. The edge velocity distribution over the cylinder is then defined by a potential flow solution which is used directly to obtain the the integral variables. The potential flow solution over the cylinder

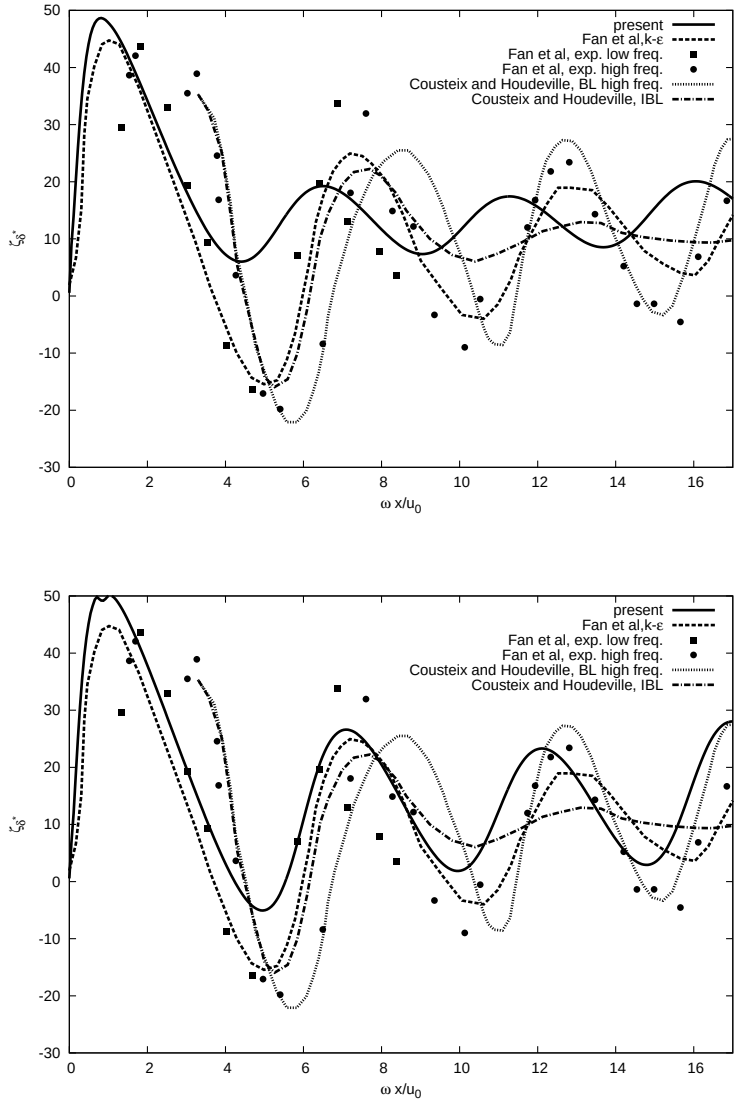

Figure 7.17: Relative phase shift of the displacement thickness δ^*,(top) using equilibrium closure, (bottom) using non-equilibrium closure

is given by (also see figure(7.21))

$$u_e = 2\,u_0 \sin(x), \quad x = [0, \pi].$$

First determined by Goldstein the steady separation point for the cylinder is about $\alpha = 104.6\ ^\circ$. The separation location is somewhat different from the steady case, based on singularity studies of the boundary layer equations Dommelen and Shen, Cebeci and Cowley determined that the separation point for the unsteady boundary layer flow over a cylinder is approximately located at $\alpha = 111\ ^\circ$, also see section (I.3.4). The separation of the boundary layer should be accompanied with a convergence of characteristics of the quasi-linear system (see e.g. Matsushita[91]) and the separation indicator as defined in section(5.4) should thus show a maximum value. Near the separation point the shape factor H and the displacement thickness δ^* should grow very large over a short distance, the separation point is then characterised by a steeply diminishing momentum thickness(see figure (J.22)) and a sharply rising displacement thickness(see figure

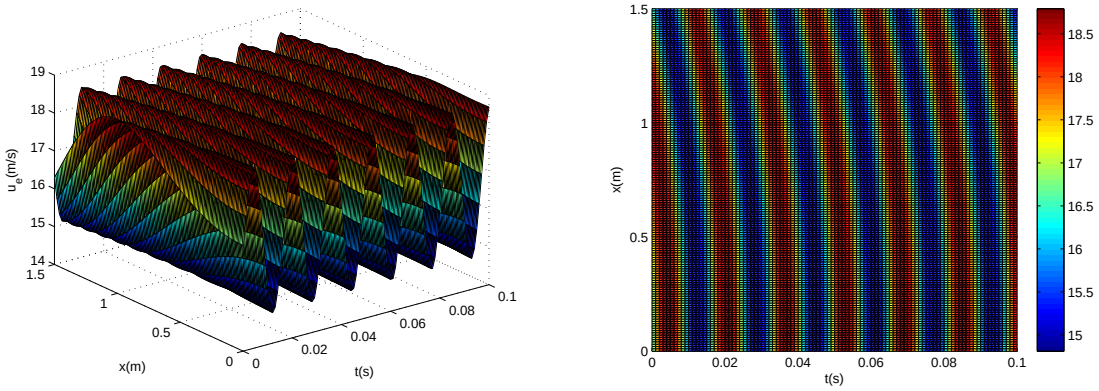

Figure 7.18: $x-t$ edge velocity distribution for high-frequency unsteady flat plate

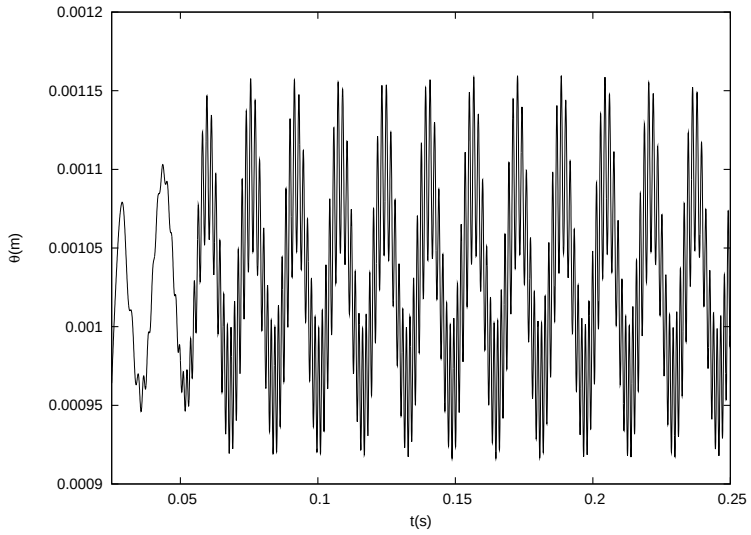

Figure 7.19: Time evolution of the momentum thickness at half of the plate length

(7.25)) and shape factor(see figure (7.22)).

The global settings for this test case are given in table(7.6). This test case is purely

parameter	value	unit
plate length	π	$[m]$
run time	until breakdown	$[s]$
spatial scheme	QUICK	$[n/a]$
temporal scheme	Runge-Kutta 1/2/4	$[n/a]$
refinement	left-boundary	$[n/a]$
kinematic viscosity	1.0	$[\frac{kg}{ms}]$
undisturbed velocity u_0	0.5, 1.0	$[\frac{m}{s}]$

Table 7.6: Global variables for the boundary layer flow over an impulsively moved cylinder

theoretical for the laminar case since for the used settings the boundary layer thickness is of the same order of magnitude as the radius of the cylinder. The finite difference schemes perform equally well, there were no noteworthy differences, see figure (7.22).

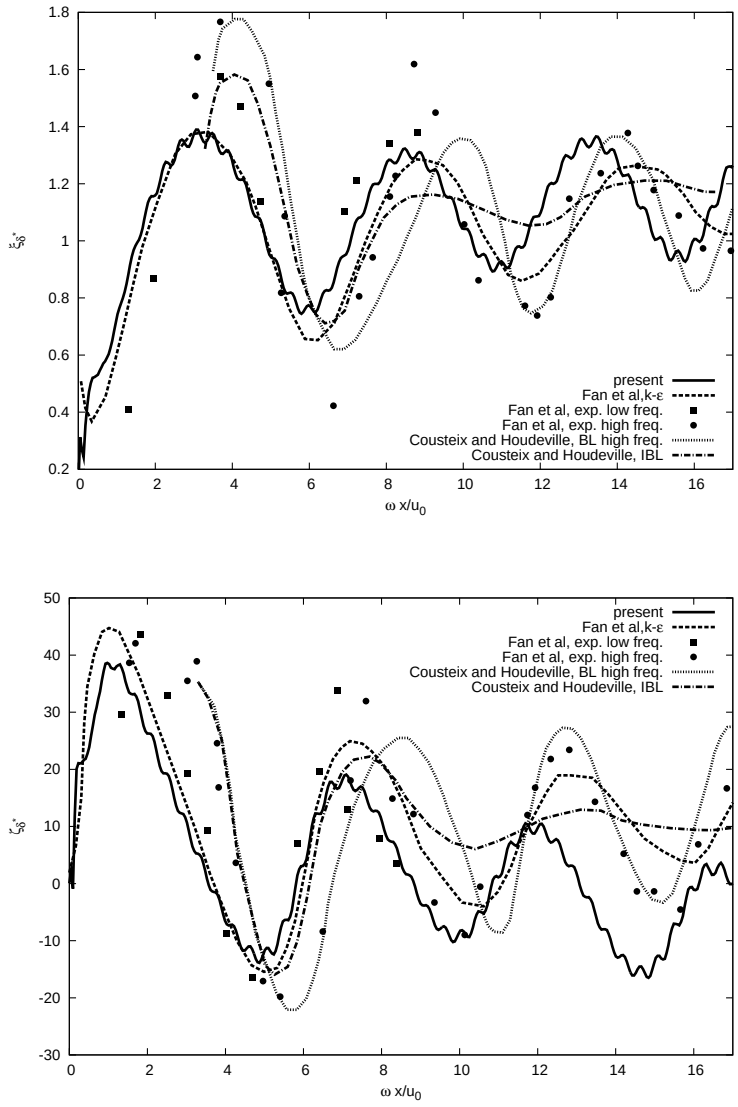

Figure 7.20: Harmonic results for the displacement thickness δ^* for the high frequency case using the non-equilibrium closure, (top) ratio of relative amplitude , (bottom) ratio of phase shift

grid refinement near the left boundary near the stagnation point improves the result and does not necessarily decrease the overall temporal step size since the eigenvalues near the stagnation point are very small, it is therefore recommended to be used for stagnation flows. For the left boundary condition several values were used, namely, the stagnation point values used by Nishida and Milewski, the value following from one step of Thwaites integral equation and the value for the Rayleigh flow at $t = \Delta t$. It was found that the overall solution was practically indifferent to the type of boundary condition used. In figure (7.23) the results using the Milewski left boundary value are shown for the wall shear stress and the points of zero friction, it is in good agreement with the reference result by Cebeci, the agreement deteriorates as the degree of separation increases.

It was shown that the degree to which the separation could be simulated is at least dependent on the closure relations, the closure relations due to Matsushita and Akamatsu were better able to handle separated boundary layer flow than the closure relations

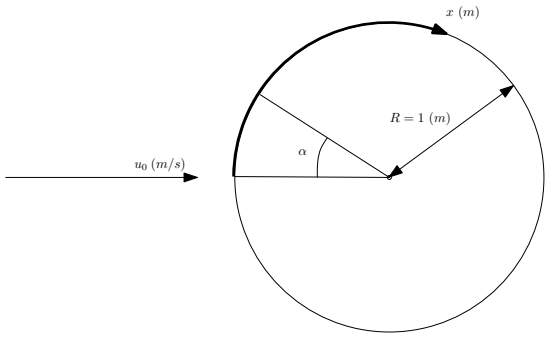

Figure 7.21: Problem definition of impulsively moved cylinder

due to Drela. The explanation has already been given earlier in the text, Matsushita and Akamatsu simply consider a wider range of (semi)-similarity solutions to obtain the closure relations. Although the Drela closure relations are more accurate for the non-separated flow, with increasing shape factor Drela's Falkner-Skan based closure relations are pushed beyond their envelope and the solution blows up. For a negative inversed shape factor E the closure relations by Matsushita and Akamatsu also lose their validity. For high values of the shape factor the momentum thickness goes to zero and the displacement thickness levels out (see figure (7.24)). The separation indicator produces a clear spike at/near the separation point, also the momentum thickness θ and Re_θ have a maximum near the separation point (see figure(J.28)). From the tests with the impulsively moved cylinder it is clear that the Falkner-Skan based closure relations as used by Drela performs better than the closure relations by Matsushita and Akamatsu for low values of the shape factor which inversely performed better at the higher values of the shape factor (approximately $H > 3$), this may be due to extrapolation inaccuracies. From the convergence plots (7.26) it is clear that divergence starts with the shape factor,

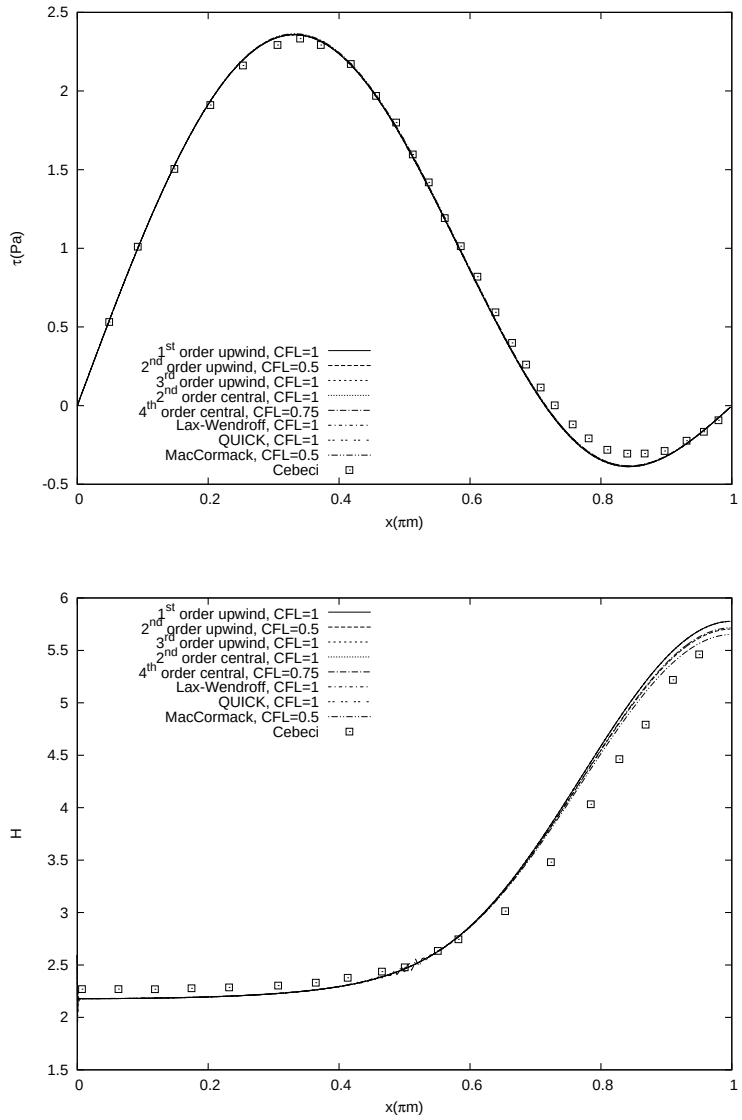

Figure 7.22: Comparison of results obtained for impulsively moved cylinder with various schemes for $u_e = 2\sin(x)$, with grid refinement near the left boundary, $\Delta x = 0.01$, (top) Wall shear stress, (bottom) Shape factor

Purely based on the eigenvalue plots (see figure (7.27)) a flux limiter is not necessary. This is because no discontinuity is present and because long before the expected discontinuity will appear the current set of IBL equations fails due the shape factor H going to infinity as the momentum thickness θ goes through zero. In case the equation set from Matsushita et al is used the discontinuity **can** be reached. In the final coupled procedure however the discontinuity is likely to be avoided due to the strong interaction between the boundary layer and the outer flow.

Turbulent Flow

The impulsively moved cylinder case is performed again but now with a turbulent boundary layer flow, the global variables can be found in table (7.7).

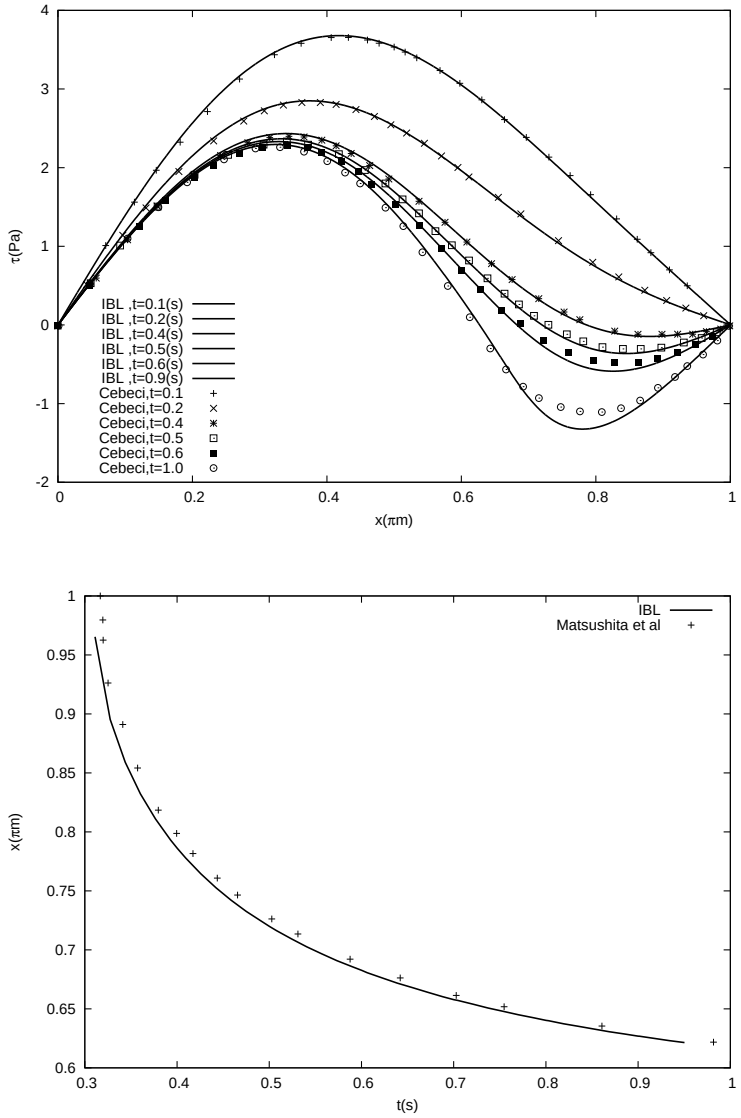

Figure 7.23: Comparison of results obtained with QUICK scheme for $u_e = 2\sin(x)$, with grid refinement near the left boundary, RK2 time integration, $\Delta x = 0.001$, $CFL = 0.5$, (top) Wall shear stress, (bottom) point of zero friction

parameter	value	unit
plate length	2π	$[m]$
run time	0.5	$[s]$
spatial scheme	QUICK	$[n/a]$
temporal scheme	Runge-Kutta 2	$[n/a]$
spatial stepsize	0.001	$[m]$
refinement	left-boundary	$[n/a]$
kinematic viscosity	1.5e-5	$\left[\frac{kg}{ms}\right]$
edge velocity	1.8	$\left[\frac{m}{s}\right]$

Table 7.7: Global variables for the turbulent boundary layer flow of an impulsively moved cylinder

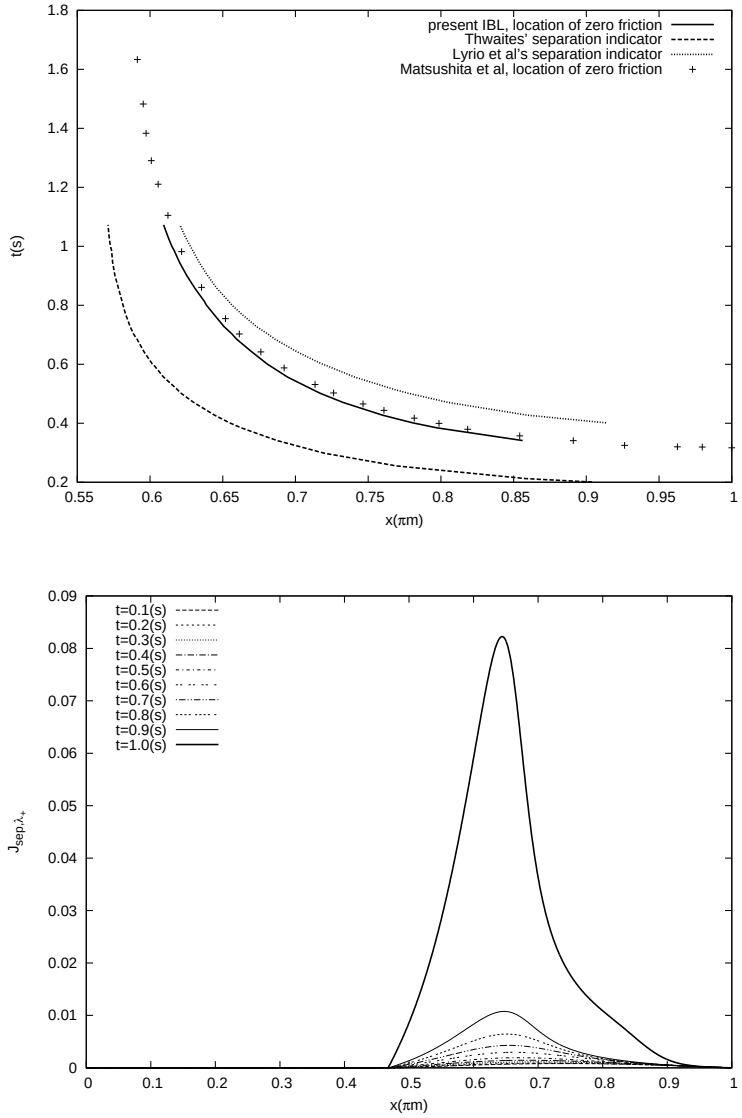

Figure 7.24: Separation indicators for $u_e = 2\sin(x)$, obtained with smoothed QUICK scheme, RK1 time integration, $CFL = 1.75$, with grid refinement near the left boundary, (top) Separation predictions,(bottom) Separation indicator J

The reference result was obtained using the commercial flow solver CFX, the $k-\omega$ SST turbulence model from Menter was used for the turbulence modeling. The stepsize over the cylinder was $25\ mm$, the boundary layer was meshed with 20 layers starting with $0.1\ mm$ and a growth factor of 20%, the boundary layer thickness is about $19\ mm$. The intermittency over the entire cylinder was about 7%. The intermittency for the entire boundary layer was pre-set at 7%, i.e the boundary layer is 7% turbulent. Only the wall shear stress τ was compared, it is clear from figure (7.29) that the IBL fails completely using a non-equilibrium closure model. Using the equilibrium closure model the best result was obtained at the beginning of the cylinder, it seems that a separation bubble moves upwind which causes the friction zero point to move upwind also, literature suggests that turbulent separation over a cylinder takes places at about $\alpha = 126\ ^\circ$ (see e.g. Li et al[81]), this brings the validity of the reference result into question. Given the higher mixing rate of the turbulent boundary layer with the flow outside the boundary

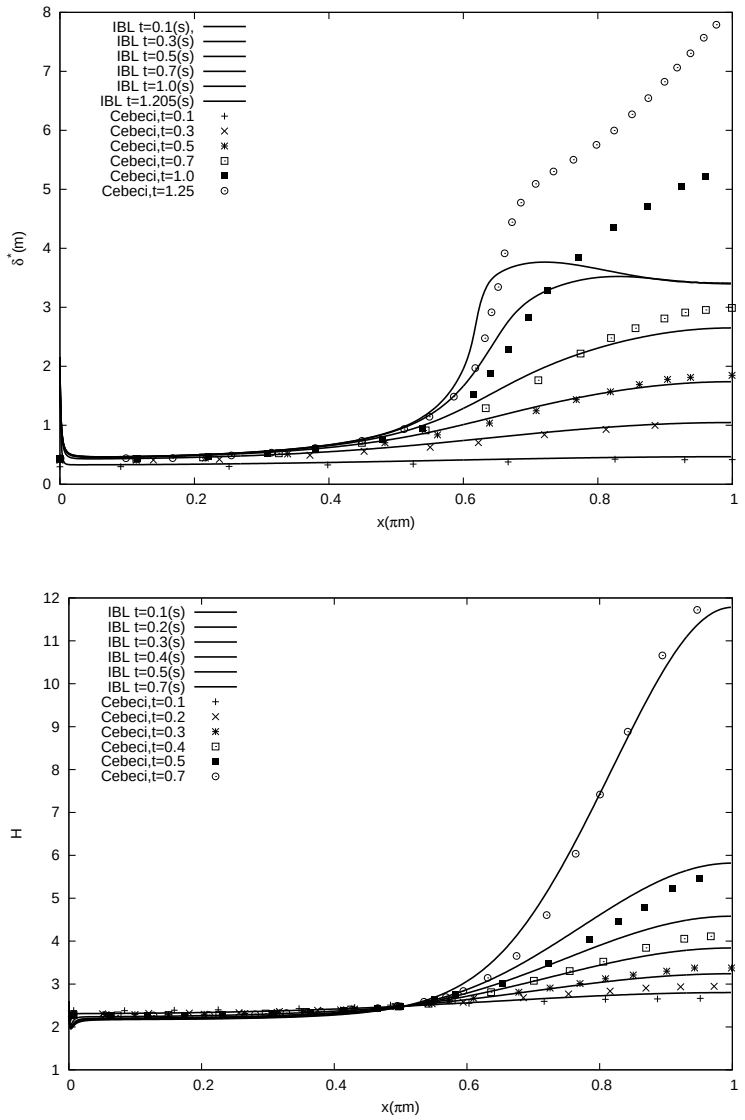

Figure 7.25: Results obtained using the smoothed QUICK scheme, RK1 time integration, $CFL = 1.75$, $\Delta x = 0.01$ with grid refinement near the left boundary, (top) displacement thickness δ^*,(bottom) shapefactor H

layer it should be able to overcome higher pressure gradients than the laminar boundary layer.

The closure relation for the friction was the model by Swafford, see section (3.4), applying the friction model by Cousteix and Houdeville[30](see section (3.4)) did not improve the result.

7.3 Comparison of Run times

As a coarse means of establishing a coarse comparison between the different numerical methods in terms of computational loading a simple test case is executed. For this purpose the Blasius case is simulated for three different grid resolutions, namely $\Delta x =$

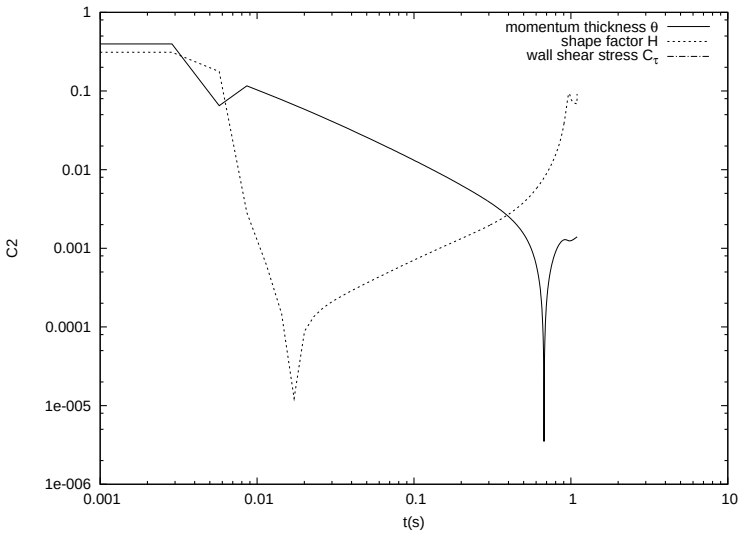

Figure 7.26: Convergence criterium $C2$ for $u_e = 2\sin(x)$, obtained with smoothed QUICK scheme, RK1 time integration, $CFL = 1.75$, $\Delta x = 0.01$ with grid refinement near the left boundary

scheme	$\Delta x = 0.01$	$\Delta x = 0.005$	$\Delta x = 0.0025$
2^{nd} order DG	8.1	31	116
Roe FVM	1.3	5.1	19.3
MacCormack FDM	1.5	6	23.9
1^{st} order upwind	0.85	3.4	13.5

Table 7.8: Computation run time, with $RK1$ time integration,$CFL = 0.5$

0.01, 0.005, 0.0025 with $CFL = 0.5$. Koo et al[76] find that a 2^{nd} order DG method is 12.5 times slower than a non-limited 2^{nd} order FVM for a one dimensional scalar problem and about 3 times slower for a two dimensional Euler problem. In this case the 2^{nd} order DG method is about 9 times slower than the first order upwind differencing scheme and about $5-6$ times slower than the Roe scheme and the MacCormack scheme. It should be kept in mind that the code is not optimised yet, the mass and the Gaussian[6] matrices are very sparse so this can be achieved easily by LU-decomposition.

7.4 Summarising

The results show that the current formulation of the IBL equations plus the chosen closure relations can handle unsteady laminar and turbulent boundary layer flows quite well despite the usage of steady closure models. No smoothing was required for the central schemes. Smoothing was required for the very high Reynolds number flat plate case which may have been caused by an unsuitable left boundary condition. Grid refinement at the left boundary for the cylinder case (i.e. the stagnation case) showed no significant change in the global time step while improving the solution quality. At the same time different stagnation point values (i.e. the left boundary condition) showed no significant difference for the results for the cylinder case. The prediction of separation and transition for unsteady boundary layers is still a matter of ongoing research, especially given the extra difficulties of severe cross flow and added body forces in the case of three dimensional wind turbine flow, as has been discussed earlier.

[6]for each element there is matrix with the Gaussian nodes and weights

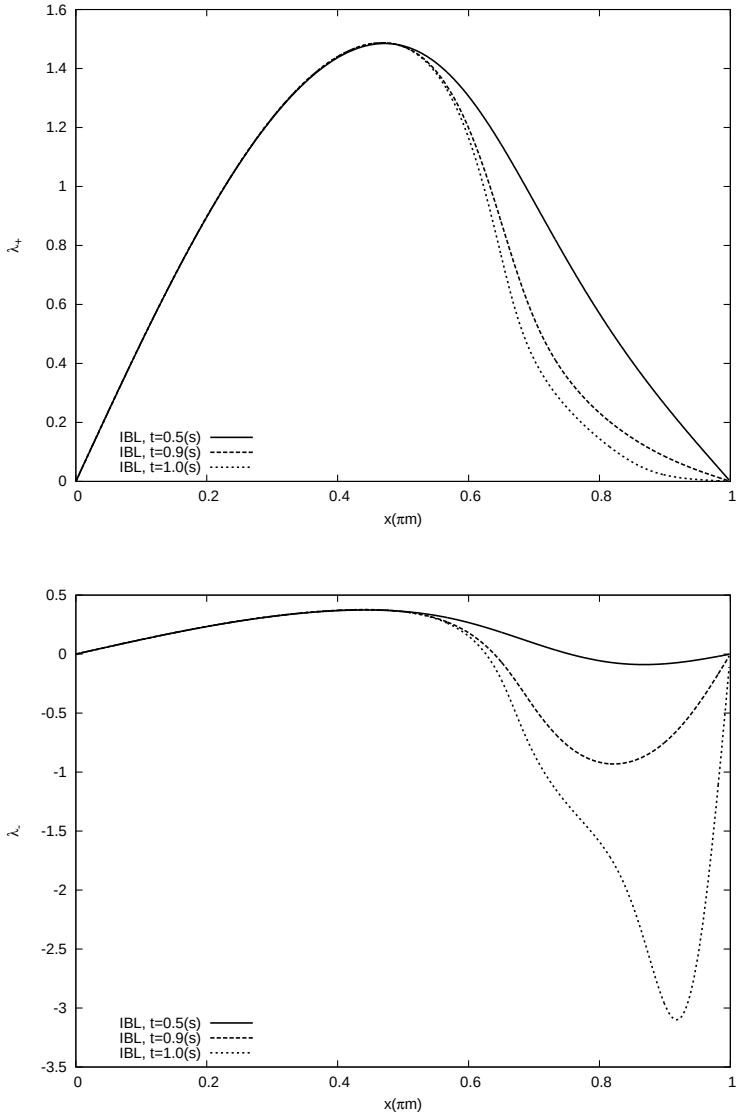

Figure 7.27: Results obtained using the smoothed QUICK scheme, RK1 time integration, $CFL = 1.75$, $\Delta x = 0.0025$ with grid refinement near the left boundary, (top) eigenvalue λ_+,(bottom) λ_-

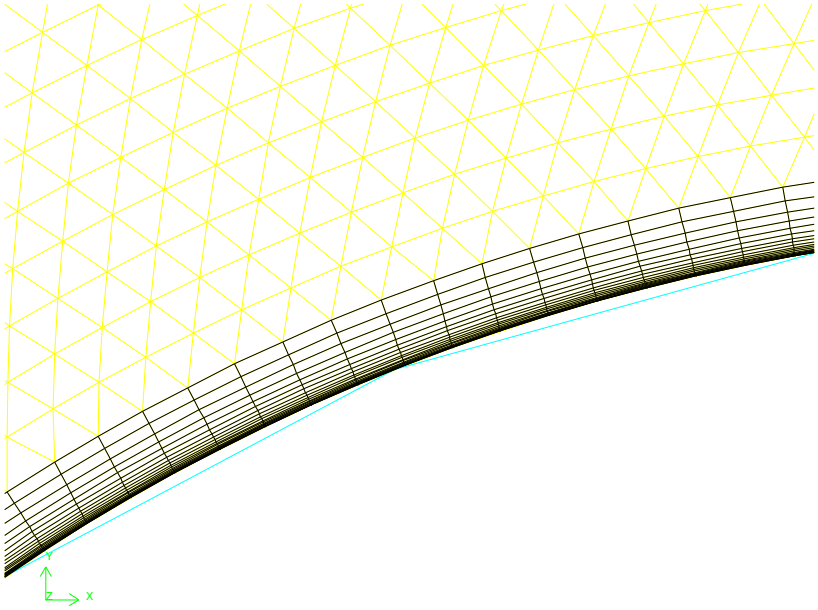

Figure 7.28: A section of the grid near the cylinder wall for the CFX simulation

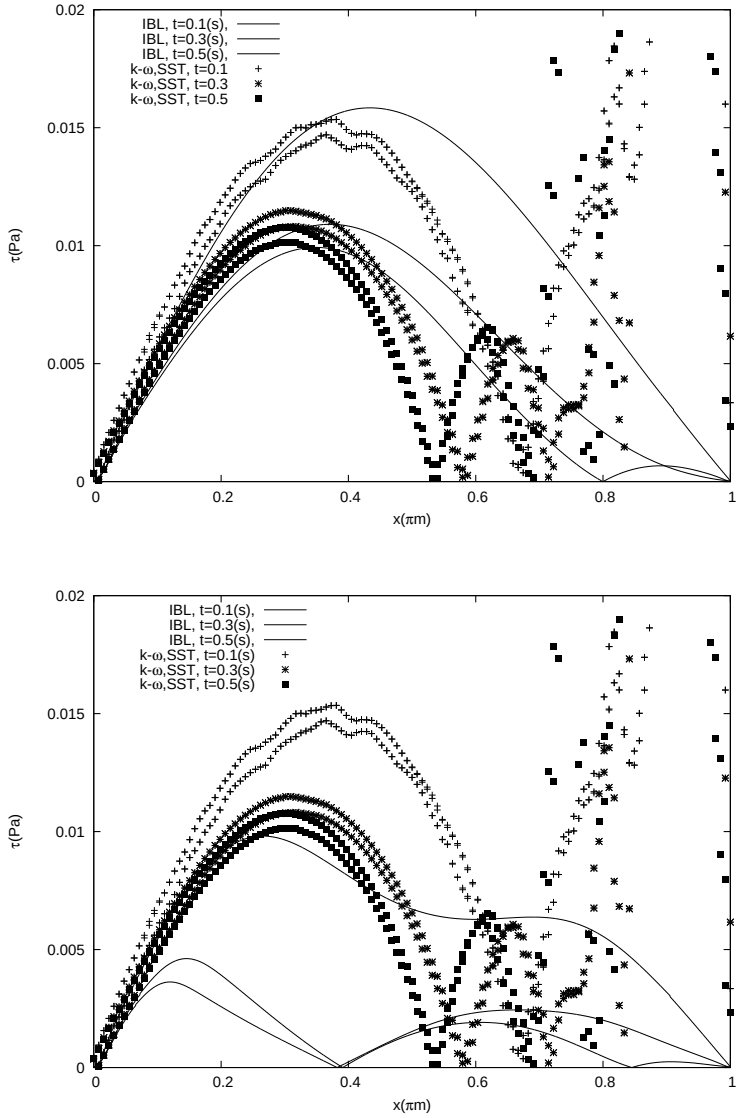

Figure 7.29: Comparison of results between for the impulsively moved cylinder with turbulent boundary layer flow,(top) using the equilibrium closure relation for the diffusion coefficient C_D, (bottom) using the non-equilibrium closure relation for the diffusion coefficient C_D

Chapter 8

Conclusions and Recommendations

Following the results of the test cases and the earlier discussions, several conclusions and recommendations are presented.

8.1 Conclusion

The usage of steady flow based closure models do not seem to bother the transient solution quality in a qualitative sense, for a quantitative conclusion unsteady closure models are necessary for comparison.

The usage of closure relations may bring severe limitations for the Discontinuous Galerkin method since heuristically it prohibits the use of an expansion in basis functions for the source vector and the exact flux vector. Further investigation is required comparing the results of the expansion in basis functions with the results obtained through Gaussian quadrature.

The fully turbulent cases have more stringent requirements on the step size, most likely due to the mixed signs of the eigenvalues. Also, the stability was more affected by the left boundary condition, this seemed to affect the upwind methods the most. The latter can be explained by the fact that the upwind method is stable only for the characteristics in the upwind direction.

Numerical smoothing stabilised the solution in all cases, for zero or low pressure gradient boundary layer flows the solution quality will be affected as was experienced for the laminar flat plate.

The use of an equilibrium closure relation or a non-equilibrium closure relation for the diffusion coefficient C_D significantly influenced the results, the non-equilibrium closure relation produces more physical temporal results for the unsteady turbulent cases. However, this increase in physical accuracy was accompanied by decrease stability compared to the equilibrium case.

The solution quality for the Finite Difference Methods was degraded to first order for the steady state solutions, this might be explained by the fact that first order differencing is used for the first steps on the left boundary.

For several reasons the comparison should be considered as provisory, all of which lie in the simplification of the problem considered and the fact that only two-dimensional boundary layer flow was considered. The simplifications are, the negligence of curvature terms, the treatment of two dimensional instead of three dimensional boundary layer equations, and the omittance of fictitious forces. One of the downsides of implementing the finite difference method in case of curved surfaces is the requirement that

the geometric gradients are directly incorporated in the differential equations. The subsequent presence of goniometric formulae will affect the computational efficiency and large geometric gradients may cause very large differential terms. As a consequence the comparative results are likely skewed, it is therefore advised to run a comparative study for the two dimensional integral boundary layer equations with curvature terms. Also it is advised to test the hyperbolicity of the current system in case fictitious forces are added and in case a dimension is added, this is simply a matter of obtaining the eigenvalues for realistic values of the primary variables.

The temporal step size for the explicit time integration scheme is approximately equal to the spatial stepsize divided by the edge velocity which may have a negative impact on the coupling of the unsteady integral boundary layer equations to the unsteady potential solver which will have a time step several orders larger, this supports the investigation of an implicit time integration scheme for the unsteady integral boundary layer equations.

8.2 Recommendations

Based on the results obtained it is advised to use a flux limiter for the transition region in case the conservative equations are solved. It is clear from the results that negative friction preceding separating flow does not give rise to a discontinuity of the eigenvalues. This discontinuity does appear for a transition from a laminar to a turbulence boundary layer, over the transition region the closure relations are switched from laminar to turbulent which indirectly causes a discontinuity in the primary variables.

It is recommended to consider test cases which specifically aim to test the non-linearity and the stability characteristics of the system for specific schemes, especially in relation to stability preserving schemes, flux limiters and perhaps an equivalent entropy-fix for the Roe scheme.

As a reference result in general it is recommended to use the field form of the boundary layer equations, since it is more flexible than a full incompressible Navier Stokes-solver and since it forms a direct reference value for the integral boundary layer equations, i.e. results maybe differ from the incompressible Navier Stokes-solver due to physical effects which are not modeled by the integral boundary layer equations, in this respect the boundary layer equations should be of equal value.

In general, to investigate the suitability of the integral form of the boundary layer equations to model unsteady behavior an analytical analysis should be performed of the integral equations by substitution of the velocity distribution.

Literature shows that the steady integral boundary layer equations can be used in a coupled procedure to model unsteady flow phenomena such as flutter, it is therefore advised to consider implementing and testing a quasi-steady integral boundary layer formulation, see e.g. Howlett[67], Edwards[44],Zhang[160] and Sekar[120].

Some notes by the author

The initial thesis assignment was to compare numerical methods for the unsteady two-dimensional integral boundary layer equations, this quickly shifted to a more general comparison of complete solution methods, including the closure models and the transition detection, mainly because the application of closure models to the unsteady integral boundary layer equations is not straightforward and it is not well described in literature. Be that as it may, purely looking at the thesis assignment the closure models were of secondary importance. Because of this dilution of effort I humbly admit that the numerical comparison has perhaps not attained the relative size it deserves[1], topics like total

[1] which surely attributed to incorrectly applying the non-conservative equations to the finite volume and the finite element method

variation diminishing, strong stability preserving, space-time discontinuous Galerkin, adaptive grids, etc. etc. could have been discussed in more detail if at the start of my thesis work a quick selection was made for the closure models. It is my opinion that the listing/discussion of a wide range of closure models is certainly useful for anyone interested in applying integral boundary layer equation and especially for my successor. For a future study I strongly recommend to apply focus on either the closure models or the numerical methods.

Bibliography

[1] B. Abu-Ghannam and R. Shaw. Natural transition of boundary layers the effects of turbulence, pressure gradient and flow history. *J. of Mech. Eng. Sci.*, 22:213–228, 1980. [cited at p. 24]

[2] R.C. Ackerberg and J.H. Phillips. The unsteady laminar boundary layer on a semi-infinite flat plate due to small fluctuations in the magnitude of the free-stream velocity. *Journal of Fluid Mechanics*, 51(1):137–157, 1972. [cited at p. 234]

[3] N. Akhter and F. Ken-Ichi. Development of prediction method of boundary layer bypass transition using intermittency transport equation. *Internation journal of gas turbine, propulsion and power systems*, 1(1):30–38, October 2007. [cited at p. 27]

[4] J.D. Anderson. *Computational Fluid Dynamics, the basics with applications*. McGraw-Hill, 1995. ISBN- 0-07-113210-4. [cited at p. 83]

[5] John D. Anderson. *Fundamentals of Aerodynamics (Mcgraw-Hill Series in Aeronautical and Aerospace Engineering)*. McGraw-Hill Science/Engineering/Math, 3 edition, 2000. [cited at p. 7]

[6] Paul Andersson, Martin Berggren, and Dan S. Henningson. Optimal disturbances and bypass transition in boundary layers. *Physics of Fluids*, 11(1):134–150, 1999. [cited at p. 25]

[7] H.L. Atkins and C.W. Shu. Quadrature-free implementation of discontinuous galerkin method for hyperbolic equations. *AIAA*, 36(5):775–782, May 1998. [cited at p. 101]

[8] C. Bak. Research in aeroelasticity efp-2007, July 2008. ISBN 978-87-550-3685-7. [cited at p. 26]

[9] W.H.H. Banks and G.E. Gadd. Delaying effect of rotation on laminar separation. *AIAA*, 1(4):941–943, 1964. [cited at p. 86]

[10] H. Bhanderi and H. Babinsky. Improving the lag entrainment method in the case of transonic shock wave / boundary layer interaction. TR AIAA 2004-2147, AIAA, 2004. [cited at p. 30]

[11] R. Biswas, K.D. Devine, and J.E. Flaherty. Parallel, adaptive finite element methods for conservation laws. *Applied Numerical Mathematics*, 14:255–283, 1994. Sandia National Laboratories Tech. Rep. SAND92-7341. [cited at p. 119]

[12] C. Blom. *Discontinuous Galerkin method on tetrahedral elements for aeroacoustics*. PhD thesis, University of Twente, September 2003. [cited at p. 104, 106, 107, 110, 113, 114]

[13] J.I. Bong. *A numerical model for two-dimensional unsteady flow calculations with a surface panel method*. PhD thesis, Texas Tech University, December. [cited at p. 35, 66]

[14] J. Bongers. Implementation of a new transition prediction method in xfoil predicting transition in suction boundary layers. Master's thesis, Delft University of Technology, Kluyverweg 1, August 2006 2006. [cited at p. 23, 24, 26, 195, 267]

[15] P. Bradshaw. Singularities in unsteady boundary layers. *AIAA J.*, 17(7):790–793, 1979. [cited at p. 34]

[16] R.L. Burden and J.D. Faires. *Numerical Analysis*. Brooks/Cole, 7 edition, 2001. [cited at p. 111]

[17] L.W. Carr. A compilation of unsteady turbulent boundary layer experimental data. technical memorandum 81317, NASA, September 1981. [cited at p. 143]

[18] C.E. Castro and E.F. Toro. Solvers for the high-order riemann problem, for hyperbolic balance laws. *Journal of Computational Physics*, 227(1):2481–2513, November 2007. [cited at p. 107]

[19] T. Cebeci. Unsteady two-dimensional laminar and turbulent boundary layers with fluctuations in external velocity. *Proceedings of the Royal society of London. Series A, Mathematical and physical sciences*, 355(1681):225–238, June 1977. [cited at p. 13, 75, 237, 257, 260]

[20] T. Cebeci and P. Bradshaw. *Momentum transfer in boundary layers*, volume 1 of *thermal and fluid engineering*. Hemisphere publishing, London, 1 edition, 1977. [cited at p. 74]

[21] T. Cebeci and L.W. Carr. Prediction of boundary layer characteristics of an oscillating airfoil. IUTAM Symposium on Unsteady Turbulent shear flows, 1981. [cited at p. 75]

[22] T. Cebeci and J. Cousteix. *Modeling and computation of boundary-layer flows*. Springer, Berlin Heidelberg, 2 edition, 2005. ISBN-3-540-65010-5. [cited at p. 17, 22, 23, 24, 27, 28, 29, 30, 185, 209, 233, 256, 257, 259, 263]

[23] T. Cebeci, A. Khattab, and S.M. Schimke. Can the singularity be removed in time-dependent flows. *Workshop on unsteady seperated flow*, page 96, 1984. [cited at p. 35]

[24] T. Cebeci and A.M.O Smith. *Analysis of turbulent boundary layers*. Academic Press, New York, 1974. [cited at p. 22, 28, 257, 267]

[25] B. Cockburn and C.W. Shu. Rungekutta discontinuous galerkin methods for convection-dominated problems. *Journal of Scientific Computing*, 16(3):173–261, April 2001. [cited at p. 90, 107, 112, 116, 117, 118, 119, 126]

[26] E.G.M. Coenen. *Viscous-Inviscid Interaction with the Quasi-Simultaneous Method for 2D and 3D Aerodynamic Flow*. PhD thesis, Rijksuniversiteit Groningen, 2001. ISBN: 90-367-1472-9. [cited at p. 22, 29, 32, 36, 37, 38, 75, 121, 214, 228]

[27] J.C. Cooke. Approximate calculation of three-dimensional laminar boundary layers. Technical Report 3201, Ministry of aviation,aeronautical research council, London, 1961. [cited at p. 20]

[28] J. Cousteix. Three-dimensional and unsteady boundary layer computations. *Ann. Rev. Fluid Mech.*, 18:173–196, 1986. [cited at p. 13, 35, 77, 121, 143, 144, 234]

[29] J. Cousteix and R. Houdeville. Singularities in three-dimensional turbulent boundary-layer calculations and separation phenomena. *AIAA*, 19(8):976–985, August 1981. [cited at p. 30, 44, 50, 57]

[30] J. Cousteix and R. Houdeville. *Effects of unsteadiness on turbulent boundary layers*. Von Karman institute for fluid dynamics, 1988. [cited at p. 32, 75, 143, 154]

[31] S. Cowley. Mechanics for a new millennium, August 2000. Proceedings of the 20th International Congress of Theoretical and Applied Mechanics Chicago, Illinois, USA. [cited at p. 25, 74]

[32] A.G.T. Cross. Boundary layer calculation and viscous-inviscid coupling, 1986. [cited at p. 29]

[33] P.A. Davidson. *Turbulence, an introduction for scientists and engineers*. Oxford University press, Cambridge, 1 edition, 2004. ISBN 019852948 1. [cited at p. 256]

[34] B. De Maerschalk. Space-time least-squares spectral element method for unsteady flows. Master's thesis, Delft University of Technology, Kluyverweg 1, February 2003. [cited at p. 102, 106]

[35] M. Drela. *Two-Dimensional Transonic Aerodynamic Design and Analysis using the Euler Equations*. PhD thesis, Massachusetts Institute of Technology, 1984. [cited at p. 20, 21, 22, 23, 27, 30, 33, 37, 44, 47, 51, 57, 58, 60, 61, 69, 72, 86, 121, 195, 213, 222]

[36] M. Drela. Xfoil: An analysis and design system for low reynolds number airfoils, 1989. [cited at p. 23]

[37] M Drela. Improvements in low reynolds number airfoil flow predictions with ises and xfoil. Cfdl tr, Massachusetts Institute of Technology, June 1990. [cited at p. 20]

[38] M. Drela. Mises implementation of modified abu-ghanam/shaw transition criterion. Report, MIT Aero-Astro, 1995. [cited at p. 24]

[39] M. Drela. Implicit implementation of the full e^n transition criterion. TR AIAA 2003-4066, AIAA, June 2003. 21st applied aerodynamics conference, Orlando,Florida. [cited at p. 23]

[40] M. Drela and M.B. Giles. Viscous-inviscid analysis of transonic and low reynolds number airfoils. *AIAA*, 25(10):1347–1356, 1986. [cited at p. 22]

[41] Z. Du and M.S. Selig. A 3-d stall-delay model for horizontal axis wind turbine performance prediction. In *Collection of Technical Papers*, chapter 21, pages 9–20. AIAA, 1998. A98-16844 03-44. [cited at p. 24, 32, 86]

[42] Z. Du and M.S. Selig. The effect of rotation on the boundary layer of a wind turbine blade. *Renewable Energy*, 20, 2000. [cited at p. 86]

[43] H. Dumitrescu and V. Cardos. Rotational effects on the boundary-layer flow in wind turbines. *AIAA*, 42(2):408–412, 2003. [cited at p. 259]

[44] J.W. Edwards. Transonic shock oscillations and wing flutter calculated with an interactive boundary layer coupling method. Technical Memorandum 110284, NASA, 1996. [cited at p. 37, 68, 160]

[45] J.W. Edwards. Calculated viscous and scale effects on transonic aeroelasticity. *Journal of Aircraft*, 45(6):1863–1872, 2008. [cited at p. 68]

[46] J. Erhel, K. Burrage, and B. Pohl. Restarted gmres preconditioned by deflation. *Journal of Computational and Applied Mathematics*, January 1995. [cited at p. 115]

[47] F. Eulitz and K. Engel. Numerical investigation of wake interaction in a low pressure turbine, July 1997. Joint Propulsion conference and exhibit, 33th, AIAA=1997-3027. [cited at p. 22, 195]

[48] V.M. Falkner and S.W. Skan. Some approximate solutions of the boundary layer equations. *Phil. Mag.*, 12(7):865–896, 1931. [cited at p. 57]

[49] S. Fan, B. Lakshminarayana, and M. Barnett. Low-reynolds-number k-epsilon model for unsteady turbulent boundary-layer flows. *AIAA*, 31(10):1777–1785, October 1993. [cited at p. 142, 144, 145]

[50] C. Fenno, H. Hassan, and N. Perry. Unsteady viscous-inviscid interaction procedures for transonic airfoils using cartesian grids. Technical Report AIAA 1988-2591, AIAA, 1988. [cited at p. 31, 63, 68, 137]

[51] J.H.A.A. Ferziger, A.A. Lyrio, and J.C. Bardina. New skin friction and entrainment correlations for turbulent boundary layers. *Journ.Fluids Eng.*, 104:537–540, 1982. [cited at p. 16]

[52] A. Garrel Van. Integral boundary layer methods for wind turbine aerodynamics. Literature Survey ECN-C–04-004, ECN, 2003. [cited at p. 10, 86]

[53] M.I. Gerritsma. Computational fluid dynamics,incompressible flows, December 2002. [cited at p. 92, 120]

[54] S. Gottlieb and C.W. Shu. Total variation diminishing runge-kutta schemes. *Mathematics of computation*, 67(221):73–85, January 1998. [cited at p. 112]

[55] S. Gottlieb, C.W. Shu, and E. Tadmor. Strong stability-preserving high-order time discretization methods. *SIAM Review*, 43(1):89–112, March 2001. [cited at p. 113, 114, 115]

[56] J. Green, D. Weeks, and J. Brooman. Prediction of turbulent boundary layer and wakes in compressible flow by a lag-entrainment method. R&M 3791, Aeronautical research council, 1977. [cited at p. 30, 47, 51]

[57] J.E. Green. Application of headś entrainment method to the prediction of turbulent boundary layers a and wakes in compressible flow. Memorandum, Aerodynamics Dept. R.A.E. Farnborough, 1972. [cited at p. 29, 30, 32, 48, 52]

[58] K.C. Hall and E.H. Dowell. Reduced-order models of unsteady viscous flows in turbomachinery using viscous-inviscid coupling. *Journal of Fluids and Structures*, 1(15):255–273, 2001. [cited at p. 16, 30, 37, 38, 49, 52, 63, 68, 69, 75]

[59] M.G. Hall. A numerical method for calculating unsteady two-dimensional laminar boundary layers. *Ing.Arch.*, 38:97, 1969. [cited at p. 187, 234, 236]

[60] D.R. Hartree. On an equation occuring in falkner and skan's approximate treatment of the equations of the boundary layer. *Proc. Cambridge Phil. Soc.*, 33:223–239, 1937. [cited at p. 21, 57]

[61] N. Hayasi. On the approximate solution of the unsteady quasi-two dimensional incompressible laminar boundary-layer equations. *J.Phys.Soc.Japan*, 17(1):203–211, 1962. [cited at p. 16, 18, 21, 35, 53, 56, 66, 185]

[62] L. He and J.D. Denton. Inviscid-viscous coupled solution for unsteady flows through vibrating blades: part 1, description of the method. *ASME*, 115:94–101, January 1993. [cited at p. 16, 21, 60, 66, 210]

[63] M.R. Head. Entrainment in the turbulent boundary layer. Memorandum, Aerodynamics Dept. R.A.E. Farnborough, 1958. [cited at p. 29]

[64] J.S. Hesthaven and T. Warburton. *Nodal discontinuous Galerkin methods, algorithms, analysis and applications*. Springer, 1 edition, 2008. [cited at p. 90, 106, 113, 118, 119]

[65] W Höhn, R. Gombert, and A. Kraus. Unsteady aerodynamical blade row interaction in a new multistage research turbine,part 2:numerical investigation. *Proceedings of IGTI'01, ASME turbo expo 2001*, 2001. [cited at p. 24]

[66] M. Holt. *Numerical methods in fluid dynamics*. Springer-Verlag, Berlin Heidelberg, 2 edition, 1984. [cited at p. 257]

[67] J.T. Howlett. Calculation of unsteady transonic flows with mild separation by viscous-inviscid interaction. Technical report NASA-TP-3197, NASA Langley Research Center, Hampton,VA 23665-5225, June 1992. [cited at p. 37, 43, 49, 52, 68, 160]

[68] A. James, W. Schmidt, and E. Turkel. Numerical solution of the euler equations by finite volume methods using runge-kutta time-stepping schemes. In *Fluid and Plasma Dynamics Conference, 14th*, Palo Alto, CA, June 23-25 1981. AIAA-1981-1259. [cited at p. 83]

[69] A. Jameson, D. Whitfield, and W. Schmidt. Viscid-inviscid interaction on airfoils using euler and inverse boundary-layer equations, 1981. http://aerocomlab.stanford.edu/Papers/jameson_DFVLR-AAVA.pdf. [cited at p. 38]

[70] J. Johansen and J.N. Sø rensen. Prediction of laminar/turbulent transition in airfoil flows. *J. Aircraft:engineering notes*, 36(4):731–735, 1999. [cited at p. 61]

[71] Jeppe Johansen and Sørensen J.N. Prediction of laminar/turbulent transition in airfoil. TR AIAA-1998-702, AIAA, January 1998. Aerospace Sciences Meeting and Exhibit, 36th, Reno, NV. [cited at p. 23]

[72] C.A. Kennedy, M.H. Carpenter, and R.M. Lewis. Low-storage, explicit runge-kutta schemes for the incompressible navier-stokes equations. Report ICASE 99-22, Nasa, June 1999. [cited at p. 113, 114]

[73] D.I. Ketcheson and A.C. Robinson. On the practical importance of the ssp property for runge-kutta time integrator for some common godunov-type schemes. *International journal for numerical methods in fluids*, (48):271–303, January 2005. [cited at p. 113, 114]

[74] S. Khan, A. Khan, M. Khan, and N. Ahmed. Unsteady falkner-skan flow of a second grade fluid. *Proc. Pakistan Acad. Sci*, 43(3):157–163, 2006. [cited at p. 18, 186]

[75] C.M. Klaij. *Space-time discontinuous Galerkin method for compressible flow*. PhD thesis, Universiteit Twente, September 2006. [cited at p. 83, 100]

[76] H. Koo, C. Kim, and .K.-H. Kim. Some characteristics and limitations of discontinous galerkin methods on inviscid compressible flow. *JKSIAM*, 10(2):85–103, 2006. [cited at p. 155]

[77] A. Krainer. A numerical method for computing unsteady 2-d boundary layer flows. TR NASA contractor report 4198, NASA, 1988. [cited at p. 13, 34, 263]

[78] S. Kubachi, K. Lodefier, R. Zarzycki, W. Elsner, and E. Dick. Further development of a dynamic intermittency model for wake-induced transition. *Flow Turbulence Combust*, pages 1–30, March 2009. DOI 10.1007/s10494-009-9206-2. [cited at p. 22, 27, 195]

[79] J.E. Kubatko, C. Dawson, and J.J. Westerink. Time step restriction for runge-kutta discontinuous galerkin methods on triangular grids. *Journal of computational physics*, 227:9697–9710, 2008. [cited at p. 116, 117]

[80] R.B. Langtry. *A correlation-based transition model using local variables for unstructured paralellized CFD codes*. PhD thesis, University of Stuttgart, May 2006. [cited at p. 27]

[81] Y. Li, R. Shock, R. Zhang, and H. Chen. Numerical study of flow past an impulsively started cylinder by the lattice-boltzmann method. *J. Fluid Mech*, 519:273–300, 2004. DOI: 10.1017/S0022112004001272. [cited at p. 153]

[82] Y. Lian and W. Shyy. Laminar-turbulent transition of a low reynolds number rigid or flexible airfoil. *AIAA*, 45(7):1501–1513, July 2007. [cited at p. 62]

[83] P.A. Libby. Critical study of integral methods in compressible laminar boundary layers. Memorandum 2655, NACA & Polytechnic institute of Brooklyn, 1952. [cited at p. 18, 19, 20, 21]

[84] M.J. Lighthill. The reponse of laminar skin friction and heat transfer to fluctuations in the stream velocity. *Proceedings of the Royal Society of London*, 224(1156):1–23, June 1954. [cited at p. 73, 74, 141, 234, 236, 237]

[85] C.C. Lin. Motion in the boundary layer with a rapidly oscillating external flow. *Proc.9th inter. congress appl. mech. Brussels*, 4:155–167, 1957. [cited at p. 234]

[86] D.W. Lobitz. Flutter speed predictions for mw-sized wind turbine blades. Technical report, Sandia National Laboratories, Albuquerque, New Mexico 87185, 2004. dwlobit@sandia.gov. [cited at p. 231]

[87] F. Lörcher, G. Gassner, and C.D. Münz. *New Results in Numerical and Experimental Fluid Mechanics VI*, volume 96/2008 of *Notes on Numerical Fluid Mechanics and Multidisciplinary Design*, chapter The Space-Time Expansion DG Method. Springer-Link, 2008. 978-3-540-74458-0. [cited at p. 83]

[88] H. Luo, J.D. Baum, and R. Löhner. Fast p-multigrid discontinuous galerkin method for compressible flows at all speeds. *AIAA*, 46(3):635–653, March 2008. [cited at p. 100]

[89] Thomas A. Manteuffel and Jr. White, Andrew B. The numerical solution of second-order boundary value problems on nonuniform meshes. *Mathematics of Computation*, 47(176):511–535, 1986. [cited at p. 120, 262]

[90] M. Matsushita and T. Akamatsu. Numerical computation of unsteady laminar boundary layers with separation using one-parameter integral method. *JSME*, 28(240):1044–1048, June 1985. [cited at p. 16, 18, 33, 57, 67, 71, 74, 77, 93, 187]

[91] M. Matsushita, S. Murata, and T. Akamatsu. Studies on boundary-layer separation in unsteady flows using an integral method. *J.Fluid Mech.*, 149:477–501, 1984. [cited at p. 11, 16, 18, 19, 21, 32, 33, 34, 56, 67, 69, 82, 147, 187, 188, 268]

[92] F.R. Menter and R.B. Langtry. Transition modeling for general cfd applications in aeronautics, January 2005. AIAA 2005-522. [cited at p. 26, 27]

[93] J.A. Michelsen and N.N. Sø rensen. Current developments in navier-stokes modelling of wind turbine rotor flow. In P. Helm and A. Zervos, editors, *2001 European wind energy conference*, pages 367–372. Technical University of Denmark AND Risønational laboratory, 2001. [cited at p. 22]

[94] W.M. Milewski. *Three-dimensional viscous flow computations using the integral boundary layer equations simultaneously coupled with a low order panel method*. PhD thesis, Massachusetts Institute of Technology, June 1997. [cited at p. 26, 37, 38, 75, 121]

[95] S. Miller and P.J. Morris. Rotational effects on the aerodynamics and aeroacoustics of wind turbine airfoils. In *12th AIAA/CEAS Aeroacoustics Conference*, 2006. AIAA 2006-2575. [cited at p. 86]

[96] F.K. Moore. Unsteady laminar boundary-layer flow. technical note TN 2471, NACA, Lewis flight propulsion laboratory, Cleveland,Ohio, September 1951. [cited at p. 17, 21, 234]

[97] R.B. Morgan. Restarted block-gmres with deflation of eigenvalues. *Applied numerical mathematics*, 54:222–236, November 2004. [cited at p. 115]

[98] B.H. Mughal. A calculation method for the three dimensional boundary layer equations in integral form. Master's thesis, Massachusetts Institute of Technology, September 1992. [cited at p. 15, 33, 71, 121]

[99] B.H. Mughal. *Integral methods for three-dimensional boundary layers*. PhD thesis, Massachusetts Institute of Technology, February 1998. [cited at p. 11, 18, 20, 28, 29, 32, 37, 68, 76, 84, 85, 121, 187, 268]

[100] D.F. Myring. An integral prediction method for three-dimensional turbulent boundary in incompressible flows. Tech. Rep. TR-70147, RAE, August 1970. [cited at p. 121, 227]

[101] J. Naber. A runge-kutta discontinuous-galerkin level-set method for unsteady compressible two-fluid flow. Master's thesis, Delft University of Technology, Kluyverweg 1,Delft, December 2005. [cited at p. 90, 99, 101, 107, 112, 118, 119]

[102] K. Nanbu. Unsteady falkner-skan flow. *Zeitschrift für Angewandte Mathematik und Physik*, 22:1167, 1971. [cited at p. 18, 186]

[103] B.A. Nishida. *Fuly simultaneous coupling of the full potential equation and the integral boundary layer equations in three dimensions*. PhD thesis, Massachusetts Institute of Technology, February 1996. [cited at p. 26, 30, 37, 75, 121]

[104] E. Nordin. *Development of body and viscous contribution to a panel program for potential flow computation*. PhD thesis, Linköpings universitet, SE-581 83 Linköping, March 2006. Master Thesis. [cited at p. 210]

[105] J.W. Oler, J.H. Strickland, B.J. Im, and G.H. Graham. Dynamic stall regulation of the darrieus turbine. Contractor report SAND83-7029, Sandia National Laboratories Albuquerque, Lubbock, Texas 79409, August 1983. [cited at p. 16, 29, 32, 35, 66, 142]

[106] H. Özdemir. *High-order Discontinuous Galerkin Method on Hexahedral elements for aeroacoustics*. PhD thesis, University of Twente, 2006. [cited at p. 101, 102, 103, 104, 107, 112, 113, 114]

[107] H. Özdemir. Derivation of integral boundary layer equations. Reference XXXX, ECN, 2008. [cited at p. 12, 173]

[108] H. Özdemir, May 2009. Personal communication. [cited at p. 106]

[109] P.O. Persson and J. Peraire. An efficient low memory implicit dg algorithm for time dependent problems. *AIAA*, 2006. Massachusetts Institute of Technology. [cited at p. 115]

[110] K. Philip, H. Ma, and W.H. Hui. Similarity solutions of the two-dimensional unsteady boundary-layer equations. *J.Fluid Mech.*, 216:537–559, 1990. [cited at p. 18, 33, 186]

[111] I. Proudman and K. Johnson. Boundary-layer growth near a rear stagnation point. *Journal of Fluid Mechanics*, 12(2):161–168, 1961. [cited at p. 19, 57, 187]

[112] N. Riley. Unsteady laminar boundary layers. *SIAM review*, 17(2):274–297, 1975. [cited at p. 73, 236, 237, 270]

[113] L. Rosenhead. *Laminar boundary layers*. Oxford Univ. press, London, 1963. [cited at p. 20, 21, 185, 208, 211, 224]

[114] L. Rosenhead. *Laminar boundary layers*. Dover, New york, 1966. [cited at p. 20]

[115] N. Rott and M.L. Rosenzweig. On the response of the laminar boundary layer fluid to small fluctuations in the free stream velocity. *J. of the aeronautical sciences*, 27:741–747,787, 1960. [cited at p. 234]

[116] L.A. Rozin. The growth of a laminar boundary layer on a flat plate set impulsively into motion. *Prik. Mat. Mekh.*, 21:615, 1957. [cited at p. 16]

[117] Y. Saad and M. Schultz. Gmres: A generalised minimal residual algorithm for solving nonsymmetric linear systems. *SIAM J. Sci. Stat. Comput.*, 7(3):856–870, July 1986. [cited at p. 115]

[118] H. Schlichting. *Boundary layer theory*. Springer, Berlin, 8 edition, 2000. ISBN 3-540-66270-7. [cited at p. 10, 15, 16, 17, 18, 19, 23, 24, 25, 26, 34, 196, 208, 209, 235, 236, 258]

[119] M.T. Schobeiri and L. Wright. Advances in unsteady boundary layer transition research, part i: Theory and modeling. *International Journal of Rotating Machinery*, 1(9):1–9, 2003. DOI: 10.1080/10236210390147308. [cited at p. 26, 27, 257]

[120] W.K. Sekar. *Viscous-Inviscid Interaction Methods for flutter calculations*. PhD thesis, Technical University of München, August 2006. [cited at p. 32, 37, 41, 63, 68, 69, 87, 129, 160, 198, 209, 263]

[121] C. Sicot, P. Devinant, S. Loyer, and J. Hureau. *Wind Energy*, chapter Rotation and Turbulence Effects on a HAWT Blade Airfoil Aerodynamics, pages 221–226. Spring Berlin Heidelberg, 2007. ISBN: 978-3-540-33865-9. [cited at p. 25]

[122] A.M.O Smith. Transition, pressure gradient, and stability theory. *Proceedings IX international congress of applied mechanics*, 4:234–244, 1956. [cited at p. 23]

[123] F.T. Smith. Steady and unsteady boundary-layer separation. *Ann. Rev. Fluid Mech.*, 18:197–220, 1986. [cited at p. 34, 66]

[124] P.D. Smith. An integral prediction method for three-dimensional compressible turbulent boundary layers. Tech. Rep. 3739, RAE R&M, December 1972. [cited at p. 73, 76, 235, 264]

[125] P.D. Smith and A.D. Young. Approximate solutions of the three-dimensional laminar boundary layer momentum integral equations. Technical Report cp 1064, Ministry of technology(UK),aeronautical research council, 1969. [cited at p. 19]

[126] K. Stewartson. On the impulsive motion of a flat plate in a viscous fluid. *Quart. Journ. Mech. and Applied Math.*, 4(2):182–198, 1951. [cited at p. 73, 235]

[127] H.W. Stock and W. Haase. Navier-stokes airfoil computations with e^n transition prediction including transitional flow regions. *AIAA J.*, 38(11):2059–2066, November 2000. [cited at p. 61]

[128] T. W. Swafford, 1985. http://www.springerlink.com/content/784723q1q3733375. [cited at p. 67, 89]

[129] T.W. Swafford. Analytical approximation of two-dimensional seperated turbulent boundary-layer velocity profiles. *AIAA Journal*, 21(6):923–926, 1963. [cited at p. 17, 27, 29, 32, 33, 67, 68, 72]

[130] T.W. Swafford. Three-dimensional,time-dependent, compressible, turbulent integral boundary layer equations in general curvilinear coordinates and their numerical solution. Final Report AEDC-TR-83-37, Arnold Engineering Development Center/DOT, 1983. [cited at p. 36, 67, 75, 83]

[131] T.W. Swafford and Whitfield D.L. Time-dependent solution of three-dimensional compressible turbulent integral boundary-layer equations. *AIAA J.*, 23(7):1005–1013, 1985. [cited at p. 72, 121]

[132] I. Tani. On the approximate solution of the laminar boundary layer equations. *J. Aero. Sci.*, 21:487, 1954. [cited at p. 18, 21, 53, 55, 56, 57, 187]

[133] I. Tani and Yu. Unsteady boundary layer over a flat plate started from rest. *Recent research on unsteady boundary layers*, page 886, 1972. [cited at p. 18, 187]

[134] D.P. Telionis and D.Th. Tsahalis. Unsteady laminar separation over impulsively moved cylinders. *Acta Astronautica*, 1(1):1487–1505, March 1974. [cited at p. 74]

[135] E.F. Toro and V.A. Titarev. Solution of the generalized riemann problem for advection-reaction equations. *Proceedings:Mathematical,physical and engineering sciences*, 458(2018):271–281, February 2002. [cited at p. 107]

[136] B. Van den Berg, D.A. Humphreys, E. Krause, and J.P.F. Lindhout. Three-dimensional turbulent boundary layers - calculation and experiments, 1988. [cited at p. 13]

[137] R. Van der Bas. Least-squares spectral element method for 2d hyperbolic systems of equations. Master's thesis, Delft University of Technology, Kluyverweg 1, September 2007. [cited at p. 106]

[138] J. Van Ingen. The en method for transition prediction. historical review of work at tu delft, June 2008. 38th Fluid Dynamics Conference and Exhibit. [cited at p. 23]

[139] J.L. Van Ingen. A suggested semi-empirical method for the calculation of the boundary-layer region. Report VTH74, Technical University of Delft, Delft,Holland, 1956. [cited at p. 23]

[140] J.L. Van Ingen. A new e^n database method for transition prediction. Delft University of Technology, September 2006. [cited at p. 25, 26]

[141] J. Van Kan, A. Segal, and F. Vermolen. *Numerical methods in scientific computing*. VSSD, 1 edition, 2005. [cited at p. 115]

[142] B. Van Oudheusden, 2008. Personal Communication. [cited at p. 36, 60, 208]

[143] A.E.P. Veldman. Computational fluid dynamics, December 2002. [cited at p. 92, 120]

[144] A.E.P. Veldman. Quasi-simultaneous viscous-inviscid interaction for transonic airfoil flow. *AIAA*, pages 1–13, June 2005. Theoretical Fluid Mechanics Meeting,Toronto,AIAA paper 2005-4801. [cited at p. 121]

[145] A.E.P. Veldman. *Boundary Layers in Fluids*. University of Groningen, p.o. Box 407, 9700 AK Groningen, 04 2008. Lecture Notes in Applied Mathematics. [cited at p. 10, 29, 34, 36, 37, 80, 257, 267]

[146] A.E.P. Veldman and R. Houwink. Steady and unsteady serparated flow computation for transonic airfoil. *AIAA*, June 1984. Paper 84-1618. [cited at p. 37]

[147] L. J. Vermeer, J. N. Srensen, and A. Crespo. Wind turbine wake aerodynamics. *Progress in Aerospace Sciences*, 39(6-7):467 – 510, 2003. [cited at p. 49]

[148] J.C. Wai and H. Yoshihara. *Seventh International Conference on Numerical Methods in Fluid Dynamics*, chapter Viscous transonic flow over airfoils, pages 417,422. Springerlink, 1981. http://www.springerlink.com/content/y34631324pk7r08j. [cited at p. 52]

[149] A. Walz. *Strömungs und Temperatur grenzschichten*. Verlag G.Braun, Karlsruhe, 1 edition, 1966. [cited at p. 20]

[150] Z.U.A. Warsi. Motion in a three-dimensional boundary with a rapidly oscillating external flow. *J.Phys.Soc.Japan*, 19(1), September 1963. 121-124. [cited at p. 237]

[151] Z.U.A. Warsi. *Fluid dynamics, theoretical and numerical approaches*. CRC Press, Florida, 1 edition, 1993. ISBN 0-8493-4436-0. [cited at p. 7, 15, 28]

[152] A.R. Wazzan, Jr. C. Gazley, and A.M.O. Smith. $h-r\_x$ method for predicting transition. *AIAA J.*, 19(6):810–812, 1981. [cited at p. 24, 26]

[153] P. Wesseling. *Principles of computational fluid dynamics*. Springer-Verlag, Berlin Heidelberg, 1 edition, 1991. ISBN-7-03-016677-9. [cited at p. 45, 96, 97, 119]

[154] F.M. White. *Viscous fluid flow*, volume 1. McGraw-Hill, 2 edition, 1991. ISBN 0-07-100995-7. [cited at p. 8, 9, 12, 13, 15, 17, 19, 23, 25, 28, 29, 31, 32, 61, 174, 182, 209, 214, 216, 218, 229, 257]

[155] D.L. Whitfield. Analytical description of the complete turbulent boundary. *AIAA J.*, 17(10):1145–1147, 1979. [cited at p. 29, 33]

[156] J.C. Williams. Flow development in the vicinity of the sharp trailing edge on bodies impulsively set into motion. *Journal of Fluid Mechanics*, 115(1):27–37, 1982. [cited at p. 19, 187]

[157] J.C. Williams and W.D. Johnson. Semisimilar solutions to unsteady boundary-layer flows including separation. *AIAA J.*, 12:1388–1393, 1974. [cited at p. 57]

[158] H. Wirz. Computation of unsteady boundary layers, 1975. [cited at p. 13, 234]

[159] W.J. Yang and H.S. Huang. Unsteady compressible laminar boundary-layer flow over a flat plate, 1969. [cited at p. 236]

[160] Z. Zhang, F. Liu, and D.M. Schuster. Calculations of unsteady flow and flutter by an euler and integral boundary-layer method on cartesian grids, 2004. [cited at p. 27, 37, 41, 43, 49, 68, 160]

Appendices

Appendix A

Integral Boundary Layer Equations

$n = 0$

For $n = 0$ equation (2.20) gives[1]

$$\frac{\partial u}{\partial t} + u\frac{\partial u}{\partial x} + v\frac{\partial u}{\partial y} + (u - u_e)\left(\frac{\partial u}{\partial x} + \frac{\partial v}{\partial y}\right) = \frac{\partial u_e}{\partial t} + u_e\frac{\partial u_e}{\partial x} + \nu\left(\frac{\partial^2 u}{\partial y^2}\right).$$

Collecting terms results in

$$\frac{\partial(u - u_e)}{\partial t} + 2u\frac{\partial u}{\partial x} - u_e\frac{\partial u}{\partial x} - u_e\frac{\partial u_e}{\partial x} + v\frac{\partial u}{\partial y} + (u - u_e)\frac{\partial v}{\partial y} = \nu\left(\frac{\partial^2 u}{\partial y^2}\right).$$

Since $u\partial v = \partial uv - v\partial u$ this can be rewritten

$$\begin{aligned}
\frac{\partial(u - u_e)}{\partial t} + 2u\frac{\partial u}{\partial x} - \frac{\partial(u\,u_e)}{\partial x} + u\frac{\partial u_e}{\partial x} - u_e\frac{\partial u_e}{\partial x} + v\frac{\partial u}{\partial y} + \frac{\partial v(u - u_e)}{\partial y} - v\frac{\partial(u - u_e)}{\partial y} &= \nu\frac{\partial^2 u}{\partial y^2},\\
\frac{\partial(u - u_e)}{\partial t} + \frac{\partial u^2}{\partial x} - \frac{\partial(u\,u_e)}{\partial x} + u\frac{\partial u_e}{\partial x} - u_e\frac{\partial u_e}{\partial x} + \cancel{v\frac{\partial u_e}{\partial y}} + \frac{\partial v(u - u_e)}{\partial y} &= \nu\frac{\partial^2 u}{\partial y^2},\\
\frac{\partial(u - u_e)}{\partial t} + \frac{\partial u(u - u_e)}{\partial x} + (u - u_e)\frac{\partial u_e}{\partial x} + \frac{\partial v(u - u_e)}{\partial y} &= \nu\frac{\partial^2 u}{\partial y^2}.
\end{aligned}$$

Integrating over y from 0 to some $y = y^* > y_e$ the displacement thickness and the momentum thickness can be retrieved, also using $\nu\frac{\partial^2 u}{\partial y^2} = \frac{1}{\rho}\frac{\partial \tau}{\partial y}$ results in

$$\begin{aligned}
\frac{\partial}{\partial t}\int_0^{y^*}(u - u_e)dy + \frac{\partial}{\partial x}\int_0^{y^*}u(u - u_e)dy + \frac{\partial u_e}{\partial x}\int_0^{y^*}(u - u_e)dy&\\
+ \frac{\partial}{\partial y}\int_0^{y^*}v(u - u_e)dy = -\frac{\tau_w}{\rho}.&
\end{aligned} \quad \text{(A.1)}$$

[1] The unsteady Kármán integral can also be found by direct integration,(see i.e. Özdemir[107]).

Writing out individual terms

$$\begin{aligned}\frac{\partial}{\partial t}\int_0^{y^*}(u-u_e)dy &= -\frac{\partial}{\partial t}\int_0^{y^*}u_e\left(1-\frac{u}{u_e}\right)dy \\ &= -\frac{\partial u_e\delta^*}{\partial t} \quad , \end{aligned} \tag{A.2}$$

$$\begin{aligned}\frac{\partial}{\partial x}\int_0^{y^*}u(u-u_e)dy &= -\frac{\partial}{\partial x}\int_0^{y^*}u_e^2\frac{u}{u_e}\left(1-\frac{u}{u_e}\right)dy \\ &= -\left(u_e^2\frac{\partial\theta}{\partial x}+2\theta u_e\frac{\partial u_e}{\partial x}\right) \quad , \end{aligned} \tag{A.3}$$

$$\begin{aligned}\frac{\partial u_e}{\partial x}\int_0^{y^*}(u-u_e)dy &= -\frac{\partial u_e}{\partial x}\int_0^{y^*}u_e\left(1-\frac{u}{u_e}\right)dy \\ &= -\frac{\partial u_e}{\partial x}\delta^*u_e \quad , \end{aligned} \tag{A.4}$$

$$\begin{aligned}\frac{\partial}{\partial y}\int_0^{y^*}v(u-u_e)dy &= \left[v(u-u_e)\right]_0^{y^*}, \\ &= 0. \end{aligned} \tag{A.5}$$

where (see appendix (B))

$$\text{displacement thickness:} \quad \delta^* = \int_0^{y_e}\left(1-\frac{u}{u_e}\right)dy, \tag{A.6}$$

$$\text{momentum thickness:} \quad \theta = \int_0^{y_*}\frac{u}{u_e}\left(1-\frac{u}{u_e}\right)dy. \tag{A.7}$$

Substitution of equations (A.2), (A.3), (A.4) and (A.5) in equation (A.1) results in

$$\frac{\partial u_e\delta^*}{\partial t}+u_e^2\frac{\partial\theta}{\partial x}+(2\theta+\delta^*)u_e\frac{\partial u_e}{\partial x}=\frac{\tau_w}{\rho}. \tag{A.8}$$

Dividing by u_e^2 results in the common form of the unsteady Kármán integral [154] relation

$$\frac{1}{u_e^2}\frac{\partial(u_e\delta^*)}{\partial t}+\frac{\partial\theta}{\partial x}+(2+H)\frac{\theta}{u_e}\frac{\partial u_e}{\partial x}=\frac{C_f}{2}. \tag{A.9}$$

Where

$$H=\frac{\delta^*}{\theta},$$
$$C_f=\frac{\tau_w}{\frac{1}{2}\rho u_e^2}.$$

$n = 1$

A similar procedure as for the momentum integral equation is followed to find a mechanical energy integral relation, using $n = 1$ equation (2.20) results in

$$2u\frac{\partial u}{\partial t} + 2u^2\frac{\partial u}{\partial x} + 2uv\frac{\partial u}{\partial y} + (u^2 - u_e^2)\left(\frac{\partial u}{\partial x} + \frac{\partial v}{\partial y}\right) = 2u\frac{\partial u_e}{\partial t} + 2uu_e\frac{\partial u_e}{\partial x} + 2u\nu\frac{\partial^2 u}{\partial y^2}.$$

Collecting terms results in

$$2u\frac{\partial(u-u_e)}{\partial t} + u^2\frac{\partial u}{\partial x} - u_e^2\frac{\partial u}{\partial x} - 2u\,u_e\frac{\partial u_e}{\partial x} + 2uv\frac{\partial u}{\partial y} + u^2\frac{\partial v}{\partial y} - u_e^2\frac{\partial v}{\partial y} = 2u\nu\frac{\partial^2 u}{\partial y^2}.$$

Again using the fact that $u\partial v = \partial uv - v\partial u$ this can be rewritten as

$$\begin{aligned}
2u\frac{\partial(u-u_e)}{\partial t} + 2u^2\frac{\partial u}{\partial x} - u_e^2\frac{\partial(u)}{\partial x} + u^2\frac{\partial u}{\partial x} - 2u\,u_e\frac{\partial u_e}{\partial x} + 2uv\frac{\partial u}{\partial y} - u_e^2\frac{\partial v}{\partial y} + u^2\frac{\partial v}{\partial y} &= 2u\nu\frac{\partial^2 u}{\partial y^2},\\
2u\frac{\partial(u-u_e)}{\partial t} + \frac{\partial u^3}{\partial x} - u_e^2\frac{\partial(u)}{\partial x} - 2u\,u_e\frac{\partial u_e}{\partial x} + v\frac{\partial u^2}{\partial y} + u^2\frac{\partial v}{\partial y} - u_e^2\frac{\partial v}{\partial y} &= 2u\nu\frac{\partial^2 u}{\partial y^2},\\
2u\frac{\partial(u-u_e)}{\partial t} + \frac{\partial u(u^2-u_e^2)}{\partial x} + \frac{\partial u^2 v}{\partial y} - \frac{\partial u_e^2\,v}{\partial y} + \cancel{v\frac{\partial u_e}{\partial y}} &= 2u\nu\frac{\partial^2 u}{\partial y^2},\\
2u\frac{\partial(u-u_e)}{\partial t} + \frac{\partial u(u^2-u_e^2)}{\partial x} + \frac{\partial v(u^2-u_e^2)}{\partial y} &= 2u\nu\frac{\partial^2 u}{\partial y^2}.
\end{aligned}$$

Again integrating over y from 0 to some $y = y^* > y_e$ and using $\nu\frac{\partial^2 u}{\partial y^2} = \frac{1}{\rho}\frac{\partial \tau}{\partial y}$

$$\begin{aligned}
2\int_0^{y^*} u\frac{\partial(u-u_e)}{\partial t}dy + \frac{\partial}{\partial x}\int_0^{y^*} u(u^2-u_e^2)dy + \frac{\partial}{\partial y}\int_0^{y^*} v(u^2-u_e^2)dy&\\
= \cancel{\frac{2}{\rho}[u\tau]_0^{y^*}} - \frac{2}{\rho}\int_0^{y^*}\tau\frac{\partial u}{\partial y}dy.& \quad \text{(A.10)}
\end{aligned}$$

Writing out the individual terms

$$
\begin{aligned}
2\int_0^{y^*} u\frac{\partial(u-u_e)}{\partial t}dy &= -2\frac{\partial}{\partial t}\int_0^{y^*} u(u_e-u)dy + 2\int_0^{y^*}(u_e-u)\frac{\partial u}{\partial t}dy \\
&= -2\frac{\partial}{\partial t}\int_0^{y^*} u(u_e-u)dy + 2\int_0^{y^*}\frac{\partial u\,u_e}{\partial t}dy - 2\int_0^{y^*} u\frac{\partial u_e}{\partial t}dy - \int_0^{y^*}\frac{\partial u^2}{\partial t}dy \\
&= -\frac{\partial}{\partial t}\int_0^{y^*} u(u_e-u)dy + \int_0^{y^*}\frac{\partial u_e\,u}{\partial t}dy - 2\int_0^{y^*} u\frac{\partial u_e}{\partial t}dy \\
&= -\frac{\partial}{\partial t}\int_0^{y^*} u(u_e-u)dy + \int_0^{y^*}\frac{\partial u_e\,u}{\partial t}dy - 2\int_0^{y^*} u\,u_e^{-1}\,u_e\frac{\partial u_e}{\partial t}dy \\
&= -\frac{\partial}{\partial t}\int_0^{y^*} u(u_e-u)dy + \int_0^{y^*}\frac{\partial u_e\,u}{\partial t}dy - \int_0^{y^*}\frac{u}{u_e}\frac{\partial u_e^2}{\partial t}dy \\
&= -\frac{\partial}{\partial t}\int_0^{y^*} u(u_e-u)dy + u_e^2\frac{\partial}{\partial t}\int_0^{y^*}\frac{u}{u_e}dy \\
&= -\frac{\partial}{\partial t}\int_0^{y^*} u_e^2\frac{u}{u_e}(1-\frac{u}{u_e})dy - u_e^2\frac{\partial}{\partial t}\int_0^{y^*}(1-\frac{u}{u_e})dy \\
&= -\frac{\partial u_e^2\theta}{\partial t} - u_e^2\frac{\partial\delta^*}{\partial t} \\
&= -u_e^2\frac{\partial\theta}{\partial t} - \theta\frac{\partial u_e^2}{\partial t} - u_e^2\frac{\partial\delta^*}{\partial t} \\
&= -u_e^2\frac{\partial(\theta+\delta^*)}{\partial t} - 2\theta u_e\frac{\partial u_e}{\partial t}, \qquad \text{(A.11)}
\end{aligned}
$$

$$
\begin{aligned}
\frac{\partial}{\partial x}\int_0^{y^*} u(u^2-u_e^2)dy &= -\frac{\partial}{\partial x}\int_0^{y^*} u_e^3\frac{u}{u_e}\left(1-\frac{u^2}{u_e^2}\right)dy \\
&= -\frac{\partial u_e^3\delta^k}{\partial x}, \qquad \text{(A.12)}
\end{aligned}
$$

$$
\begin{aligned}
\frac{\partial}{\partial y}\int_0^{y^*} v(u^2-u_e^2)dy &= \left[v(u^2-u_e^2)\right]_0^{y^*}, \\
&= 0. \qquad \text{(A.13)}
\end{aligned}
$$

Introducing the dissipation integral D and the kinetic energy thickness δ^k

$$D = \int_0^{y^*}\tau\frac{\partial u}{\partial y}dy, \qquad \text{(A.14)}$$

$$\delta^k = \int_0^{y^*}\frac{u}{u_e}\left(1-\frac{u^2}{u_e^2}\right)dy. \qquad \text{(A.15)}$$

The kinetic energy integral is obtained by substituting the individual terms (A.11), (A.12), (A.13) in equation (A.10) and subsequently dividing by u_e^3

$$\frac{1}{u_e}\frac{\partial(\theta+\delta^*)}{\partial t} + 2\frac{\theta}{u_e^2}\frac{\partial u_e}{\partial t} + \frac{1}{u_e^3}\frac{\partial(u_e^3\delta^k)}{\partial x} = C_D, \qquad \text{(A.16)}$$

where

$$C_D = \frac{2D}{\rho u_e^3}.$$

$n = 2$

Following the same procedure as for the momentum integral and the kinetic energy integral a third integral can be obtained. Using $n = 2$ equation (2.20) results in

$$3\frac{\partial u}{\partial t} + 3u^3\frac{\partial u}{\partial x} + u^2 v\frac{\partial u}{\partial y} + \left(u^2 - u_e^2\right)\left(\frac{\partial u}{\partial x} + \frac{\partial v}{\partial y}\right) = 3u^2\frac{\partial u_e}{\partial t} + 3u^2 u_e\frac{\partial u_e}{\partial x} + 3u^2 v\frac{\partial^2 u}{\partial y^2}.$$

Collecting terms results in

$$3u^2\frac{\partial(u-u_e)}{\partial t} + 4u^3\frac{\partial u}{\partial x} - u_e^3\frac{\partial u}{\partial x} - 3u^2 u_e\frac{\partial u_e}{\partial x} + 3u^2 v\frac{\partial u}{\partial y} + \left(u^3 - u_e^3\right)\frac{\partial v}{\partial y} = 3u^2\nu\frac{\partial^2 u}{\partial y^2}.$$

Again using $\partial uv = u\partial v + v\partial u$ this can be rewritten

$$3u^2\frac{\partial(u-u_e)}{\partial t} + 4u^3\frac{\partial u}{\partial x} - \frac{\partial u\, u_e^3}{\partial x} + u\frac{\partial u_e^3}{\partial x} - 3u^2 u_e\frac{\partial u_e}{\partial x} + 3u^2 v\frac{\partial u}{\partial y} \frac{\partial v\left(u^3 - u_e^3\right)}{\partial y} - v\frac{\partial(u^3 - u_e^3)}{\partial y} = 3u^2\nu\frac{\partial^2 u}{\partial y^2},$$

$$3u^2\frac{\partial(u-u_e)}{\partial t} + \frac{\partial u^4}{\partial x} - \frac{\partial u\, u_e^3}{\partial x} + 3u_e^2 u\frac{\partial u_e}{\partial x} - 3u^2 u_e\frac{\partial u_e}{\partial x} + \cancel{v\frac{\partial u^3}{\partial y}} + \frac{\partial v\left(u^3 - u_e^3\right)}{\partial y} - v\frac{\partial(\cancel{u^3} - \cancel{u_e^3})}{\partial y} = 3u^2\nu\frac{\partial^2 u}{\partial y^2},$$

$$3u^2\frac{\partial(u-u_e)}{\partial t} + \frac{\partial u\left(u^3 - u_e^3\right)}{\partial x} - 3\left(u_e u\left(u-u_e\right)\right)\frac{\partial u_e}{\partial x} + \frac{\partial v\left(u^3 - u_e^3\right)}{\partial y} = 3u^2\nu\frac{\partial^2 u}{\partial y^2}.$$

Again integrating over y from 0 to some $y = y^* > y_e$ and using $\nu\frac{\partial^2 u}{\partial y^2} = \frac{1}{\rho}\frac{\partial \tau}{\partial y}$

$$3\int_0^{y^*} u^2\frac{\partial(u-u_e)}{\partial t}dy + \frac{\partial}{\partial x}\int_0^{y^*} u\left(u^3 - u_e^3\right)dy - 3\frac{\partial u_e}{\partial x}\int_0^{y^*} u_e u(u-u_e)dy + \frac{\partial}{\partial y}\int_0^{y^*} v\left(u^3 - u_e^3\right)dy = \cancel{\frac{3}{\rho}\left[\tau u^2\right]_0^{y^*}} - \frac{3}{\rho}\int_0^{y^*}\tau\frac{\partial u^2}{\partial y}dy \quad \text{(A.17)}$$

Writing out individual terms

$$
\begin{aligned}
3\int_0^{y^*} u^2\frac{\partial(u-u_e)}{\partial t}dy &= -3\frac{\partial}{\partial t}\int_0^{y^*} u^2(u_e-u)dy + 3\int_0^{y^*}(u_e-u)\frac{\partial u^2}{\partial t}dy \\
&= -3\frac{\partial}{\partial t}\int_0^{y^*} u^2(u_e-u)dy + 3\int_0^{y^*}\frac{\partial u^2\,u_e}{\partial t}dy - 3\int_0^{y^*} u^2\frac{\partial u_e}{\partial t}dy - 2\int_0^{y^*}\frac{\partial u^3}{\partial t}dy \\
&= -\frac{\partial}{\partial t}\int_0^{y^*} u^2(u_e-u)dy + \int_0^{y^*}\frac{\partial u_e\,u^2}{\partial t}dy - 3\int_0^{y^*} u^2\frac{\partial u_e}{\partial t}dy \\
&= -\frac{\partial}{\partial t}\int_0^{y^*} u\left(u_e^2-u^2\right)dy - \frac{\partial}{\partial t}\int_0^{y^*}\left(u_e^3-u_e^2u\right)dy - \cancel{\frac{\partial}{\partial t}\int_0^{y^*} u_e u^2 dy} \\
&\quad + \frac{\partial}{\partial t}\int_0^{y^*} u_e^3 dy + \cancel{\frac{\partial}{\partial t}\int_0^{y^*} u_e u^2 dy} - 3\int_0^{y^*} u^2\frac{\partial u_e}{\partial t}dy \\
&= -\frac{\partial}{\partial t}\int_0^{y^*} u\left(u_e^2-u^2\right)dy - \frac{\partial}{\partial t}\int_0^{y^*}\left(u_e^3-u_e^2u\right)dy + 3\int_0^{y^*}\left(u_e^2-u^2\right)\frac{\partial u_e}{\partial t}dy \\
&= -\frac{\partial}{\partial t}\int_0^{y^*} u\left(u_e^2-u^2\right)dy - \frac{\partial}{\partial t}\int_0^{y^*}\left(u_e^3-u_e^2u\right)dy + 3\frac{\partial u_e}{\partial t}\int_0^{y^*}\left(u_eu-u^2\right)dy \\
&\quad + 3\frac{\partial u_e}{\partial t}\int_0^{y^*}\left(u_e^2-u_eu\right)dy \\
&= -\frac{\partial}{\partial t}\int_0^{y^*} u_e^3\frac{u}{u_e}\left(1-\frac{u^2}{u_e^2}\right)dy - \frac{\partial}{\partial t}\int_0^{y^*} u_e^3\left(1-\frac{u}{u_e}\right)dy \\
&\quad + 3\frac{\partial u_e}{\partial t}\int_0^{y^*} u_e^2\frac{u}{u_e}\left(1-\frac{u}{u_e}\right)dy + 3\frac{\partial u_e}{\partial t}\int_0^{y^*} u_e^2\left(1-\frac{u}{u_e}\right)dy \\
&= -\frac{\partial u_e^3\delta^k}{\partial t} - \frac{\partial u_e^3\delta^*}{\partial t} + 3u_e^2\frac{\partial u_e}{\partial t}\theta + 3u_e^2\frac{\partial u_e}{\partial t}\delta^* \\
&= -\frac{\partial u_e^3\delta^k}{\partial t} - u_e^3\frac{\partial\delta^*}{\partial t} + 3u_e^2\frac{\partial u_e}{\partial t}\theta, \qquad \text{(A.18)}
\end{aligned}
$$

$$
\begin{aligned}
\frac{\partial}{\partial x}\int_0^{y^*} u(u^3-u_e^3)dy &= -\frac{\partial}{\partial x}\int_0^{y^*} u_e^4\frac{u}{u_e}\left(1-\frac{u^3}{u_e^3}\right)dy \\
&= -\frac{\partial u_e^4\delta^{k+}}{\partial x}, \qquad \text{(A.19)}
\end{aligned}
$$

$$
3u_e\frac{\partial u_e}{\partial x}\int_0^{y^*} u(u-u_e)dy = -3u_e^3\frac{\partial u_e}{\partial x}\theta, \qquad \text{(A.20)}
$$

$$
\begin{aligned}
\frac{\partial}{\partial y}\int_0^{y^*} v(u^3-u_e^3)dy &= \left[v(u^3-u_e^3)\right]_0^{y^*} \\
&= 0. \qquad \text{(A.21)}
\end{aligned}
$$

Introducing the following integral variables

$$
\begin{aligned}
K &= 6\nu\int_0^{y^*} u\left(\frac{\partial u}{\partial y}\right)^2 dy, \\
\delta^{k+} &= \int_0\frac{u}{u_e}\left(1-\frac{u^3}{u_e^3}\right)dy.
\end{aligned}
$$

Now the third momentum equation is obtained by substituting the individual terms (A.18), (A.19), (A.20) and (A.21) in equation (A.17) and dividing by u_e^4

$$
\frac{1}{u_e^4}\left(\frac{\partial u_e^3\delta^k}{\partial t} + \frac{\partial u_e^4\delta^{k+}}{\partial x} + u_e^3\frac{\partial\delta^*}{\partial t} - 3u_e^2\frac{\partial u_e}{\partial t}\theta - 3u_e^3\frac{\partial u_e}{\partial x}\theta\right) = 6C_K, \qquad \text{(A.22)}
$$

(A.23)

where

$$C_K = 6\frac{\nu}{u_e^4}\int_0^{y^*} u\left(\frac{\partial u}{\partial y}\right)^2 dy.$$

Appendix B

Boundary Layer Characteristics

The boundary layer along objects is caused by the viscosity which deters the flow near the surface of the object, in fact in normal practice it is assumed that the surface velocity is identically zero. This boundary condition together with the diffusive nature of the viscosity terms gives rise to a boundary layer in which the body attached flow diffuses with the external flow. The velocity perpendicular to a solid surface is also assumed to be zero, therefore the common boundary condition for boundary layers is

$$\bar{u} = 0 \quad \bar{x} \subset \Gamma_{surface} \tag{B.1}$$

The boundary layer has a tangential velocity profile which is characterized first and foremost by the boundary layer thickness δ (see figure (B.1)).

$$\delta = y_{u=m\,u_e} \tag{B.2}$$

A typical value for m is 99%, i.e. the boundary layer is considered until the velocity inside the boundary layer is 99% of the external velocity. Other characteristics are the displacement thickness δ^*, the momentum thickness θ and the wall friction τ_w.

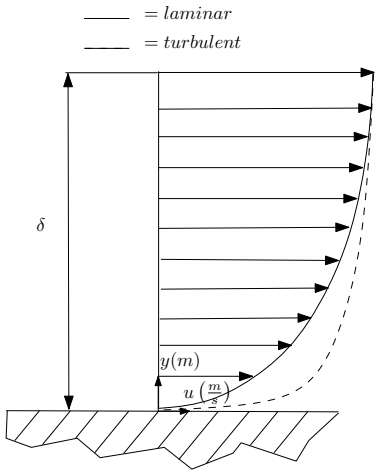

Figure B.1: Velocity distribution in the boundary layer

The displacement thickness δ^* of the boundary layer is defined as the thickness needed for the external flow to produce the reduced mass flow. The reduced massflow

for an incompressible flow is given by

$$m_{red} = \rho u_e y_e - \rho \int_0^{y_e} u dy \tag{B.3}$$

The displacement thickness then follows directly from

$$\delta^* = \frac{m_{red}}{\rho u_e} \tag{B.4}$$

or

$$\delta^* = \int_0^{y_e} \left(1 - \frac{u}{u_e}\right) dy \tag{B.5}$$

Here y_e is unknown a priori but a semi-arbitrary value for y can be chosen since the integral has no contributions for $y > y_e$. Suppose $y = y^* > y_e$

$$\delta^* = \int_0^{y^*} \left(1 - \frac{u}{u_e}\right) dy \tag{B.6}$$

$$= \int_0^{y^e} \left(1 - \frac{u}{u_e}\right) dy + \cancel{\int_{y_e}^{y^*} \left(1 - \frac{u}{u_e}\right) dy} \tag{B.7}$$

The momentum thickness θ of the boundary layer is defined as the additional thickness (on top of the displacement thickness) needed for the external flow to produce the reduced momentum. The reduced momentum for an incompressible flow is given by

$$\zeta_{red} = \rho \int_{\delta^*+\theta}^{y_e} u_e^2 dy - \rho \int_0^{y_e} u^2 dy \tag{B.8}$$

The derivation is completely analogous to the derivation of the displacement thickness and results in

$$\theta = \int_0^{y_*} \frac{u}{u_e} \left(1 - \frac{u}{u_e}\right) dy \tag{B.9}$$

Note that the momentum thickness is a direct measure for the specific wall shear force over a flat plate ([154]) through

$$\tau_w(x) = 2\rho u_e^2 \theta \tag{B.10}$$

The same procedure can be followed to obtain higher order integral variables, also see figure(B.2)

$$\delta^k = \int_0^{y_*} \frac{u}{u_e} \left(1 - \left(\frac{u}{u_e}\right)^2\right) dy, \quad \delta^{k+} = \int_0^{y_*} \frac{u}{u_e} \left(1 - \left(\frac{u}{u_e}\right)^3\right) dy, \cdots$$

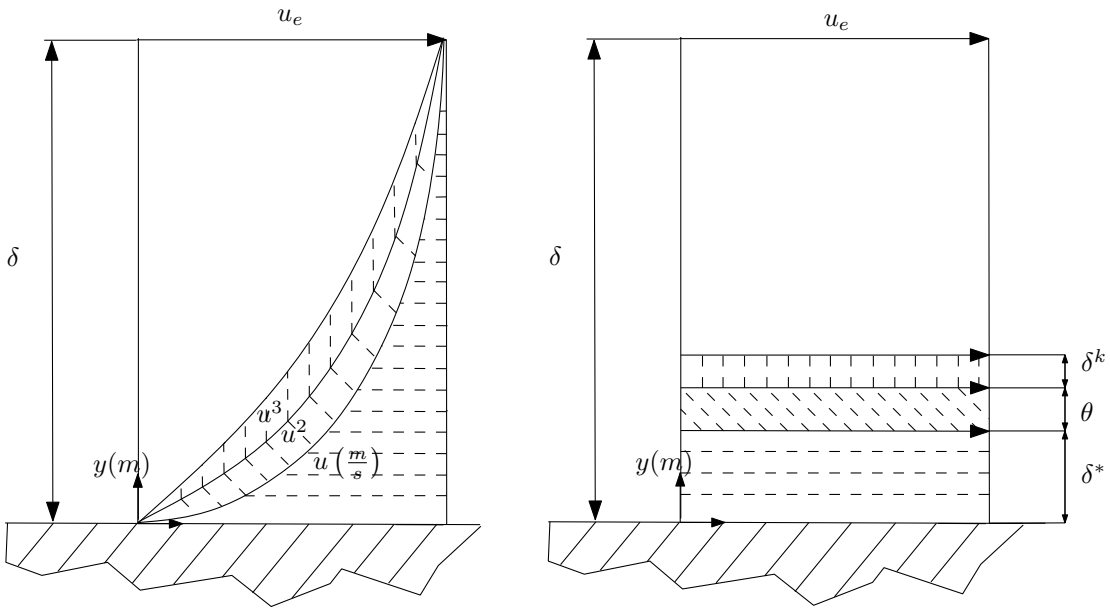

Figure B.2: Physical interpretation of integral variables

Appendix C

Similarity Solutions

Starting from the boundary layer equations it is possible for certain external velocity profiles to write a single ODE or a system of ODE's dependent on one variable usually denoted as $\eta(x, y, t)$. This means that a solution for some η simply scales in any direction for which η is constant, the solution is called self-similar in that direction. The first similarity solution was for a flat-plate boundary layer flow, due to Blasius in 1908. A subset of the similarity solutions are the semi-similarity solutions where the problem variable are reduced to two variables, see i.e. Hayasi[61].
Note that the flat-plate is defined as such through the external velocity profile, i.e. $u_e = Constant$. This should not be confused with the current flat-plat problem where the flat-plate is assumed merely for the ease of using an orthogonal coordinate system.

The similarity solution of the Falkner-Skan equation is given by

$$\begin{gathered} f''' + \frac{m+1}{2} f f'' + m\left(1 - f'^2\right) = 0 \\ \eta = \sqrt{\frac{u_e}{\nu x}}\, y, \quad f(\eta) = \frac{\psi(x,y)}{\sqrt{u_e \nu x}}, \quad m = \frac{x}{u_e}\frac{du_e}{dx} \\ \textit{boundary conditions :} f(0) = 0\,, f'(0) = 0\,, f'(\infty) = 1, \end{gathered} \tag{C.1}$$

which was adapted by Hartree (as reference by Cebeci and Cousteix[22]) to a more convenient form

$$\begin{gathered} f'''(\eta) + f(\eta) f''(\eta) + \beta\left(1 - f'^2(\eta)\right) = 0, \\ \eta = y\sqrt{\frac{m+1}{2}\frac{u_e(x)}{\nu x}}, \quad u(x,y) = u_e(x)\sqrt{\frac{m+1}{2}} f'(\eta), \quad \beta = \frac{2m}{1+m}, \\ \textit{boundary conditions :} f(0) = 0\,, f'(0) = 0\,, f'(\infty) = 1, \end{gathered} \tag{C.2}$$

where β is a measure of the pressure gradient, $\beta = 0$ results in the Blasius equation for a flat plate. The Falkner-Skan equation has a unique solution for (see Rosenhead[113])

$$0 < \eta < \infty, \quad \beta^* < \beta < 2, \quad 0 < f'(\eta) < 1, \quad f''(\eta) > 0,$$

here β^* is the value of β for which $f''(0) = 0$.

The external velocity is assumed to be consistent with a power-law freestream velocity distribution

$$u_e(x) = K\, x^m.$$

To obtain a Falkner-Skan like equation for the unsteady form of the boundary layer equations the time derivative has to be incorporated. Specific unsteady similarity solutions for the impulsively started semi-infinite wedge are given by Nanbu [102], Khan et al (2006)[74] and Philip et al[110]. Using a perturbation method Khan et al derived the unsteady variant of the Falkner-Skan equation for a second-grade fluid, the zeroeth order system is given as [74]

$$f''' + \left(f + \frac{\eta}{2}\right) f'' + f'(1 - f') = 0,$$
$$\eta = \frac{y^*}{\sqrt{t^*}},\ \psi^* = \frac{x^*}{\sqrt{t^*}} f(\eta),$$
$$\textit{boundary conditions :} f(0) = 0\,, f'(0) = 0\,, f'(\infty) = 1,$$

where

$$x^* = \frac{x}{L}, \quad y^* = \sqrt{Re(x)}\frac{y}{L}, \quad t^* = \frac{t\,u_e}{L}.$$

Khan does not give parameters that describe the wedge shape since the solution by Khan assumes $u_e = u_0 \left(\frac{x}{t}\right)^m$ with $m = 1$, it is not clear where and how m enters the differential equations. Philip et al derived general classes of similarity solutions for the unsteady boundary layer equations and found that the earlier specific solutions were indeed subsets of the more general solutions. Philip et al found 6 classes of solutions, one particular class prescribes the external velocity as $u_e = x\,g(t)$.
Within this class a solution exists for $g(t) = A > 0$ and $g(t) = \frac{A}{t}$, where A is some constant. The solution for $g(t) = A > 0$ is given by

$$f''' + ff'' + 1 - f'^2 = 0,$$
$$\eta = \sqrt{A}y, \quad u_e = Ax, \quad u = Axf'(\eta), \quad v = -A^{\frac{1}{2}} f(\eta), \tag{C.3}$$
$$\textit{boundary conditions :} f(0) = 0\,, f'(0) = 0\,, f'(\infty) = 1.$$

This is of course equal to the Falkner-Skan equation with $\beta = 1$. More interesting is the solution for $g(t) = \frac{A}{t}$ which is given by

$$f''' + (Af + \frac{1}{2}\eta) f'' + (1 - Af')f' + A - 1 = 0,$$
$$\eta = \frac{y}{\sqrt{t}}, \quad u_e = \frac{A}{t}x, \quad u = \frac{A}{t}xf'(\eta), \quad v = -\frac{A}{\sqrt{t}} f(\eta), \tag{C.4}$$
$$\textit{boundary conditions :} f(0) = 0\,, f'(0) = 0\,, f'(\infty) = 1.$$

The zeroeth-order system of Khan can indeed be recognized as a specific similarity solution if A is set to 1.

Whereas system (C.3) has a unique solution, system (C.4) has more than one solution for all $A > 0$. For $A = 1$ one solution represents attached flow and one solution represents seperated flow, in general there is flow seperation for $A < 1$ and flow attachment for $A > 1$ Philip[110].
The power-law flow that determined the Falkner-Skan flow is not retrieved as an unsteady flow similarity solution by Philip et al, however Nanbu [102] specifically investigated the time dependent similarity solution for a power-law velocity distribution and found 2 seperate solution methods. For $m < 1$

$$\left(1 - (1 - m)u^*t^*\right) \frac{\partial u^*}{\partial t^*} = \frac{1 + m}{2} \frac{\partial^2 u^*}{\partial \eta^2} + m(1 - u^{*2}) + \left(\frac{1 - m}{2}\eta u^* + v^*\right) \frac{\partial u^*}{\partial \eta},$$
$$\frac{\partial v^*}{\partial \eta} = mu^* - 1\frac{1 - m}{2}\eta \frac{\partial u^*}{\partial \eta} - (1 - m)t^* \frac{\partial u^*}{\partial t^*},$$

and for $m \geq 1$

$$\xi^{1-m}\frac{\partial u^*}{\partial \tau} = \frac{1+m}{2}\frac{\partial^2 u^*}{\partial \eta^2} + m(1-u^{*2}) - (1-m)\xi^{1-m}u^*\frac{\partial u^*}{\partial \xi^{1-m}} + \left(v^* + \frac{1-m}{2}\eta u^*\right)\frac{\partial u^*}{\partial \eta},$$
$$\frac{\partial v^*}{\partial \eta} = mu^* + (1-m)\xi^{1-m}\frac{\partial u^*}{\partial \xi^{1-m}} - \frac{1-m}{2}\eta\frac{u^*}{\eta},$$

where

$$\tau = \frac{u_0 t}{L}, \quad \xi = \frac{x}{L}, \quad t^* = \frac{\tau}{\xi^{1-m}}, \quad \eta = \sqrt{\frac{(m+1)u_0}{2\nu L}}\xi^{\frac{1-m}{2}},$$
$$u = u_0\xi^m u^*, \quad v = -\sqrt{\frac{2u_0\nu}{(m+1)L}}\xi^{\frac{1-m}{2}}v^*.$$

Both methods require a two-way approach, firstly the equations need to be integrated in time to end up with an instantaneous form of a non-linear differential equation, secondly the differential equations needs to be integrated to obtain a final solution. Note that these are coupled partial differential equations, decoupling this for the plate problem can be done by simply ignoring the y-velocity component in the x-momentum equations.

A detailed solution procedure can be found in Hall [59]. Yet another approach was used by Matsushita[91], who employed the original Falkner-Skan formulation using a slipping wall boundary condition, i.e. $f^{'}(0) = u_{wall}$, see section (4.2.4). Matsushita refers to Tani[133] in stating that the Falkner-Skan profiles are especially suitable for accelerating flows, also see for instance Mughal[99].

Downside of the similarity solutions is their reliance on a velocity prescription $u_e = f(x,t)$, this limits their applicability since an actual unsteady flow can in general not be described through an analytical relation. However for laminar (boundary/wake) flow the velocity distributions produced by the similarity solutions or semi-similarity solutions can be used to create relations for the shape factors. To that end similarity and semi-similarity solutions have been used to specifically approximate accelerating boundary layer flow, decelerating boundary layer flow, stagnating boundary layer flow and wake flow. As was said, the Falkner-Skan solution for power-law flow provides a reference for accelerating boundary layer flows.
Often used for decelerating flow is the quartic profile due to Tani, the shape factors are tabulated in his paper[132].
For the stagnating boundary layer flow, Matsushita and Akamatsu[90] use a similarity solution by Proudman and Johnson, and Robins and Howarth which they based on the rear stagnation point of a moving cylinder. The similarity solution is given by

$$f_{yt} - f_{yyy} + ff_{yy} + 1 - f_y^2 = 0,$$
$$u = -xF_y, \quad v = F, \quad x = \sqrt{\frac{\alpha}{\nu}}\overline{x}, \quad y = \sqrt{\frac{\alpha}{\nu}}\overline{y}, t = \alpha\overline{t}$$
$$\textit{boundary conditions :} (f(0,t) = f(0,t)_y = 0, f(\infty,t)_y = 1, f(x,0)_y = 1.$$

For $0 < t < 5$ the shape factors are assumed to be variable, for large t the boundary layer will approach the similarity solution found by Hiemenz (see Proudman[111]).
In case the wake is laminar, the following semi-similar solution due to Williams[156] can be used

$$\frac{\partial^2 w}{\partial \eta^2} + \alpha_1\frac{\partial w}{\partial \eta} + \alpha_2 w + \alpha_3 = \alpha_4\frac{\partial w}{\partial \xi}, \quad \frac{\partial f}{\partial w} = w,$$
$$w(\xi,0) = f(\xi,0) = 0, \quad w(\xi,\infty) = 1,$$

where

$$\alpha_1 = -\left[m\xi + \frac{1}{2}(1-m)\left[\xi + (1-\xi)\ln(1-\xi)\right] f + \frac{1}{2}(1-\xi)\eta + (m-1)(1-\xi)\ln(1-\xi)\frac{\partial f}{\partial \xi}\right],$$

$$\alpha_2 = m\xi\frac{\partial f}{\partial \eta},$$

$$\alpha_3 = -m\xi,$$

$$\alpha_4 = (1-\xi)\left[\xi + (m-1)\ln(1-\xi)\frac{\partial f}{\partial \eta}\right].$$

At $\xi = 0$ the solution is started using

$$\frac{\partial^3 f}{\partial \eta^3} + \frac{\eta}{2}\frac{\partial^2 f}{\partial \eta^2} = 0.$$

The solution due to Williams was applied by Matsushita et al[91] for $0.2 < m < 1.3$. The similarity solutions cannot be applied directly to solve general boundary layer problems, the one-parameter integral methods however can, these will be discussed in the next section.

Appendix D

Alternative Velocity Profiles

Starting from the general polynomial $\sum_{i=1}^{N} a_i p^i$ several alternative profiles are derived using different combinations of the boundary conditions. For purpose of illustration *sextic* profiles will be used, the polynomial order can be increased arbitrarily using more boundary conditions at the edge of the boundary layer.

D.1 Profile 1

D.1.1 a

Using five boundary conditions at the edge and one at the wall will result in a single parameter profile.

$$
\begin{aligned}
f(\eta) &= a_1\eta + a_2\eta^2 + a_3\eta^3 + a_4\eta^4 + a_5\eta^5 + a_6\eta^6 \\
f(1) &= a_1 + a_2 + a_3 + a_4 + a_5 + a_6 = 1 \\
f^{'}(1) &= a_1 + 2a_2 + 3a_3 + 4a_4 + 5a_5 + 6a_6 = 0 \\
f^{''}(1) &= 2a_2 + 6a_3 + 12a_4 + 20a_5 + 30a_6 = 0 \\
f^{'''}(1) &= 6a_3 + 24a_4 + 60a_5 + 120a_6 = 0 \\
f^{''''}(1) &= 24a_4 + 120a_5 + 360a_6 = 0 \\
f^{''}(0) &= 2a_2 = -\frac{\delta^2}{\nu}\left(\frac{\partial u_e}{\partial x} + \frac{1}{u_e}\frac{\partial u_e}{\partial t}\right) = -\Lambda
\end{aligned}
$$

Resulting in the following coefficients.

$$
\begin{aligned}
a_1 &= \frac{1}{10}\Lambda + 3 \\
a_2 &= -\frac{1}{2}\Lambda \\
a_3 &= -10 + \Lambda \\
a_4 &= -\Lambda + 15 \\
a_5 &= \frac{1}{2}\Lambda - 9 \\
a_6 &= 2 - \frac{1}{10}\Lambda
\end{aligned}
$$

Again this order can be increased arbitrarily using the boundary conditions at the edge. However in focusing the requirements of the polynomial on the edge conditions the more important region near the wall is neglected. Therefore in the next section a boundary condition at the wall is added.

D.1.2 b

Adding a boundary condition for $f'''(0)$ and removing a boundary condition at the edge will result in a the following single parameter profile.

$$\begin{aligned}
f(\eta) &= a_1\eta + a_2\eta^2 + a_3\eta^3 + a_4\eta^4 + a_5\eta^5 + a_6\eta^6 \\
f(1) &= a_1 + a_2 + a_3 + a_4 + a_5 + a_6 = 1 \\
f^{'}(1) &= a_1 + 2a_2 + 3a_3 + 4a_4 + 5a_5 + 6a_6 = 0 \\
f^{''}(1) &= 2a_2 + 6a_3 + 12a_4 + 20a_5 + 30a_6 = 0 \\
f^{'''}(1) &= 6a_3 + 24a_4 + 60a_5 + 120a_6 = 0 \\
f^{''}(0) &= 2a_2 = -\Lambda \\
f^{'''}(0) &= a_3 = 0
\end{aligned}$$

Resulting in the following coefficients.

$$\begin{aligned}
a_1 &= \frac{1}{5}\Lambda + 2 \\
a_2 &= -\frac{1}{2}\Lambda \\
a_3 &= 0 \\
a_4 &= \Lambda - 5 \\
a_5 &= -\Lambda + 6 \\
a_6 &= -2 + \frac{3}{10}\Lambda
\end{aligned}$$

In literature $f^{'''}$ is taken as zero at the wall due to the assumption of incompressibility, it follows from the assumption of incompressibility that

$$\frac{\partial u}{\partial x} = -\frac{\partial v}{\partial y} \Rightarrow \left.\frac{\partial u}{\partial x}\right|_{y=0} = -\left.\frac{\partial v}{\partial y}\right|_{y=0} = 0,$$

Since the velocity gradient of v normal to the plate is not prescribed as zero and since such an assumption was not used for the derivation of the boundary layer equations or the integral boundary layer equations it effectively means that $\left.\frac{\partial v}{\partial y}\right|_{y=0} = 0$ is an added boundary condition resulting from the assumption of incompressibility. Using $f^{'''} = 0$ leads to a very instable approximate method, for Falkner-Skan flows with $m = 1, 2 \ldots 5$ there was no stable solution. Setting $f^{'''}$ to a positive value improved the results, in fact much better results were obtained using $f^{'''}(0) = \frac{1}{2}\Lambda$. Perhaps the prescription of a zero valued third derivative at the wall leads to oscillatory behaviour for higher orders of the polynomial, a non-zero boundary condition at the wall seemed to the oscillatory behaviour.

Re-assessing the boundary conditions

$$\times \frac{\partial^n}{\partial y^n}: \quad \left.\frac{\partial^{n+1}u}{\partial t \partial y^n}\right|_{y=0} + u\left.\frac{\partial^{n+1}u}{\partial x \partial y^n}\right|_{y=0} + v\left.\frac{\partial^n u}{\partial y^{n+1}}\right|_{y=0} = \left.\frac{\partial^n}{\partial y^n}\left(\frac{\partial u_e}{\partial t} + u_e\frac{\partial u_e}{\partial x}\right)\right|_{y=0} + \nu\left.\frac{\partial^{n+2}u}{\partial y^{n+2}}\right|_{y=0}, \quad n = 0 \ldots N$$

these $N+1$ equations will describe the following boundary conditions for $f(\eta)$

$$f^{n+2}(0), \quad n = 0 \dots N$$

In general the value for each term which is not differentiated with y explicitly is equal to the boundary value, also the external velocity terms are constant throughout the boundary layer in the direction normal to the wall, this means for the time derivative that

$$\frac{\partial^{n+1} u}{\partial t \partial y^n} \neq 0, \quad n = 1, \dots N. \tag{D.1}$$

If $\frac{\partial u}{\partial t}$ is not neglected the boundary conditions at the wall are given by

$$\begin{aligned}
f(0) &= 0 \\
f^{'}(0) &= \frac{u_e \delta}{2\nu} C_f \\
f^{''}(0) &= -\frac{1}{2}\Lambda \\
f^{'''}(0) &= \frac{3\delta^3}{u_e \nu^2} \left(C_f \frac{\partial u_e^2}{\partial t} + u_e^2 \frac{\partial C_f}{\partial t} \right)
\end{aligned}$$

D.2 Profile 2

If the time derivatives are incorporated in the boundary conditions an unsteady profile can be produced which is dependent on C_f and Λ.

D.2.1 a

First a profile is created with four conditions at the edge and two at the wall.

$$\begin{aligned}
f(\eta) &= a_1\eta + a_2\eta^2 + a_3\eta^3 + a_4\eta^4 + a_5\eta^5 + a_6\eta^6 \\
f(1) &= a_1 + a_2 + a_3 + a_4 + a_5 + a_6 = 1 \\
f^{'}(1) &= a_1 + 2a_2 + 3a_3 + 4a_4 + 5a_5 + 6a_6 = 0 \\
f^{''}(1) &= 2a_2 + 6a_3 + 12a_4 + 20a_5 + 30a_6 = 0 \\
f^{'''}(1) &= 6a_3 + 24a_4 + 60a_5 + 120a_6 = 0 \\
f^{'}(0) &= a_1 = \frac{u_e \delta}{2\nu} C_f \\
f^{''}(0) &= 2a_2 = -\Lambda
\end{aligned}$$

Resulting in the following coefficients.

$$\begin{aligned}
a_1 &= \frac{u_e \delta}{2\nu} C_f \\
a_2 &= -\frac{1}{2}\Lambda \\
a_3 &= 2\Lambda - 10\frac{u_e \delta}{2\nu} C_f + 20 \\
a_4 &= -3\Lambda + 20\frac{u_e \delta}{2\nu} C_f - 45 \\
a_5 &= -15\frac{u_e \delta}{2\nu} C_f + 2\Lambda + 36 \\
a_6 &= 4\frac{u_e \delta}{2\nu} C_f - \frac{1}{2}\Lambda - 10
\end{aligned}$$

D.2.2 b

Now a condition at the wall is added and a condition at the edge is removed.

$$
\begin{aligned}
f(\eta) &= a_1\eta + a_2\eta^2 + a_3\eta^3 + a_4\eta^4 + a_5\eta^5 + a_6\eta^6 \\
f(1) &= a_1 + a_2 + a_3 + a_4 + a_5 + a_6 = 1 \\
f^{'}(1) &= a_1 + 2a_2 + 3a_3 + 4a_4 + 5a_5 + 6a_6 = 0 \\
f^{''}(1) &= 2a_2 + 6a_3 + 12a_4 + 20a_5 + 30a_6 = 0 \\
f^{'}(0) &= a_1 = \frac{u_e\delta}{2\nu}C_f \\
f^{''}(0) &= 2a_2 = -\Lambda \\
f^{'''}(0) &= 6a_3 = \frac{3\delta^3}{u_e\nu^2}\left(C_f\frac{\partial u_e^2}{\partial t} + u_e^2\frac{\partial C_f}{\partial t}\right)
\end{aligned}
$$

Resulting in the following coefficients.

$$
\begin{aligned}
a_1 &= \frac{u_e\delta}{2\nu}C_f \\
a_2 &= -\frac{1}{2}\Lambda \\
a_3 &= \frac{\delta^3}{2u_e\nu^2}\left(C_f\frac{\partial u_e^2}{\partial t} + u_e^2\frac{\partial C_f}{\partial t}\right) \\
a_4 &= 3\Lambda - \frac{3\delta^3}{2u_e\nu^2}\left(C_f\frac{\partial u_e^2}{\partial t} + u_e^2\frac{\partial C_f}{\partial t}\right) - 10\frac{u_e\delta}{2\nu}C_f + 15 \\
a_5 &= 15\frac{u_e\delta}{2\nu}C_f - 4\Lambda + \frac{3\delta^3}{2u_e\nu^2}\left(C_f\frac{\partial u_e^2}{\partial t} + u_e^2\frac{\partial C_f}{\partial t}\right) - 24 \\
a_6 &= -6\frac{u_e\delta}{2\nu}C_f + \frac{3}{2}\Lambda - \frac{\delta^3}{2u_e\nu^2}\left(C_f\frac{\partial u_e^2}{\partial t} + u_e^2\frac{\partial C_f}{\partial t}\right) + 10
\end{aligned}
$$

These 2-parameter profiles can only be solved if an extra equation is used, i.e. the energy integral equation or the moment-of-moment equation. Again the order of the polynomial can be increased arbitrarily using more or less boundary conditions at the edge.

Appendix E

Closure Relations

E.1 Laminar Boundary Layer Flow

$$
\begin{aligned}
\text{Wieghardt:}\quad \frac{u}{u_e} &= f_1(\eta) + a f_2(\eta) + b f_3(\eta),\\
f_1 &= 1-(1-\eta)^8(1+8\eta+36\eta^2+120\eta^3),\\
f_2 &= (1-\eta)^8\eta(1+8\eta+36\eta^2),\\
f_3 &= -(1-\eta)^8\eta^2(1+8\eta),\\
a &= \frac{\tau_w\delta}{\mu u_e}, \quad b = \frac{1}{2}\Lambda.
\end{aligned}
\tag{E.1}
$$

$$
\begin{aligned}
\text{Timman:}\quad \frac{u}{u_e} &= 1-\int_\eta^\infty e^{-\eta^2}\left(a+c\eta^2\right)d\eta - e^{-\eta^2}\left(b+d\eta^2\right),\\
a &= \frac{4}{3\sqrt{\pi}}(1-b),\\
c &= \frac{4}{3\sqrt{\pi}}(1-b),\\
b &= \begin{cases} -\Lambda, & \frac{\theta^2}{\nu}\frac{du_e}{dx} < 0,\\ -\frac{1}{2}\Lambda, & \frac{\theta^2}{\nu}\frac{du_e}{dx} \geq 0. \end{cases}\\
d &= \begin{cases} -\frac{1}{2}\Lambda, & \frac{\theta^2}{\nu}\frac{du_e}{dx} < 0,\\ 0, & \frac{\theta^2}{\nu}\frac{du_e}{dx} \geq 0. \end{cases}
\end{aligned}
\tag{E.2}
$$

$$
\begin{aligned}
\text{Cooke:}\quad \frac{u}{u_e} &= f+\zeta g,\\
f &= 1-\frac{2}{3\sqrt{\pi}}\eta e^{-\eta^2} - 2\frac{2}{\sqrt{\pi}}\int_\eta^\infty e^{-\eta^2}d\eta,\\
g &= \frac{1}{2}\left(1-e^{-\eta^2}-f\right),\\
\zeta &= \left(\frac{1}{0.293}\right)\frac{\theta^2}{\nu}.
\end{aligned}
\tag{E.3}
$$

$$
\begin{aligned}
\text{Mughal:}\quad \frac{u}{u_e} &= 1-(1-\eta)^\zeta\left(1+a_1\eta+a_2\eta^2\right)\\
a_1 = \frac{2}{3}(\zeta-1)+\frac{\Lambda}{\zeta+1}, &\quad a_2 = \frac{\zeta(\zeta-1)}{6}(\zeta-1)+\frac{\Lambda}{2}, \quad \zeta = -\frac{7}{40}\Lambda+5
\end{aligned}
\tag{E.4}
$$

$$C_D = \frac{H^*}{Re_\theta}\begin{cases} 0.207 + 0.00205\,(4-H)^{5.5}, & H < 4, \\ 0.207 - 0.003\,(H-4)^2, & H > 4, \end{cases} \tag{E.5}$$

where

$$H^* = \begin{cases} 1.515 + 0.076\frac{(H-4)^2}{H}, & H < 4, \\ 1.515 + 0.040\frac{(H-4)^2}{H}, & H > 4. \end{cases} \tag{E.6}$$

$$\text{Lyrio et al:} \quad C_f = 2\,\frac{(1.91 - 4.13\Lambda)}{Re_{\delta^*}}, \tag{E.7}$$

with

$$\lambda = \frac{\theta^2}{\nu}\left(\frac{\partial u_e}{\partial x} + \frac{1}{u_e}\frac{\partial u_e}{\partial t}\right), \quad \Lambda = 0.325 - 0.13\lambda H^2, \quad H = \frac{1}{0.68 - 0.922\Lambda}. \tag{E.8}$$

$$\text{Sekar:} \quad C_f = \begin{cases} \frac{1}{Re_\theta}\left[0.0727\frac{(5.5-H)^3}{H-1} - 0.07\right] & H < 5.4 \\ \frac{2}{Re_\theta}\left[-0.067 + 0.01977\frac{(7.4-H)^2}{H-1}\right] & 7.4 > H > 5.4 \\ \frac{2}{Re_\theta}\left[-0.067 + 0.022\left(1 - \frac{1.4}{H-6}\right)^2\right] & H > 7.4 \end{cases}. \tag{E.9}$$

E.2 Laminar to Turbulent Transition

$$\text{Granville:} \quad Re_{\theta,tr} \geq 375 + e^{6.1+55\overline{\lambda}_\theta} + Re_{\theta,crit}, \quad -0.04 \leq \overline{\lambda}_\theta \leq 0.024, \tag{E.10}$$

$$\begin{aligned} \text{Arnal et al:} \quad Re_{\theta,tr} &= R_{\theta,crit} - 206e^{25.7\overline{\lambda}_\theta}\left[\ln(16.8Tu) - 2.77\overline{\lambda}_\theta\right], \\ \text{turbulence intensity:} \quad Tu &= \frac{\sqrt{\frac{1}{2}\left(\overline{u'^2} + \overline{v'^2}\right)}}{u_e}. \end{aligned} \tag{E.11}$$

where

$$Re_{\theta_{crit}} = \begin{cases} \frac{54.2124}{H(H-2.48)} + \frac{31.6}{H} & H > 2.591 \\ \frac{520}{H} + \frac{2.5\exp 6}{H}\left(\frac{1}{H} - \frac{1}{2.591}\right)^{1.95} & H \leq 2.591 \end{cases}, \tag{E.12}$$

here $\overline{\lambda_\theta}$ is the mean Thwaites parameter

$$\overline{\lambda_\theta} = \frac{1}{x - x_{cr}}\int_{x_{cr}}^{x} \frac{\theta^2}{\nu}\frac{du_e}{dx}dx. \tag{E.13}$$

$$\text{Abbu-Ghannam/Shaw:} \quad Re_{\theta,crit} = 155 + 89(n_{crit})^{5/4}\left[1 + \frac{1}{4}\tanh\left(\frac{10}{H-1} - 5.5\right)\right], \tag{E.14}$$

with e.g.

$$\text{Mack:} \quad n_{crit} = -8.43 - 2.4\ln[0.027\tanh(Tu/2.7)]. \tag{E.15}$$

$$\text{Henkes and Van Ingen:} \quad \begin{cases} n_{crit} = 2.13 - 6.18\log^{10}(Tu) \\ n_{trans} = 5 - 6.18\log^{10}(Tu) \end{cases}. \tag{E.16}$$

$$\text{Anderson et al:} \quad n_{tr} = -8.43 - 2.4\ln(Tu), \quad 0.1\% < Tu < 2\%, \tag{E.17}$$

$$\text{Coenen:} \quad Re_{\theta_{crit}} = \exp\left(\frac{52}{H} - 14.8\right). \tag{E.18}$$

$$\text{Bongers[14]:} \quad Re_{\theta_{crit}} = \exp\left(26.3 - 8H\right), \quad 2.2 < H < 3. \tag{E.19}$$

$$\text{Wazzan et al:} \quad \log_{10}(Re_{x,tr}) \approx -40.4557 + 64.8066H - 26.7538H^2 + 3.3819H^3, \quad 2.1 < H < 2.8, \tag{E.20}$$

$$\text{Drela[35]:} \quad \log_{10}\left(Re_{\theta,crit}\right) = \left(\frac{1.415}{H-1} - 0.489\right)\tanh\left(\frac{20}{H-1} - 12.9\right) + \frac{3.295}{H-1} + 0.44,] \tag{E.21}$$

$$\text{Drela and Giles:} \quad \log_{10}\left(Re_{\theta,crit}\right) = 0.7\tanh\left(\frac{14}{H-1} - 9.24\right) + 2.492\left(\frac{1}{H-1}\right)^{0.43} + 0.62, \tag{E.22}$$

$$\text{Abu et al[47]:} \quad Re_{\theta,crit} = 163 + 74.3[0.94n_{crit} + 1]\left[0.55\tanh\left(\frac{10}{H-1} - 5.5\right) + 1\right], \tag{E.23}$$

$$\text{Abu et al[78]:} \quad Re_{\theta,crit} = 163 + \exp\left(f - \frac{f}{6.91}Tu\right) \tag{E.24}$$

$$f = \begin{cases} 6.91 + 12.75\lambda_\theta + 63.64\lambda_\theta^2, & \lambda_\theta < 0 \\ 6.91 + 2.48\lambda_\theta - 12.28\lambda_\theta^2, & \lambda_\theta \geq 0 \end{cases} \qquad \lambda_\theta = \frac{\theta^2}{\nu}\frac{\partial u_e}{\partial x}.$$

E.3 Turbulent Boundary Layer Flow

$$1/7^{th} \text{ power law:} \quad \delta^* = \frac{1}{8}\frac{0.16x}{\sqrt[7]{Re_x}}, \quad \theta = \frac{7}{72}\frac{0.16x}{\sqrt[7]{Re_x}}, \quad H = \frac{9}{7}. \tag{E.25}$$

$$\text{Spalding:} \quad y^+ = u^+ + e^{-\kappa\, c}\left(e^{\kappa u^+} - 1 - \kappa u^+ - \frac{(\kappa u^+)^2}{2} - \frac{(\kappa u^+)^3}{6}\right). \tag{E.26}$$

$$\text{Swafford:} \quad u = \frac{u_e\, s}{u_e^+ 0.09}\arctan\left(0.09y^+\right) + \frac{u_e}{u_e^+}\left(u_e^+ - \frac{s\pi}{0.18}\right)\sqrt{\tanh\left[a\left(\frac{y}{\theta}\right)^b\right]}, \tag{E.27}$$

where

$$
\begin{aligned}
C_f &= \frac{0.3e^{-1.33H}}{(\log_{10} Re_\theta)^{1.74+0.31H}} + 0.00011\left[tanh\left(4-\frac{H}{0.875}\right)-1\right] \\
u_e^+ &= \sqrt{\frac{2}{|C_f|}} \\
s &= \frac{c_f}{|c_f|} \\
\frac{u}{u_e}(2) &= \frac{1}{1.95}\left[\tanh^{-1}\left(\frac{8.5-H}{7.5}\right)-0.364\right] \\
\frac{u}{u_e}(5) &= 0.155 + 0.795\mathbf{sech}[0.51(H-1.95)] \\
g(2) &= \frac{\left[\frac{u}{u_e}(2) - \frac{2}{0.09u_e^+}\tan^{-1}\left(\frac{0.18Re_\theta}{u_e^+}\right)\right]}{1-\frac{s\pi}{0.18u_e^+}} \\
g(5) &= \frac{\left[\frac{u}{u_e}(5) - \frac{2}{0.09u_e^+}\tan^{-1}\left(\frac{0.45Re_\theta}{u_e^+}\right)\right]}{1-\frac{s\pi}{0.18u_e^+}} \\
b &= \frac{\ln\left(\frac{\tanh(g^2(5))}{\tanh(g^2(2))}\right)}{\ln\frac{2}{5}} \\
a &= \frac{1}{2^b\tanh\left(g^2(2)\right)}
\end{aligned}
$$

$$
\text{Cross:}\quad \begin{cases} u = \frac{u_e u_\tau \cos(\beta_w)}{\kappa}\left(\frac{1}{2}\ln\left(Re_\delta u_\tau \eta\right)^2\right) + q_e B\left(\sin\left(\frac{\pi}{2}\eta\right)\right)^\chi \\ u_c = \frac{u_e u_\tau \sin(\beta_w)}{\kappa}\left(\frac{1}{2}\ln\left(Re_\delta u_\tau \eta\right)^2\right) + q_e B_c\left(\sin\left(\frac{\pi}{2}\eta\right)\right)^{\chi_c} \end{cases}, \tag{E.28}
$$

where

$$
B = 1 - \frac{u_\tau cos(\beta_w)}{\kappa}\left[\frac{1}{2}\ln\left(Re_\delta u_\tau\right)^2 + A\right], \quad B_s \quad = -\frac{u_\tau sin(\beta_w)}{\kappa}\left[\frac{1}{2}\ln\left(Re_\delta u_\tau\right)^2 + A\right],
$$

A is the law of the wall constant which is 5.0 for a smooth wall and 8.0 for a fully rough wall (see Schlichting[118, p.523]). The cross flow exponents χ and χ_c are not given by Cross, he does suggest that χ and χ_c are correlations of $\chi, \beta_w, atan\left(\frac{B_c}{B}\right)$ where χ is the wake exponent.

$$
\text{White:}\quad f(\eta) \approx \sin\left(\frac{\pi}{2}\eta\right)^2, \quad f(\eta) \approx 3\eta^2 - 2\eta^3. \tag{E.29}
$$

$$
\text{Granville:}\quad u^+ = \frac{1}{\kappa}\ln y^+ + c + \frac{1}{\kappa}\left[\Pi(1 - cos\pi\eta + (\eta^2 - \eta^3))\right], \quad y^+ \geq 30. \tag{E.30}
$$

$$
\text{Thompson:}\quad u^+ = \begin{cases} y^+, & y^+ \leq 4, \\ 1.0828 - 0.414\ln y^+ + 2.2661\left(\ln y^+\right)^2 - 0.324\left(\ln y^+\right)^3, & 4 < y^+ < 30. \end{cases} \tag{E.31}
$$

$$
\text{White:}\quad \beta = -0.4 + 0.76\Pi + 0.42\Pi^2 \tag{E.32}
$$

$$
\begin{aligned}
\text{White:}\quad \beta &= -\lambda^2 H\frac{\theta}{u_e}\frac{du_e}{dx}, \\
\lambda &= \frac{2 + 3.179\Pi + 1.5\Pi^2}{\kappa(1+\Pi)}\frac{H}{H-1},
\end{aligned} \tag{E.33}
$$

$$\frac{\overline{u}}{u_e} \approx 1 - \zeta + 0.4\zeta^{\frac{3}{2}}\sqrt{\left(\frac{y}{\delta^*}\right)} + 0.6\zeta \sin\left(\frac{\pi}{2}\zeta\frac{y}{2.86\delta^*}\right), \quad \zeta = \frac{u_s}{u_e}, \tag{E.34}$$

where u_s is defined as a characteristic velocity scale

Ludwieg and Tillman: $$C_f = 0.246\, 10^{-0.678H}\left(\frac{u_e\theta}{\nu}\right)^{-0.268}. \tag{E.35}$$

White, adverse pressure gradient: $$C_f = \frac{0.3e^{-1.33H}}{(\log_{10} Re_\theta)^{1.74+0.31H}} \tag{E.36}$$

White, flat plate flow: $$C_f = \left(\frac{0.027}{Re_x^{\frac{1}{7}}}\right). \tag{E.37}$$

Green, adverse pressure gradient:: $$C_f = C_{f_0}\left(\frac{0.9}{0.4\frac{H}{H_0}} - 0.5\right), \tag{E.38}$$

where C_{f_0} is the friction coefficient for zero pressure gradient, this is taken as

Green 1972 $$C_{f_0} = \frac{0.012}{\log_{10} Re_\theta - 0.64} - 0.00093,$$

Green et al 1977 $$C_{f_0} = \frac{0.01013}{\log_{10} Re_\theta - 1.02} - 0.00075,$$

and

Green 1972 $$H_0 = \frac{1}{1 - 6.8\sqrt{\frac{C_{f0}}{2}}},$$

Green et al 1978 $$H_0 = \frac{1}{1 - 6.55\sqrt{\frac{C_{f0}}{2}}}.$$

Ferziger et al: $$C_f = 0.1017\,|1 - 2\zeta|^{1.732}\left(\frac{\zeta}{H\, Re_\theta}\right)^{0.268} sign(1 - 2\zeta), \tag{E.39}$$

where the so-called blockage factor ζ is given by

$$\zeta = \frac{\delta^*}{\delta},$$

this expression for C_f is used in conjunction with the following expression which is derived from Coles wall-wake law

$$\frac{H-1}{H} \approx 1.5\zeta + 0.309\sqrt{C_f} + 0.955\frac{C_f}{\zeta}.$$

Du and Selig: $$C_f = 0.172 Re_\theta^{-0.268} 10^{-0.678H}\left(1 + B_1\sqrt{\tan\left(\beta_w\frac{x - x_{trans}}{c}\right)}\right), \quad B_1 = 0.52. \tag{E.40}$$

where β_w is the crossflow angle.

$$C_f = \frac{0.3e^{-1.33H}}{(\log_{10} Re_\theta)^{1.74+0.31H}} + 0.00011\left[\tanh(A) - 1\right], \tag{E.41}$$

where Sekar[120] uses

$$A = \begin{cases} 4 - \frac{H}{0.875} & H > 5.25 \\ 104 - \frac{H}{0.875} & H \leq 5.25 \end{cases},$$

Sekar also replaces the logarithm by the value 3 for a momentum thickness Reynolds number lower than 20.

$$\begin{aligned} \text{Cousteix and Houdeville:} G &= \frac{H-1}{H}\sqrt{\frac{2}{C_f}}, \\ D &= 2G - 4.25\sqrt{G} + 2.12, \\ C_f &= \frac{2}{\left(\frac{1}{\kappa}\ln\left(Re_{\delta^*}\right) + D\right)^2}. \end{aligned} \tag{E.42}$$

$$\text{Mughal:} \quad C_D = 2\left(0.009 - 0.011\exp\left(-0.15H^{2.1}\right) + 0.00003\exp\left(0.117H^2\right) + aRe_\theta^{-0.574}\right), \tag{E.43}$$

where

$$a = \begin{cases} 0.438 - 0.280H, & H \leq 3.5, \\ 0.160\left(H - 3.5\right) - 0.55, & H > 3.5. \end{cases}$$

$$\text{Drela:} \quad C_D = H^*\left[\frac{C_f}{2}\left(\frac{4}{H} - 1\right)\frac{1}{3} + 0.03\left(\frac{H-1}{H}\right)^3\right], \tag{E.44}$$

where

$$H^* = \begin{cases} 1.505 + \frac{4}{Re_\theta} + \left(0.165 - \frac{1.6}{\sqrt{Re_\theta}}\right)\frac{(H_0 - H)^{1.6}}{H}, & H < H_0, \\ 1.505 + \frac{4}{Re_\theta} + (H - H_0)^2\left(\frac{0.04}{H} + 0.007\frac{\ln Re_\theta}{\left(H - H_0 + \frac{4}{\ln Re_\theta}\right)^2}\right), & H > H_0, \end{cases} \tag{E.45}$$

with

$$H_0 = 3 + \frac{400}{Re_\theta}, \quad H_0 = \min(H_0, 4).$$

$$\text{Drela:} \quad C_D = H^*\left[\frac{C_f}{2}\left(\frac{4}{H} - 1\right)\frac{1}{3} + \frac{2}{H^*}C_\tau(1 - u_s)\right], \tag{E.46}$$

where

$$u_s = \frac{H^*}{6}\left(\frac{4}{H} - 1\right).$$

E.3.1 Unsteady Entrainment and Shear Stress Lag

$$\begin{aligned} \text{Head:} \quad F(H_1) &= 0.0306(H_1 - 3)^{-0.6169}, \\ H_1 &= \begin{cases} 0.8234(H - 1.1)^{-1.287} + 3.3, & H < 1.6 \\ 1.5501(H - 0.6778)^{-3.064} + 3.3, & H \geq 1.6 \end{cases}. \end{aligned} \tag{E.47}$$

$$\text{Coenen:} \quad H_1 = \begin{cases} 2 + 1.5\left(\frac{1.12}{H-1}\right)^{1.093} + 0.5\left(\frac{H-1}{1.12}\right)^{1.093}, & H < 4. \\ 4 + \frac{1}{3}(H - 4), & H \geq 4, \end{cases}, \tag{E.48}$$

$$\text{Coenen:}\quad H_1 = \begin{cases} \frac{(0.5H+1)H}{H-1}, & H < 2.732, \\ \frac{(0.5G+1)G}{G-1}, & G \le 4 \quad \& \quad H \ge 2.732, \\ 1.75 + \frac{5.2273G}{G+5.818181}, & G > 4 \quad \& \quad H \ge 2.732. \end{cases} \quad , \tag{E.49}$$
$$G = 0.5(H - 2.732) + 2.732.$$

Drela:

$$\begin{aligned} C_{\tau,eq} &= \frac{0.015H^*(H-1)^3}{(1-U_s)H^3}, \\ \frac{u_s}{u_e} = U_s &= 0.5H^*\left(1 - \frac{H-1}{0.75H}\right), \\ \delta &= \theta\left(3.15 + \frac{1.72}{H-1} - 0.01\,(H-1)^2\right) + \delta^* \end{aligned} \tag{E.50}$$

where the energy shape factor H^* is defined by

$$H^* = \frac{\delta^k}{\theta},$$

,

$$\text{Nishida:}\quad \sqrt{C_\tau}_{init} = 1.8\exp\left(\frac{-3.3}{H-1}\right)\sqrt{C_{\tau,eq}} \tag{E.51}$$

Cebeci and Cousteix:

$$\begin{aligned} \text{flat plate friction:}\quad C_{f0} &= \frac{0.01013}{\log Re_\theta - 1.02} - 0.00075, \\ \text{equilibrium entrainment:}\quad F_{eq} &= H_1\left[\frac{C_f}{2} - (H+1)\left(\frac{\theta}{u_e}\frac{du_e}{dx}\right)_{eq}\right], \\ \text{shear stress coefficient:}\quad \sqrt{C_\tau} &= \sqrt{-0.32C_{f0} + 0.024F + 1.2F^2}, \\ \text{equilibrium shear stress coefficient:}\quad \sqrt{C_{\tau,eq}} &= \sqrt{0.32C_{f0} + 0.024F_{eq} + 1.2F_{eq}^2}, \\ \left(\frac{\theta}{u_e}\frac{du_e}{dx}\right)_{eq} &= \frac{1.25}{H}\left[\frac{C_f}{2} - \left(\frac{H-1}{6.432H}\right)^2\right], \\ \left(\frac{\delta}{u_e}\frac{du_e}{dx}\right)_{eq} &= (H_1 + H)\left(\frac{\theta}{u_e}\frac{du_e}{dx}\right)_{eq}. \end{aligned} \tag{E.52}$$

Green et al:

$$\begin{aligned} C_f &= C_{f_0}\left(\frac{0.9}{0.4\frac{H}{H_0}} - 0.5\right), \\ H_0 &= \frac{1}{1 - 6.55\sqrt{\frac{C_{f_0}}{2}}}, \\ H_1 &= 3.15 + \frac{1.72}{H-1} - 0.01(H-1)^2. \end{aligned} \tag{E.53}$$

Appendix F

Blasius correlation

First the boundary conditions are related through

$$\frac{f^{''}(0)}{f^{'}(\infty)} = B, \tag{F.1}$$

where B is the value of $f^{''}(0)$ for which $f^{'}(\infty) = 1$.
Note that a boundary condition can be rewritten

$$f^{'}(\infty) = 1 \quad \rightarrow \quad \left[f^{'}(\infty)\right]^{n} = 1$$

Then note that if $f_0(\eta)$ fulfills the Blasius equation this also holds for $af_0(a\eta)$. The boundary conditions are fulfilled if

$$a^3 f_0^{''}(0) = B, \quad a^2 f_0^{'}(\infty) = 1$$

or

$$a^3 f_0^{''}(0) = B, \quad \left[a^2 f_0^{'}(\infty)\right]^{n} = 1$$

Again relating the boundary conditions and equating with equation (F.1) for f_0:

$$\frac{f_0^{''}(0)}{f_0^{'}(\infty)} = a^{3-2n}\frac{f_0^{''}(0)}{f_0^{'}(\infty)}$$
$$a^{3-2n} = 1 \rightarrow n = \frac{3}{2}$$

Given a first iteration through integration, the final value for B is obtained with

$$f^{''}(0) = \left(\frac{f^{''}(0)}{\left[f^{'}(\infty)\right]^{\frac{3}{2}}}\right)_{iter}$$

Appendix G

Profile Comparison for Falkner-Skan flows

In the following tables m is the power of the power-law velocity distribution, the errors are considered for the end of the plate, the number of steps was set to 500.

	m	$\epsilon_\delta(\%)$			$\epsilon_{\delta*}(\%)$			$\epsilon_\theta(\%)$			$\epsilon_{C_f}(\%)$		
Method	...	Ti	Dr	P4	Ti	Dr	P4	Ti	Dr	P4	Ti	Dr	P4
	-0.09043	n/a	n/a	-16.8	n/a	11.3	16.6	n/a	-10.7	-15	n/a	n/a	n/a
	0.25	48.3	n/a	-14.1	0.61	0.43	0.33	20.8	0.53	1.8	13.7	1.0	1.5
	1	52.2	n/a	-11.9	2.1	-0.35	1.2	21.2	-0.45	4.0	11.6	0.13	3.0
	3	53.3	n/a	-14.4	2.5	-0.30	1.5	20.8	-0.26	4.4	10.7	0.03	3.2
	5	53.5	n/a	-16.2	2.6	-0.02	1.6	20.7	-0.14	4.5	10.3	-0.06	3.2

Table G.1: Ti:Timman, Pn:Pohlhausen of n^{th} order, Dr: two parameters with Drela closure, An:Alternative of n^{th} order, Wi: Wieghardt profile

	m	$\epsilon_\delta(\%)$		$\epsilon_{\delta*}(\%)$		$\epsilon_\theta(\%)$		$\epsilon_{C_f}(\%)$	
Method	...	A4	Wi	A4	Wi	A4	Wi	A4	Wi
	-0.09043	12.5	-56.6	8.3	-8.3	5.2	-4.8	n/a	n/a
	0.25	-13.5	-131.8	1.4	-4.8	3.0	-12.4	0.78	-8.1
	1	n/a	-109.4	n/a	-6.5	n/a	-15.5	n/a	-10.2
	3	n/a	-99.3	n/a	-7.1	n/a	-16.3	n/a	-10.7
	5	n/a	-97.2	n/a	-7.1	n/a	-16.4	n/a	-10.9

Table G.2: Ti:Timman, Pn:Pohlhausen of n^{th} order, Dr: two parameters with Drela closure, An:Alternative of n^{th} order, Wi: Wieghardt profile

	m	$\epsilon_\delta(\%)$			$\epsilon_{\delta*}(\%)$			$\epsilon_\theta(\%)$			$\epsilon_{C_f}(\%)$		
Method	...	Tw	P6	A6	Tw	P6	A6	Tw	P6	A6	Tw	P6	A6
	-0.09043	n/a	-63.3	-16.9	19.0	20.6	18.1	-3.8	-22.9	-5.6	n/a	n/a	n/a
	0.25	n/a	-56.0	-28.7	-1.8	-0.45	0.24	2.0	-2.1	0.91	1.62	-1.17	0.89
	1	n/a	-46.1	n/a	-0.02	0.7	n/a	5.0	1.7	n/a	2.8	1.7	n/a
	3	n/a	-43.0	n/a	0.21	1.2	n/a	5.5	3.0	n/a	3.1	2.4	n/a
	5	n/a	-42.1	n/a	0.4	1.4	n/a	5.3	3.4	n/a	2.8	2.5	n/a

Table G.3: Pn:Pohlhausen of n^{th} order,An:Alternative of n^{th} order,Tw: Thwaites

	m	$\epsilon_\delta(\%)$		$\epsilon_{\delta*}(\%)$		$\epsilon_\theta(\%)$		$\epsilon_{C_f}(\%)$	
Method	...	P9	A9	P9	A9	P9	A9	P9	A9
	-0.09043	-134.3	-65.9	20.4	20.9	-28.40	-12.0	n/a	n/a
	0.25	-121.2	-76.2	-1.2	-0.01	-5.5	-1.1	-3.5	-0.43
	1	-104.3	n/a	0.01	n/a	-0.89	n/a	0.11	n/a
	3	-98.3	n/a	0.6	n/a	0.71	n/a	1.04	n/a
	5	-97.2	n/a	0.8	n/a	1.13	n/a	1.21	n/a

Table G.4: Pn:Pohlhausen of n^{th} order,An:Alternative of n^{th} order,Tw: Thwaites

	m	$\epsilon_\delta(\%)$		$\epsilon_{\delta^*}(\%)$		$\epsilon_\theta(\%)$		$\epsilon_{C_f}(\%)$	
Method	...	Ti	A4	Ti	A4	Ti	A4	Ti	A4
	-0.09043	n/a	3.5	n/a	14.8	n/a	-8.2	n/a	n/a
	0.25	57.6	-28.7	1.1	0.24	5.6	0.91	4.9	0.89
	1	61.3	31.3	2.1	5.0	8.4	18.0	5.5	11.6
	3	62.6	34.1	2.4	5.7	9.1	19.3	5.6	11.9
	5	62.8	34.7	2.5	5.9	9.3	19.7	5.5	11.9

Table G.5: Altered profiles,Ti:Timman($\eta = 2\eta_{original}$), An:Alternative profile($f'''(0) = \frac{1}{2}\Lambda$)

	m	$\epsilon_\delta(\%)$		$\epsilon_{\delta^*}(\%)$		$\epsilon_\theta(\%)$		$\epsilon_{C_f}(\%)$	
Method	...	A6	A9	A6	A9	A6	A9	A6	A9
	-0.09043	-23.0	-70.4	18.4	20.8	-10.6	-14.4	n/a	n/a
	0.25	-121.2	-76.2	-1.2	-0.01	-5.5	-1.1	-3.5	-0.43
	1	-8.0	-59.8	2.4	1.3	7.9	3.5	5.5	2.9
	3	-6.2	-58.6	2.8	1.6	8.6	4.1	5.7	3.1
	5	-5.9	-58.7	2.9	1.7	8.7	4.3	5.7	3.1

Table G.6: Altered profiles,Ti:Timman($\eta = 2\eta_{original}$), An:Alternative profile($f'''(0) = \frac{1}{2}\Lambda$)

Appendix H

Parameter File

```
cDebug=0                  ! Debug mode
!
! Run parameters, grid
!
cDeltaX0=0.005d0          ! (initial) distance step
cDeltaT0=0.005d0          ! (initial) time step, timestep shall never be larger than this value
cZeroRange=1.d-14         ! margin for zero value
cT0=0.d0                  ! starting time
cX0=0.d0                  ! starting distance
cPlateLength=1.0d0        ! 0.75 for high frequency, 1.6 for low frequency
cBCValue=4                ! BC-left,1: Nishida, 2: Milewski, 3: Coenen(turb), 4: Thwaites, 5: flat
plate(1/7th power law or Blasius/Rayleigh)
cInitValue=1              ! Init: 1: Rayleigh solution, 2: Use value equal to boundary value
cRightBC=0                ! 0 = no BC, 1 = Neumann BC (for flat plate)
cInitM1=8                 ! number of steps using Thwaites to determine the initial value for theta
cMaxTimeSteps=40000       ! max number of time steps
cMaxDistanceSteps=100000  ! max number of distance steps
cGridGenInterval=20       ! Grid Generation interval in number of time steps
cGapDx=0.01               ! if adaptive grid refinement, this step is used to fill the gap at the end
cVariableTimeStep=0       ! will fix the distance step and base the timestep on the largest maximum
eigenvalue
cVariableDistanceStep=0    ! variable distance step,will create non-uniform grid for the left bc
cSpline=1                  ! Cubic spline, use to interpolate velocity
cRefPerc=0.10d0            ! max. region which is refined, is between [0,1]
cDxFactor=10.d0            ! if variable distance step,will divide cDeltaX0 by this number as initial
step
cDxGrowth=1.085d0          ! successive growth for each next distance step
!
! Run parameters, solution
!
cConvergenceCriterium=10.d-15   ! Convergence Criterium for the RMS
cCFL=0.25                       ! CFL number, stability requirement
cUpWrun=0                       ! this number determines how many initial points are based on upw1ind
 differencing,min. 1 for 4th central, set to 0 for Roe/Steger Warming!
cLamPerc=0.0d0                  ! max. quasi-laminar region from left boundary compared to platelength, is
between [0,1], intermittency will increase linearly
cUinf=1.5d0                     ! 150.d0  !1.4717 !21.9 !16.8    ! outside velocity  (25 m/s for flat plat
cNu=1.5d-5                      !1.4717d-5    !1.4717d-5  ! 1.5e-5 ! kinematic viscosity
cRho=1.                         ! 1.2 density
cTu=0.00                        ! turbulence intensity
cFrequency=50.d0                ! frequency for oscillation test cases
```

```
cTurbInit=0                    ! Turbulent boundary layer from the get-go
cTransitionCheck=              ! Do transition check
cTransitionInterval=25         ! interval count(in time level) for transition check
cEquilibrium=1                 !  equilibrium turb. boundary layer
cSeparationCheck=0             ! check for separation or not
cSeparationInterval=15         ! interval count(in time level) for separavarition check
cPreSetIntermittency=0.00d0    ! set intermittency over entire plate, set to zero for laminar !!!
cUseIntMitt=4                  ! use intermittency factor, 0:none, 1:linear pre, 2:linear post,
3: exp pre, 4: exp post, 5: poly pre, 6:poly post, 7 : Drela post
cIntMittShape=10.d0            ! shape value for intermittency function
cInterInsertIntoSolution=0     ! 0: insert averaged variables into K/L, 1: average K/L
cBCSmoothing=0                 ! Smooth BC using internal value,1: 1 internal value,....3:
cSmoothing=0                   ! nr. of smoothed internal values starting from left boundary
cKc=5.6d0                      ! 4.2 or 5.6, constant for lag entrainment
csepIndicatorMax=1.            ! value for separation indicator
cNmax=8.9                      ! Maximum value amplification factor
cNref=9.1                     ! Value of amplification factor at which transition is assumed complete
cUseMatsushitaClosure=0        ! Use Matsushita closure for laminar flow
cSepStrong=1                   ! for strong separation,H/theta is expected to flip
!
! output parameters
!
cPrintTimeStep=.5              ! min time step with which the results are printed
cRunTime=4.5                   ! Maximum solution time, 0.41935 for high frequency, 0.6842   for low
 frequency
cPrintAll=0                    ! print all timesteps
cPrintToEps=1                  ! Save plots as .eps
cShowPlots=1                   ! show plots
cShowLambdaPlots=0             ! show plots with eigenvalues,sep. indicator,
cShowRefPlot=1                 ! 0 = none, 1 = flat plate, 2 = cylinder
cAlphaElliptic=0.25            ! times pi for the angle of attack of the elliptic cylinder
cMessageInterval=200           ! every xx steps print runtime time
!
! Numerical scheme
!
cDifference=9                !  1,2 = first/second order upwind differencing/ 3,4 = second/fourth order
  ! central /5 = Lax-Wendroff(one step) /  6 3rd upw /7 QUICK differencing/ 8,9
  ! = Roe/Steger-Warming  Note that 2nd Order central +
  ! smoothing is equiv. to Lax-Friedrich/ 10 = StegerWarming 2nd order / 11
  ! StegerWarming 3rd order / 12 = MacCormack / 13=Kurganov-Tadmor
cFluxLimiter=0               ! Flux limiter for Roe, only if flux limiter is used
cMuscl=0                     ! use MUSCL for higher order  Roe
cFluxLimiterRegion=0         ! 0 : over entire profile, 1 : over transition region
cEntropyFix=0                ! use entropy scheme for Roe
cEntropyFixValue=1.0d-1      ! value when eigenvalue is considered to small and entropyfix is used
cRKorder=1                   ! order of Runge-Kutta time integration, 1..
```

Extra input parameters for the DG algorithm

```
cUseFormulation=0            ! 0 = Gaussian int. order greater than 0,
 1 = Expansion in Basis functions, order=0
cUseBasisFunction=0          ! 0 = unweighted monomials, 1 = weighted monomials
cInitPolOrder=1              ! Initial polynomial order for the basis functions, also determines Gauss nod
cVaryingPolyOrder=0          ! p-refinement
cGaussPolyCreate=128         ! Create table with Gaussian nodes/weights
cSSP=0                       ! 0=LSRK(Blom,Ozdemir),1= use SSPRK, 2=LSRK(Kennedy), 3= LSRK3SSP(Ketcheson)
cUseHigherOrderFlux=0        ! 0= only centered values used for the flux,1= all coefficients are used
cTheta=1.d0                  ! parameter to determine the weight of the characteristic flux, see phd van
Ozdemir and thesis of Bram van Es
```

Appendix I

Test Cases

I.1 Steady Methods

I.1.1 Von Kármán Equation and Pohlhausen Velocity Profile

First consider the steady Von Kármán equation

$$\frac{d\theta}{dx} + \frac{\theta}{u_e}(2+H)\frac{du_e}{dx} = \frac{1}{2}C_f. \tag{I.1}$$

Here θ, H and C_f are unknown and u_e is prescribed. A direct way of resolving θ, H and C_f with one closure model is by assuming a velocity profile, for instance the Pohlhausen profile. Restating the Pohlhausen profile

$$f(\eta) = \left(2 - 2\eta^2 - \eta^3\right)\eta + \frac{1}{6}\Lambda\eta\left(1-\eta\right)^3,$$
$$\Lambda = \frac{\delta^2}{\nu}\frac{du_e}{dx}.$$

Applying the definitions for the integral variables gives in general

$$\delta^* = f_\delta(\delta, u_e),$$
$$\theta = f_\theta(\delta, u_e),$$

and the same for the friction coefficient; $C_f = f_{C_f}(\delta, u_e)$, i.e. θ, H and C_f can be written as functions of δ and the Von Kármán equation reduces to an ODE which can be solved. Writing out the integral variables for the Pohlhausen velocity profile and simplifying results in

$$\delta^* = -\frac{1}{120}\frac{\delta}{\nu}\left(-36\nu + \delta^2\frac{due}{dx}\right),$$
$$\theta = -\frac{1}{45360}\frac{\delta}{\nu^2}\left(-5328\nu^2 + 48\delta^2\frac{du_e}{dx}\nu + 5\delta^4\left(\frac{du_e}{dx}\right)^2\right),$$
$$C_f = \frac{\nu}{u_e\delta}\left(4 + \frac{1}{3}\frac{\delta^2}{\nu}\frac{du_e}{dx}\right).$$

Using the chain rule for $\frac{d\theta}{dx}$

$$\frac{d\theta}{dx} = \frac{d\theta(\eta,\lambda)}{d\delta}\frac{d\delta}{dx},$$

Where

$$\theta(\eta,\lambda) = -\frac{\delta}{45360}\left(-5328 + 48\Lambda + 5\Lambda^2\right). \tag{I.2}$$

rewriting the Von Karman equation

$$\frac{d\delta}{dx} = \left(\frac{d\theta}{d\delta}\right)^{-1}\left[-\frac{\theta}{u_e}(2+H)\frac{du_e}{dx} + \frac{1}{2}C_f\right]. \tag{I.3}$$

This can be solved numerically given an initial value for $\frac{d\delta}{dx}$, obviously the initial value for δ is zero. To initialize the Pohlhausen method for an initial flat plate flow note that $\delta \sim \sqrt{x}$ at the beginning of the plate (i.e. see Schlichting[118]), this means $\delta = C\sqrt{x}$.
Now the expression for the integral variables are substituted in equation(I.3), and if $x \to 0$ only the lowest order remains, the following expression for C is found

$$C = 2\sqrt{x}\frac{\frac{2\nu}{Cu_e\sqrt{x}}}{\frac{37}{315}} = 4\frac{315}{37}\frac{\nu}{Cu_e},$$
$$C = 2\sqrt{\frac{315}{37}\frac{\nu}{u_e}}.$$

So for $x \to 0$ the solution is obtained from

$$\delta = 2\sqrt{\frac{315x\nu}{37u_e}}. \tag{I.4}$$

Now equation (I.3) can be solved given the expressions for the integral variables, starting with equation (I.4) for the first integration steps the solution can be obtained for $0 < x < L$.

In case of a forward stagnation point, i.e. u_e is zero, there will be a singularity if $\frac{du_e}{dx} \neq 0$, to remove the singularity the term $\theta(2+H)$ should be zero, to that end Rosenhead[113] suggests as starting values at the stagnation point

$$\theta = \sqrt{\frac{0.077\nu}{\frac{du_e}{dx}}}, \quad \delta^* = \theta\sqrt{\frac{\Lambda}{0.077}},$$

now δ follows from the expression for θ

$$\sqrt{\frac{0.077\nu}{\frac{du_e}{dx}}} = -\frac{1}{45360}\delta\left(-5328\nu^2 + 48\delta^2\frac{du_e}{dx}\nu + 5\delta^4\left(\frac{du_e}{dx}\right)^2\right),$$

which can be solved iteratively. If $u_e = 0$ and $\frac{du_e}{dx} = 0$ then C_f is set to zero and $\frac{1}{u_e}\frac{du_e}{dx}$ follows from l'Hôpital's rule. This is not possible for the Falkner-Skan solutions ($m \neq 0$) which will give $\frac{1}{u_e}\frac{du_e}{dx}\Big|_{x\to 0} = \frac{1}{x} \to \infty$. However, general external velocity distributions may be initialised using a Falkner-Skan solution with

$$m(0) = \left(\frac{x}{u_e}\frac{du_e}{dx}\right)_{x\to 0}, \tag{I.5}$$

this however requires the solution of an arbitrary Falkner-Skan profile[142].

As was in said section 3.1.2 and explained further in D, the guessed velocity profile can be chosen to fit an arbitrary number of boundary conditions. This can lead to higher order polynomials using a single parameter but it can also produce higher order polynomials with more than one parameter, the former will be discussed in section I.1.3, the latter will be omitted. Likewise, it is possible to introduce velocity profiles for the entire turbulent BL, for instance the sin-squared law , thus the guessed velocity profile approach can lead to a complete description of the attached boundary layer. Using higher order velocity profiles with the moment of moment equations C_f becomes

a primary variable together with δ, C_d still requires a closure relation. The strength of this approach is the relative generic nature of the closure which can describe any profile as long as the profile parameters stay within certain bounds. The weakness is the dependency on the rather superfluous boundary layer thickness δ and the fact that the polynomial profiles may give $\frac{u}{u_e} > 1$ somewhere in the profile for certain values of the profile parameters. Mughal used assumed velocity profiles to obtain the integral variables 'on-the-fly'. The apparent weakness of the Von Kármán -Pohlhausen method, or any velocity profile method for that matter, is the initial boundary layer profile to start the procedure. To create a generic initial profile the method due to Thwaites is considered in the next section.

I.1.2 Method of Thwaites

Thwaites produced the most used one-parameter integral method for laminar boundary layers. His method uses a parameter (say λ) which is dependent on the momentum thickness θ, and Thwaites introduces a universal function $l(\lambda)$

$$\lambda = \frac{\theta^2}{\nu}\frac{du_e}{dx},$$
$$l(\lambda) = \frac{\theta}{u_e}\frac{du}{dy}.$$

Substituting this in the steady Von Kármán equation and rewriting results in

$$F(\lambda) = \frac{u_e}{\nu}\frac{d\theta^2}{dx} = 2\left[l(\lambda) - \lambda\left(H+2\right)\right].$$

Using a wide range of empirical data, Thwaites approximated this using a linear function

$$F(\lambda) = 0.45 - 6\lambda, \tag{I.6}$$

which results in a single differential term after substitution in the Von Kármán equation, now θ can be found by integration

$$\frac{\theta^2 u_e^6}{\nu} = 0.45\int_0^x u_e^5 dx + \left(\theta^2\frac{u_e^6}{\nu}\right)_0$$
$$\Rightarrow \tag{I.7}$$
$$\theta = \sqrt{\frac{\nu}{u_e^6}\left[0.45\int_0^x u_e^5 dx + \left(\theta^2\frac{u_e^6}{\nu}\right)_0\right]}, \tag{I.8}$$

see i.e. White[154], schlichting[118] and Cebeci[22]. With the empirical data used to extract the linear correlation l and H can be related to the Thwaites parameter λ by (see Cebeci[22], sekar[120])

$$\left.\begin{array}{l} l = 0.22 + 1.57\lambda - 1.8\lambda^2 \\ H = 2.61 - 3.75\lambda + 5.24\lambda^2 \end{array}\right\} \; 0 \le \lambda \le 0.1, \tag{I.9}$$

$$\left.\begin{array}{l} l = 0.22 + 1.402\lambda + \frac{0.018\lambda}{0.107+\lambda} \\ H = \frac{0.0731}{0.14+\lambda} + 2.088 \end{array}\right\} \; -0.0898 \le \lambda \le 0, \tag{I.10}$$

$$\left.\begin{array}{l} l = 0.3590 \\ H = 2.2874 \end{array}\right\} \; \lambda > 0.1. \tag{I.11}$$

For $\lambda < -0.0898$ it is assumed that the flow separates. Alternatively White gave the following curve fits for $-0.09 < \lambda < 0.25$

$$l = (\lambda + 0.09)^{0.62},$$
$$H = 2 + 4.14z - 83.5z^2 + 854z^3 - 3337z^4 + 4576z^5, \quad z = 0.25 - \lambda.$$

Now the friction coefficient and the density thickness follow from the definitions for l and H

$$C_f = 2\frac{l}{Re_\theta},$$
$$\delta^* = H\theta.$$

The starting value for θ is obtained by considering the differential (see [104])

$$\frac{d}{dx}\left(u_e^6\Big|_{x\to 0}\theta^2\right) = 0.45\nu,\, u_e^5\Big|_{x\to 0} \tag{I.12}$$

this is valid even for non-stagnation flows. Consider a 2^{rd} order Taylor expansion of the velocity near the starting point ($x = 0$)

$$u_e = u_e(0) + x\left.\frac{du_e}{dx}\right|_{x=0} + \frac{x^2}{2}\left.\frac{d^2u_e}{dx^2}\right|_{x=0}.$$

Substituting in equation (I.12) and solving gives

$$\theta(0) = \sqrt{\frac{9}{140}\nu\left.\frac{u_e}{\frac{du_e}{dx} + \frac{1}{2}\frac{d^2u_e}{dx^2}}\right|_{x=0}}, \tag{I.13}$$

or if $u_e = 0$, taking the first order Taylor expansion for u_e near $x = 0$

$$\theta(0) = \sqrt{0.075\left.\frac{\nu}{\frac{du_e}{dx}}\right|_{x=0}}. \tag{I.14}$$

of course the above is only valid if $\left|\frac{du_e}{dx}\right| > 0 \bigvee \left|\frac{d^2u_e}{dx^2}\right| > 0$. In case $u_e|_{x\to 0} = Constant$ it is assumed that $\theta(0) = 0$. Using for instance the Falkner-Skan solutions relations can be found for h, θ and δ.

Unsteady Thwaites

An unsteady method was found in a paper by He and Denton[62] using Thwaites' integral, the unsteady Von Kármán equation and the unsteady Thwaites parameter they arrive at

$$\frac{\partial(\theta^2u_e^6)}{\partial x} = \left[0.45 - \frac{2\theta}{\nu u_e}\left(u_e\frac{\partial\delta^*}{\partial t} + \theta\frac{\partial u_e}{\partial t}\right)\right]\nu u_e^5.$$

They use the correlations based on the steady Thwaites' parameter i.e., quasi-unsteadiness is assumed which automatically limits the method to low reduced frequencies. Unsteady Thwaites' will not be considered beyond this point simply because of the inherent quasi-unsteadiness.

I.1.3 Von Kármán Equation and a Higher Order Polynomial Velocity Profile

Libby notes that a 6^{th} order profile is comparable in accuracy to a two parameter method of the same order, this makes the 6^{th} order profile attractive for use with the integral boundary layer method. Moreoever the polynomial order can be extended easily if the number of boundary conditions is increased since there are in principle infinitely many

boundary conditions for the boundary layer profile, see appendix D. Using two conditions at the wall and four at the edge gives (see appendix D.1.2)

$$f(\eta) = \left(\frac{1}{5}\Lambda + 2\right)\eta + \left(-\frac{1}{2}\Lambda\right)\eta^2 + (\Lambda - 5)\,\eta^4 + (-\Lambda + 6)\,\eta^5 + \left(-2 + \frac{3}{10}\Lambda\right)\eta^6. \quad \text{(I.15)}$$

The sixth order profile using one condition at the wall and five at the edge is given by (see appendix D.1.1)

$$f(\eta) = \left(\frac{1}{10}\Lambda +\right)\eta + \left(-\frac{1}{2}\Lambda\right)\eta^2 + (-10 + \Lambda)\,\eta^3 + (-\Lambda + 15)\,\eta^4 + \left(\frac{1}{2}\Lambda - 9\right)\eta^5 + \left(2 - \frac{1}{10}\Lambda\right)\eta^6. \quad \text{(I.16)}$$

The latter profile is basically an extension of the boundary conditions used for the original Pohlhausen method, where the number of edge conditions is simply increased, this profile will be denoted as the Pohlhausen type. The former profile will be denoted as the alternative type. Implementation with the Von Kármán equation is of course identical to the Pohlhausen profile. Besides the polynomial velocity profile there are also exponential profiles, for instance due to Timman which is discussed in the next section.

I.1.4 Von Kármán Equation and Timman Velocity Profile

The steady Von Kármán equation is combined with the velocity profile by Timman (see i.e. [113]). The Timman profile meets infinitely many boundary conditions at the edge and four boundary conditions at the wall. The Timman profile is written as

$$\begin{aligned}
\frac{u}{u_e} &= 1 - \int_\eta^\infty \exp\left(-\eta^2\right)\left(a + c\eta^2\right)d\eta - \exp\left(-\eta^2\right)\left(b + d\eta^2\right), \\
a &= \frac{4}{3\sqrt{\pi}}(1-b), \\
c &= \frac{4}{3\sqrt{\pi}}(1-b), \\
b &= \begin{cases} -\Lambda, & \frac{\theta^2}{\nu}\frac{du_e}{dx} < 0, \\ -\frac{1}{2}\Lambda, & \frac{\theta^2}{\nu}\frac{du_e}{dx} \geq 0, \end{cases} \\
d &= \begin{cases} -\frac{1}{2}\Lambda, & \frac{\theta^2}{\nu}\frac{du_e}{dx} < 0, \\ 0, & \frac{\theta^2}{\nu}\frac{du_e}{dx} \geq 0. \end{cases}
\end{aligned}$$

The integral can be solved

$$\int_\eta^\infty \exp\left(-\eta^2\right)\left(a + c\eta^2\right)d\eta =$$
$$-\exp\left(-\eta^2\right)\left[\frac{a}{2}\pi^{1/2} erf(\eta)\exp\left(\eta^2\right) - \frac{c}{2}\eta + \frac{c}{4}\pi^{1/2} erf(\eta)\exp\left(\eta^2\right) - \frac{a}{2}\pi^{1/2}\exp\left(\eta^2\right) - \frac{c}{4}\pi^{1/2}\exp\left(\eta^2\right)\right].$$

The integral variables cannot be solved for analytically because of the error function. Either the function is integrated numerically or the error function is approximated. For the error function an 11^{th} order polynomial fit is used. Now the solution procedure is similar to the Von Kármán -Pohlhausen method. If the amount of integral parameters is increased more integral equations are needed to provide a closed system, a well known two parameter method is due to Wieghardt which is discussed in the next section.

I.1.5 Von Kármán Equation, Energy Equation and Wieghardt Velocity Profile

Using three conditions at the wall, namely $f(0)$, $f''(0)$ and $f'''(0)$ and eight conditions at the edge Wieghardt derived a two-parameter method. The velocity profile due to Wieghardt is written as

$$\begin{aligned}
\frac{u}{u_e} &= f_1(\eta) + a f_2(\eta) + b f_3(\eta),\\
f_1 &= 1-(1-\eta)^8(1+8\eta+36\eta^2+120\eta^3),\\
f_2 &= (1-\eta)^8\eta(1+8\eta+36\eta^2),\\
f_3 &= -(1-\eta)^8\eta^2(1+8\eta),\\
a &= \frac{\delta u_e}{2\nu}C_f, \quad b = \frac{1}{2}\Lambda.
\end{aligned} \tag{I.17}$$

The integral equations are written as

$$\begin{aligned}
\frac{d\theta}{dx} &= \frac{C_f}{2} - (2+H)\frac{\theta}{u_e}\frac{du_e}{dx},\\
\frac{d\delta^k}{dx} &= C_D - 3\delta^k\frac{du_e}{dx}.
\end{aligned}$$

Since all integral variables can be written as functions of C_f and δ, two first order ordinary differential equations emerge. The implementation of the Wieghardt profile is rather laborious due to the extremely elaborate expressions which makes it difficult to debug. The Wieghardt method is initialised in the same way as the Von Kármán - Pohlhausen method. The Wieghardt method requires the parameters to be solved through an iteration process, whereby through the application of two integral equations a single equation emerges from which one parameter is solved iteratively. The parameter b is chosen as preset using the old value for δ, once parameter a is found approximately the flux $\frac{d\delta}{dx}$ can be calculated. For the iteration process a Newton-Rhapson iteration step is chosen for it's efficiency given an accurate guess, which in this case follows directly from the old value for the friction coefficient C_f. The solution was found to be very sensitive to changes in the convergence requirement and the number of iteration steps.
Comparing the values for the parameters following from the Wieghardt solution with the values following from the Falkner-Skan solution the following modification was added

$$\frac{du_e}{dx} > 0, \begin{cases} a = \frac{5}{3}a \\ b = \frac{3}{2}b \end{cases}, \quad \frac{du_e}{dx} < 0 \begin{cases} a = \frac{3}{5}a \\ b = \frac{2}{3}b \end{cases}.$$

The original Wieghardt method defines the parameters as follows

$$\begin{aligned}
a &= \frac{\delta}{\theta}t, \quad b = \frac{1}{2}\left(\frac{\delta}{\theta}\right)^2\lambda,\\
T &= C_f\frac{\nu u_e}{2}\theta, \quad \lambda = \frac{\theta^2}{\nu}\frac{du_e}{dx}.
\end{aligned}$$

Multiplying the dimensional energy equation by $2u_e^3\delta^k$ the momentum thickness θ is found by integrating

$$\lambda = \frac{4}{K^2u_e^6}\frac{du_e}{dx}\int_0^x u_e^5 KL dx,$$

where

$$K = \frac{\delta^k}{\theta}, \quad L = \frac{\theta D}{\mu u_e^2}.$$

Now the momentum integral can be written as

$$T = \lambda(H-1) + 2\frac{L}{K} - \lambda\frac{u_e\frac{dK}{dx}}{\frac{du_e}{dx}K}. \tag{I.18}$$

Since $\frac{\delta}{\theta}$, L, H and K can be expressed in a and b and since a and b are functions of the parameters T and λ a closed system of equations emerges.

I.1.6 Von Kármán Equation, Energy Equation and laminar Drela Closure

Drela[35] defined the following shape factors

$$H = \frac{\delta}{\theta}, \quad H^* = \frac{\delta^k}{\theta}, \quad J = \frac{\delta^{**}}{\theta},$$

where

$$\delta^{**} = \int_0^\infty \left(1 - \frac{\rho}{\rho_e}\right) \frac{u}{u_e} dy.$$

Since for the present case the density ρ is considered constant $\delta^{**} = J = 0$. Using these shape factors Drela rewrote the momentum and energy integral to

$$\frac{d\theta}{dx} = \frac{C_f}{2} - (H+2)\frac{\theta}{u_e}\frac{du_e}{dx},$$
$$\frac{dH^*}{dx} = \frac{1}{\theta}C_D - \frac{H^*}{\theta}\frac{C_f}{2} - (1-H)\frac{H^*}{u_e}\frac{du_e}{dx}.$$

Now in case of incompressibility Drela assumes H^*, C_f and C_D are dependent on H and Re_θ. Using Falkner-Skan profiles Drela determines the following relations for H^*, C_f and C_D in case of a laminar boundary layer flow.

$$H^* = \begin{cases} 1.515 + 0.076\frac{(H-4)^2}{H} & , H < 4, \\ 1.515 + 0.040\frac{(H-4)^2}{H} & , H > 4, \end{cases}$$

$$C_f = \frac{2}{Re_\theta}\begin{cases} -0.067 + 0.01977\frac{(7.4-H)^2}{H-1} & , H < 7.4, \\ -0.067 + 0.022\left(1 - \frac{1.4}{H-6}\right)^2 & , H > 7.4, \end{cases}$$

$$C_D = \frac{H^*}{Re_\theta}\begin{cases} 0.207 + 0.00205\,(4-H)^{5.5} & , H < 4, \\ 0.207 - 0.003\,(H-4)^2 & .H > 4. \end{cases}$$

If the above is substituted in the differential equations a set of ordinary differential equations is attained which can be solved numerically.
The energy integral can be written as

$$\frac{dH}{dx} = \frac{1}{\kappa H(H+4)}\left[\frac{1}{H^*\theta}C_D - \frac{1}{\theta}\frac{C_f}{2} - (1-H)\frac{1}{u_e}\frac{du_e}{dx}\right],$$
$$H < 4, \quad \kappa = 0.076,$$
$$H > 4, \quad \kappa = 0.040.$$

To initiate the solution the method of Thwaites can be used to retrieve θ in combination with Falkner-Skan derived relations to obtain δ^* and C_f, see section I.1.2. The benefit of this method is that in case of transition to turbulence the closure relations are changed and not the solution method. Also the dependency on δ is removed, this might benefit the availability of closure models since empirical data for δ is dependent on the definition of the boundary layer thickness. Also the system of equations is less likely to behave erratic since the shape factors vary mildly compared to the integral variables.

I.1.7 Von Kármán Equation and Head's entrainment Equation

The method due to Head makes use of the entrainment equation together with the Von Kármán equation. Using closure relations for C_f and H_1 the two differential equations can be solved for the two primary variables θ and H. The differential equations are

$$\frac{1}{2}C_f = \frac{d\theta}{dx} + \frac{\theta}{u_e}(2+H)\frac{du_e}{dx},$$
$$\frac{1}{u_e}\frac{du_e\theta H_1}{dx} = 0.0306(H_1-3)^{-0.6169}.$$

For closure of the friction coefficient C_f will be approximated using the correlation from White and for H_1 the relations from Cebeci and Bradshaw will be used (see [154])

$$C_f = \frac{0.3\exp(-1.33H)}{(\log_{10} Re_\theta)^{1.74+0.31H}},$$
$$H_1 = \begin{cases} 0.8234(H-1.1)^{-1.287}+3.3, & H<1.6, \\ 0.5501(H-0.6778)^{-3.064}+3.3, & H\geq 1.6. \end{cases}$$

Using the closure relation from Cebeci and Bradshaw and applying the product rule the entrainment equation can be written as

$$\frac{dH}{dx} = \frac{1}{\gamma\theta}\left[0.0306\,(H_1-3)^{-0.6169} - H_1\frac{d\theta}{dx} - \frac{\theta H_1}{u_e}\frac{du_e}{dx}\right],$$
$$\gamma = \begin{cases} -1.0597(H-1.1)^{-2.287} & H<1.6, \\ -1.6855(H-0.6778)^{-4.064} & H\geq 1.6. \end{cases}$$

Alternatively, C_f can be closed with the C_f relation described in the previous section. The differential equations can now be solved numerically using the method of Thwaites for the initialisation. Benefit of using Head's entrainment method is the relative straightforward extension to unsteady flow and the fact that in theory it is able to describe laminar as well as turbulent boundary layer flow. A laminar closure relation was found in Coenen[26] (in reference to Cousteix)

$$\frac{H_1}{H_{10}} + a\frac{H_{10}}{H_1} = b\left(\frac{1}{H} + \frac{H}{4.02923^2}\right) + c,$$

where $H_{10} = 12.37$ and

$$H_{10} \leq 4.02923: \quad a = 1.2706, \quad b = -1.5022, \quad c = 3.1924,$$
$$H_{10} > 4.02923: \quad a = 0.33044, \quad b = 0.31993, \quad c = 1.03094.$$

This can be solved for $H > 2$, below which the solution is complex valued, the solution has two roots for each range, the actual closure for H_1 is comprised of the smallest root value λ_- of the lower range and the largest root value λ_+ of the upper range, see figure (I.1). The minimum value for H_1 occurs at $H = H_{10}$. The above relationship is combined with the closure relations by Drela for the laminar case and does not lead to meaningful results which may be due to the relation for $F(H)$ which is still based on the turbulent BL.

I.2 Steady Test Cases

Before the unsteady methods are treated some basic steady test cases are performed with the methods described in section (I.1).

I.3 Basic Test cases using Falkner-Skan

To test the methods, a solution will be obtained for an external velocity distribution which is described by

$$u_e = x^m.$$

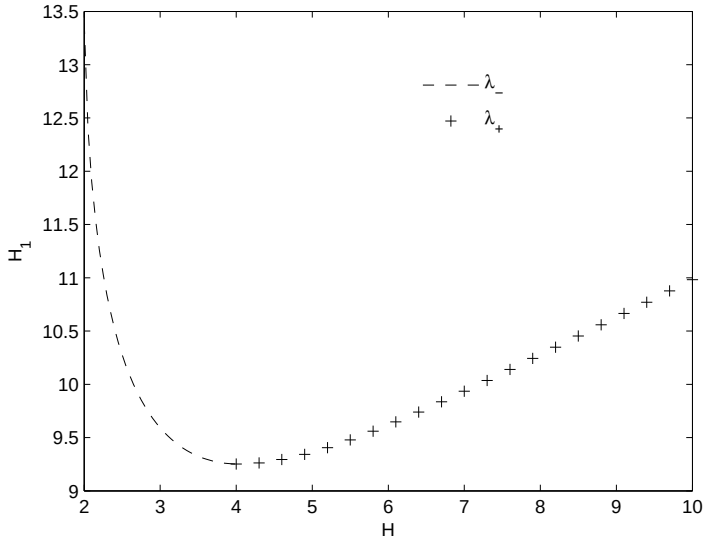

Figure I.1: H_1 versus H for the laminar boundary layer

For comparison a relative error will be calculated for $x = L$, this error is defined as

$$\epsilon_{value} = 100 \frac{value_{ref} - value_{approx}}{value_{ref}}.$$

For the unsteady case the average error over time will be plotted for $x = L$. The external parameters used for the test cases can be found in table I.1. Note that the amount of steps is fixed at 500. All test cases will be initialised using a flat plate boundary layer

description	symbol	value	units
viscosity	μ	$1.5e^{-5}$	$\frac{N\,s}{m^2}$
density	ρ	1.2	$\frac{kg}{m^3}$
profile length	L	1	m
end time	T	1	s
distance	x	$0 < x < L$	m
time	t	$0 < t < T$	s
number of spatial integration steps	N	500	-
number of temporal integration steps	M	50	-

Table I.1: Parameters used for the test cases

flow with the integral variables set to zero, subsequently two steps are computed using a flat plate solution, a refinement of the initialisation will take place in section I.3.3.

I.3.1 $m = 0$, Blasius Solution

The boundary layer flow over a flat plate can be described by the Blasius solution if the external velocity is constant, the Blasius solution is a similarity solution which directly

follows from the more generic Falkner-Skan relations (see equation (C.1)) by taking $m = 0$. The Blasius solution is described by

$$\begin{gathered} f''' + \frac{1}{2} f f'' = 0, \\ \eta = \sqrt{\frac{u_e}{\nu x}} y, \quad f(\eta) = \frac{\psi(x,y)}{\sqrt{u_e \nu x}}, \\ \textit{boundary conditions :} f(0) = 0\,, f'(0) = 0\,, f'(\infty) = 1. \end{gathered} \tag{I.19}$$

The boundary condition $f'(\infty) = 1$ has to be replaced by a boundary condition $f''(0) = B$ to be able to integrate the ODE. If the boundary condition is found the ODE can be integrated. The correct value for $f''(0)$ is found by integrating the ODE with some assumed value for $f''(0)$ and by using the fact that (see appendix(F))

$$\frac{f''(0)}{\left[f'(\infty)\right]^{\frac{3}{2}}} = B.$$

The approximate value for $f''(0)$ is found through

$$f''(0) = \left(\frac{f''(0)}{\left[f'(\infty)\right]^{\frac{3}{2}}} \right)_{iter}.$$

It follows that $f''(0) = 0.332057$, see i.e. White[154]. Now that the ODE is fully described the boundary layer (integral) variables can be found:

$$\begin{gathered} \frac{\delta}{x} = \frac{5}{\sqrt{Re_x}}, \quad \frac{\delta^*}{x} = \frac{1.7208}{\sqrt{Re_x}}, \quad \frac{\theta}{x} = \frac{0.664}{\sqrt{Re_x}}, \\ H = 2.592, \quad C_f = \frac{0.664}{\sqrt{Re_x}}, \end{gathered} \tag{I.20}$$

Also important is the stability of the Blasius flow, from White[154, table 5-1]

$$Re_{\delta^*,crit} = 520, \quad Re_{\theta,crit} = 201.$$

Note that the initial solution used for the numerical procedure can be written as

$$\frac{\delta}{x} = 2\sqrt{\frac{315}{37}}\sqrt{\frac{\nu}{u_e x}} \approx \frac{5.84}{\sqrt{Re_x}}, \tag{I.21}$$

which is already close to the Blasius solution. If for the Von Kármán-Pohlhausen method a flat plate flow is assumed with constant external velocity the following results are obtained through equation I.3

$$\begin{gathered} \frac{\delta}{x} = 2\frac{\sqrt{\frac{315}{37}}}{\sqrt{Re_x}}, \quad \frac{\delta^*}{x} = \frac{3}{5}\frac{\sqrt{\frac{315}{37}}}{\sqrt{Re_x}}, \quad \frac{\theta}{x} == 2\frac{\sqrt{\frac{37}{315}}}{\sqrt{Re_x}}, \\ H = 2.5541 \quad , C_f = 2\frac{\sqrt{\frac{37}{315}}}{\sqrt{Re_x}}, \end{gathered}$$

The differences can thus be found immediately by comparing the factors, this gives

$$\epsilon_\delta = -16.7\%, \quad \epsilon_{\delta^*} = -1.7\%, \quad \epsilon_\theta = -3.2\%, \quad C_f = -3.3\%.$$

The results are tabulated in table I.2. Most notable are the relatively large errors for the boundary layer thickness δ and the fact that this error increased for polynomial order. The boundary layer thickness is an arbitrary variable since the criterion for the thickness is met assymptotically with increasing height above the profile. In other words,

profile	ϵ_δ(%)	ϵ^*_δ(%)	ϵ_θ(%)	ϵ_{C_f}(%)
Pohlhausen[4^{th} order profile]	-16.7	-1.7	-3.2	-3.3
Alternative[4^{th} order profile]	13.6	-0.37	6.2	7.00
Pohlhausen[6^{th} order profile]	-64.5	-2.4	-9.4	-10.0
Alternative[6^{th} order profile]	-20.9	-0.36	0.5	0.34
Pohlhausen[9^{th} order profile]	-136.6	-3.1	-14.2	-14.6
Alternative[9^{th} order profile]	-73.1	-0.60	-4.1	-4.4
Timman($\eta = 2\eta_{original}$]	42.3(52.8)	-4.0(-0.58)	18.6(-0.08)	19.9(2.1)
Thwaites	n/a	-1.1	-1.8	1.1
Drela [two parameter]	n/a	0.58	0.65	-0.32
Wieghardt [two parameter]	-26.4	7.2	18.9	19.3

Table I.2: Results for the Blasius flat plate solution.

if say the velocity distribution of the Falkner-Skan solution is taken for some velocity profile x^n and the boundary layer thickness is set as the height for which $\frac{u}{u_e} \leq 0.99$, the value of δ_{approx} for the approximate solution will differ from the Falkner-Skan solution largely due to the fact that δ_{approx} is taken at $\frac{u}{u_e} = 1.0$, i.e. the approximate method tries to solve for the exact boundary layer height whilst the reference method assumes some realistic criterium. Therefore, the boundary layer thickness is not a proper comparator for the different methods.

The Pohlhausen profile of the 4^{th} order fits the Blasius profile more closely than the higher order profiles, this is reflected in lower accuracies for the higher order Pohlhausen profiles. In general the polynomial profiles become flatter near $\eta = 1$ for increasing polynomial order. This can be explained by the fact that in this case an increase in polynomial order means that more boundary conditions at the edge are used for the determination of the polynomial coefficients. These boundary conditions state that $f^n(1) = 0$, now if more derivatives for a given point are set to zero the more closely the expression surrounding that point will match a constant value (1 in this case), the solution will basically flatten near the edge, see appendix(D). Heuristically, the amount of boundary conditions at the edge should be of the same order as the amount of boundary conditions at the wall. The two parameter method by Drela performs well as does the altered Timman profile. Surprisingly the Wieghardt profile is least accurate which should not be the case, however as was noted the Wieghardt profile is extremely laborious to debug and will therefore be kept as is. It is suspected that computer accuracy comes into play for the iterations due to the large numerical factors in the product terms combined with 5^{th} order powers. To consider the convergence more directly some error norm is defined. Defining the relative error norm L_2 for the displacement thickness as

$$L_{2\delta^*} = \sqrt{\frac{\sum \left(\delta_{ref} - \delta^*\right)^2}{\sum \delta^2_{ref}}}.$$

The L_2 convergence behavior suggests that the Von Kármán - Pohlhausen method reaches the model accuracy quite quickly. To a lesser degree this also applies to the alternative profile and the method by Drela, Timman shows linear convergence for a grid resolution of up to 5000 elements (see figure I.3).

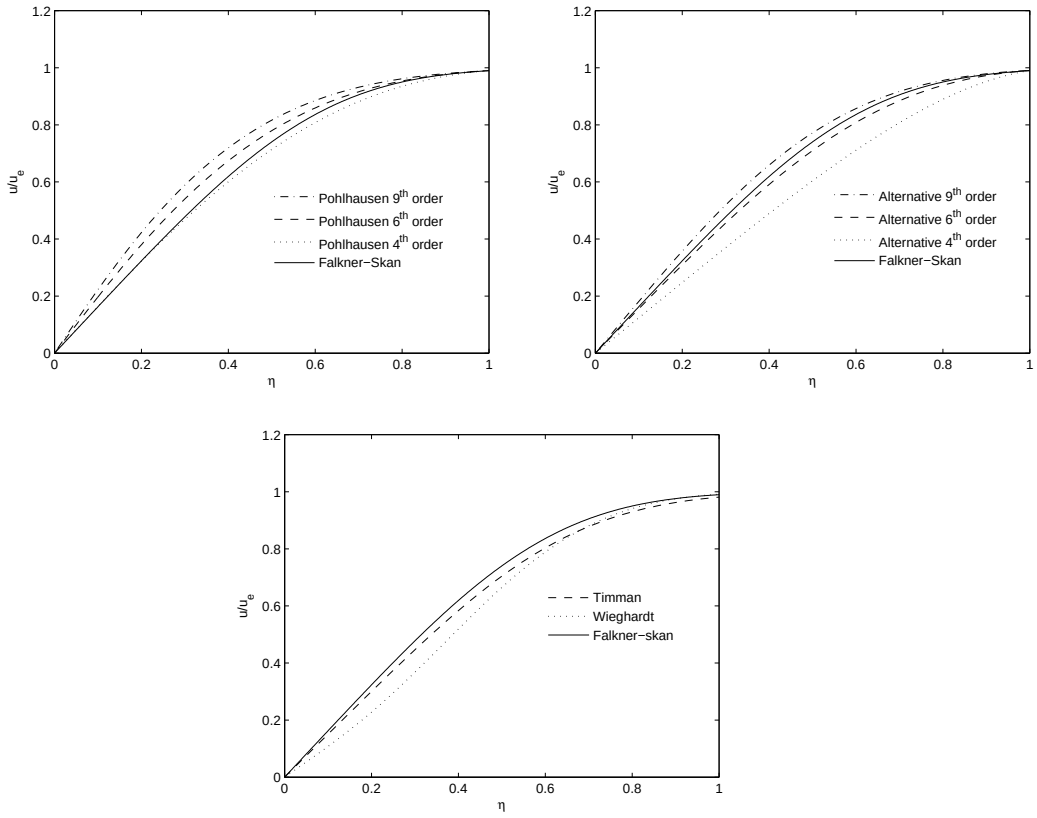

Figure I.2: Blasius solution, (left) Pohlhausen velocity profiles, (right) Alternative velocity profiles, (bottom) Wieghardt velocity profile.

I.3.2 $m \neq 0$, Similarity Solutions

The solution for $u_e = x^m$ follows from the Falkner-Skan equation (C.1), the problem represents a decelerating flow for $m < 0$ and an accelerating flow for $m > 0$. The values for m are chosen as

Slowly retarded flow:	$m = -0.09043, \beta = -0.19884$
Mildly accelerating flow:	$m = 0.25, \beta = 0.4$
Linearly accelerating flow:	$m = 1, \beta = 1$
Exponentially accelerating flow 1:	$m = 3, \beta = 1.5$
Exponentially accelerating flow 2:	$m = 5, \beta = \frac{5}{3}$

Before the Falkner-Skan equation can be integrated some value for C in $f''(0) = C$ has to be found for which $f'(\infty) \rightarrow 1$. Following White[154] the solution is assumed to behave asymptotically for $\eta = 10$. Using the shooting method in combination with guessed values for η_{99}, $f''(0)$ can be found recursively. This will be especially useful for finding shape factor relations for a large range of external velocity distributions. The

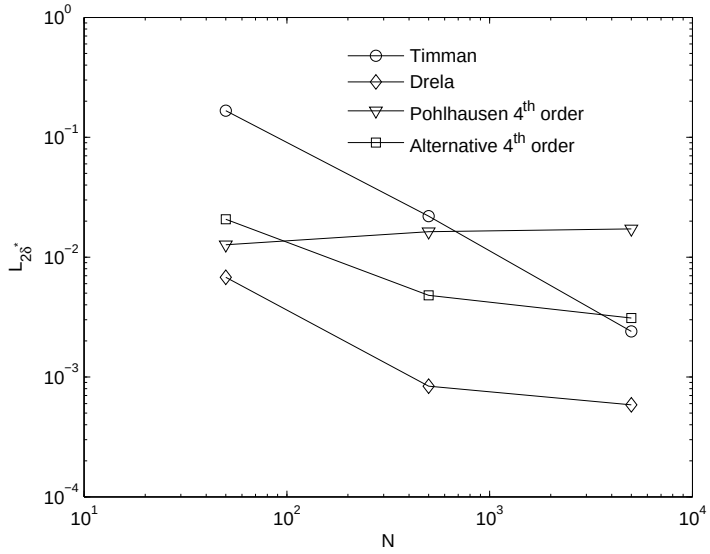

Figure I.3: L_2 error norm for δ^* versus number of steps in x-direction.

following values for $f^{''}(0)$ are found assuming $f^{'}(\infty) = 1$ is 99% accurate.

Slowly retarded flow:	$f_w^{''} = 0,$	$\eta_{99\%} = 4.79$
mildly accelerating flow:	$f_w^{''} = 0.855,$	$\eta_{99\%} = 2.79$
Linearly accelerating flow:	$f_w^{''} = 1.23259,$	$\eta_{99\%} = 2.37$
Exponentially accelerating flow 1:	$f_w^{''} = 1.47724,$	$\eta_{99\%} = 2.13$
Exponentially accelerating flow 2:	$f_w^{''} = 1.55035,$	$\eta_{99\%} = 2.06$

Using $df(x)y = f(x)dy$ the integral variables and the friction coefficient can be retrieved with

$$\delta^* = \sqrt{\frac{2}{m+1}\frac{\nu x}{u_e}}\int_0^{\eta_{99\%}} \left(1 - f^{'}\right) d\eta,$$
$$\theta = \sqrt{\frac{2}{m+1}\frac{\nu x}{u_e}}\int_0^{\eta_{99\%}} f^{'}\left(1 - f^{'2}\right) d\eta,$$
$$C_f = \sqrt{\frac{2(m+1)\nu}{u_e x}} f_w^{''}.$$

Given $\eta_{99\%}$, δ follows from

$$\delta = \frac{\eta_{99\%}}{\sqrt{\frac{m+1}{2}\frac{u_e(x)}{\nu x}}}.$$

The accelerating flow starts with significant wiggles indicating instability, this is most likely caused by the initial values of u_e and $\frac{du_e}{dx}$. The term in $\frac{1}{u_e}\frac{du_e}{dx}$ will be very large for very small u_e, since the external flow has a power-law distribution

$$\frac{1}{u_e}\frac{du_e}{dx}\bigg|_{x\to 0} = m\frac{x^{m-1}}{x^m}\bigg|_{x\to 0} = m\frac{1}{x}\bigg|_{x\to 0} \to \infty,$$

this can be relieved by choosing the appropriate initial profile or alternatively, the dimensional Von Kármán equation is used. The initial wiggle for the accelerating flow is

compared for $m = 1$ using Timman and a 4^{th} order Pohlhausen profile, it can be seen that Timman recovers much more quickly than the 4^{th} order Pohlhausen profile, (see figure I.4). The magnitude of the wiggle is much larger for the Timman profile and when the polynomial order is increased the Pohlhausen profile was much improved with a decreasing amplitude and recovery distance for higher polynomial order. Over time the

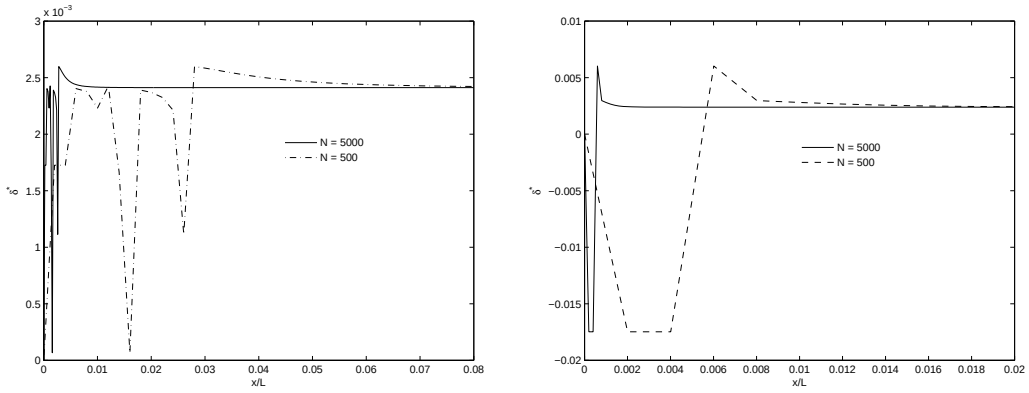

Figure I.4: Comparison δ^* convergence for $m = 1$, (left) Pohlhausen 4^{th} order, (right) Timman.

difference between the exact Falkner-Skan solution and the numerical solution levels out for the accelerating flow, also the approximate solution was fairly insensitive to different assumed initial profiles. Furthermore, notwithstanding the initial wiggles, there was convergence for a low number of grid points. For the decelerating flow the solution is very instable, requiring a much finer grid for a grid-independent solution, also it is more sensitive to the initial conditions. In refining the grid the Wieghardt profile exhibited anomalous behavior, with spurious wiggles depending on the grid resolution and number of iterations. As can be seen in figure I.5, the convergence for the retarded flow

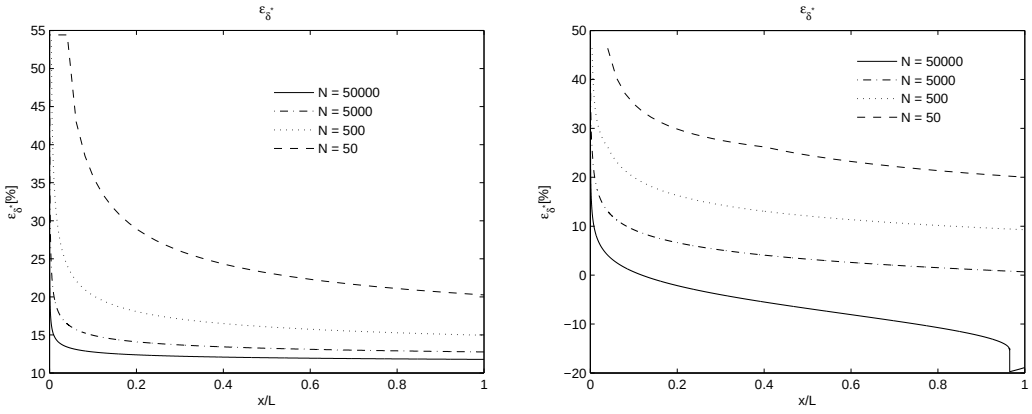

Figure I.5: Comparison $\epsilon_{\delta*}$ convergence for $m = -0.09043$,(left) Pohlhausen 4^{th} order,(right) Drela.

case is slow but there are no instabilities, this was seen for all polynomial orders (4,6,9) both for the Pohlhausen profile and the alternative profile, the method using Drela's closure did not show convergence for $m = -0.09043$, for $m = -0.08$ however Drela does show convergence similar to the convergence seen with the Pohlhausen profile.

The L_2 error norm is approximately constant (see figure I.6) , which can mean for example that the truncation error is dominating. The slightly increasing error norms can be explained by an approximation which starts near the exact solution and drifts off to it's

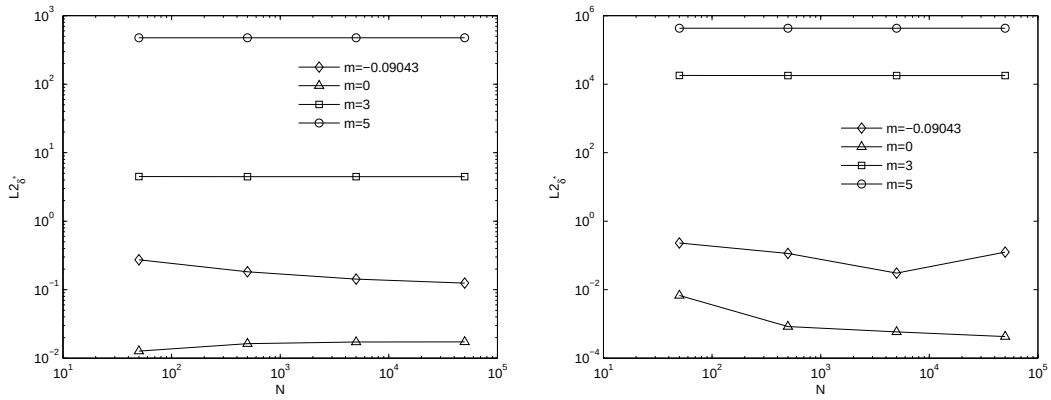

Figure I.6: L_2 error norm for δ^* versus number of steps in x-direction, (left) Pohlhausen 4^{th} order, (right) Drela.

final incorrect value. The latter is the case for $m = 0$, the final more converged approximation is less accurate than the solution for a less converged approximation, see figure I.7. It could already be seen from figures I.4 and I.5 that the solution does converge for

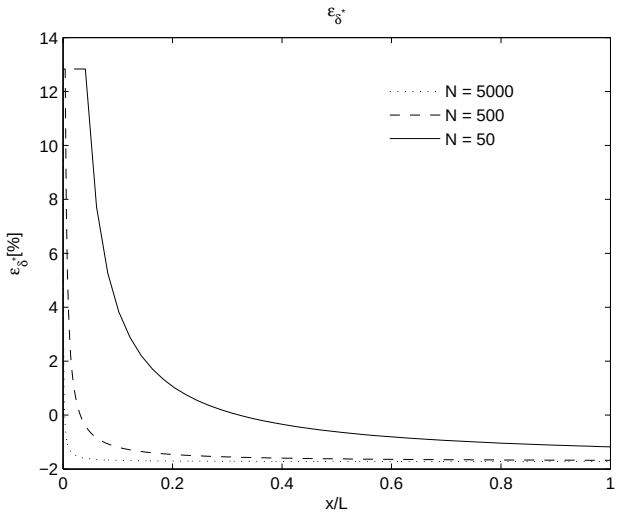

Figure I.7: ϵ_{δ^*} convergence for $m = 0$ using the Pohlhausen guessed velocity profile

$m > 1$. Taking a closer look at the solution it seems that the initial wiggle, going from initial solution to the approximate solution, dominates the error norm (see figure I.8), it stays exactly the same in magnitude for exactly the same points, hence the dominating error term and thus grossly the total error stays constant. This sensitivity to the initial solution can be decreased by applying two different grid resolutions at the start of the solution, taking a resolution two times the intended solution will suffice to remove the wiggle. The wiggle is absent for $m = 0$, this is expected since the initial solution for the guessed velocity profiles is based on the flat plate solution. The magnitude of the wiggle deteriorates with increasing value for m, also for higher polynomial orders the magnitude decreases.

Using the Von Kármán equation in combination with a Pohlhausen velocity profile, the accelerating flow cases give very good results for θ, δ^* and C_f , however the decelerating

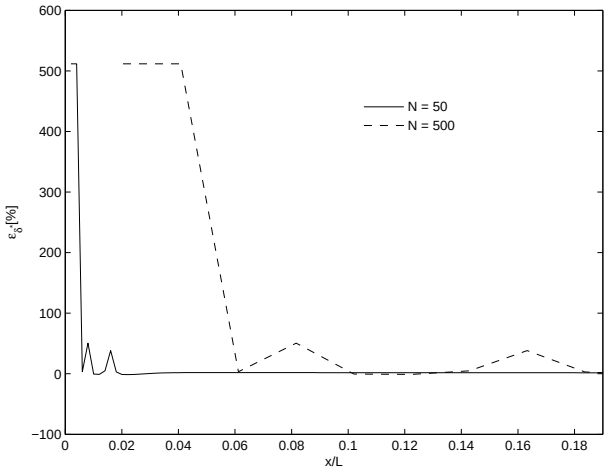

Figure I.8: Initial ϵ_{δ^*} wiggle for $m = 3$, pohlhausen 4^{th} order method for two numbers of grid points N.

flow cases are very instable and produce much poorer results. The alternative velocity profiles give somewhat better results for the decelerating flow cases compared to the Pohlhausen profiles, however for accelerating flow cases the alternative velocity profiles fail completely. The failure of the alternative profile could not be attributed to the shape of the profile, in fact it matched quite well with the Falkner-Skan profile (see figure(I.10)), instead it was suspected that a non-zero value at the wall for the third derivative may cause instabilities. It was found that $f''' = \frac{1}{2}\Lambda$ stabilized the solution for $-0.09043 < m < 5$, this altered alternative procedure is plotted in figure (I.9) and is also indicated in the results table (see appendix (G)). The Timman velocity profile does not seem to have much merit in the given cases, notable was the relatively constant error for different values for m. It was noted that the velocity profile as described by Timman did not reach $\frac{u}{u_e} = 1$ until about $\eta \approx 2$, subsequently upon increasing the integration interval to $\eta = 2$ for the integral variables the results for Timman improved substantially. The two parameter method due to Drela is clearly the best overall with a fairly constant error, which was to be expected since the closure relations used are based on Falkner-Skan profiles. It is assumed that in general laminar boundary layers will adhere closely to Falkner-Skan solutions given the same shape factor H, see i.e. Drela[35].
It must be noted that the relative errors reached a quasi-constant value for all steady cases except for the retarded flow case. The Wieghardt profile matches the velocity profile quite closely. The Timman profile fails for the retarded flow case $m = -0.09043$[1], yet for less retarded flows $m = -0.025$, $m = -0.05$, $m = -0.08$ the agreement is excellent, see table(I.3). This in itself is not unphysical since the steady boundary layer should separate for $m = -0.09043$, indeed the solution deteriorates towards the separation value for m. Overall large differences were observed for the boundary layer thickness δ, which

m	ϵ_δ(%)	ϵ_{δ^*}(%)	ϵ_θ(%)	ϵ_{C_f}(%)
-0.025	65.1	2.6	5.7	0.82
-0.05	53.9	-2.6	-1.7	5.3
-0.08	47.9	-25.3	-14.4	61.8

Table I.3: Timman profile with $\eta = 2\eta_{original}$, retarded flows

[1]The velocity profile for Timman at $m = -0.09043$ is produced using the Falkner-Skan value for Λ

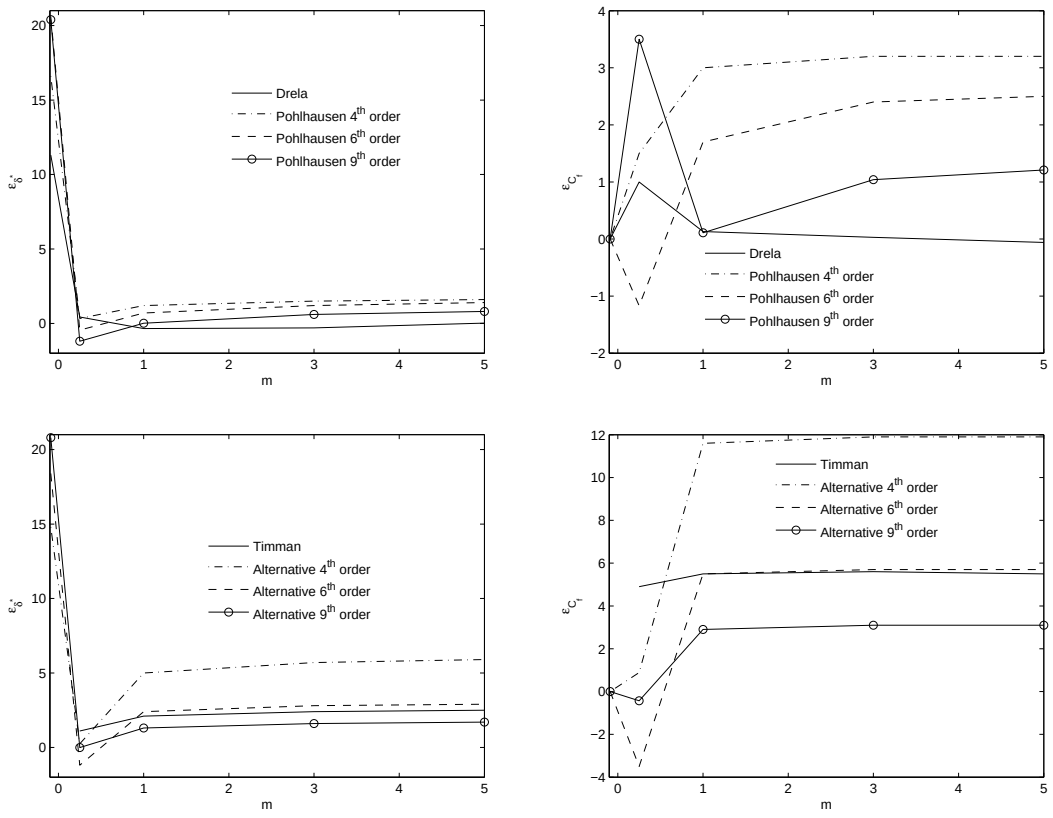

Figure I.9: ϵ_{δ^*} and ϵ_{C_f} comparison of relative errors for number of grid points $N = 500$.

was explained earlier. Note that the integral variables can be written as

$$\delta^* = \delta \int_0^1 \left((1 - \frac{u}{u_e} \right) d\eta, \quad \theta = \delta \int_0^1 \frac{u}{u_e} \left(1 - \frac{u}{u_e} \right) d\eta,$$
$$\delta^k = \delta \int_0^1 \frac{u}{u_e} \left(1 - \left(\frac{u}{u_e} \right)^2 \right) d\eta, \quad \delta^{k+} = \delta \int_0^1 \frac{u}{u_e} \left(1 - \left(\frac{u}{u_e} \right)^3 \right) d\eta.$$

If shape factors are used as primary variables δ does not influence the behaviour of the differential equation and thus it is likely to be more accurate. Finally it is noted that the Von Kármán equation in combination with a guessed velocity profile may have a non-unique solution; in testing the code solutions were obtained which were the negated value of the correct approximation indicating the existence of at least two solutions. This resulted from using inappropriate initial solutions which gave negative values for the integral variables, this is not expected to give problems if appropriate initial solutions are used.

I.3.3 Initial Conditions Revisited

As can be seen in the plots of the previous section, and as could be expected, for the similarity solutions the flat-plate initial solution is not appropriate. The subsequent wiggles are a consequence of a mismatch between the two connecting solutions, this is especially the case when the initial solution does not represent the actual flow problem.

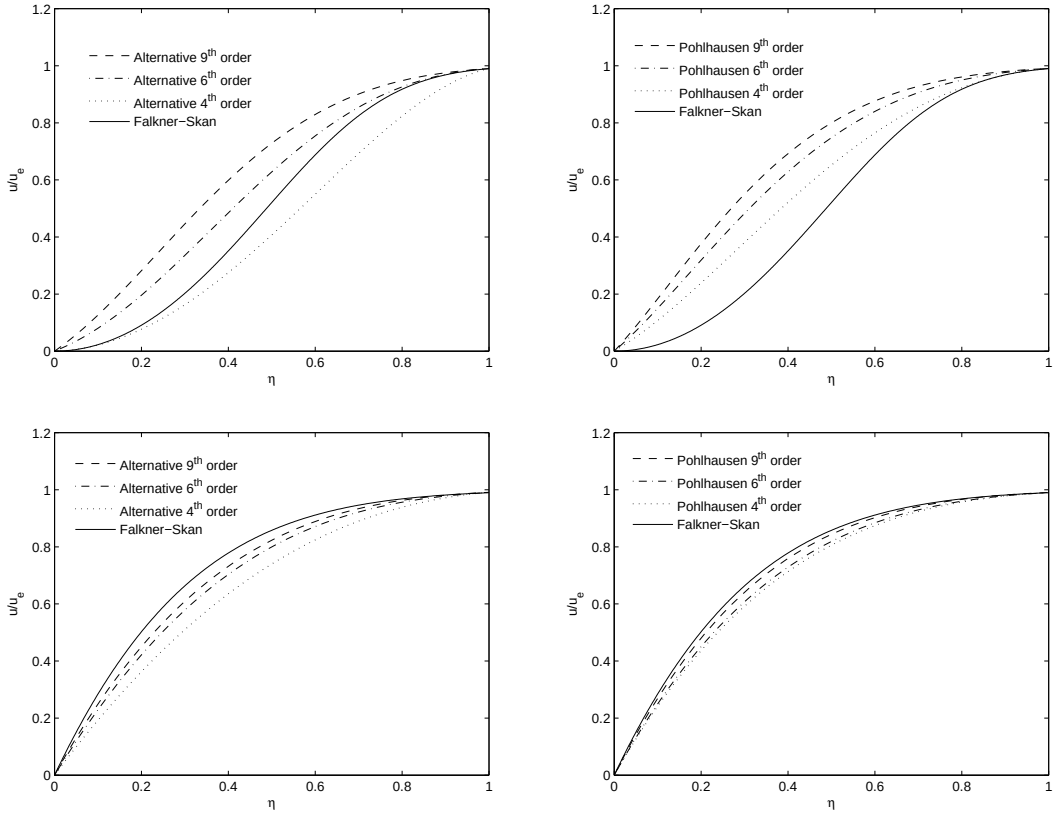

Figure I.10: (top left) Alternative profile, $m = -.09043$, (top right) Pohlhausen, $m = -.09043$, (bottom left) Alternative profile, $m = 5$, (bottom right) Pohlhausen profile, $m = 5$.

It was also noted in the previous section that a negative valued initial solution may cause the subsequent solution to be negative valued.

Looking at the problem at hand a specific treatment of the initial condition can be chosen. For the assumed velocity profile methods a flat plate boundary layer flow with constant velocity was used as the initial BL solution. The present case is meant as a benchmark for a solver that is to be used for the simulation of flow over wind turbine blades. This allows for the assumption that the initial boundary layer flow starts from some forward stagnation point.

A first approach comes from the method of Thwaites; using Thwaites' integral (see equation (I.8)) with $\left(\theta^2 \frac{u_e^6}{\nu}\right)_0 = 0$ for a stagnation flow in combination with Drela's closure for δ (see equation (E.50)) the first steps can be resolved. For the initial value of θ equation (I.14) may be used, which is equivalent to a relation from Rosenhead([113, p.297,300]) which he suggested for the Von Kármán method

$$\theta = \sqrt{\frac{0.077\nu}{\frac{du_e}{dx}}},$$

which is similar to equation (I.14). The above relations are meant to keep the methods consistent for u_e is zero and this only works if $\frac{du_e}{dx} \neq 0$. To avoid the use of a series solution equation (I.12) can be integrated directly to obtain an estimate for $\theta(0)$, in case

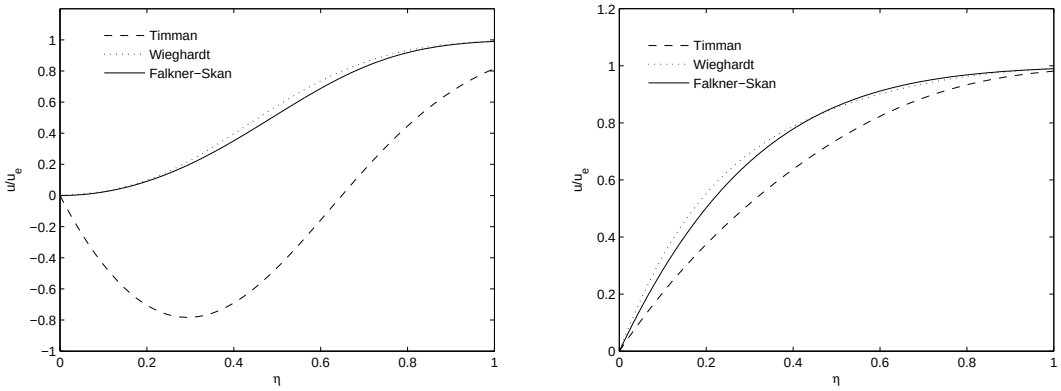

Figure I.11: (left) Wieghardt profile, $m = -.09043$, (right) Wieghardt profile, $m = 5$.

the external velocity is analytical prescribed some multiple point integration scheme might be used to increase the accuracy of the guess

$$\theta(0) = \sqrt{\frac{0.45\nu}{u_e^6\,(\Delta x)}\frac{\Delta x}{m}\left(u_e^5(0) + u_e^5\left(\frac{\Delta x}{m}\right) + \cdots + u_e^5\left(\frac{(m-1)\Delta x}{m}\right) + u_e^5(\Delta x)\right)}, \qquad \text{(I.22)}$$

, in case of a numerical prescribed external velocity a simple two point integration can be used

$$\theta(0) = \sqrt{\frac{0.45\nu}{u_e^6\,(\Delta x)}\frac{\Delta x}{2}\left(u_e^5(0) + u_e^5(\Delta x)\right)}, \qquad \text{(I.23)}$$

if more accuracy is needed, a higher order extrapolation scheme might be considered or a higher grid resolution near the stagnation point. Another approach can be constructed with the equivalent Falkner-Skan solution; A Falkner-Skan solution is used where the power m for $x = 0$ is dependent on the external velocity distribution, this Falkner-Skan solution is used for the first steps of the solution procedure. It was suggested in section (I.1.1) to use an estimate for the equivalent m given by the limit value

$$m(0) = \left(\frac{x}{u_e}\frac{\partial u_e}{\partial x}\right)_{x\to 0}. \qquad \text{(I.24)}$$

This will produce an indeterminate value for $u_e(0) = 0$ and l'Hôpital will not resolve the problem for higher order power law distributions, to generalize the approximation it is suggested to approximate $m(0)$ using the values at $x = \Delta x$

$$m(0) \approx \left(\frac{\Delta x}{u_e}\frac{\partial u_e}{\partial x}\right)_{x=\Delta x}, \qquad \text{(I.25)}$$

in case of a numerically prescribed external velocity, as it would be in an actual viscid-inviscid method, then $m(0)$ can be found by

$$m(0) \approx \left(\frac{\Delta x}{u_e}\frac{\Delta u_e}{\Delta x}\right)_{x=\Delta x}. \qquad \text{(I.26)}$$

The Falkner-Skan solution for the above arbitrary value for m can be found by interpolating earlier found values for $f_0^{''}$ and m (see figure (3.3)). The Falkner-Skan solution is very sensitive to the initial value for $f^{''}$, as the solution for larger values for η varies strongly for different values $f_0^{''}$, this has a negative effect on the quality of the initial solution. The sensitivity can be compensated by using a less strict criterium for the

boundary layer thickness; instead of the $\eta_e = 99\%$ used for the main boundary layer calculation it is proposed to use $\eta_e = 95\%$, this avoids the large variance for higher η and it will not introduce a large error in the integral variables since $u \approx u_e$ near the boundary layer edge. Alternatively the shooting method might be employed using a guessed value for $\eta_{99\%}$. Alternatively the guessed value for m can be directly coupled to a value for the shape factor H.

The above approach can be used for methods using a guessed velocity profile and methods using empirical closure relations. if the equivalent Falkner-Skan power $m(0)$ is smaller than 1, δ, δ^* and θ are set to zero and C_f follows from the equivalent Falkner-Skan solution for at $x = F\Delta x$. For $m(0) \leq 1$ all the integral variables follow from the equivalent Falkner-Skan solution at $x = F\Delta x$. The Falkner-Skan values are taken at $x = F\Delta x$ since the solution is singular for $x = 0$, here F is some factor $\langle 0, 1]$, this done to extract the initialisation as close to the stagnation point as possible.

In his PhD-thesis Nishida defines (in reference to White) an attachment line (in spanwise direction) to initiate the boundary layer solution. The values of the momentum thickness and the displacement thickness are taken at a certain arc length from the stagnation point using a stagnation Falkner-Skan solution. The arc length represents the attachment region in which the stagnated flow transitions to an attached boundary layer flow, here it is assumed by default that the transition takes place in maximally one distance step Δx. Following Nishida and Milewski the values for the momentum thickness and the displacement thickness are given by

$$\text{Nishida}: \quad H = 2.21, \quad \theta = 0.29234\sqrt{\frac{\Delta x}{Re_\infty u_{\Delta x}}}, \delta^* = 0.64791\sqrt{\frac{\Delta x}{Re_\infty u_{\Delta x}}}, \tag{I.27}$$

$$\text{Milewski}: \quad H = 2.35, \quad \theta = 0.38574\sqrt{\frac{\Delta x}{Re_\infty u_{\Delta x}}}, \delta^* = 0.90649\sqrt{\frac{\Delta x}{Re_\infty u_{\Delta x}}}. \tag{I.28}$$

The following approach is suggested for the steady IBL equations;

1. Guess momentum thickness through direct integration or use the suggested value by Nishida or Milewski
2. Apply the closure relations for the method of Thwaites to extract the remaining integral variables
3. Apply the method of Thwaites for the first steps

For the purpose of demonstration only 2 stagnation flows will be considered $m = 1$ and $m = 3$, where $\frac{\partial u_e}{\partial x} \neq 0$ and $\frac{\partial u_e}{\partial x} = 0$ respectively. It should be noted that the initial value for the error in the following figures starts at $x = \Delta x$ since the Falkner-Skan solution is not a number for $x = 0$. For $m = 1$ and $m = 3$ the stagnation values for the momentum thickness are approximately equal for Nishida(equation (I.27)) and direct integration (equation (I.23)) , for this reason one stagnation value approach will be used for the plots. For $m = 1$ starting from the initial value the approximate solution for the power law distribution is within % 10 after only two steps in x-direction, increasing the number of steps in x-direction compresses the region in which the initialisation error dominates but this has no notable effect on the error magnitude (see figure I.12). The parameter L indicates the number of steps that the method Thwaites is used after the initialisation, adding one more step using Thwaites brings the initial solution closer to the approximate solution. For $m = 3$ two important observations were made, a minimum of four steps was required using the method of Thwaites, secondly a minimum of 4-point integration was needed to attain a stable solution for the method of Thwaites. Various integration accuracies were tested, the lowest being 4-point integration and the highest being 14-point integration, the number of integration points for the method of Thwaites is indicated by the parameter K.

The dependency of the solution quality on the initial resolution indicates the need for

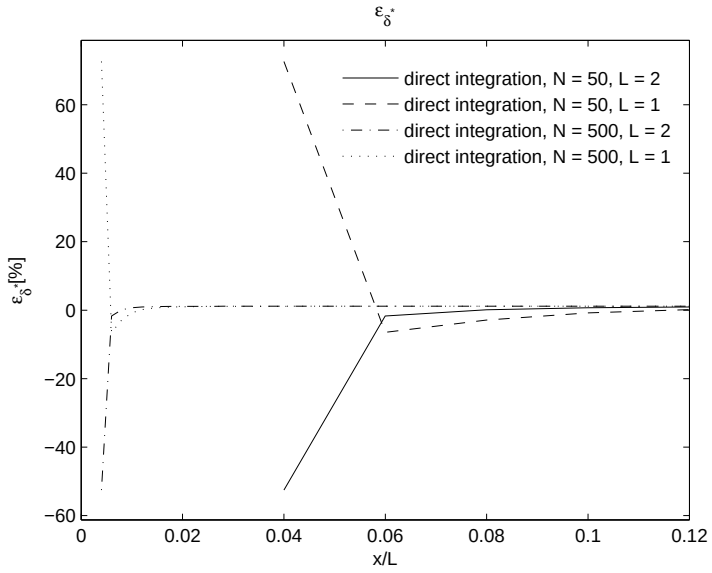

Figure I.12: Initial error using Von Kármán - Pohlhausen method for power law flow with $m = 1$, direct integration stagnation values.

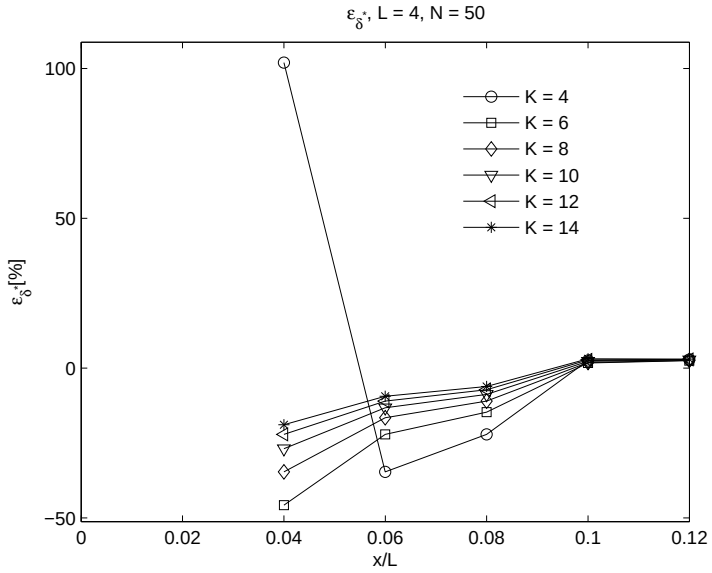

Figure I.13: Initial error using Von Kármán - Pohlhausen method for power law flow with $m = 3$, direct integration stagnation values.

a non-uniform grid and in fact an adaptive grid since the solution near the forward stagnation point will change for each timestep. It is observed by Myring[100] that the unsteady boundary layer equations are very sensitive to initial irregularities if the integration is done in upstream direction and subsequently he recommends to integrate in the downstream direction. This relates to the direction in which the information is transported, and it was already seen that a backward differencing method is required for characteristics which travel in positive direction.

The above initialisation pertains the laminar boundary layer flow, however it has become clear from the text that a turbulent initial boundary layer is possible in wind turbine flow which requires specific initial values, one such initialisation was found in Coenen[26] and is given by

$$\theta = \frac{0.005}{\sqrt[5]{Re}}, \quad H = 1.35. \tag{I.29}$$

I.3.4 Separating Flows

A direct way to determine the robustness of the integral boundary layer formulation is to consider limit cases which lead to an unstable solution and which have physical significance. The occurrence of separation is such a case and many separation cases exist for which there is an exact (theoretical) solution, this allows an important benchmark since the prediction of separation is important for the size of the wake which in turn is the largest contributor to the total pressure drag of any profile or indeed an entire wind turbine. Several velocity distribution will be considered, the focus is on the prediction of the separation location. The exact separation values are taken from White[154, tab.4-5], the criterion used to establish separation is

$$\lambda = \frac{\theta^2}{\nu}\frac{du_e}{dx} = -0.09$$

The tested methods are reasonably close to the exact separation values, the Timman

velocity profile ↓	Exact	Pohl.	Alt.	Drela	Thwaites	Timman
Separation point$[m]$ →						
$1-x$	0.120	0.114	0.133	0.123	0.123	0.136
$1-x^2$	0.271	0.258	0.285	0.257	0.268	0.286
$1-x^4$	0.462	0.440	0.468	0.442	0.449	0.464
$1-x^8$	0.640	0.615	0.638	0.618	0.621	0.631
$x-x^3$	0.655	0.642	0.662	0.636	0.648	0.657
$\sqrt{1-x}$	0.218	0.207	0.239	0.202	0.221	0.243
$(1-x)^2$	0.0637	0.0602	0.0709	0.0584	0.0652	0.0728
$(1+x)^{-1}$	0.151	0.1436	0.1733	0.1384	0.158	0.181
$(1+x)^{-2}$	0.0713	0.0675	0.0807	0.0653	0.0739	0.0835
$\sin(x)$	1.823	1.778	1.840	1.757	1.800	1.828
$\cos(x)$	0.389	0.368	0.408	0.366	0.384	0.407
$\lvert$average deviation$\rvert$	...	4.46%	6.67%	2.98%	2.27%	8.06%

Table I.4: Comparison of separation values for a range of external velocity profiles, For Timman $\lambda_{min} = -0.0832$ was used

profile in combination with the Von Kármán equation resulted in a minimum for the profile parameter λ near the exact separation value. It was observed that Timman resulted in $C_f = 0$ very close to the exact separation values which is in accordance with the generally accepted idea that the wall friction C_f is zero at separation. A reversed result was found for the closure of Drela with the Von Kármán equation and the energy equation, although the accordance was good using the earlier defined separation criterion Drela did not reach $C_f = 0$ near the separation point based on the separation criterion.

The integral variables increase exponentially surrounding the separation point for the $sin(x)$ velocity distribution (see figure I.14) a development which is much less pronounced for the $1-x$ velocity distribution(see figure I.15).

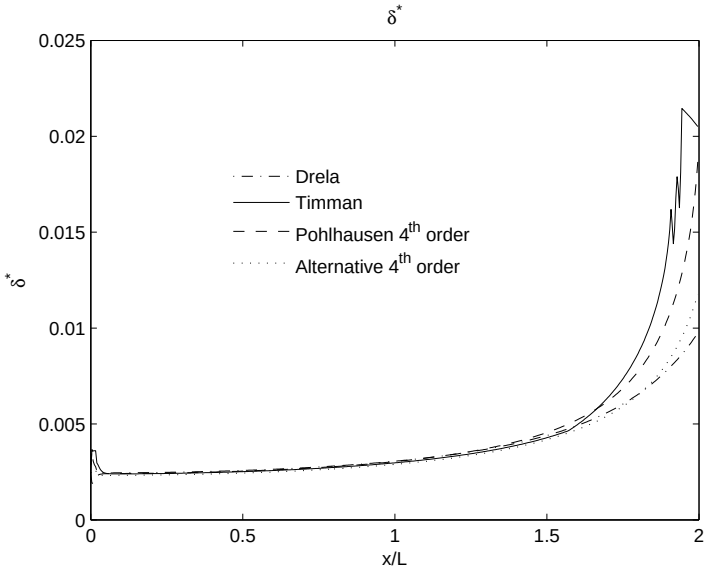

Figure I.14: Comparison of δ^* for different profiles with a $\sin(x)$ velocity distribution

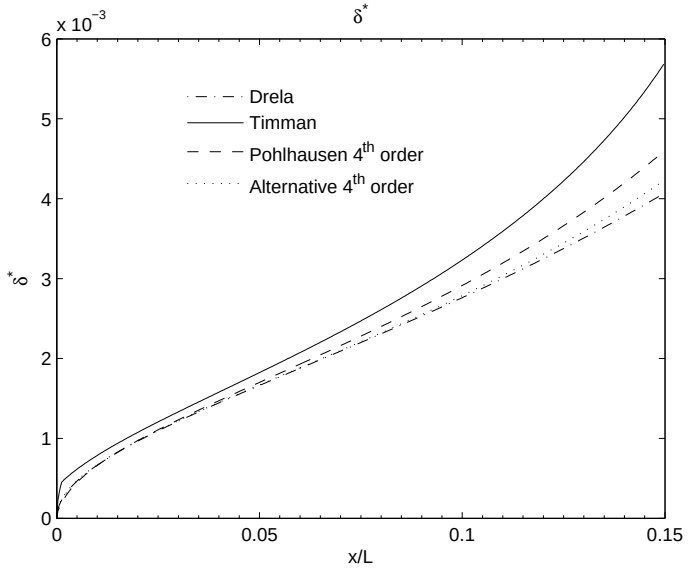

Figure I.15: Comparison of δ^* for different profiles with a $1 - x$ velocity distribution

It is apparent that increasing the order of the polynomial velocity profile does not increase the accuracy of the separation prediction (see figure (I.16)).

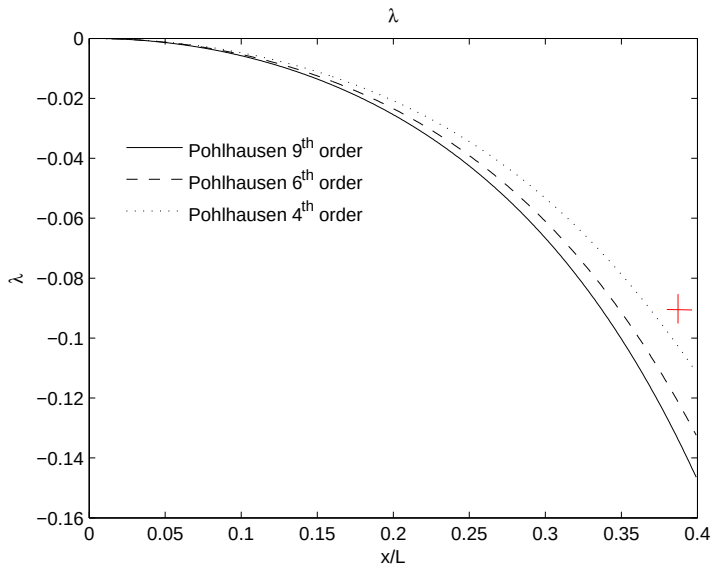

Figure I.16: Comparison of λ for different profiles with a $\cos(x)$ velocity distribution, here the exact separation location is indicated by the red cross

I.4 Unsteady Test Cases

I.4.1 Actual Blade Profile with Unsteady Perturbations

As was mentioned the current treatise on the two dimensional integral boundary layer equations is meant to assist in the selection of the closure models and the discretisation methods to be used in a three dimensional unsteady integral boundary layer solver for windturbine analysis. Henceforth the external velocity profile should be representative of unsteady boundary layer flow over a typical profile section used in windturbines. It makes sense to test the integral boundary layer solver seperately from the unsteady potential flow solver. Given a known set of velocity distributions for e.g. various angles of attack the behavior of the integral boundary layer equations can be tested without coupling. For a typical profile consider the NACA 64(3)618, see figure (I.17). To find the velocity distribution using a potential flow the program XFOIL is applied. The unsteadiness is assumed to be caused by flutter and turbulence, the flutter induced instantaneous unsteadiness will cause the external velocity distribution over the entire profile to change more or less uniformly. Turbulence is assumed to behave like a small periodic perturbation from the resulting velocity. The flutter induced velocity in the normal direction is of equal order as the flutter induced velocity in the tangential direction but both induced velocities are about two orders of magnitude smaller than the free stream velocity (see Lobitz[86]). The frequency of the flutter is assumed to be constant at $0.7\ Hz$(see Lobitz[86]), whereas the perturbation due to turbulence is assumed to be oscillating at a frequency two orders higher, $700\ Hz$. The assumed perturbation is now represented using sines

$$u_{e,pert} = \beta_{turb} \sin(1400\pi t) + \beta_{flut} \sin(1.4\pi t),$$
$$\beta_{turb} \ll \beta_{flut} \approx \frac{1}{100} V_{inf}.$$

This perturbation is then added to the velocity profile for the inviscid potential flow over the NACA 643618 profile (see figure I.18). The mean velocity profile is given by the potential flow solution of the airfoil at various angles of attack. Now to simulate flutter the angle of attack of the airfoil is changed over time, then using the potential flow

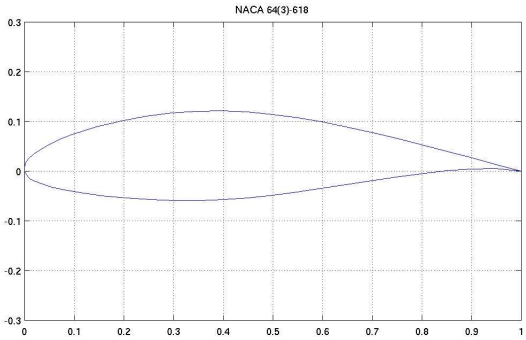

Figure I.17: airfoil profile NACA 643618.

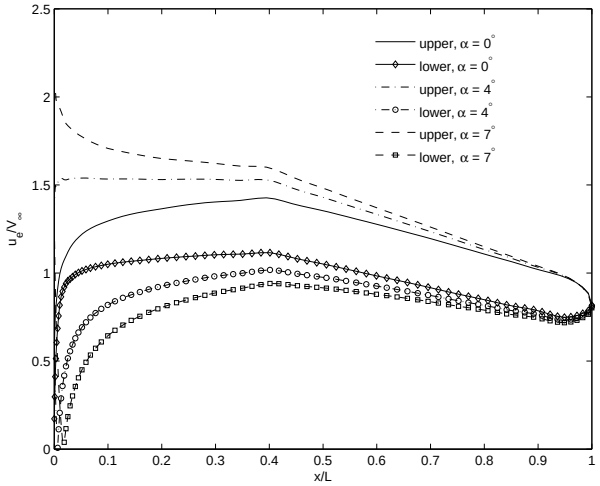

Figure I.18: NACA 643618 Potential flow velocity distribution.

results for a set of angles the values for the specific angle of attack is retrieved through interpolation. Now β_{flut} follows from interpolation for a specific angle $\alpha = \alpha_{max} \sin 1.4\pi t$. For comparison the numerical reference solution will be used. Due to the external turbulence the transition checks which employ the Falkner-Skan solution should be to generous. The external turbulence is likely to shift the transition point upstream, therefore a bypass transition model will be used for comparison.

I.4.2 Double Harmonic for the Finite Flat Plate

The oscillations considered so far assume that there is some velocity distribution over the flat plate which is perturbed periodically independent of x, meaning the temporal and spatial dependence of the external velocity are decoupled. A more realistic test case involves harmonic behaviour of the external flow in both temporal and spatial

dimension. The simplest form involves a mean velocity with harmonic fluctuations, i.e.

$$u_e = u_{e,0}\left(1 + Af(x,t)\right),$$

where $|A| \ll 1$ and $f(x,t)$ is arbitrarily chosen as e.g.

$$f(x,t) = \sin(2\pi\omega_1\zeta) * cos(2\pi\omega_2\alpha). \tag{I.30}$$

where $\alpha = \frac{x}{L}$ is the relative distance with respect to the plate length and $\zeta = \frac{t}{t_{end}}$ is the relative time with respect to the end time. Note that the velocity distribution in x-

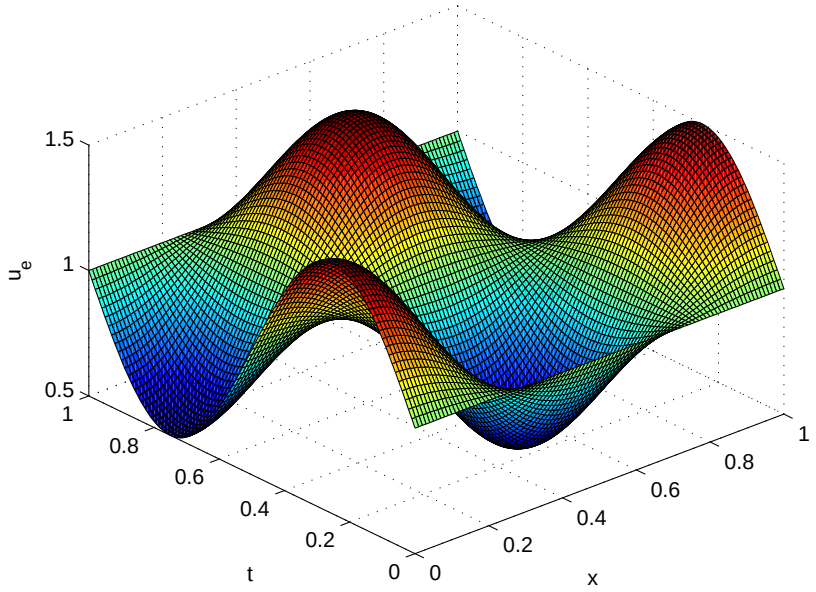

Figure I.19: Velocity distribution(equation(I.30)) with $\omega_1 = 1, \omega_2 = 1, A = 0.5$.

direction implies a non-flat plate geometry, however since the perturbation is assumed to be very small with respect to the mean velocity this can still be considered a physically meaningful test case. This test case lacks a reference result, this may be found by applying the field form of the boundary layer equations. Also, with respect to the example form of the double harmonic , the frequencies of the space dependent part and the time dependent part can be varied independently which allows for a good benchmark of the robustness of the IBL code. Since a flat plate geometry is still assumed no coordinate transformation is necessary.

I.4.3 Literature on Unsteady Test Cases

Experimental data on unsteady flat plate flow is rather limited to oscillatory external velocity inputs (see Cebeci[22, §9.10]) for both laminar and turbulent flow. There also exist limit solutions of the BL equations for the case of the flat plate which allow for direct integration, the most basic limit solution is the case of quasi-unsteadiness, this is however directly reflected in the (adapted) Pohlhausen parameter and thus in the solution and is therefore ignored as a trivial case. The impulsively started semi-infinite flat plate was treated by Stokes(1856) and Rayleigh(1911). Later in the fifties and sixties work concentrated on oscillating free streams and oscillating flat plates. The limit

solutions arose for small amplitude and/or for low and high frequency oscillations.
For the more challenging case of arbitrary external velocity there are series solutions for the unsteady flat plate BL flow, these series solutions should hold for small times,see i.e. Moore[96], Cousteix[28], Wirz[158]. Moore[96] gave a series solution for the flat plate boundary layer flow with arbitrary time-dependent external velocity, Ostrach(1955) continued his work as did Kestin et al(1960) and Yang,King(1966) and Huang(1969), these solutions are however limited to very short or very long times. The boundary layer solutions using series solutions and asymptotic expansions are, for the present work, to involved to use as a reference result. There are however analytical solutions possible in the limit of certain solutions or for certain limit problems, i.e. for large time or for an infinite flat plate.
The simplest unsteady case with the flat plate was analysed by Lord Rayleigh in 1911, this problem involves an infinite flat plate which is moved instantaneously. The Rayleigh problem has an analytical solution as does the case of the oscillating infinite flat plate which is described by Stokes solution. The instantaneously moved semi-infinite flat plate has been solved by for instance Hall [59].
Lighthill[84] gave a solution for a steady external flow with very high or very low frequency disturbance, the results were confirmed by Lin [85] and Phillips[2]. Another simplified model due to Rott and Rosenzweig [115] which also uses a two component periodic external flow assumes there is a weak periodic perturbation, this model allows for high and low frequencies.

I.4.4 Impulsively Started Infinite Flat Plate

The problem is defined as follows, a flat plate is moved such that it instantaneously achieves a velocity u_w which is subsequently constant in time, since it is infinitely long there are no gradients in the direction of the plate. Also known as the first Stokes problem, the first limit case that will be considered is the impulsively started infinite flat plate in a fluid at rest. The flat plate is set into motion with velocity u_w. Given the

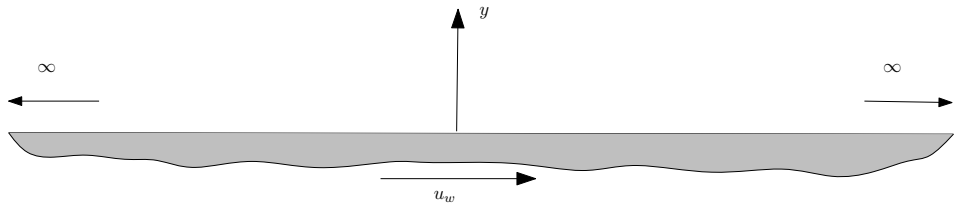

Figure I.20: Infinite flat plate problem.

infinite length of the plate variation in x-direction can be ignored, the BL momentum equation is now reduced to the simplest parabolic equation

$$\frac{\partial u}{\partial t} = \nu \frac{\partial^2 u}{\partial y^2}, \tag{I.31}$$

with boundary conditions

$$\begin{aligned} t \leq 0, \quad & y \geq 0, \quad u = 0, \\ t > 0, \quad & y = 0, \quad u = u_w, \\ & y \to \infty, \quad u = 0. \end{aligned}$$

Introducing the dimensionless variable $\eta = \frac{y}{2\sqrt{\nu t}}$ the heat equation can be rewritten as

$$\begin{aligned} f^{''} + 2\eta f^{'} &= 0, \\ f(0) = 1, \quad f(\infty) &= 0, \end{aligned}$$

where $f(\eta) = \frac{u}{u_w}$.
The solution is now given by

$$\begin{aligned} f &= 1 - erf(\eta), \\ \text{error function: } erf(\eta) &= \frac{2}{\sqrt{\pi}} \int_0^\eta e^{-\eta^2} d\eta. \end{aligned} \tag{I.32}$$

As was said the boundary condition for the IBL relations assume the wall is fixed, the solution can be altered easily to fit the case where the external flow velocity u_e is set into motion impulsively; this is equivalent to the case where the plate is moved impulsively to the left with $u_w = -u_e$, then fixing the reference frame on the plate results in

$$f = 1 - \big(1 - erf(\eta)\big) = erf(\eta).$$

This result is used to initialise the flat plate simulation with the IBL equations, this approach is naturally suited to handle the laminar BL. For the turbulent case

I.4.5 Oscillating Infinite Flat Plate

This step-solution can be extended to arbitrary $u_w(t)$; since boundary layer equation (I.31) is linear the solutions for velocity steps Δu_w can be integrated through convolution to obtain a solution for $u_w(t)$. This will lead to Duhamel's folding integral (see i.e. Schlichting[118])

$$u_D(y,t) = \frac{y}{2\sqrt{\pi\nu}} \int_{-\infty}^{t} \frac{u_w(\tau)}{(t-\tau)^{\frac{3}{2}}} e^{-\frac{y^2}{4\nu(t-\tau)}} d\tau. \tag{I.33}$$

A specific solution is the second Stokes problem which deals with an oscillating infinite flat plate, where the oscillation is defined as

$$u_w(0,t) = u_0 \cos(\omega t), \tag{I.34}$$

with the solution

$$\frac{u}{u_w} = \frac{e^{-\eta}\cos(\omega t - \eta)}{\cos(\omega t)}, \tag{I.35}$$

where $\eta = \sqrt{\frac{\omega}{2\nu}} y$.
It was already mentioned that this solution assumes the wall to move oscillatory whereas in the present case the wall is considered static. As was said the solution can be adapted in a straightforward manner to the boundary condition $u_e = |u_w|$ by considering a reference frame fixed to a moving flat plate with velocity $u_w = -u_e$, the equivalent solution is

$$\frac{u}{u_e} = 1 - \frac{e^{-\eta}\cos(\omega t - \eta)}{\cos(\omega t)}, \tag{I.36}$$

and in general given Duhamel's folding integral

$$\frac{u}{u_e} = 1 - \frac{u_D(y,t)}{u_e}. \tag{I.37}$$

I.4.6 Impulsively moved Semi-Infinite Flat Plate

For the semi-infinite flat plate the sudden change is convected through the flow until the entire flow domain at the boundary is steady, i.e. the velocity distribution differs in x-direction (see figure (I.21)). The final solution is readily available through the Blasius equation. For small times the solution can be approximated by the Rayleigh solution at the edge of the boundary layer, from Stewartson[126], Smith[124] :

$$\begin{aligned} u_e\, t < x \quad & \frac{u}{u_e} = erf\left(\frac{y}{2\sqrt{\nu\, t}}\right), \\ u_e\, t > x \quad & \frac{u}{u_e} = erf\left(\frac{y}{2}\sqrt{\frac{u_e}{\nu\, x}}\right). \end{aligned}$$

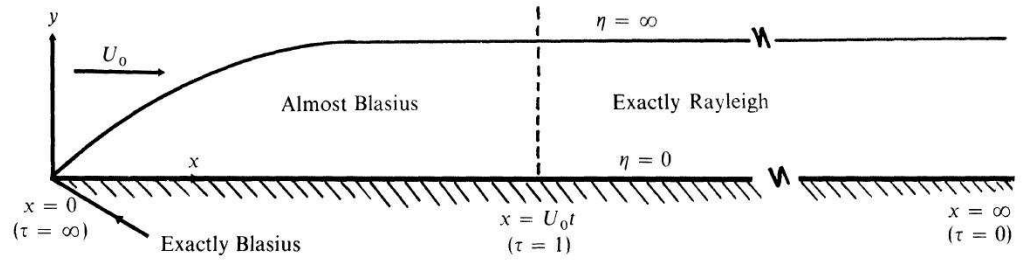

Figure I.21: Impulsively started flow over a semi-infinite flat plate, see Riley[112].

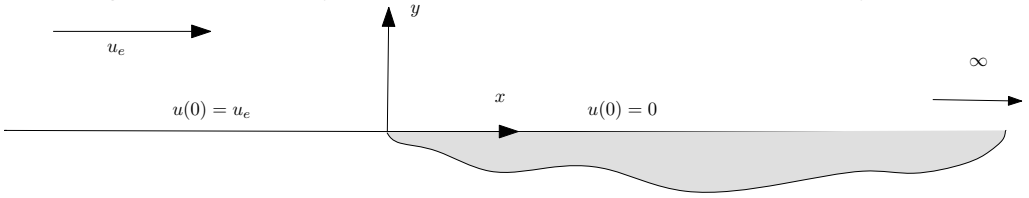

Figure I.22: Sketch of semi-infinite flat plate problem.

Stewartson gives the following approximation for the drag for $u_e\, t < x$

$$\frac{\tau_w}{\mu} = \frac{u_e}{\sqrt{\pi \nu B}}, \quad B = \min\left(t, \frac{x}{u_e}\right).$$

Using the momentum-integral Stewartson derived a solution for the wall shear force which should agree well with both the Rayleigh method and the Blasius solution

$$u_e t \leq 2.65x, \quad \left(\mu \frac{\partial u}{\partial y}\right)_0 = 0.534 \rho\, u_e \sqrt{\frac{\nu}{t}},$$
$$u_e t \geq 2.65x, \quad \left(\mu \frac{\partial u}{\partial y}\right)_0 = 0.328 \rho\, u_e \sqrt{\frac{u_e\, \nu}{x}}.$$

If the disturbance at the leading edge does not influence the solution, the solution is independent in chordwise direction, in case of an instantaneously moved flat plate this results in a Rayleigh solution and in case of an oscillating profile the solution due to Stokes can be applied. Extending this idea it should be possible to use Duhamel's folding integral for arbitrary velocity distributions (over time), the range over which this solution can be considered is then (also see Yang[159])

$$\int_0^t u_e(t) dt \leq x.$$

After approximately four seconds the steady state should be reached, in other words the Blasius solution is attained, see e.g. Hall[59].

I.4.7 Oscillating Free Stream Velocity for the Semi-Infinite Flat plate

Instead of an oscillating infinite flat plate, now imagine that the free stream over the semi-infinite flat plate is perturbed slightly and imagine that the perturbation can be described by a periodic function. Consider for the free stream the following function (see i.e. Schlichting[118], Lighthill[84])

$$u_e = u_{e,0}(x)\left(1 + \epsilon e^{i\omega t}\right),$$

and for the response

$$u = u_0 + \epsilon u_1 e^{i\omega t}, \quad v = v_0 + \epsilon v_1 e^{i\omega t}.$$

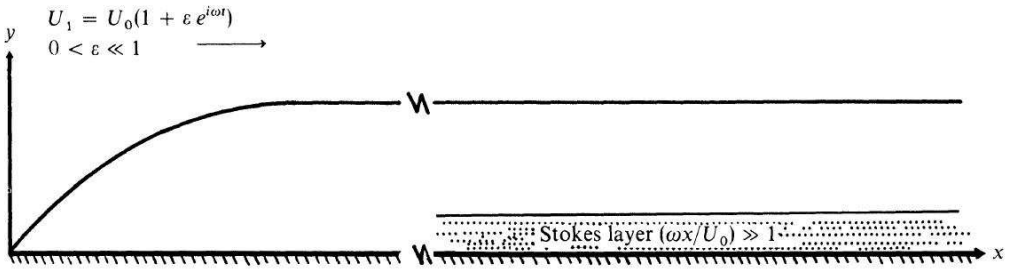

Figure I.23: Free stream with oscillation around the mean, see Riley[112].

The response evolves around the mean, for a constant mean velocity $u_{e,0}$, u_0 and v_0 are represented by the Blasius solution. Lighthill[84] substitutes the new variables in the boundary layer equations and separates the real and complex solutions. Lighthill treats the case for high and low frequency separately, high and low frequency are based on the frequency ω_0 which is defined as

$$\omega_0 = \frac{3\tau_0}{\rho u_{e,0}\delta_0^*}.$$

The real valued solutions for u are approximated by

$$\omega \ll \omega_0, \quad u = u_{e,0}\left(1 - (1-\eta)^2\left(1 - \left(1 + \frac{1}{4}\Lambda\right)\eta - \left(3 - \frac{1}{2}\Lambda\right)\eta^2\right)\right),$$

$$\omega \gg \omega_0, \quad u = u_{e,0}\left(1 - e^{-y\sqrt{\frac{\omega}{2\nu}}}\cos\left(y\sqrt{\frac{\omega_0}{2\nu}}\right)\right),$$

where $\Lambda = \frac{\delta^2}{\nu}\frac{du_e}{dx}$ and $\eta = \frac{y}{\delta}$. For the skin friction coefficient Cebeci extracted the following from Lighthill's paper (see Cebeci[19] and Lighthill[84])

$$C_f = \frac{1}{2}\sqrt{Re_x}\begin{cases} 0.332 + \epsilon\left(0.498\cos(\omega t) - 0.849\frac{\omega x}{u_e}\sin(\omega t)\right), & \lambda(x) \ll 1, \\ 0.332 + \epsilon\sqrt{\frac{\omega x}{u_e}}\cos(\omega t + \frac{1}{4}\pi), & \lambda(x) \gg 1, \end{cases}$$

where $\lambda(x) = \frac{\omega x}{u_e}$ is called the frequency parameter. If for the present case the Blasius solution is assumed for the mean flow then

$$A = 0.15, \quad \tau_0 = 2\frac{\mu u_{e,0}}{\delta}, \quad \delta_0^* = 0.3\delta.$$

According to Riley the solution for $\lambda(x) \gg 0$ is a combination of the Blasius solution for the outer layer (the Prandtl layer) and the Stokes solution near the wall (the Stokes layer).

Simplifying a method due to Lin, Warsi[150] gives the solution for large values of the frequency parameter λ with normal sized amplitudes. The input oscillation in x-direction is

$$u_e^{'} = u_{e,0}\sin(nt). \tag{I.38}$$

The solution for $\zeta \to \infty$ is then given by

$$u^{'} = u_{e,0}\left[\sin(nt) - e^{-\frac{\eta}{\delta_0}}\sin(nt - \frac{\eta}{\delta_0})\right], \tag{I.39}$$

with for the boundary layer thickness

$$\delta_0 \sim \sqrt{\frac{2\nu}{n}}. \tag{I.40}$$

The previous infinite cases are useful as theoretical reference results, however they will not suffice as final test cases since their infinite nature prevents a numerical implementation. The cases considered are basically of semi-infinite nature since no wake interaction will be incorporated, as has been said, it is assumed that no changes in the solution are introduced through the right boundary.

Appendix J

Additional Plots

J.1 Laminar Flat Plate

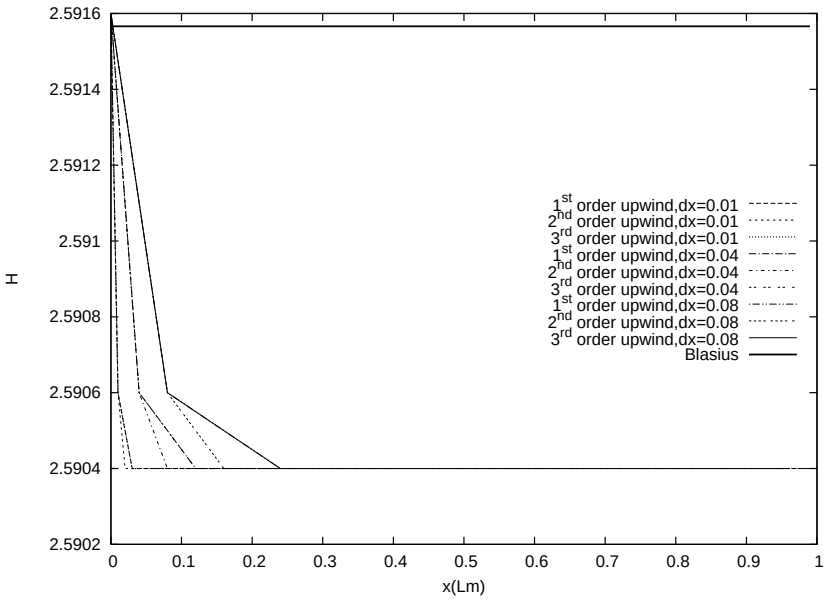

Figure J.1: Result for the upwind schemes,$RK = 2$,$CFL = 0.5$ at $t = 4.5(s)$

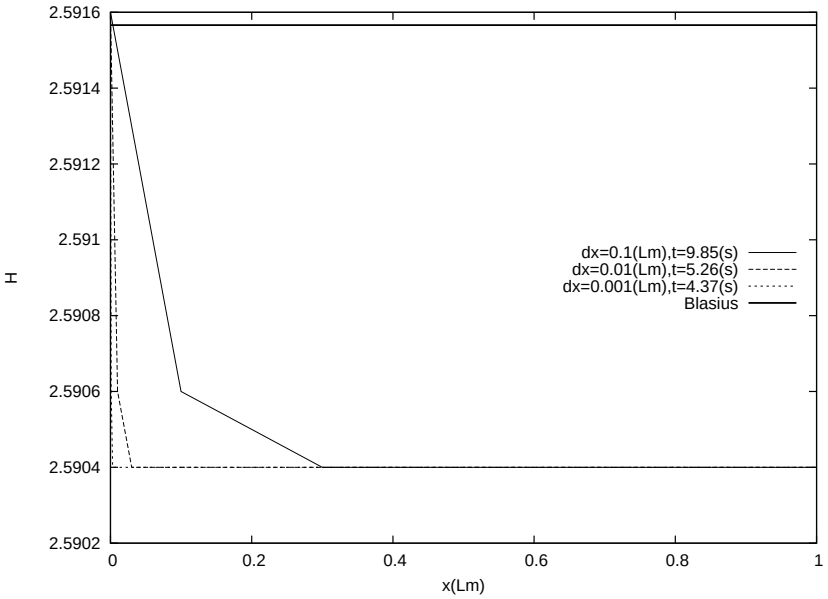

Figure J.2: Shape factor H converged solution for the first order upwind scheme, RK2 time integration, $\Delta x = 0.001\ m$

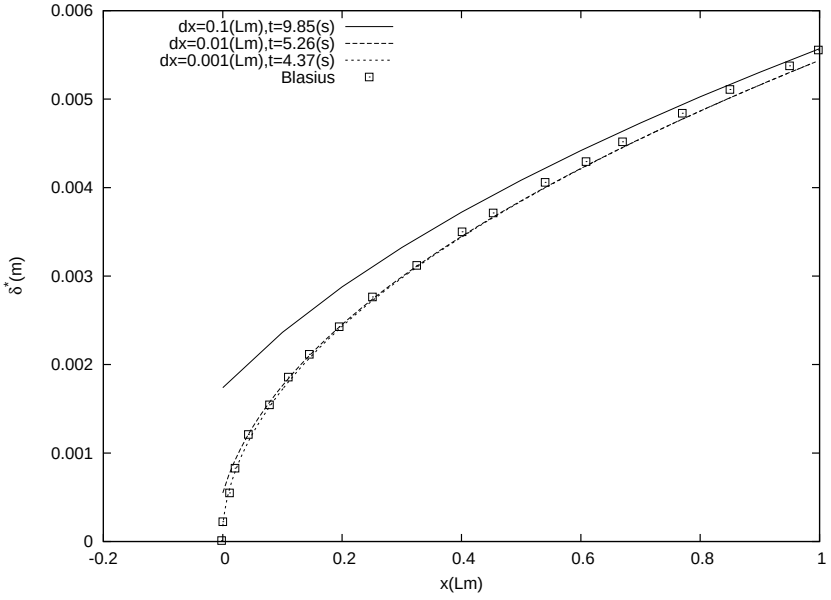

Figure J.3: Shape factor δ^* converged solution for the first order upwind scheme, RK2 time integration, $\Delta x = 0.001\ m$

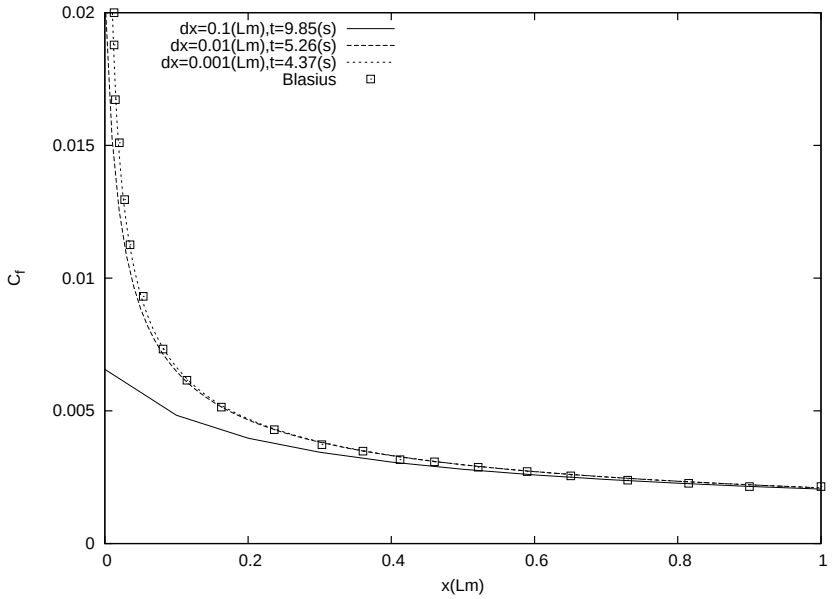

Figure J.4: Shape factor C_f converged solution for the first order upwind scheme, RK2 time integration, $\Delta x = 0.001\ m$

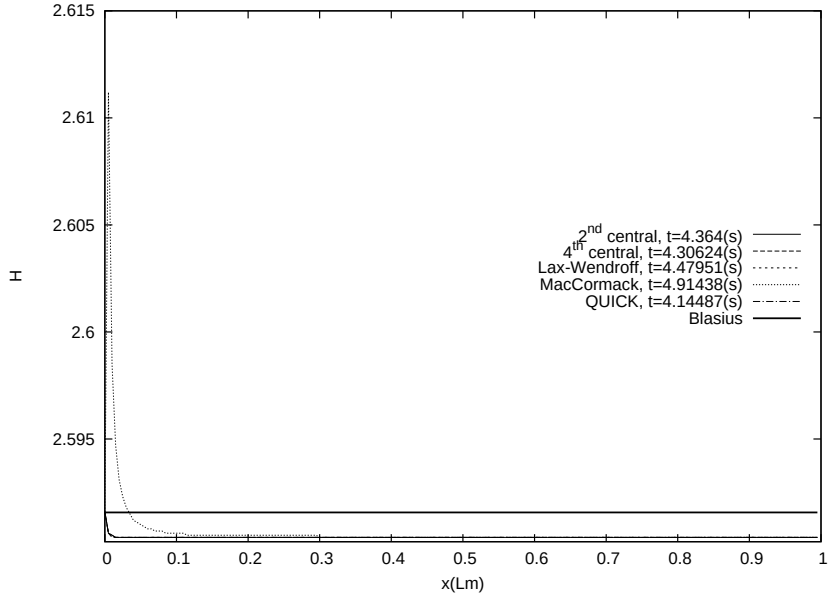

Figure J.5: The various FDM schemes with converged result

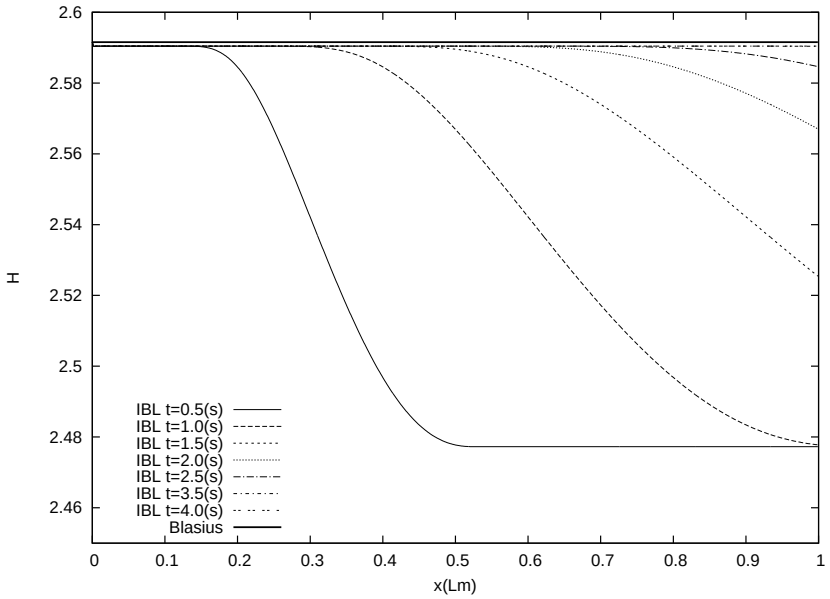

Figure J.6: Shape factor$H$ from transient solution for second order upwind with RK2 time integration,$CFL = 0.5$

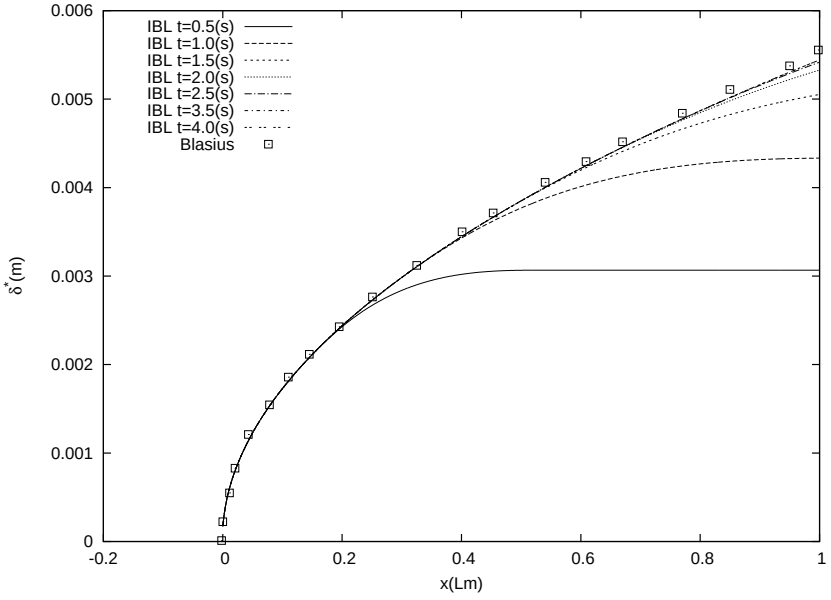

Figure J.7: Displacement thickness δ^* from transient solution for second order upwind with RK2 time integration,$CFL = 0.5$

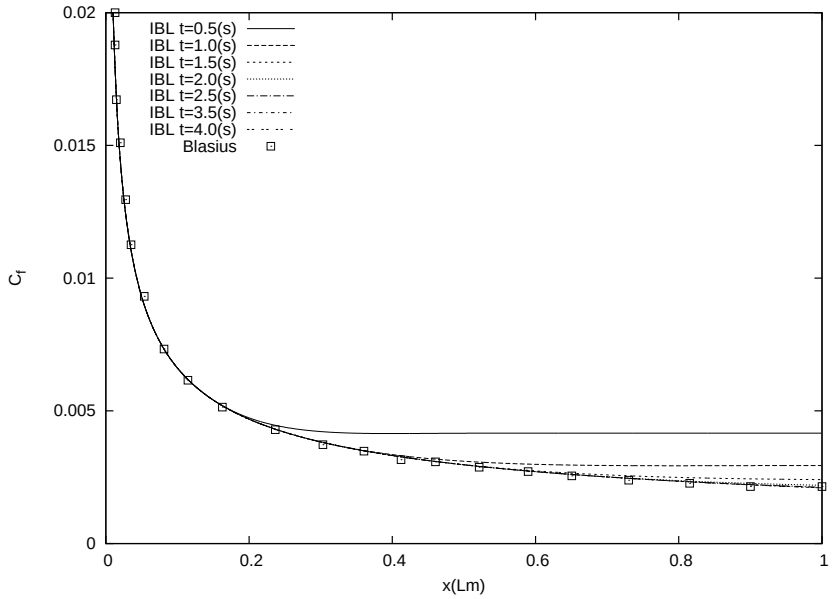

Figure J.8: Friction coefficient C_f from transient solution for second order upwind with RK2 time integration,$CFL = 0.5$

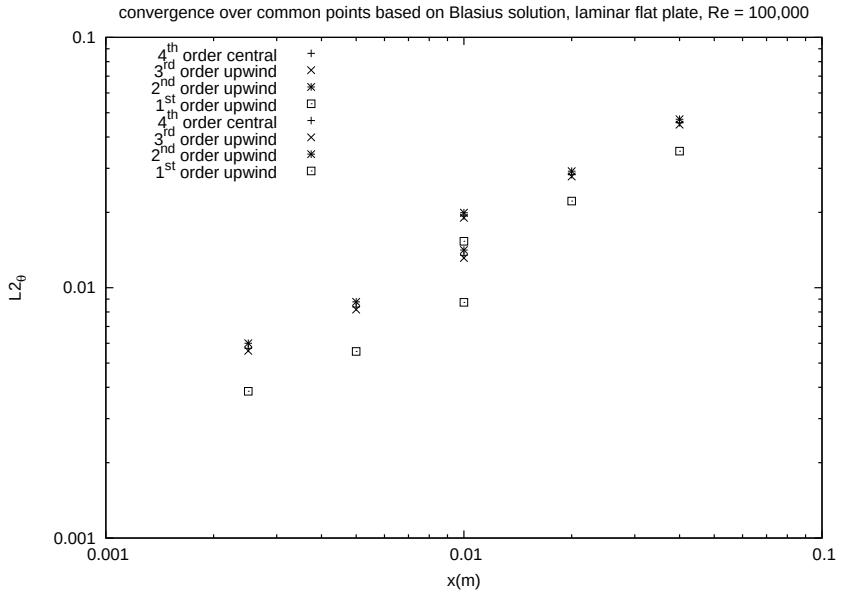

Figure J.9: L2 error norm over common points

J.2 Turbulent Flat Plate

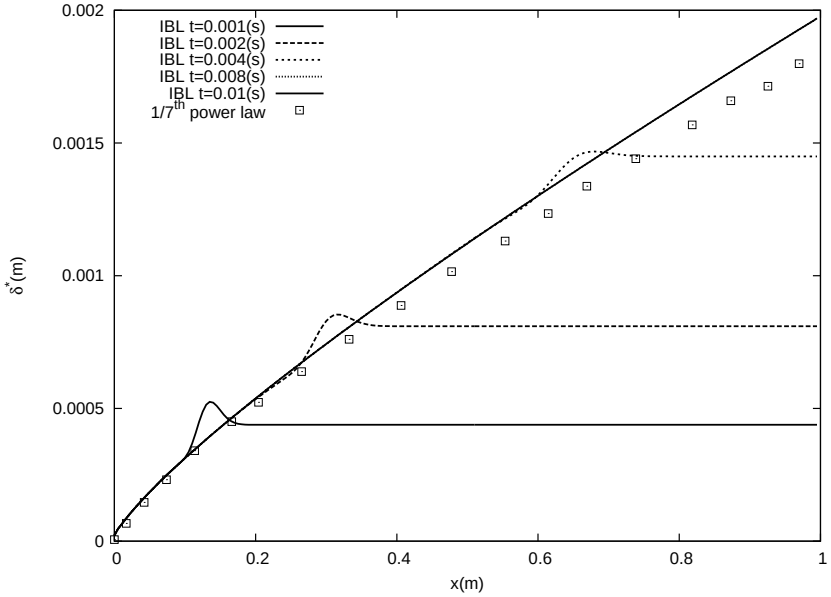

Figure J.10: Turbulent flat plate, $Re = 10e6$, run with MacCormack scheme, $\Delta x = 0.01$,$CFL = 0.25$

J.3 Transition Flow over Flat Plate

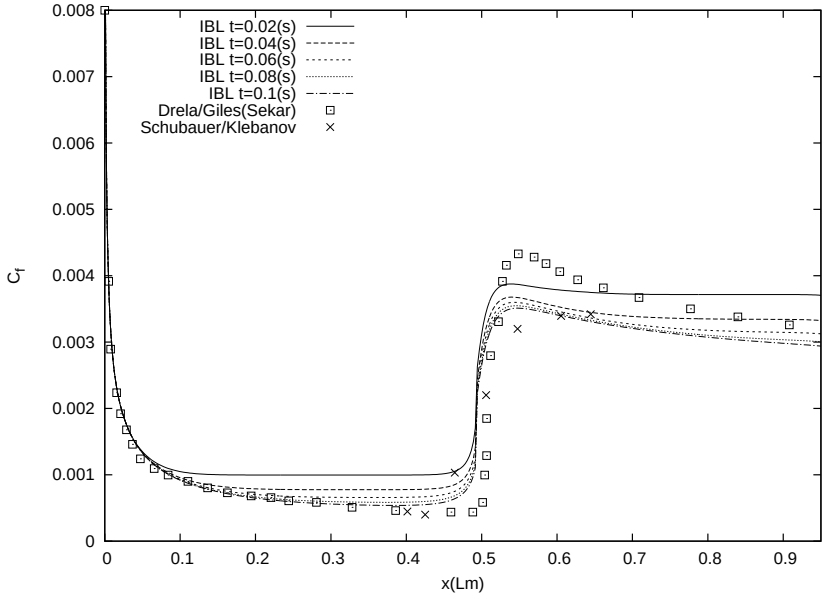

Figure J.11: Friction coefficien C_f for transition flow over flat plate without intermittency function, $Re = 6.25e6$, run with first order upwind scheme, $\Delta x = 0.01$,$CFL = 0.25$

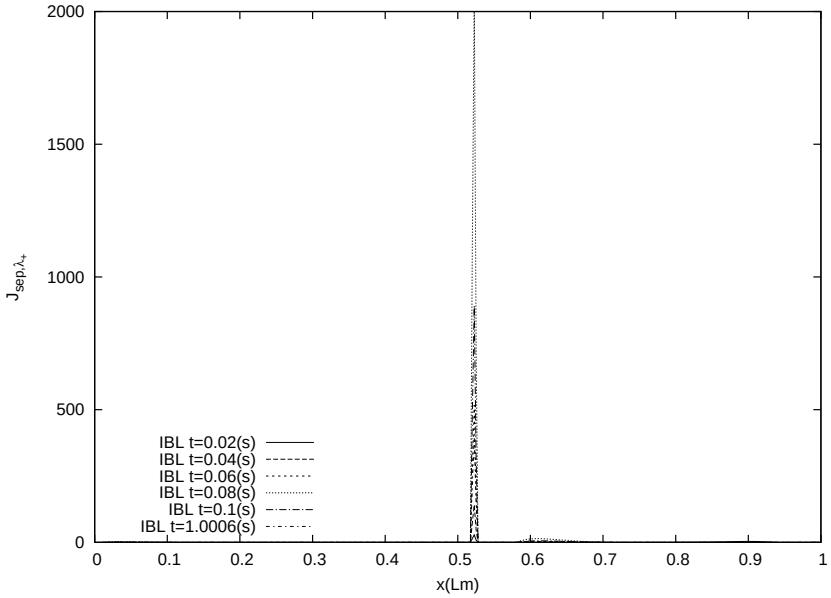

Figure J.12: Separation indicator J_{sep,λ_+} for transition flow over flat plate without intermittency function, $Re = 6.25e6$, run with fourth order central scheme, $\Delta x = 0.01$,$CFL = 0.25$

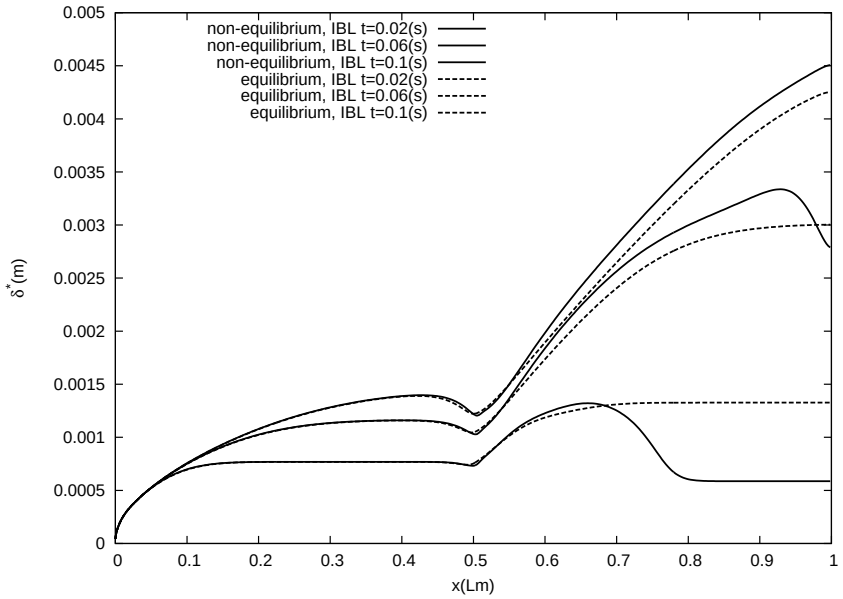

Figure J.13: Displacement thickness δ^* for transition flow over flat plate without intermittency function, $Re = 6.25e6$, run with QUICK scheme, $\Delta x = 0.01$,$CFL = 0.25$

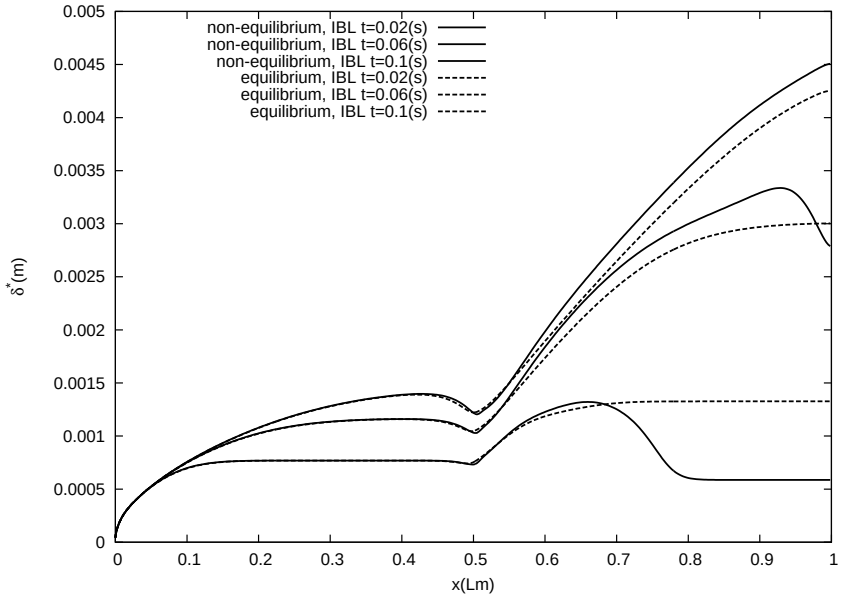

Figure J.14: Displacement thickness δ^* for transition flow over flat plate with and without smoothing

J.4 Unsteady Laminar flow over Flate Plate

J.5 Unsteady Turbulent flow over Flate Plate

J.6 Impulsively Moved Cylinder

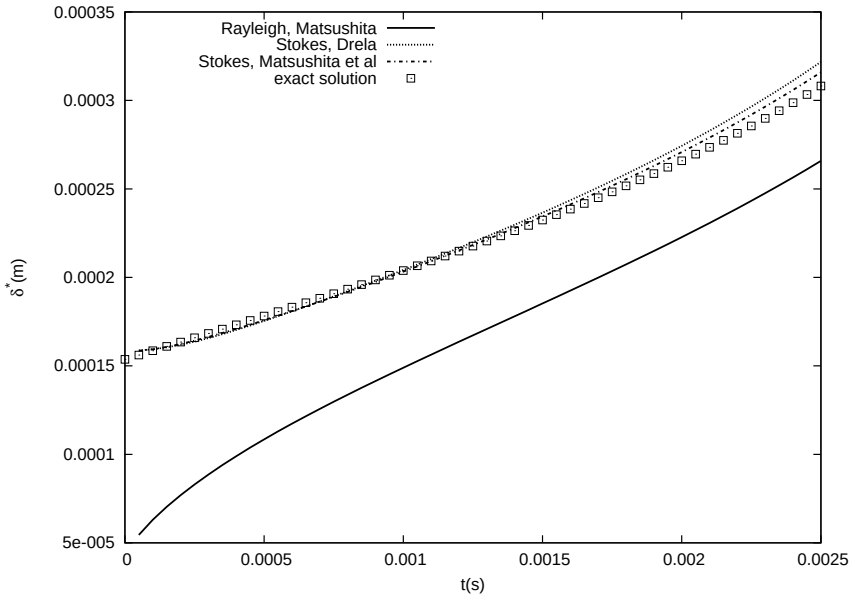

Figure J.15: Oscillating flate plate, displacement thickness δ^* at center of plate, run with QUICK scheme, RK4 time integration, $\Delta x = 0.00025$,$CFL = 0.5$, $\delta_{100\%}$

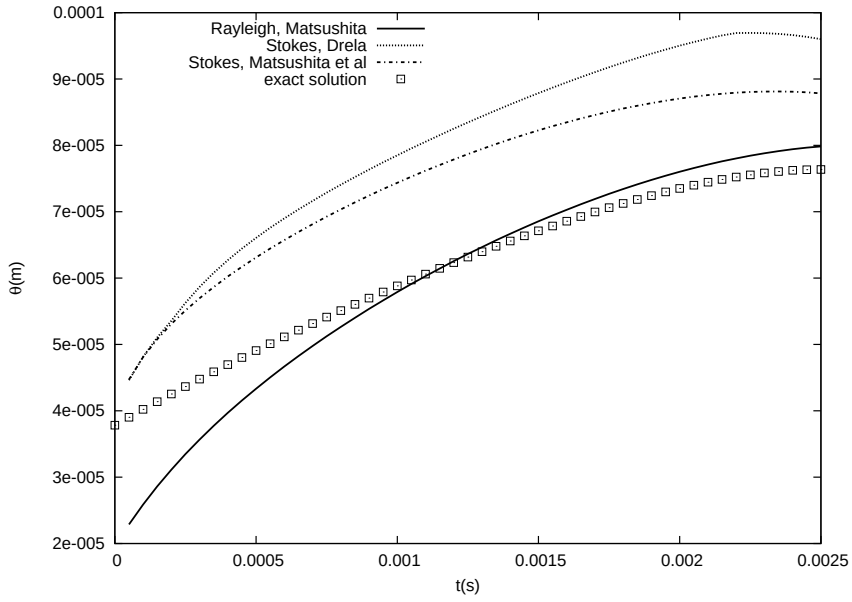

Figure J.16: Oscillating flate plate, momentum thickness θ at center of plate, run with QUICK scheme, RK4 time integration, $\Delta x = 0.00025$,$CFL = 0.5$, $\delta_{100\%}$

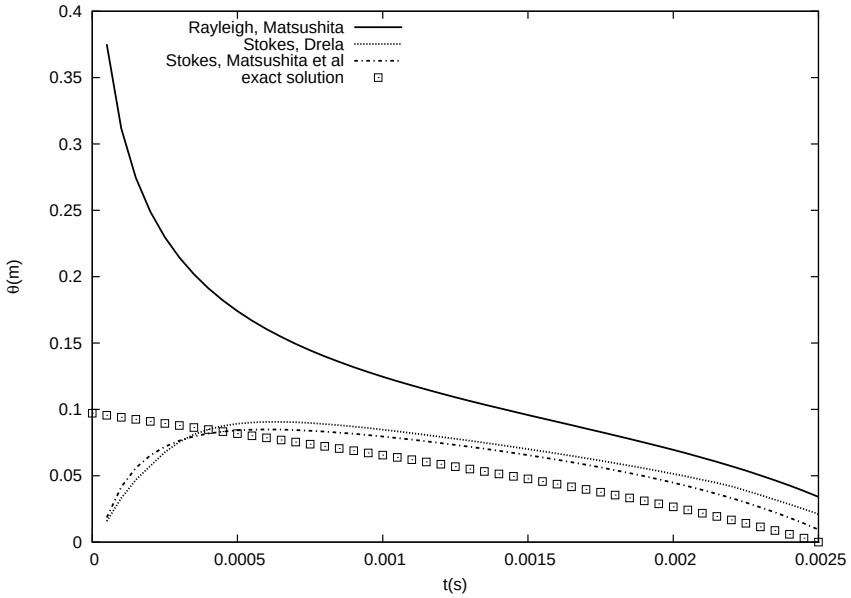

Figure J.17: Oscillating flate plate, momentum thickness θ at center of plate, run with QUICK scheme, RK4 time integration, $\Delta x = 0.00025$,$CFL = 0.5$, $\delta_{100\%}$

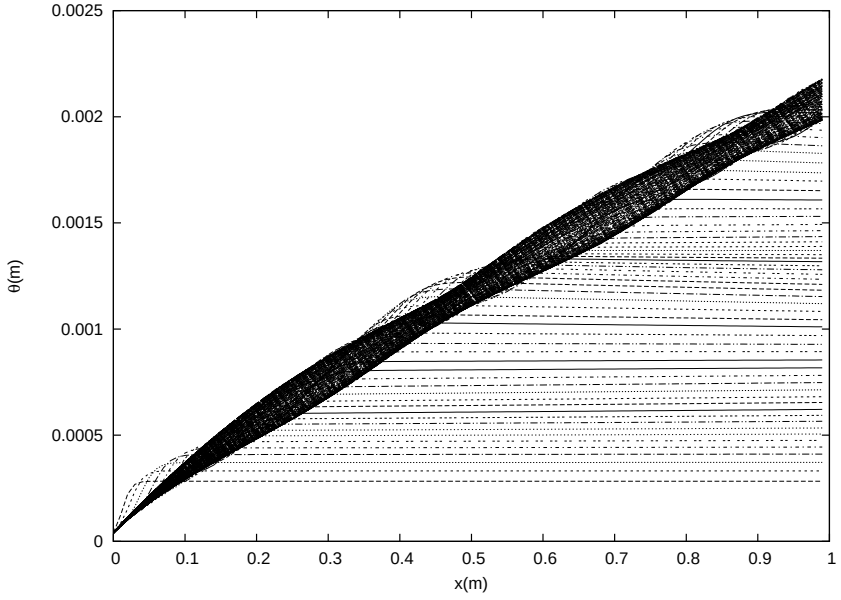

Figure J.18: Momentum thickness θ over ≈ 10 periods for the low frequency case with equilibrium closure

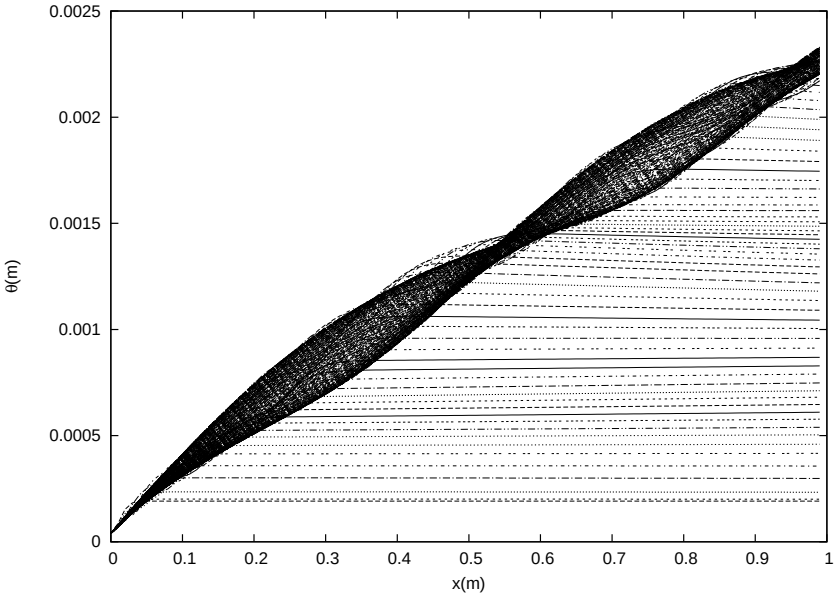

Figure J.19: Momentum thickness θ over ≈ 10 periods for the low frequency case(left) with non-equilibrium closure

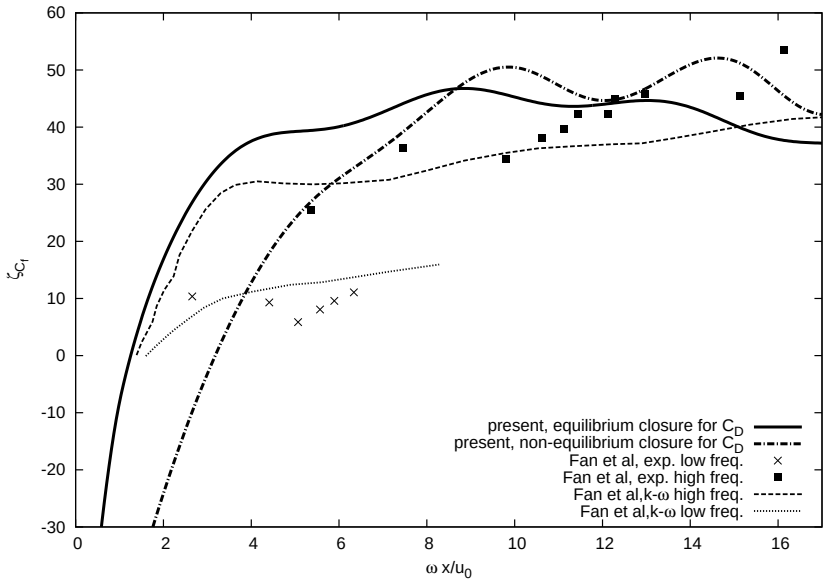

Figure J.20: Oscillating turbulent flate plate with non-equilibrium closure, RK2 , run with QUICK scheme, $\Delta x = 0.002$,$CFL = 0.25$

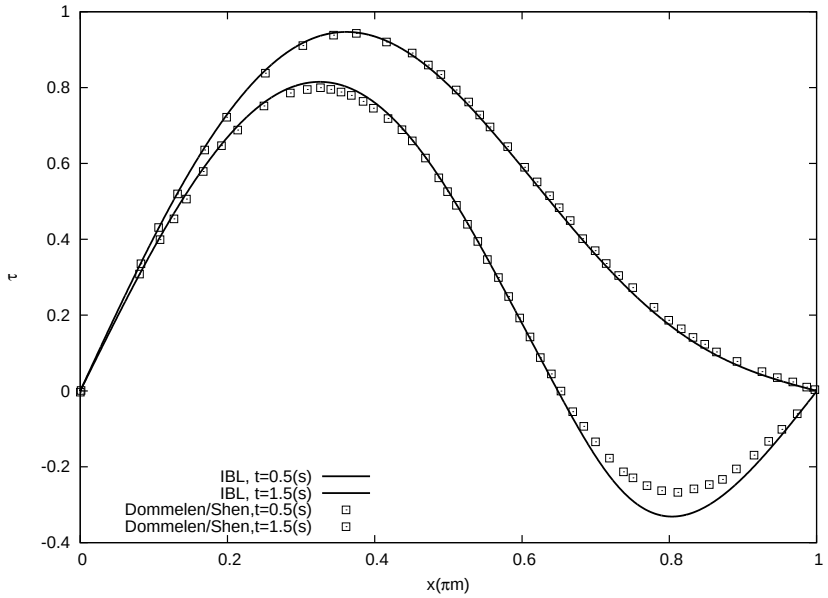

Figure J.21: Wall shear stress C_τ obtained with QUICK scheme for $u_e = sin(x)$, RK2 time integration, Matsushita closure, Thwaites as left BC, with grid refinement near the left boundary, $\Delta x = 0.001$, $CFL = 0.5$

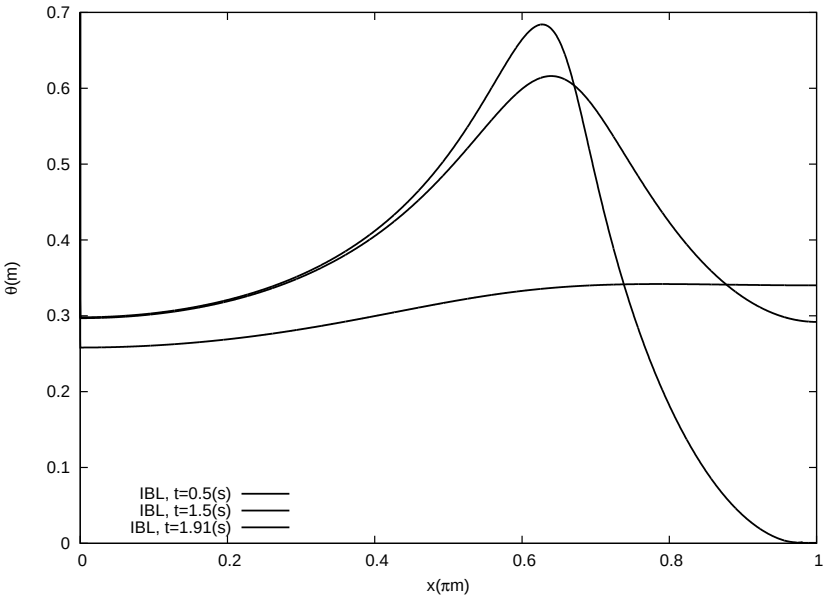

Figure J.22: Momentum thickness θ obtained with QUICK scheme for $u_e = sin(x)$, RK2 time integration, Matsushita closure, Thwaites as left BC, with grid refinement near the left boundary, $\Delta x = 0.001$, $CFL = 0.5$

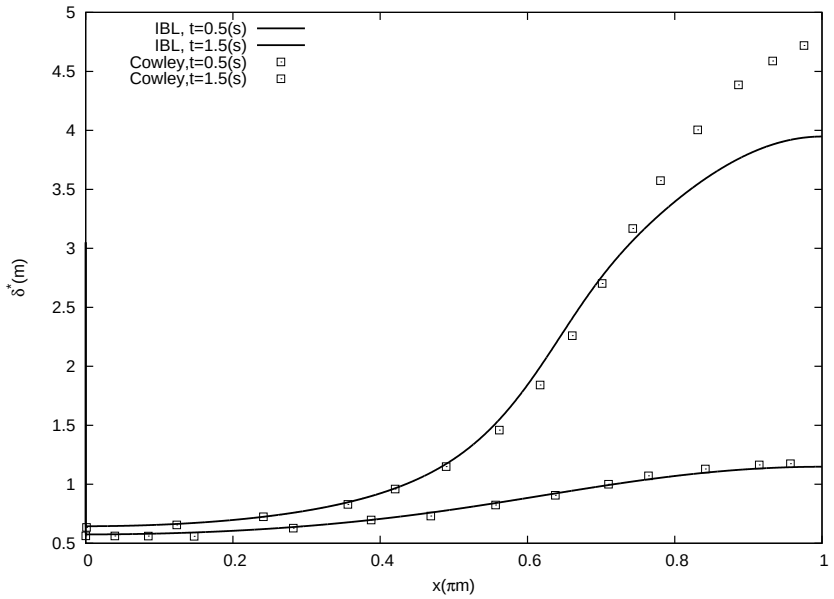

Figure J.23: Displacement thickness δ^* obtained with QUICK scheme for $u_e = sin(x)$, RK2 time integration, Matsushita closure, Thwaites as left BC, with grid refinement near the left boundary, $\Delta x = 0.001$, $CFL = 0.5$

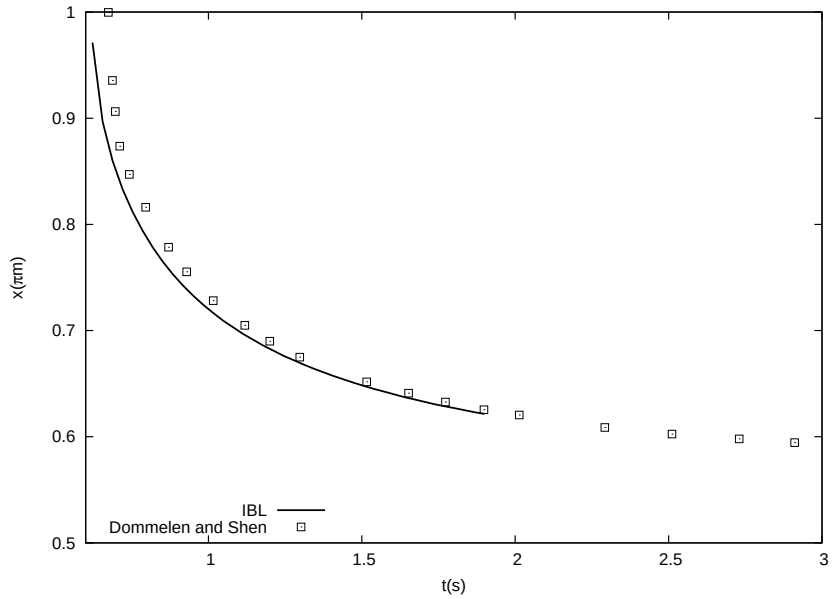

Figure J.24: Zero friction point obtained with QUICK scheme for $u_e = sin(x)$, RK2 time integration, Matsushita closure, Thwaites as left BC, with grid refinement near the left boundary, $\Delta x = 0.001$, $CFL = 0.5$

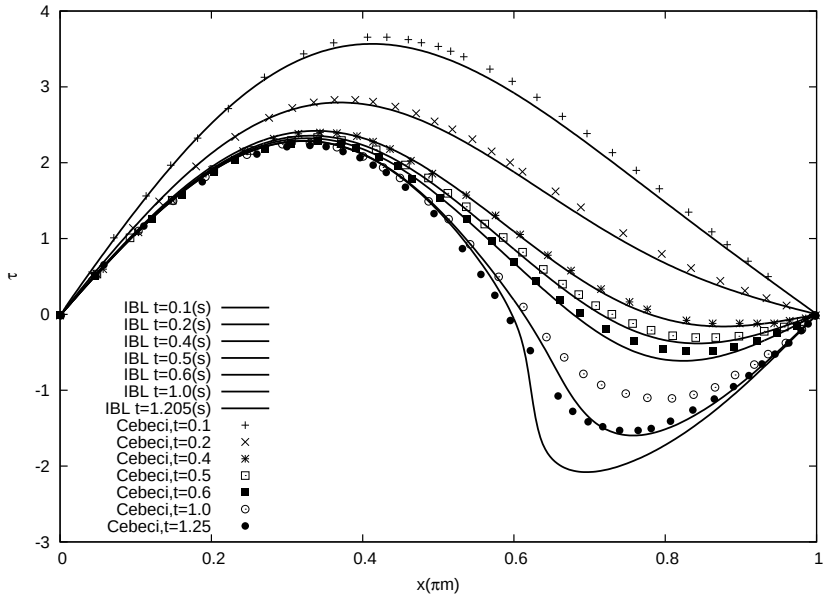

Figure J.25: Shear stress obtained with QUICK scheme, RK1 time integration for $u_e = 2sin(x)$, Matsushita closure, Thwaites as left BC, with grid refinement near the left boundary, $\Delta x = 0.01$, $CFL = 1.75$

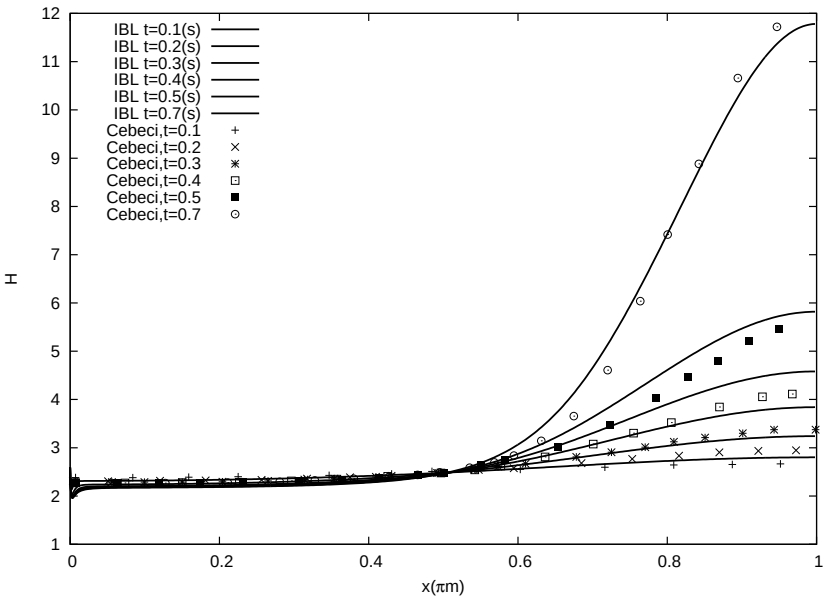

Figure J.26: Shape factor H obtained with QUICK scheme, RK1 time integration for $u_e = 2sin(x)$, Matsushita closure, Thwaites as left BC, with grid refinement near the left boundary, $\Delta x = 0.01$, $CFL = 1.75$

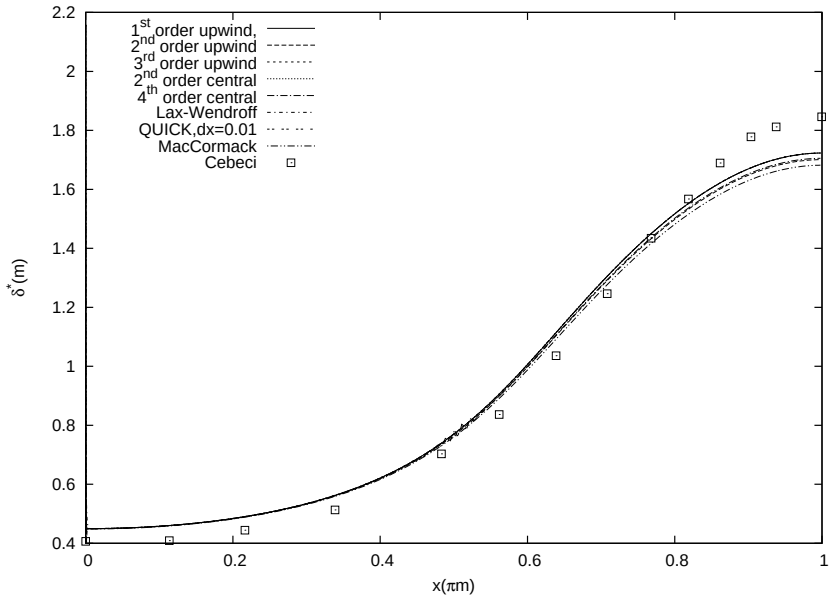

Figure J.27: Displacement thickness δ^* obtained with QUICK scheme, RK1 time integration for $u_e = 2sin(x)$, Matsushita closure, Thwaites as left BC, with grid refinement near the left boundary, $\Delta x = 0.01$, $CFL = 1.75$

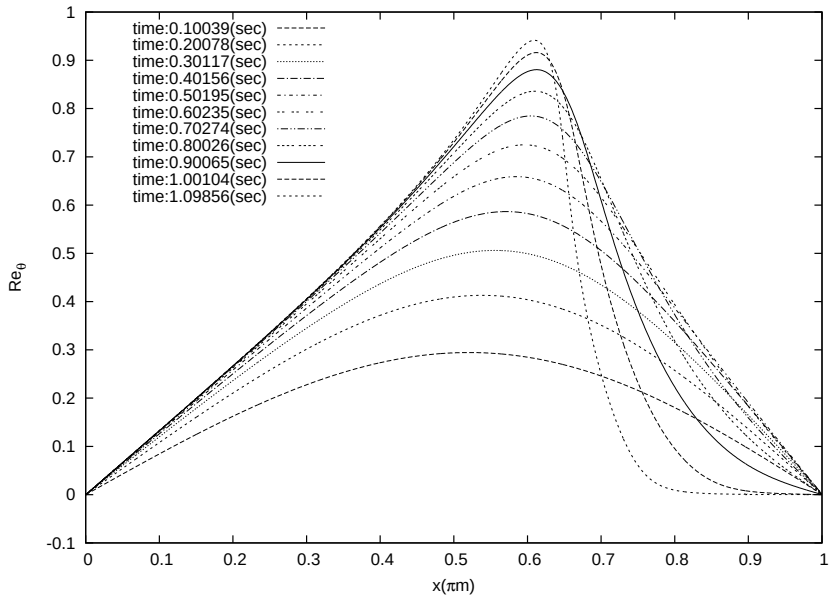

Figure J.28: Re_θ obtained with smoothed QUICK scheme, RK1 time integration for $u_e = 2sin(x)$, Matsushita closure, Milewski as left BC, with grid refinement near the left boundary, $\Delta x = 0.0025$, $CFL = 1.75$

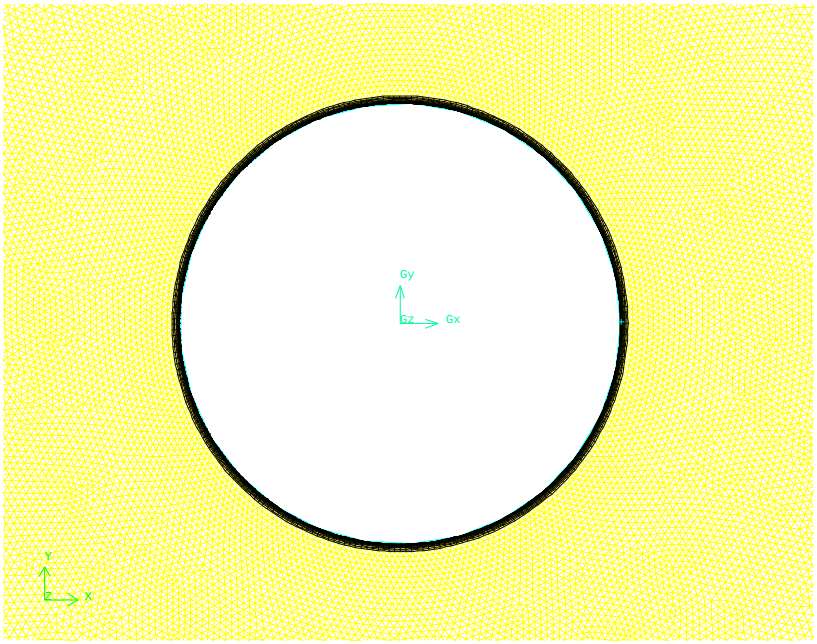

Figure J.29: Mesh for CFX simulation of impulsively moved cylinder

Appendix K

Reynolds Averaged Boundary Layer Equations

The ostensibly chaotic process of turbulence (see figure (K.1)) can be described in detail through the unsteady NS equations, however this requires the resolution of all turbulence scales which becomes too expensive for large Reynolds numbers. For this reason turbulence models have been developed which are intended to capture dominating behavior of turbulence through simplified models.

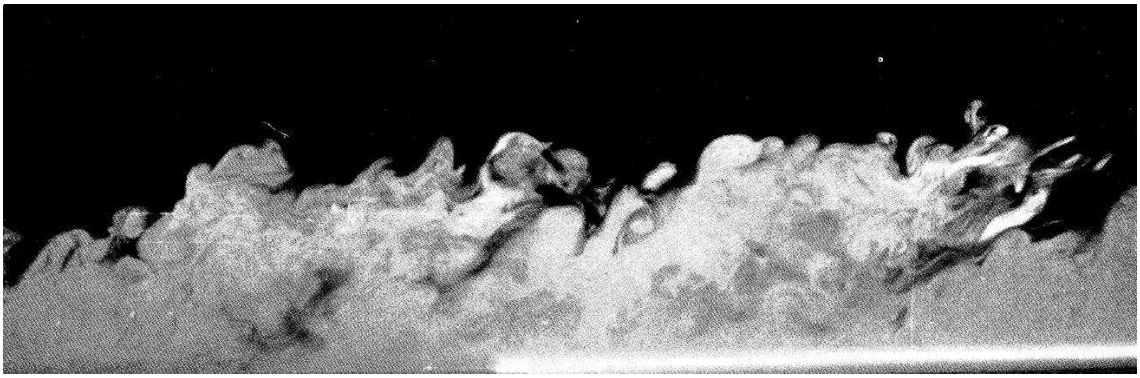

Figure K.1: Turbulent boundary layer.

The start of turbulence modeling is the assumption that the flow velocities can be divided into a mean part and a fluctuating part, i.e.

$$u = \overline{u} + u^{'}, \quad v = \overline{v} + v^{'}, \quad p = \overline{p} + p^{'},$$

where[1]

$$\overline{u} = \lim_{N \to \infty} \frac{1}{N} \sum_{i=0}^{N} u_i,$$

where N denoted the number of samples, i.e. the value at some point over the profile is sampled N times. This is usually called the Reynolds decomposition.

[1] Applicable to all variables with the bar

The following rules, called the Reynolds conditions, apply

$$\begin{aligned}\overline{f+g} &= \overline{f}+\overline{g},\\ \overline{\alpha f} &= \alpha\overline{f},\\ \overline{\frac{\partial f}{\partial s}} &= \frac{\partial \overline{f}}{\partial s},\\ \overline{\overline{f}g} &= \overline{f}\,\overline{g}.\end{aligned}$$

From this several relations can be derived (see i.e. Davidson[33])

$$\overline{\overline{u}} = \overline{u}, \quad \overline{\overline{f}\,\overline{g}} = \overline{f}\,\overline{g}.$$

The basic statistical characteristic of the fluctuating part is that it has a symmetric probability distribution (a Gaussian distribution is commonly used), i.e. $\overline{u'} = 0$.
Applying the Reynolds decomposition to (2.19) gives [2]

$$\frac{\partial\left(\overline{u}+u'\right)}{\partial t} + \frac{\partial\left(\overline{u}+u'\right)^2}{\partial x} + \frac{\partial\left(\overline{v}+v'\right)\left(\overline{u}+u'\right)}{\partial y} = \frac{\partial u_e}{\partial t} + u_e\frac{\partial u_e}{\partial x} + \nu\frac{\partial^2\left(\overline{u}+u'\right)}{\partial y^2}. \tag{K.1}$$

Averaging equation (K.1), applying the Reynolds conditions and derived rules and omitting bars for the mean terms results in

$$\frac{\partial u}{\partial t} + \cancel{\frac{\partial \overline{u'}}{\partial t}} + \frac{\partial u^2}{\partial x} + \frac{\partial \overline{u'^2}}{\partial x} + \cancel{2\frac{\partial \overline{u}\,\overline{u'}}{\partial x}} + \frac{\partial uv}{\partial y} + \cancel{\frac{\partial \overline{u'}\,v}{\partial y}} + \cancel{\frac{\partial \overline{v'}\,u}{\partial y}} + \frac{\partial \overline{u'v'}}{\partial y} = \frac{\partial u_e}{\partial t} + u_e\frac{\partial u_e}{\partial x} + \nu\frac{\partial^2 u}{\partial y^2} + \nu\cancel{\frac{\partial^2 \overline{u'}}{\partial y^2}}$$

For the boundary layer it is assumed that the fluctuating terms have the same order of magnitude (see i.e. Cebeci [22]) :

$$\overline{u'^2} \approx \overline{v'^2} \approx \overline{u'v'}. \tag{K.2}$$

Non-dimensionalising the fluctuation terms it then follows that

$$\frac{\partial \overline{u'^2}}{\partial x} \approx \frac{\delta}{L}\frac{\partial \overline{u'v'}}{\partial y},$$

and can therefore be neglected. The Reynolds Averaged Boundary Layer equation is now written as

$$\frac{\partial u}{\partial t} + u\frac{\partial u}{\partial x} + v\frac{\partial u}{\partial y} = \frac{\partial u_e}{\partial t} + u_e\frac{du_e}{dx} + \frac{\partial}{\partial y}\left(\nu\frac{\partial u}{\partial y} - \overline{u'v'}\right), \tag{K.3}$$

where $-\overline{u'v'}$ is the Reynolds Stress.
Except for the Reynolds stress equation set (K.3) is equal to the boundary layer equations derived earlier.

K.0.1 Turbulence Closure for Field Equations

The Reynolds stress is an extra term, thus a closure model is required to close the system of equations, which is now comprised of the turbulent momentum equation(K.3) and the continuity equation. In general there are multiple equation models, mixing length models and eddy viscosity models

$$\begin{aligned}\text{eddy-viscosity model:} \quad -\overline{u'v'} &= \varepsilon\frac{\partial u}{\partial y},\\ \text{mixing-length model:} \quad -\overline{u'v'} &= l^2\left|\frac{\partial u}{\partial y}\right|\frac{\partial u}{\partial y}.\end{aligned}$$

[2] Since u_e is prescribed it will not be divided into a mean and a fluctuating part.

Chakka and Schobeiri[119] add the intermittency factor to the eddy viscosity to account for the fact that transition has not fully occurred

$$\varepsilon = \gamma l^2 \left| \frac{\partial u}{\partial y} \right|,$$

the intermittency is made time-dependent through a Strouhal-number for the unsteady disturbance (in their case wake-influence). The two equations models basically use two parameters which are described separately by a differential equations, i.e. the $\kappa - \omega$ or $\kappa - \epsilon$ method. There are also the Reynolds stress models which employ five differential equations to describe the so-called Reynolds transport; the production and destruction of Reynolds stress due to convection, diffusion and external sources. For the purpose of the present research it suffices to use a so-called zero-equation model where the Reynolds stress is closed with an algebraic relation for either the eddy viscosity or the mixing length. The turbulence closure models presented below are devised specifically for the boundary layer.

The turbulence models presented below assume that the turbulent boundary layer velocity profile has two distinct regions, the inner region (close to the wall) and the outer region, the inner region is about $10-20\%$ of the entire boundary layer thickness[22], see figure(3.7). The eddy viscosity due to Spalding(1961) and Kleinstein(1967) is described as follows for the wall region (see Holt [66])

$$\varepsilon = \mu 0.04432 \left(e^{0.4u^+} - 1 - 0.4u^+ - 0.08u^{+2} \right),$$

where

$$\text{Law of the wall :} u^+ = \frac{u}{u_\tau},$$
$$\text{Friction velocity :} u_\tau = \sqrt{\frac{\tau_w}{\rho}}.$$

For the outer boundary layer the Clauser(1956) model can be used (see Holt[66])

$$\varepsilon = \mu 0.00168 Re_{\delta^*},$$

where

$$Re_{\delta^*} = \frac{u_e \delta^*}{\nu}.$$

to apply this, starting from $y = 0$ check whether the outer and inner model match, if so, the outer model should be used.

Cebeci and Smith[24] used a solution by Van Driest(1956) for the sublayer (also see Veldman[145])

$$l = \kappa y \left(1 - e^{\frac{-y^+}{A^+}} \right),$$

where $y^+ = \frac{y u_\tau}{\nu}$ and $A^+ = 26$, κ is called the Von Kármán constant which will be set at $\kappa = 0.41$ (see i.e. White[154]). For the outer layer the solution the eddy viscosity is given by the Clauser model. Cebeci[19] improved the above method for boundary layer flow with fluctuating external velocity, for the inner layer the eddy viscosity is formulated as

$$\varepsilon = \left[0.4y \left(1 - e^{-\frac{y}{A}} \right) \right]^2 \frac{\partial u}{\partial y},$$

where

$$A = \frac{26 \nu u_\tau^{-1}}{\sqrt{1 - 11.8(p_t^+ + p_x^+)}},$$
$$u_\tau = \sqrt{\frac{\tau_w}{\rho}}, \quad p_t^+ = \frac{\nu}{u_\tau^3} \frac{\partial u_e}{\partial t}, \quad p_x^+ = \frac{\nu u_e}{u_\tau^3} \frac{\partial u_e}{\partial x}.$$

For the outer layer Cebeci gives

$$\varepsilon = \alpha \int_0^\infty (u_e - u)\, dy,$$

where

$$\begin{aligned}
\alpha &= 0.0168 \frac{1.55}{1+\Pi}, \\
\Pi &= 0.55 \left[1 - e^{-0.243 z_1^{\frac{1}{2}} - 0.293 z_1} \right], \\
z_1 &= \frac{R_\theta}{425} - 1.
\end{aligned}$$

Again the inner layer formulation is used starting from $y = 0$ until it matches with the outer layer formulation.

Michel(1968) used for the mixing-length model over the entire layer (see Schlichting[118])

$$l = \lambda\delta \tanh\left(\frac{\kappa y}{\lambda\delta}\right),$$

where $\lambda = 0.085$.

For non-equilibrium flows it is advised to use at least one differential equation to described the turbulent boundary layer, see i.e. Schlichting[118].

Appendix L

Reference Solution of the BL Equations

The numerical solution of the field form of the BL equations is used for two purposes, firstly the computing time and effort required to resolve the boundary layer flow can be compared to the integral boundary layer method and secondly the flexibility of the field form can be used to give reference results. Not done for this thesis but important from the viewpoint of a future application of the IBLT is the incorporation of rotational effects and the gravitational acceleration. A direct way to start the analysis into the effects of these added terms is to apply the Field BL equations augmented with the added terms, this has been done by for instance Dumitrescu and Cardos[43]. A reference code for the incompressible unsteady boundary layer equations is given by Cebeci and Cousteix[22], this code will be used as a theoretical reference. The following discussion may likely not result in an actual implementation due to time constraints however it is relevant to consider the numerical implementation of the field method compared to the implementation of the integral method.

Using the chain rules together with the continuity equation the turbulent BL equation(K.3) can rewritten as

$$\frac{\partial u}{\partial t}+\frac{\partial u^2}{\partial x}+\frac{\partial uv}{\partial y}=\frac{\partial u_e}{\partial t}+u_e\frac{\partial u_e}{\partial x}+\frac{\partial}{\partial y}\left(\nu\frac{\partial u}{\partial y}-\overline{u'v'}\right), \tag{L.1}$$

here mass continuity is assumed implicitly, this is a second order partial differential equation. Alternatively a coupled first order system can be produced by taking out the bracketed term on the right-hand-side and by using the mass continuity explicitly

$$\begin{aligned}\frac{\partial u}{\partial t}+u\frac{\partial u}{\partial x}+v\frac{\partial u}{\partial y}&=\frac{\partial u_e}{\partial t}+u_e\frac{\partial u_e}{\partial x}+\frac{\partial \tau}{\partial y},\\ \frac{\partial u}{\partial x}+\frac{\partial v}{\partial y}&=0,\\ \tau&=\nu\frac{\partial u}{\partial y}-\overline{u'v'},\end{aligned} \tag{L.2}$$

Which can be written in matrix form

$$A\frac{\partial U}{\partial t}+B\frac{\partial U}{\partial x}+C\frac{\partial U}{\partial y}=D,$$

where

$$A = \begin{pmatrix} 1 & 0 & 0 \\ 0 & 0 & 0 \\ 0 & 0 & 0 \end{pmatrix}, \quad B = \begin{pmatrix} u & 0 & 0 \\ 1 & 0 & 0 \\ 0 & 0 & 0 \end{pmatrix}, \quad C = \begin{pmatrix} v & 0 & 1 \\ 0 & 1 & 0 \\ \varepsilon & 0 & \nu \end{pmatrix},$$

$$D = \begin{pmatrix} \frac{\partial u_e}{\partial t} + u_e \frac{\partial u_e}{\partial x} \\ 0 \\ \tau \end{pmatrix}, \quad U = \begin{pmatrix} u \\ v \\ \tau \end{pmatrix}, \quad \varepsilon \frac{\partial u}{\partial y} = -\overline{u'v'}$$

The above (ill-conditioned) formulation nicely illustrates the difference between the integral method, the latter has one coefficient matrix less but the coefficient matrices themselves have more complicated coefficients.

L.1 Approach One, Dimensional Conservative Boundary Layer Equations

Integrating the BL equation L.1 over some control volume and applying the divergence theorem

$$\int_\Omega \frac{\partial (u - u_e)}{\partial t} d\Omega + \int_{\delta\Omega} \begin{pmatrix} u^2 - \frac{1}{2}u_e^2 \\ uv - \nu \frac{\partial u}{\partial y} + \overline{u'v'} \end{pmatrix} \begin{pmatrix} n_x \\ n_y \end{pmatrix} d\Gamma = 0$$

The most convenient turbulence model is the mixing length model due to Michel which describes the entire boundary layer, since we assume the external flow to be time dependent the suggested eddy viscosity due to Cebeci[19] is also considered.The eddy viscosity models are given by

$$\text{Michel} : -\overline{u'v'} = \left[\lambda\delta \tanh\left(\frac{\kappa y}{\lambda\delta}\right)\right]^2 \left|\frac{\partial u}{\partial y}\right| \frac{\partial u}{\partial y},$$

$$\text{Cebeci} : -\overline{u'v'} = \begin{cases} \kappa^2 y^2 \left(1 - \exp\left(\frac{-y^+}{A^+}\right)\right)^2 \left|\frac{\partial u}{\partial y}\right| \frac{\partial u}{\partial y}, & \text{sub layer,} \\ \left[0.4y\left(1 - \exp\left(-\frac{y}{A}\right)\right)\right]^2 \left(\frac{\partial u}{\partial y}\right)^2, & \text{inner layer,} \\ \alpha \frac{\partial u}{\partial y} \int_0^\infty (u_e - u) dy, & \text{outer layer.} \end{cases},$$

where the constants have been presented in section (2).

The transition check is the same as used for the integral equations. Once a transition point is detected the eddy viscosity is directly placed in the formulation. Given the above formulation the discretisation follows from the definition of the control volume. This is treated in the next section.

L.1.1 Discretisation

For the FVM formulation the differential equation should be integrated over some control volume. Typically if a finite difference method is employed the Keller Box scheme is used, this can also be done for the FVM formulation, see figure (L.1) According to Veldman the Keller box scheme is very sensitive for wiggles, this is due to the central differences used in both x-direction and y-direction. This puts a more stringent requirement on the grid resolution, see stability analysis in appendix (??). Upwind differencing is less stringent for the resolution and it facilitates the direction in which the signal is transferred, however unlike central differencing there is artificial diffusion, meaning that the numerical approximation introduces a second order differential term, see Taylor-analysis in appendix (??). In the case of the BL equations artificial diffusion in x-direction does not introduce a significant error source since $\frac{\partial^2 u}{\partial x^2} \sim 0$, therefore using upwind differencing is more robust and it does not influence the accuracy if second

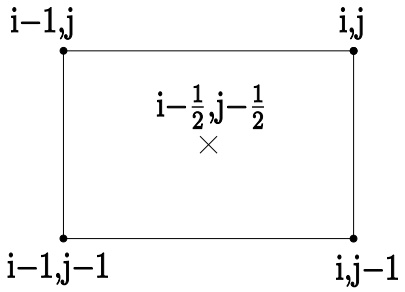

Figure L.1: Keller box, scheme.

order upwinding is used. In y-direction central differencing may be used. Now there is 2^{nd} order spatial accuracy. The control volume for this discretisation is given in figure (L.2).

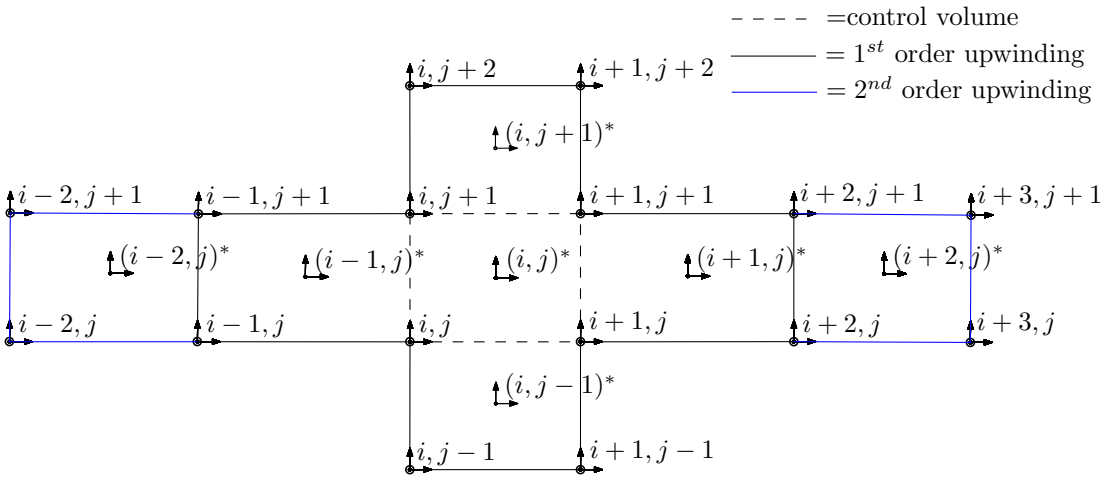

Figure L.2: Control volume and required nodal points for the discretisation scheme

Using a variable stepsize in $y-$direction the discretisation is written as

$$h_i h_j \frac{\partial(u-u_e)}{\partial t} = -h_j \left(u^2 - \frac{1}{2}u_e^2\right)_{\Delta x_{upw}} - h_i (uv)_{\Delta y_{central}} + h_i \left(\nu \frac{\partial u}{\partial y}\right)_{\Delta y_{central}} + h_i \left(\overline{u'v'}\right)_{\Delta y_{central}},$$

where the individual terms are written as

$$\begin{aligned}
\left(u^2 - \frac{1}{2}u_e^2\right)_{\Delta x_{upw}} &= \frac{1}{2}\left(1 - sign\left(u^*(i,j)\right)\right)\left[-\overline{u}^2(i+2,j) + 4\overline{u}^2(i+1,j) - (u^*)^2(i,j)\right] \\
&+ \frac{1}{2}\left(1 + sign\left(u^*(i,j)\right)\right)\left[3(u^*)^2(i,j) - 4\overline{u}^2(i+1,j) + \overline{u}^2(i-2,j)\right] \\
&- \frac{1}{2}\left(u_e^2(x(i+1),t(n)) - u_e^2(x(i),t(n))\right), \\
(uv)_{\Delta y_{central}} &= \left((uv)^*(i,j+1) - (uv)^*(i,j)\right)\Delta h^- - \left((uv)^*(i,j) - (uv)^*(i,j-1)\right)\Delta h^+, \\
\left(\nu \frac{\partial u}{\partial y}\right)_{\Delta y_{central}} &= 2\nu\left[\frac{u^*(i,j+1) - u^*(i,j)}{h_{j+1}+h_j}\Delta h^- - \frac{u^*(i,j) - u^*(i,j-1)}{h_j + h_{j-1}}\Delta h^+\right], \\
\Delta h^+ &= \frac{h_{j+1}+h_j}{h_{j-1}+h_j}, \quad \Delta h^- = \frac{h_{j-1}+h_j}{h_{j+1}+h_j}, \\
\Delta u_+^* &= \frac{u^*(i,j+1) - u^*(i,j)}{h_{j+1}+h_j}, \quad \Delta u_-^* = \frac{u^*(i,j) - u^*(i,j-1)}{h_{j-1}+h_j}, \\
\overline{u}(i,j) &= \frac{u(i,j) + u(i,j+1)}{2}, \quad u^*(i,j) = \frac{\overline{u}(i+1,j) + \overline{u}(i,j)}{2},
\end{aligned}$$

with for the eddy viscosity terms

$$\begin{aligned}
\text{Michel:} -\left(\overline{u'v'}\right)_{\Delta y_{central}} &= \left[\lambda\delta \tanh\left(\frac{\kappa y}{\lambda\delta}\right)\right]^2_{i,j+1} 4\left|\Delta u_+^*\right| \Delta u_+^* \Delta h^- - \\
&\left[\lambda\delta \tanh\left(\frac{\kappa y}{\lambda\delta}\right)\right]^2_{i,j} 4\left|\Delta u_-^*\right| \Delta u_-^* \Delta h^+, \\
\text{Cebeci,sub:} -\left(\overline{u'v'}\right)_{\Delta y_{central}} &= \left[\kappa y\left(1 - \exp\left(-\frac{y^+}{A^+}\right)\right)\right]^2_{j+1} 4\left|\Delta u_+^*\right| \Delta u_+^* \left(\Delta h^-\right)^2 - \\
&\left[\kappa y\left(1 - \exp\left(-\frac{y^+}{A^+}\right)\right)\right]^2_{j} 4\left|\Delta u_-^*\right| \Delta u_-^* \left(\Delta h^+\right)^2, \\
\text{Cebeci,inner:} -\left(\overline{u'v'}\right)_{\Delta y_{central}} &= \left[0.4y\left(1 - \exp\left(-\frac{y}{A}\right)\right)\right]^2_{j+1} 4(\Delta u_+^* \Delta h^-)^2 - \\
&\left[0.4y\left(1 - \exp\left(-\frac{y}{A}\right)\right)\right]^2_{j} 4(\Delta u_-^* \Delta h^+)^2, \\
\text{Cebeci,outer 1:} -\left(\overline{u'v'}\right)_{\Delta y_{central}} &= \left[\Delta u_+^* \Delta h^- - \Delta u_-^* \Delta h^+\right] \alpha \int_0^\infty (u_e - u) dy, \\
\text{Cebeci,outer 2:} -\left(\overline{u'v'}\right)_{\Delta y_{central}} &= 0.0168 u_e \delta^* \left[\Delta u_+^* \Delta h^- - \Delta u_-^* \Delta h^+\right].
\end{aligned}$$

The vertical velocity v is updated using the conservation of mass, i.e. $\frac{\partial u}{\partial x} = -\frac{\partial v}{\partial y}$. The weighted averaged coefficient matrices will not be (skew-)symmetric and not (positive/negative)definite, this means that the coefficient matrix may become singular. Simply using the unweighted averages will preserve symmetry and definiteness while maintaining second order accuracy (see Manteuffel and White[89]). The only adaptation of the earlier defined generic discretisation is that $\Delta h^+ = \Delta h^- = 1$.

L.1.2 Updating the Nodal Values

The time-flux is determined in the center of the cells. The nodal values for the new time step need to be extracted which can be done in two ways

- time-flux in center points, update, then extrapolate new nodal values
- time-flux in center points, extrapolate flux to nodal points, update

The latter seems preferable since the first order equation will be more smooth than the zeroeth order equation, therefore the interpolation will contain a smaller approximation error. For the explicit time integration the solution procedure can be written as

$$\left[\frac{\partial u}{\partial t}\right]^n = \left[-\frac{\left(u^2-\frac{1}{2}u_e^2\right)_{\Delta x_{upwinding}}}{h_i} - \frac{(uv)_{\Delta y_{central}}}{h_j} + \frac{\left(\nu\frac{\partial u}{\partial y}\right)_{\Delta y_{central}}}{h_j} + \frac{\left(\overline{u'v'}\right)_{\Delta y_{central}}}{h_j} + \frac{\partial u_e}{\partial t}\right]^n,$$

$$\left[\frac{\partial v}{\partial y}\right]^{n+1} = -\left[\frac{\partial u}{\partial x}\right]^{n+1}.$$

Updating the values for v requires that first $\frac{\partial u}{\partial x}$ is extracted for every point, then the values for v can be found by integrating $\frac{\partial v}{\partial y}$ in the $y-$direction. Likewise the integral variables can be found by integration in $y-$direction according to the definitions of the integral variables.

L.2 Approach B, Non-Dimensional Non-Conservative Boundary Layer Equations

The original Keller-box approach is described by the following steps[77] :

- the BL equations are reduced to a system of first order differential equations
- the differential equations are solved using central differences and two-point averages using the corner point value
- the resulting equations are linearised using Newton's method
- the resulting block tridiagonal system is solved using the block elimination method

The non-dimensionalised BL equations are described in e.g. Krainer[77, p.25], Cebeci and Cousteix[22], Sekar[120].

L.3 Boundary Conditions and Initial Conditions

The (dimensional) boundary conditions are given[1] by (also see figure(L.3))

$$\begin{aligned} u = u_e, v = 0, &\qquad x = 0, y > 0, t \geq 0, \\ u = v = 0, &\qquad x < 0, y = 0, t \geq 0, \\ u = u_e, v = 0, &\qquad x > 0, y \neq 0, t = 0, \\ u = 0.99u_e, v \approx 0, &\qquad y \to \infty, t \geq 0. \end{aligned}$$

As is done for the IBL equations, for the boundary at the far end of the plate backward

[1] the non-dimensional boundary conditions follow directly from the dimensional boundary conditions

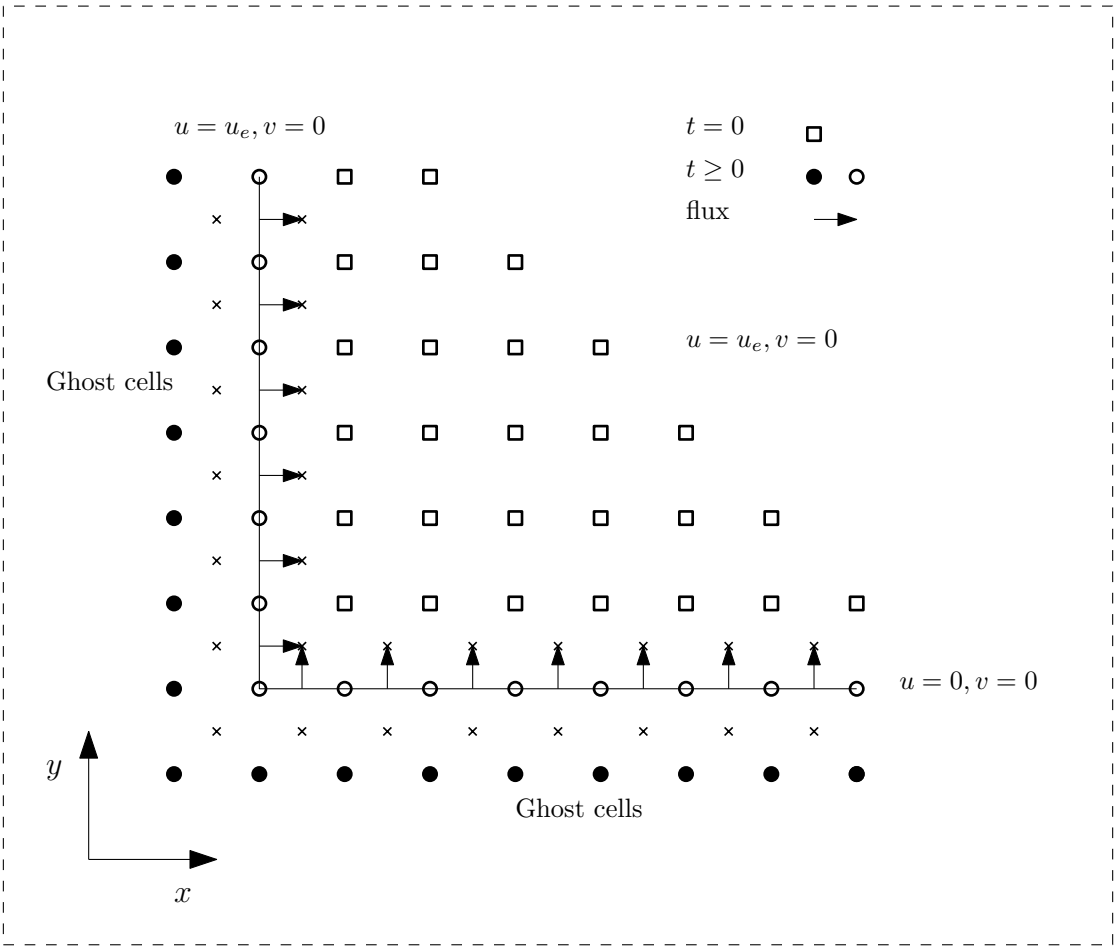

Figure L.3: Boundary conditions and initial conditions

differencing will be used, removing the need for a far-end boundary condition. This assumes the information convects downstream only (or dominantly), which is done by for instance Smith[124] who assumes that information convects downstream for the entire profile. If first order upwinding is used for the first interior points at the left boundary, no special treatment is required for the left boundary. If second order upwinding is maintained ghostcells are required (see figure (L.3)).

The final boundary condition is formed by the definition of $y \rightarrow \infty$ and it's respective value, this will be based initially on the result of an (equivalent) steady state integral boundary layer solution. To prevent that during the execution of the unsteady problem the boundary layer thickness grows outside the solution domain, the initial set boundary layer height must be overestimated or the boundary layer height (i.e. the vertical gridsize) must be variable.

List of Symbols and Abbreviations

Abbreviation	Description
AWSM	Aerodynamic Windturbine Simulation Module
BC	Boundary Condition
BEM	Blade Element Momentum Theory
CFL	Courant Friedrich Lewy
DG	Discontinuous Galerkin
ECN	Energy Research Center of the Netherlands
IBL	Integral Boundary Layer
IBLM	Integral Boundary Layer Method
FDM	Finite Difference Method
FEM	Finite Element Method
FVM	Finite Volume Method
GQR	Gaussian Quadrature Rule
LSRK	Low Storage Runge Kutta
MRS	Moore, Rott and Sears
MUSCL	Monotone Upwind Schemes for Conservation Laws
NS	Navier Stokes
ODE	Ordinary Differential Equation
PDE	Partial Differential Equation
PHATAS	Program for Horizontal Axis wind Turbine Analysis and Simulation
QUICK	Quadratic Upstream Interpolation for Convective Kinematics
RANS	Reynolds Averaged Navier Stokes
RK	Runge Kutta
SSP	Strong Stability Preserving
TVBM	Total Variation Bounded in the Mean
TVD	Total Variation Diminishing

Symbol	Description	Unit
Roman Characters		
A	coefficient matrix for temporal flux vector	n/a
B	coefficient matrix for spatial flux vector	n/a
C	coefficient matrix for source vector	n/a
C_f	friction coefficient	[-]
C_D	viscous diffusion coefficient	[-]
D	viscous diffusion	$[N/s/m$
f	conservative flux vector or frequency	n/a
F	primary variable vector	n/a
h	numerical flux vector	n/a
H	shape factor	[-]
H_1	Head's shape factor	[-]
H^*	kinetic shape factor	[-]
E	inverse shape factor	[-]
K	Jacobian matrix or coefficient matrix for spatial flux vector for conservative and non-conservative schemes respectively	n/a
K_c	Green's lag entrainment constant	[-]
L	source vector	n/a
M	right eigenvector matrix	n/a
Tu	Turbulence intensity	[%]
u_e	boundary layer edge velocity	$[m/s]$
u_s	slip velocity	$[m/s]$
Miscellaneous		
Re_x	Local Reynolds number	[-]
Re_θ	Momentum thickness Reynolds number	[-]
Re_{δ^*}	Displacement thickness Reynolds number	[-]
C_τ	Shear stress coefficient	[-]
$\mathbb{L}$	Linear operator	n/a
$C2$	Convergence number for $L2$ norm	[-]
Greek Symbols		
ρ	density or spectral radius	$[kg/m^3][m/s]$
ν	kinematic viscosity	$[m^2/s]$
μ	dynamic viscosity	$[kg/s/m]$
τ	shear stress	$[Pa]$
δ	boundary layer thickness	$[m]$
δ^*	displacement thickness	$[m]$
δ^k	kinetic energy thickness	$[m]$
θ	momentum thickness	$[m]$
η	relative height $\frac{y}{\delta}$	[-]
λ	eigenvalue	$[m/s]$
Λ	Pohlhausen parameter	[-]
γ	intermittency factor or velocity profile parameter	[%][-]
κ	Von Kármán constant	[-]
ψ	basis function	$[m]$
ϕ	test function	$[m]$
ξ	non-dimensional coordinate within FEM control element	[-]

List of Figures

List of Tables